Maria Consuelo Hart Prieto MB. BCh. MRCS(Ed).

THE APPLICATIONS OF RAMAN SPECTROSCOPY TO UROLOGY

Institute of Bioscience and Technology
&
Cranfield Postgraduate Medical School

DM Thesis

Institute of Bioscience and Technology
&

Cranfield Postgraduate Medical School

DM Thesis

Academic Year 2004/2005

Maria Consuelo Hart Prieto MB. BCh. MRCS(Ed).

THE APPLICATIONS OF RAMAN SPECTROSCOPY TO UROLOGY

Supervisors: Mr. M. Wright, Mr. A. W. Ritchie & Dr. N. Stone

July 2006

THIS THESIS IS SUBMITTED IN PARTIAL FULFILLMENT OF THE REQUIREMENTS FOR THE DEGREE OF DOCTORATE OF MEDICINE

Abstract:

Raman spectroscopy is an optical technique that can interrogate biological tissues. In doing so it gives us an understanding of the changes in the molecular structure that are associated with disease development. The Kerr gating technique uses a picosecond pulsed laser and fast temporal gating of inelastically (Raman) scattered light.

The tissue samples used were taken following fully informed consent and ethics approval. Bladder samples were obtained by taking a biopsy during a TURBT or TURP, prostate samples were taken during TURP and the liver and kidney (pigs) were bought at a supermarket. The bladder and prostate samples were snap frozen in liquid nitrogen and stored in an -80°C freezer until required for experimentation. The liver and kidney tissue were used fresh. The constituent samples were bought from Sigma – Aldrich.

Multivariate and least squares analysis were used to ascertain the biochemical basis of the differing pathologies within the bladder and the prostate gland, as well as to test diagnostic algorithms produced by a colleague in our group. Depth profiling through the bladder and prostate gland was shown to be feasible by utilizing the Kerr gating technique as was the suppression of fluorescence from dark tissue (liver and kidney).

We have shown for the first time, that we can utilise Raman spectroscopy to determine the biochemical basis of pathologies of the bladder and the prostate gland. With the help of the Kerr gating technique we also obtained spectra from different depths through them. We also suppressed fluorescence and resonantly enhanced Raman spectra from dark tissue. These have major implications in terms of understanding pathogenesis and disease progression and also the potential to accurately assess depth of tumour invasion.

Acknowledgements:

This work was funded in part by the Cobalt Unit Appeal Fund and involved a collaboration between Gloucestershire Royal Hospital and the Rutherford Appleton Laboratory.

Firstly I would like to thank Dr Nick Stone for the opportunity to undertake this project, for his supervision and for his continuing friendship. His perseverance and patience as my academic supervisor has kept me going over the last two years (especially when I decided to go to Australia to write up). If it weren't for e mail and skype I don't know what I would have done.

Mr Alastair Ritchie has proved an inspiration as a clinical supervisor. Not only did his enthusiasm and encouragement for the project help with its progression but also the Wednesday morning day case theatre sessions kept me grounded. In writing up his experience and knowledge have been invaluable.

I was very fortunate to have a second clinical supervisor and Mr Mark Wright proved to be invaluable as the project progressed. His knowledge of the project and the discussions with him helped me to explore different avenues.

Professor Hugh Barr, the leader of our research group has given me great support and encouragement over the last few years. I would like to thank him for always being there when he was needed.

I cannot overstate my gratitude to the histology department at Gloucestershire Royal Hospital and especially Dr Jeremy Uff for his help and support with this project, Jackie Rachael, Christine Braun and Jo Motte for their help with the tissue storage and cutting of all my samples and Dr Linmarie Ludeman for the histology pictures.

The group at Rutherford Appleton Laboratories proved to be very useful in exploring new spectroscopic techniques and I would like to thank them for the use of the Kerr – gating technique. I would especially like to thank Dr Pavel Matousek for his patience in explaining the technique to me as a non basic scientist. I also gratefully acknowledge the loan of a NIR CCD camera from Andor Technology for use during the experiments at the Rutherford Appleton Laboratories.

I would also like to thank the group for our daily coffee breaks and discussion. Without them new ideas and potential pathways would not have been explored.

Finally I would like to thank my long suffering husband, Tim for his understanding, encouragement and support and to my baby – Luka, who spurred me on, ensuring that I had almost finished writing up before he was born. I couldn't have done it without them.

Declaration:

This thesis is the result of my own investigations, except where otherwise stated.
Other sources are acknowledged within the text giving explicit references. A bibliography is appended.

This thesis has not previously been accepted in substance for any other degree and is not being concurrently submitted in candidature for any other degree.

This thesis has been submitted to Cranfield University on the conditions contained in the regulations and except where otherwise stated, the work was carried out as part of my course of study and not previously or subsequently.

I hereby give consent for my thesis, if accepted, to be available for photocopying and for inter-library loan, and for the title and summary to be made available to outside organisations.

Signed……. (candidate)

Date…….

Contents:

List of figures and tables.

Abbreviations:

ANOVA	Analysis of variance
AUR	Acute urinary retention
ATP	Adenosine tri-phosphate
BPH	Benign prostatic hyperplasia
CaP	Adenocarcinoma of the prostate gland
CIS	Carcinoma in situ
CS_2	Carbon Sulphide
CUR	Chronic urinary retention
DHT	Dihydroxytestosterone
DNA	Deoxyribonucleic acid
DRE	Digital rectal examination
F-crit	Critical value of F
H & E	Haematoxylin and Eosin
HGPIN	High grade prostatic intra-epithelial neoplasia
IVU	Intravenous urogram
LDA	Linear discriminant analysis
P.C	Personal computer
PC	Principal component
PCA	Principal component analysis
pH	Hydrogen ion concentration
PIN	Prostatic intra-epithelia neoplasia
PMD	Post micturition dribbling
PSA	Prostate specific antigen
RNA	Ribonucleic acid

rRNA	Ribosomal ribonucleic acid
TCC	Transitional cell carcinoma
TNM	Tumour-nodes-metastases
TRUS	Transrectal ultrasonography
TURBT	Transurethral resection of bladder tumour
TURP	Transurethral resection of the prostate gland
USS	Ultrasound scan
UTI	Urinary tract infection
5-ALA	5 – Aminolevulinic acid

Glossary of terms:

Actin	The contractile protein that makes up thin filaments in a muscle fibre (cell).
Acute	Having rapid onset, severe symptoms, and a short course.
Acute urinary retention	The painful inability to pass urine when your bladder is full.
Adenocarcinoma	A malignant neoplasm of glandular or secretory epithelium.
Adenosine Triphosphate	The universal energy-carrying molecule manufactured in all living cells as a means of capturing and storing energy. It consists of the purine base adenine and the five carbon sugar ribose, to which are added, in a linear array, three phosphate groups.
Androgen	Substance producing or stimulating masculine characteristics, such as the male hormone testosterone.
Basement membrane	Thin, extracellular layer consisting of a basal lamina secreted by epithelial cells and a reticular lamina secreted by connective tissue cells.
Biopsy	The process of removing tissue or other material from the living body for examination, usually microscopic for diagnosis.

Brachytherapy	The ultrasound guided trans-perineal insertion of radioactive rods or seeds into the prostate.
Calculus	A stone or insoluble mass of crystallized salts or other material, formed within the body.
Carcinogenesis	Mechanisms of the causation of malignant neoplasms.
Carcinoma	A malignant epithelial neoplasm.
Carcinoma in situ	A malignant epithelial neoplasm that has not yet invaded through the original basement membrane; synonymous with intra-epithelial neoplasia.
Castration	Removal of gonads, (testes or ovaries).
Cell	The basic structural and functional unit of all organisms; the smallest structure capable of performing all the activities vital to life.
Chronic	Persisting for a long period of time.
Chronic urinary retention	The painless stretching of the bladder due to outlet obstruction, resulting in the inability to completely void urine. Occurs over a long period of time.
Cyst	A cavity with an epithelial lining, containing fluid or other material.
Cystectomy	The surgical removal of the bladder.

Cystitis	inflammation of the bladder, whether used as a histologic, bacteriologic, or cystoscopic description, or a clinical syndrome that is usually accompanied by an abrupt onset of dysuria, increased frequency, urgency, and suprapubic pain.
Cystoprostatectomy	The surgical removal of the bladder and the prostate gland.
Detrusor muscle	Intermediate muscularis layer surrounding the mucosa of the urinary bladder.
Differentiation	1. Embryological – process by which a tissue develops special characteristics. 2. Pathological – degree of morphological resemblance of a neoplasm to its parent tissue.
Disease	Abnormal state causing or capable of causing ill health.
Down regulation	Phenomenon in which there is a decrease in the number of receptors in response to an excess of a hormone or neurotransmitter.
Dysplasia	Change in the size, shape and organisation of cells due to chronic irritation or inflammation; may revert to normal if the stress is removed or progress to neoplasia.
Dysuria	Pain on passing urine.

Elastic scattering	When monochromatic radiation passes through a substance it can be scattered or absorbed. Most of the scattered light is elastically scattered with the same frequency as incident light, so energy is conserved with the same number and type of particles in the initial and final state.
Ejaculatory duct	A tube that transports sperm cells from the ductus (vas) deferens to the prostatic urethra.
Epithelial tissue	tissue composed of cells that line the cavities and surfaces of structures throughout the body. Many glands are also formed from epithelial tissue. Epithelium lines both the outside (skin) and the inside cavities and lumen of bodies
False negative	The proportion of individuals with the disease that are classified as not having the disease.
False positive	The proportion of individuals without the disease that are classified as having the disease.
Gland	Single or group of specialised epithelial cell that secrete substances.
Gold standard	The standard with which all other tests or procedures are compared.
Haematoxylin and Eosin	The standard stains used in the histological processing of frozen and formalin fixed tissue for pathological analysis.

Haematuria	Blood detected in the urine; can be either microscopic or macroscopic.
Haematogenous	Via the blood vessels.
Hesitancy	The inability to commence the floww of urine immediately.
Histopathology	The study of microscopic structure of tissue used in the diagnosis of disease.
Hyperplasia	Enlargement of an organ, or tissue within it, due to an increase in the number of cells.
Incidence	The number of new cases diagnosed per 100,000 persons / year.
Inelastic scattering	When monochromatic radiation passes through a substance it can be scattered or absorbed Most of the scattered light is elastically scattered with the same frequency as that of incident light, but a small proportion of the incident light is inelastically scattered with the difference in energy changing the vibrationalstate of the molecule probed. Inelastic scattering is the process measured in Raman spectroscopy.
Inflammation	Localised, protective response to tissue injury designed to destroy, dilute, or wall off the infecting agent or injured tissue; characterised

	by redness, swelling, pain, heat and sometimes loss of function.
Inter-observer variation	Disagreement between different observers.
Intra-observer variation	Disagreement between the same observer.
Intravenous urogram	The injection of a contrast agent into a vein that is excreted by the kidneys. Plain radiographs are then taken at specific times post injection and the contrast is seen within the urinary tract. In this way filling defects from tumours can be seen as can obstruction of a kidney.
Intravesical	Within the bladder.
Lymphoedema	A condition of localized fluid retention caused by a compromised lymphatic system.
Macroscopic	Can be seen with the naked eye.
Metastasis	The spread of cancer to the surrounding tissues, (local), or to other body sites, (distant).
Microscopic	Can be seen with a microscope, but not with the naked eye.
Morbidity	Diseased, pertaining to disease.
Mortality rate	Number of deaths occurring per 100,000 persons per year.
Neoplasia	Uncoordinated and abnormal tissue growth; new growth that does not respond to normal growth controls.

Nephrostomy	The insertion of a tube into the calyceal system of the kidney through the back to relieve obstruction to the kidney i.e. ureteric obstruction.
Nocturia	The need to pass urine during the night.
Oestrogen	Female sex hormones produced by the ovaries concerned with the development and maintenance of female reproductive structures and secondary sex characteristics, fluid and electrolyte balance, and protein anabolism. In males it is produced by the peripheral conversion of testosterone and androstenedione.
Orchidectomy	The surgical removal of one or both testes.
Plasma	The extracellular fluid found in blood vessels; blood minus the formed elements.
Prevalence	The number of cases of a disease present per 00,000 persons at a given time.
Prostadynia	Pain originating from the prostate gland.
Prostatitis	Inflammation within the prostate gland.
PSA density	The PSA level divided by the volume of the prostate gland.
PSA velocity	The rate of change of serum PSA over a period of time.

Radical Cystectomy	The surgical removal of the bladder, in it's, entirety, in an attempt to cure bladder cancer.
Radical Cystoprostatectomy	The surgical removal of the bladder and the prostate gland, in it's entirety, in an attempt to cure bladder cancer.
Radical prostatectomy	The surgical removal of the prostate gland, in it's entirety, in an attempt to cure prostate cancer.
Radical external beam radiotherapy	Giving radiation to an area in the body in an attempt to cure the patient of cancer.
Radical treatment	The attempt to cure, usually cancer.
Raman spectroscopy	An inelastic scattering technique, which exploits the frequency shift that occurs in incident light due to excitation of vibrational and rotational states in illuminated molecules.
Regression	The process of estimating a mean outcome in a population for any given value of the exposure variable, using a sample of exposures and outcomes.
Regression equation	An equation describing the relationship between a continuous exposure variable and the mean of a continuous variable.
Residual	The volume of urine left in the bladder post micturition.

Retropubic prostatectomy.	The surgical removal of the prostate nodules as an open procedure, usually leaving behind the prostatic capsule.
Sensitivity	The proportion of individuals with the disease that are classified as having the disease.
Specificity	The proportion of individuals without the disease that are classified as not having the disease.
Stroma	The tissue that forms the ground substance, foundation, or framework of an organ, as opposed to its functional parts, (parenchyma).
Synergistic effect	A hormonal interaction in which the effects of two or more hormones acting together is greater or more extensive than the sum of each hormone acting alone.
Tenesmus	The sensation for the need to have the bowels opened without there being any faeces within the rectum.
Tissue	A group of similar cells and their intercellular substance joined together to perform a specific function.
Transrectal ultrasonography	An ultrasound probe passed into the rectum to gain good views of the prostate gland.

Transurethral resection of bladder tumour	The surgical removal of a bladder tumour by operating via the urethra. Therefore resulting in no cuts on the outside.
Transurethral resection of prostate	The surgical removal of part of the prostate gland by operating via the urethra. Therefore resulting in no cuts on the outside.
Ureter	The tube that carries urine from the kidney to the bladder.
Ureteric stent	Tubes passed through the ureter to relieve an obstruction and keep the ureter open.

1. Introduction.

1.1. Aims and Objectives.

The main aim of this study is to determine whether near-infrared Raman Spectroscopy can be used to build robust spectral and biochemical diagnostic models to differentiate between benign and malignant disease of the bladder and the prostate gland *in vitro*. In doing so we hope to further our understanding of carcinogenesis within these tissues.

Secondary objectives include, significantly increasing the sample size of the pilot bladder and prostate diagnostic models developed by my predecessor as well as determining whether near-infrared Raman Spectroscopy can be used for the real-time optical differentiation of benign and malignant disease of the bladder and the prostate gland *in vivo*.

Raman Spectroscopy has already shown potential for the in vivo use of a probe in the oesophagus [Shim 2000], colon [Molckovsky 2003], cervix [Mahadevan-Jansen 1998b] and skin [Caspers 1998]. At present however there is no real time diagnostic tool to diagnose pathologies within the bladder or the prostate gland, without the need for biopsy. It is hoped that Raman Spectroscopy will be helpful with the *in-situ* diagnosis of tissue as well as assessing surgical margins following excision, therefore obviating the need for subjective histology.

1.2. Raman spectroscopy.

1.2.1. Why Raman spectroscopy?

There are many spectroscopic techniques that can be used in tissue diagnosis both *in vitro* and *in vivo*. The conventional means of diagnosis is by white light cystoscopy but biopsies are needed to enable a histopathological diagnosis. The following is used for the clinical diagnosis of urological tissues at present: fluorescence spectroscopy. Fourier transform infrared (FTIR) spectroscopy , optical coherence tomography and, Raman spectroscopy are used in research to distinguish between different pathologies in urological tissues.

Fluorescence spectroscopy with the use of exogenous molecules such as 5-aminolaevulinic acid (5-ALA) has been used clinically and in-vivo within the bladder. The administration of 5-ALA results in the accumulation of proto-porphyrin IX which is tumour specific and fluoresces. This can guide the biopsy of lesions within the bladder. It does have a high false positive rate and has so far only been used the bladder and not with the prostate [Baumgartner 1999]. Work in parallel by Grimbergen et al [2006] have shown that Raman spectroscopy could be performed on biopsies post 5-ALA guided biopsy by subtracting the background fluorescence using a subtraction algorithm. The combination of the two *in vivo* may lead to a better method of obtaining optical biopsies.

Optical coherence tomography (OCT) is a cross sectional imaging technique that is similar to B-mode ultrasonography, however images are formed by detecting light reflected from subsurface tissue as opposed to sound waves. The light is reflected from the subsurface tissue microstructures [Yang 2004]. *In vivo* studies have been done in the bladder [Sergeev 1997] as well as *in vitro* in the prostate, urethra. ureter and bladder [Tearney 1997]. The latter showed an axial resolution of 16 microns which is better than any other available intraluminal imaging at present. The disadvantages with it however are that the images are subjective and artefact can be caused by peristalsis if in the ureter or movement of the bladder with respiration.

FTIR spectroscopy could be used seperately or as an adjunct to Raman spectroscopy as they are both able to probe the molecular constituents of the tissue being measured by studying the interaction of light with the molecular vibrational states.

The disadvantage of FTIR spectroscopy over Raman is that there is interference from water and therefore the tissue needs to de dry and would not be suitable for in-vivo work. As the research group's final aim is to have an in-vivo probe for the diagnosis of urological pathologies, it was felt that FTIR spectroscopy was not appropriate for these experiments [Bhargava 2001, Gazi 2004].

Raman has been demonstrated elsewhere to be highly specific, insensitive to water content of the tissue and compatible with fibre optic technologies. It was therefore felt that it would be suitable for the work in this thesis and future work of the group.

As the objective of this thesis was to look at pathologies within the bladder and the prostate gland using the same spectroscopic method and the group was hoping to

progress to in-vivo diagnoses it was felt that Raman spectroscopy was the best modality for this.

1.2.2. An overview.

In 1928, Chandrasekhara Venkata Raman first reported the Raman effect. This is a phenomenon whereby light is inelastically scattered. He initially observed that scattering from the sea gave it its colour independent of reflection or absorption of light from the sky, and later went on to focus sunlight onto a liquid. The scattered light was viewed via polarizers and filters so that it could be seen by the eye. These experiments culminated in a publication in Nature whereby he described 'a new type of secondary radiation' [Raman 1928]. Chandrasekhara Venkata Raman was later awarded a Nobel prize for his work (1930).

Raman spectroscopy is an optical technique that analyses the way that incident light is inelastically scattered from a substance. It utilises the concept of the Raman effect, whereby energy is exchanged between light and matter.

Light is an electromagnetic wave composed of both an electric field component and a magnetic field component. The electric and magnetic fields are both orthogonal to each other and orthogonal to the direction of propagation of the wave. A photon is a package of light. Therefore if the speed of light (c) is equal to the wavelength of light (λ) multiplied by its frequency (v), then the energy of a photon (E) is equal to Planks constant (h) multiplied by frequency, or Planks constant multiplied by (the speed of

light divided by the wavelength), as is shown below. The energy is inversely proportional to the wavelength.

$$c = \lambda v$$

$$E = h v \qquad \text{therefore} \qquad E = h (c/ \lambda)$$

When a beam of light, is passed through a substance, the light will either be scattered or absorbed. This occurs even if the substance is cleaned to exclude any dust particles or other material. Two types of scattering are noted, the majority will be Rayleigh scattering, this is elastic scattering i.e. the scattered light has the same frequency as the incident light, and therefore has no energy change. The second type which occurs in a very small fraction of the photons is Raman scattering (in 1 in 10^{-7}). This scattering is inelastic, i.e. the frequency of the scattered light is different to that of the incident light, and therefore there has been a gain or loss of energy. This is shown in the simplified diagram below, (Fig 1.1).

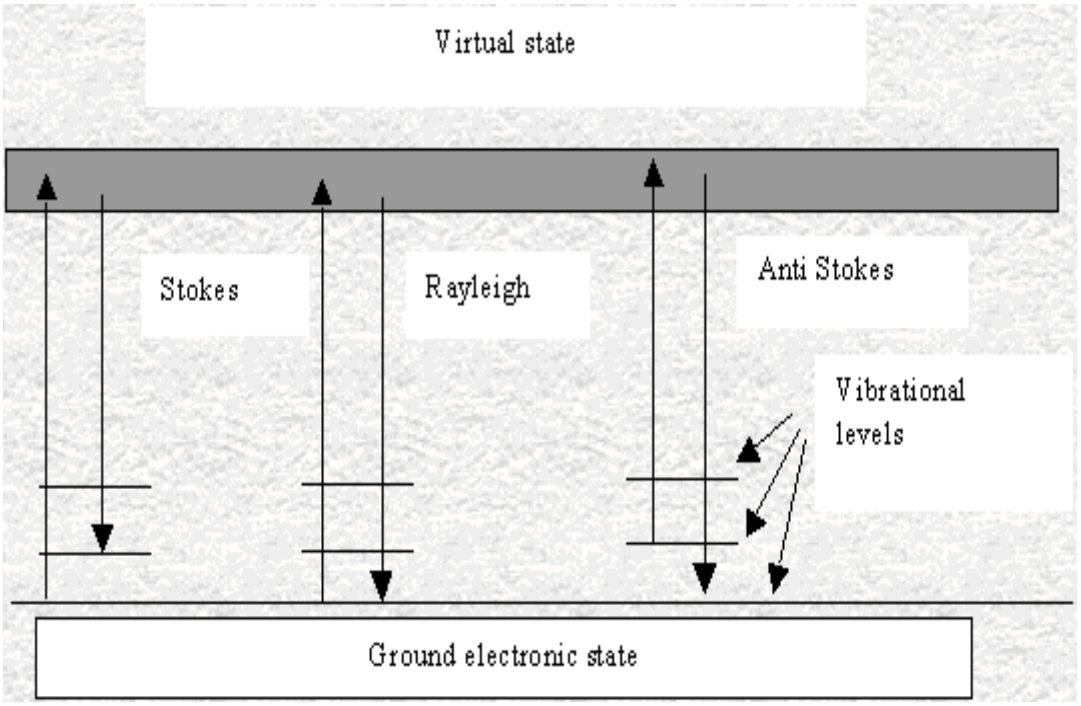

Fig 1.1: A simplified energy diagram illustrating Raman and Rayleigh scattering.

Reproduced from Anderson (2000)

http://carbon.cadenver:edu/public/chemistry/classes/chem4538/raman.htm

Raman scattering can be Stokes whereby the scattered light frequency is less than that for the incident light or vice versa for Anti-Stokes. As light energy is proportional to frequency, the change in the scattered light frequency is equal to that of the molecular vibrations of the molecule. Figure 1.2 shows how a Raman spectrum may appear in its basic form.

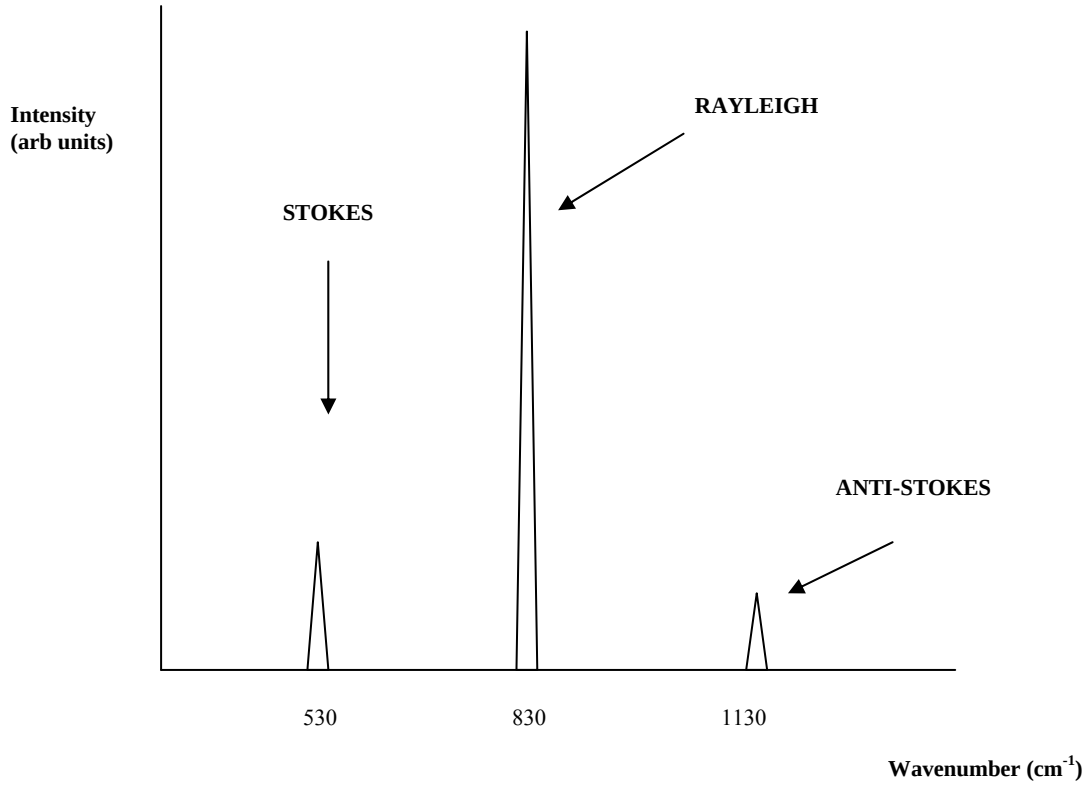

Fig 1.2: **A** diagram showing a Raman spectrum in its basic form.

Adapted from Anderson (2000).

http://carbon.cadenver:edu/public/chemistry/classes/chem4538/raman.htm

As you can see from the above diagram the Stokes line is more intense but both are equally displaced from the Rayleigh line. In view of this and the fact that Anti-Stokes is temperature dependent (because molecules have to already be in an excited state) and is less likely to occur when compared to Stokes then the Stokes spectrum is usually used.

Not all molecules are able to be Raman active. Only those that show polarizability within the vibrational motion can be Raman active. The stretching and contraction of the bonds changes the interactions between the electrons and nuclei thereby changing the molecular polarizability. It is the interaction of the polarizability with the incident

light that creates an induced dipole moment in the molecule (change in the rotation of the molecule) and the light emitted by this contains the Raman scattering as on rotating the molecule may lose polarizability and retain some of the energy.

The scattered light can be collected using a spectrometer. The position of the peaks is a function of the frequency change of the molecules, and the intensity of the peaks is proportional to the number of photons at each frequency.

As each molecular species has its own unique set of vibrations, the Raman spectrum is inherently dependent on the architecture of the tissue. Unfortunately most tissues are extremely heterogenous and prior knowledge of the tissue structure is essential for the interpretation of the spectra. In this way Raman spectroscopy can provide qualitative and quantitative information on the tissue in question.

1.2.3. Development of the instrumentation used in Raman spectroscopy.

The principles of the Raman effect and Raman spectroscopy have remained relatively unchanged since its discovery. However there have been a number of technological advances that have enabled its application to medical diagnostics.

For Raman spectroscopy to be of practical use in medical diagnostics, a Raman system must combine a high intensity monochromatic light source, with a high resolution wavelength dispersive element and a highly sensitive detector. This is needed in view of Raman scattering being a small proportion of the light scattered as was discussed above.

The initial breakthrough came when in 1960 Maiman invented an amplified light source that was monochromatic. This was to become known as a LASER (light amplification by stimulated emission of radiation). A LASER is not only monochromatic i.e. it had the same wavelength but it was also coherent therefore the light travelled in the same direction enabling focusing.

The first lasers used as the excitation source however were visible. These unfortunately caused a lot of fluorescence when used on biological tissues. The fluorescence had the effect of drowning out the Raman signal so that it could not be seen. Therefore initial studies had to be confined to biological tissues that had minimal fluorescence such as the lens of the eye [Yu 1975] and gallstones [Ishida 1987].

Then came the development of filters. These filtered out the laser wavelength prior to detection, therefore enabling the use of single grating systems. Previously it was necessary to use triple grating systems to remove the entire laser light, however, this also reduced the amount of Raman scattering light that reached the detector. Improved grating technology has improved things further. Gratings work like a prism and disperse the light so that it can be measured by the detector. We use a holographic grating with 300 lines per millimetre.

The development of NIR (near infrared) lasers enabled its use to advance Raman spectroscopy in biological tissues. The advantage of infrared light (800nm) over visible light (300nm) is that it has a longer wavelength and decreased frequency therefore making it less energetic. In this way fluorophores within the tissue tend not to get excited. It is the fluorophores that are responsible for the fluorescence seen when using the visible light.

Initially the detectors that were used were indium-gallium-arsenide (InGaAs) detectors. These detectors were able to pick up the Raman signal and were sensitive to the infrared region of the spectra, however due to the low energy of the infrared excitation light, the detectors required long acquisition times to be able to obtain a spectrum. These acquisition times were up to several hours long therefore making the possibility of in vivo acquisition not applicable [Alfano 1991, Wang 1993]. With the advent of charged coupled device (CCD) detectors acquisition times have been reduced to practical levels [Baraga 1992]. The other advantage of these detectors is that they are array detectors and therefore can measure more than one wavelength. In this way it can measure more of the spectrum at one time. This NIR excitation light source produces a stronger Raman signal in biological tissues than the infrared region, but still has little in the way of fluorescence when compared to visible light [Manoharan 1994].

Not only were the acquisition times improved by the use of CCD detectors but also by the advent of holographic notch filters. Initially a triple monochromator was used to remove the Rayleigh scattering but this tended to remove 95% of the light and therefore longer acquisition times were needed to obtain a good Raman signal. In using a holographic notch filter, a single monochromator can be used and therefore less light is lost. This allows a higher throughput of light and Raman signal therefore enabling acquisition times to be reduced.

1.3. Kerr gated Raman spectroscopy.

Raman spectroscopy is thought to have the potential for minimally invasive detection of malignancies and pre-malignancies within the bladder and the prostate gland. A potential problem with this is the inability to obtain spectra from beneath the surface. This is needed to ascertain whether there has been any local extension of the disease in the case of the bladder, or to find a focus of adenocarcinoma in an otherwise benign prostate gland.

A possible way to overcome this is by temporal gating techniques such as picosecond Kerr gating. The Kerr gating technique uses excitation with a picosecond pulsed laser in combination with a fast temporal gating of instantaneous Raman scattered light. The scattered light is collected at various time delays following the laser pulse.

The ability of depth probing using Raman was determined by two stages:

1. The laser photons have to be able to migrate to a given depth within the tissue.
2. The Raman photons that have been produced have to migrate back to the surface.

In this way Raman spectra from differing depths within the tissue will emerge at different times thereby making their separation feasible [Matousek 2005].

There have been studies utilising the Kerr gating technique to improve upon Raman spectra obtained from bone interiors [Morris 2004] as well as test experiments demonstrating the depth resolving power of the Raman Kerr gating concept on artificially prepared samples [Matousek 2005].

In an attempt to further our understanding of the heterogeneity of tissue structure the basic cell morphology will be discussed, using an epithelial cell as an example. The two tissues that make up the majority of the urologists workload – the prostate gland and the urinary bladder will then be looked at and finally the anatomy and histology of the normal prostate gland and urinary bladder as well as the main pathologies within these tissues will be discussed.

In this way the information within the Raman spectra from each of the pathologies studied will be interpreted with greater accuracy.

Other spectroscopic techniques used for tissue analysis and diagnostics will be discussed in chapter 4.

1.4. Cell morphology.

The cell is the basic, living, structural and functional unit in the body, and it is at the cellular level that disease processes originate. It is here that activities essential to life occur as well as changes determining the cell structure.

There are well over 200 different types of cell identified within the body thus far, yet despite this they possess many common features (Fig 1.3). There are three main components to the cell – the plasma membrane, the cytosol and the organelles. Inclusions are also a component of cells but they tend to be temporary. They consist of lysosomes and peroxisomes, these act to store and secrete the products of the cell, and are metabolically inactive.

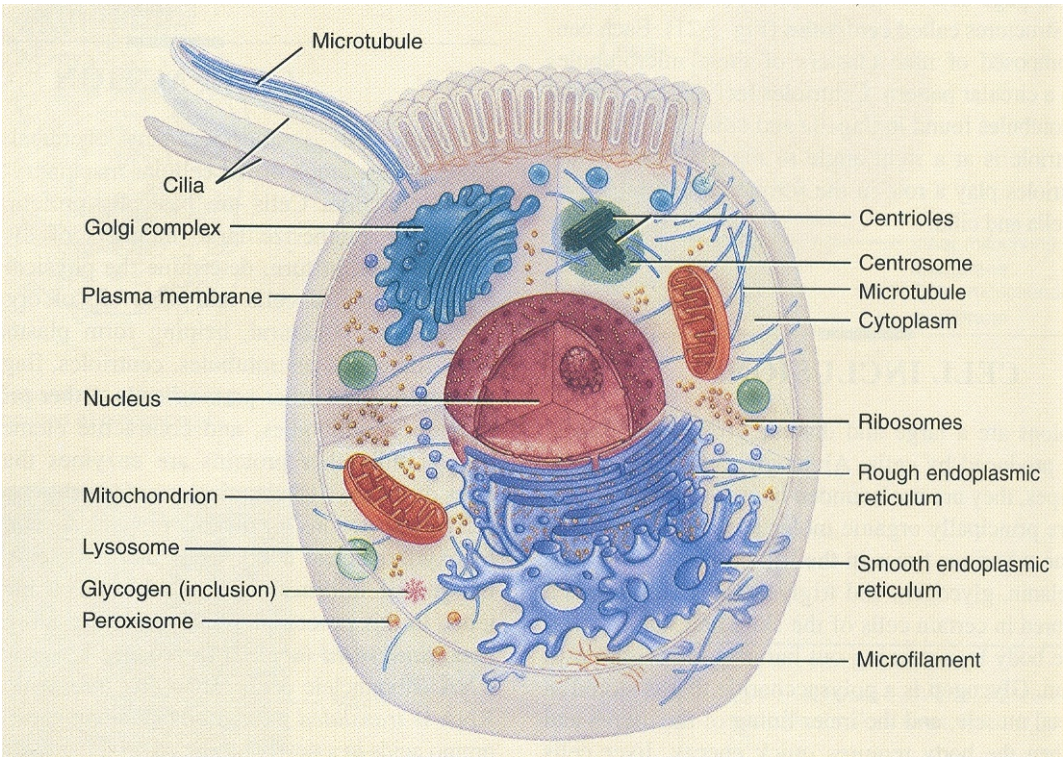

Fig 1.3: The sectional view of a generalised animal cell.

Reproduced from Principles of Anatomy and Physiology, 8th edition [Tortora 1996].

The first of the three main components of the cell to be considered is the plasma membrane (Fig 1.4). This is a thin membrane approximately 8.5-10 nm thick that surrounds the cell separating it from the extracellular material. It functions both as a barrier and a transport medium that regulates the passage of substances in and out of the cell. The plasma membrane is composed of a phospholipid bilayer, with integral and peripheral proteins embedded in it. The membrane forms a bilayer as the phospholipids are amphipathic – they have a hydrophilic phosphate head and a hydrophobic fatty acid tail.

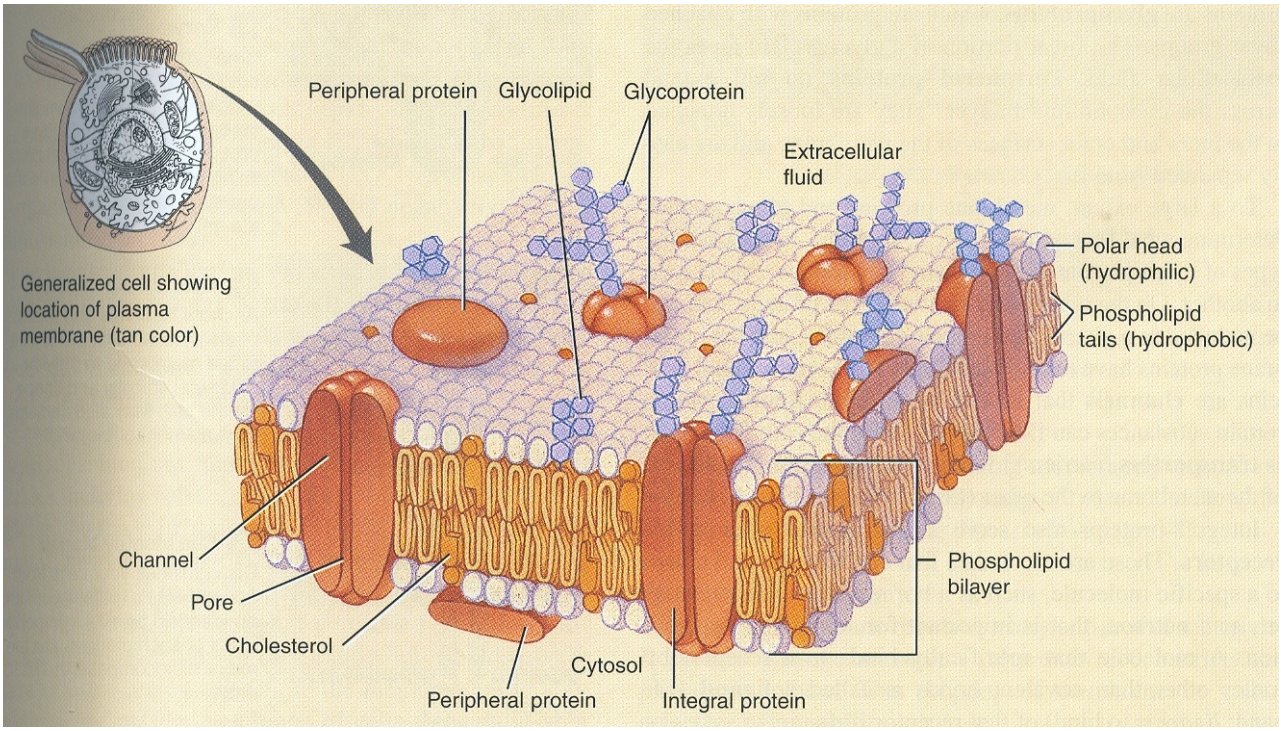

Fig 1.4: The sectional view of a plasma membrane.

Reproduced from Principles of Anatomy and Physiology, 8th edition [Tortora 1996].

The next major component of the cell is the cytosol. This is the intracellular fluid in which organelles and inclusions are suspended, and solutes are dissolved. It is a transparent, viscous, gel-like fluid that consists of 75 – 90% water [Tortora 1996]. It is within this fluid that complex metabolic reactions occur, by receiving raw materials from the extracellular fluid.

The cytosol contains a series of microtubules, microfilaments and intermediate filaments known as the cytoskeleton. Microfilaments and microtubules consist of the proteins, actin and tubulin respectively. The cytoskeleton functions to hold the cellular shape, as well as to carry out co-ordinated cellular movements. It aids phagocytosis and the movement of organelles and chemicals within the cell itself.

The last major component of cells is made up of organelles. Organelles are small compartments in which highly specialised reactions can occur. Different cells will have differing numbers and types of organelles present within them depending on their function. The organelles are as follows; the nucleus, ribosomes, endoplasmic reticulum, golgi complex, and mitochondria.

The largest organelle is the nucleus (Fig 1.5). This is spherical in shape, and is surrounded by the nuclear envelope – a phospholipid bilayer such as the plasma membrane. It contains the chromosomes where most of the genetic material is found. This genetic material controls cell structure as well as many of the cellular activities within the cell. These are made up of deoxyribonucleic acid (DNA), and histones. The nucleus also contains nucleoli, which are clusters of DNA, ribonucleic acid (RNA) and protein. Nucleoli are the sites at which ribosomes are synthesised.

Ribosomes are small granules that contain ribosomal RNA (rRNA), and ribosomal proteins. They are primarily involved in the synthesis of proteins. These proteins can be used within the cell or be destined for export out of the cell.

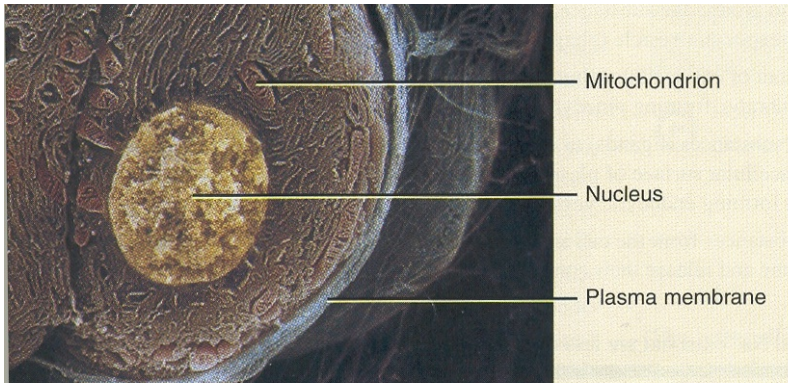

Fig 1.5: Scanning electron micrograph of a nucleus (7800x).

Reproduced from Principles of Anatomy and Physiology, 8th edition [Tortora 1996].

Endoplasmic reticulum is continuous with the nuclear envelope, being made up of a number of cisterns, (membrane – enclosed channels). There are two main types – smooth and rough, or agranular and granular. The smooth or agranular endoplasmic reticulum has no ribosomes on it and is the site of steroid, fatty acid and phospholipid synthesis. Rough or granular endoplasmic reticulum is studded with ribosomes and is the site of protein synthesis (Fig 1.6). It also acts as a temporary storage area for the newly synthesised molecules.

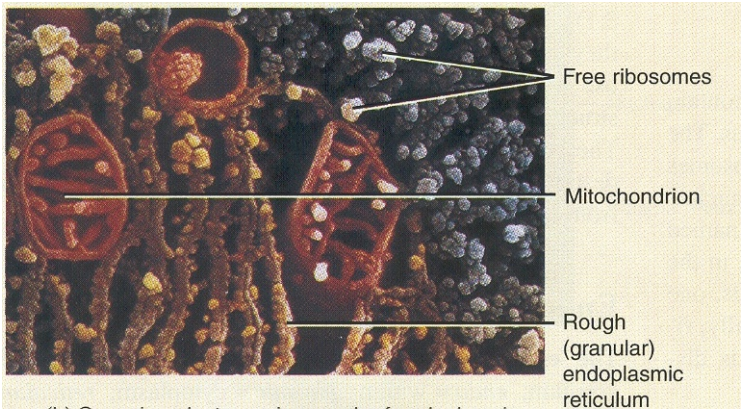

Fig 1.6: Scanning electron micrograph of endoplasmic reticulum, ribosomes and mitochondria (60,000x).
Reproduced from Principles of Anatomy and Physiology, 8th edition [Tortora 1996].

The golgi complex also consists of cisternae, and functions to package up the products of the cell and delivers them to the cell membrane (Fig 1.7).

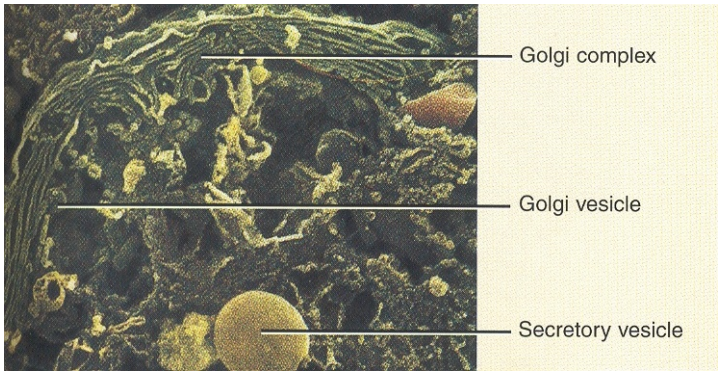

Fig 1.7: Scanning electron micrograph of a Golgi complex (20,000x).

Reproduced from Principles of Anatomy and Physiology, 8th edition [Tortora 1996].

The mitochondria are the main sites for the generation of adenosine tri-phosphate (ATP), via oxidative phosphorylation (Fig 1.6). ATP is needed for all chemical reactions to occur, therefore an active cell will have a large number of mitochondria with a high rate of ATP production. Mitochondria also have the ability to self- replicate in response to an increase in ATP demand, if the cell divides or becomes more active.

As you can appreciate from the above, the cell is very complex, with many constituents. Each of these will potentially be able to give Raman peaks on a spectrum, of which some will be stronger than others.

1.5. The Prostate Gland.

Recently the prostate gland has been mentioned a lot in the media. This is because the vast majority of men will suffer with symptoms related to disease of the prostate gland at some point in their lives.

The main concern however is of prostate cancer. As many as 40% of men aged between 60 and 70 years, have microscopic foci of well differentiated adenocarcinoma of the prostate gland (CaP). 27,000 men were diagnosed in the year 2000 in England and Wales with prostate cancer [Cancer research UK 2004]. It is the second leading cause of cancer related death in men in Western Europe and North America [Kurth 1998, Cancer research UK 2004], and the leading cause of cancer related death in the United States [Tortora 1996]. It is also a major cause of morbidity and health care related costs. 3-5% of men will die of CaP and 10% of men diagnosed with CaP will develop clinical disease [Kurth 1998]. The diagnosis of CaP is dependent on an abnormal digital rectal examination (DRE), and / or a raised level of serum prostate specific antigen (PSA). A finding of either of these in men will lead onto transrectal ultrasonography (TRUS), and biopsy (Fig 1.8). The biopsies tend to be sextant sampling with targeting if a lesion is suspected on TRUS. Unfortunately the biopsies have a high number of false negatives, and therefore a cancer can remain undiagnosed. These false negative results are mainly due to sampling error (in that the CaP may be present as a small focus within the prostate gland and the biopsy may have missed this) [Kurth 2000]. It has been shown that even if a man has two sets of negative biopsies with a persistently raised PSA, he has a 10% risk of having a cancer found on the third biopsy [Kurth 2000].

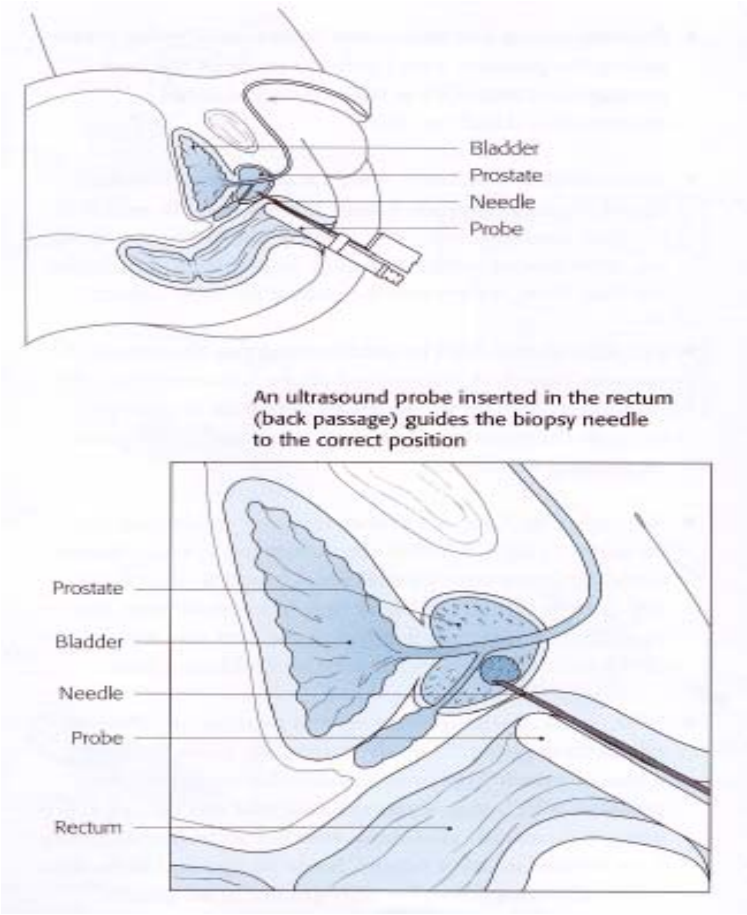

Fig 1.8: Transrectal ultrasound scan and biopsy. Reproduced with the kind permission of Health Press.

Also the biopsies are reviewed by the histo-pathologists (Fig 1.9). The samples are very small and the process is subjective, an error can occur in the diagnosing, as well as the grading of CaP. The sensitivity of TRUS for prostate cancer varies from 33 –83%, and the specificity varies from 97-100%. [Campbell 2002]

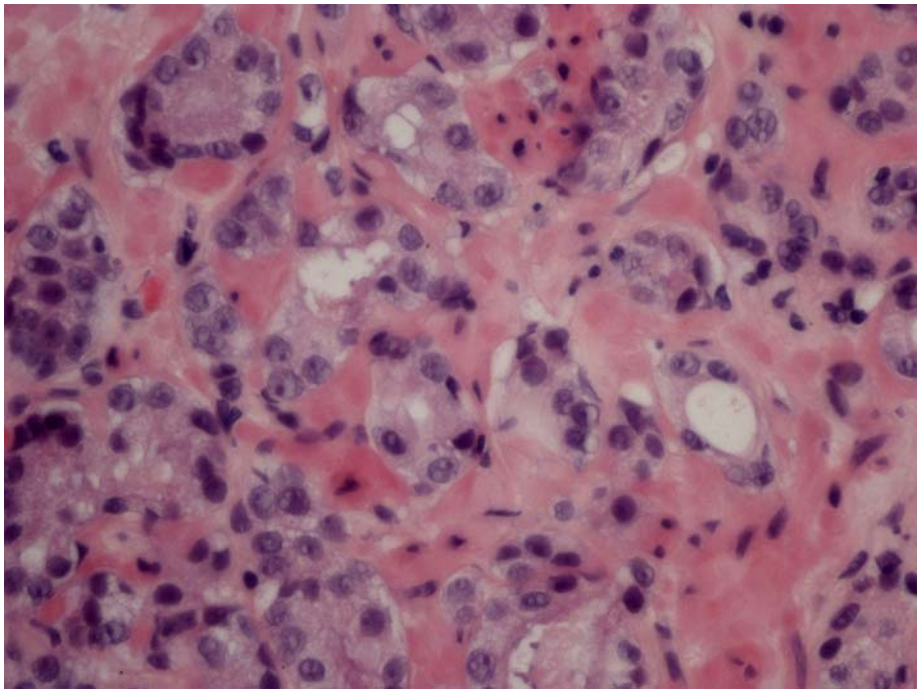

Fig 1.9: A needle biopsy showing CaP prepared at the Gloucestershire Royal hospital.

The ideal would be to diagnose CaP with a PSA in the range of 2.5-10 ng/ml, as this would increase the chances of cure with radical treatment. The reality, given the low specificity of both the PSA, and the TRUS and biopsy, is that many of the cancers are diagnosed when a cure is not possible.

The prostate gland and its pathologies will be discussed in more depth in chapter 2.

1.6. The Urinary Bladder.

There has been a lot of research work done on the bladder in the past, with the aim to provide a specific and sensitive means of distinguishing between the pathologies associated with the bladder. The most important pathology is as expected cancer.

The incidence of bladder cancer in the UK is 8% in men and 3% in women. It is the fourth most common cancer in men and the eighth in women. Each year there are 9000 cases diagnosed in men and 3600 diagnosed in women in the UK but although the figures are high there has been a reduction in the age standardised incidence since the 1980's. It is thought that the reason for this is the reduction in smoking and the banning of aromatic amines in the 1980's. Both of these are known risk factors for the development of bladder cancer [Meyer 2003].

Ninety percent of bladder cancers are transitional cell carcinomas of the bladder, and the majority of these are superficial. They tend to be found in the over 65 year olds.

The standard method for the diagnosis of bladder cancer is by means of a cystoscopy and biopsy, which ordinarily involves a general anaesthetic. Once diagnosed patients are staged by means of the TNM (tumour-nodes-metastases), classification and entered into a surveillance scheme, if no further treatment is required. The surveillance program involves 6 monthly – yearly cystoscopies for at least 10 years.

The gold standard, non-invasive test is urine cytology. This is stained with a Papanicolaou stain and has 95% specificity. However the test is only 40 – 60% sensitive (the sensitivity increases with the grade of the tumour). This is because of the significant inter and intra-observer variability, as well as the fact that urine cytology is altered by UTI, bladder instrumentation, indwelling catheters, radiotherapy and intravesical chemotherapy.

Unfortunately some of the bladder tumours, especially carcinoma *in situ* and flat superficial tumours can look just like cystitis, or normal bladder. In view of this a test that has a greater sensitivity and specificity than urine cytology is urgently needed, so that patients won't have to undergo unnecessary anaesthetic procedures.

The bladder and its pathologies will be discussed in more depth in chapter 3.

2. The Prostate Gland.

2.1. Anatomy of the Prostate Gland.

The prostate gland is a chestnut shaped gland approximately 4 cm in diameter. It lies within the true pelvis, between the bladder neck and the urogenital diaphragm, it surrounds the bladder neck and the proximal urethra in the male (Fig 2.1). It is anterior to the rectum and posterior to the inferior aspect of the symphysis pubis [Young 1998]. The prostate gland weighs approximately 20g but increases in size and weight with age [Berry 1984].

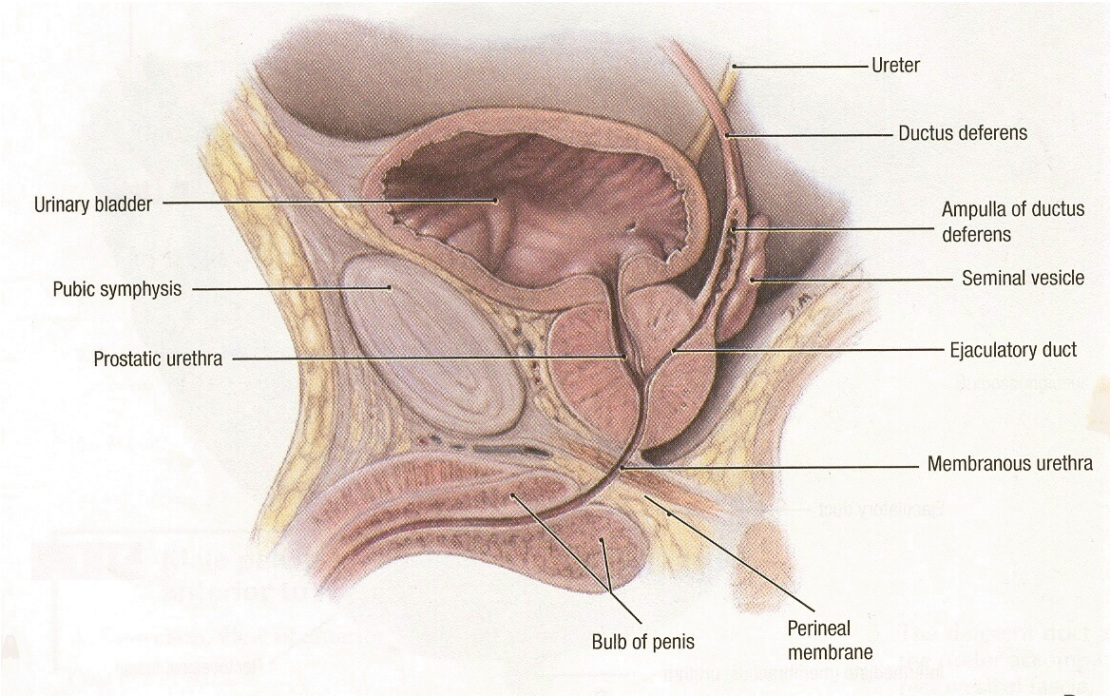

Fig 2.1: Anatomy of the male lower urinary tract.

Reproduced from Grant's Atlas of Anatomy, 10th edition [Agur 1999].

It is separated into lobes by the urethra and the ejaculatory ducts. There are five in total, two lateral lobes – these are palpable on DRE and are marked by a midline groove posteriorly, a middle lobe – this lies between the urethra and the ejaculatory ducts, an anterior lobe – this is enclosed by the urethra, and a posterior lobe – this lies behind the ejaculatory ducts. Tisell and Salander have postulated that there are actually six lobes, two each of the lateral, dorsal and median lobes [Young 1998]. In practice however, this has little application to prostatic pathology. Mc Neal's model has now replaced the concept of lobes with that of zones, and this is more widely used [Mc Neal 1988]. The prostate is divided into three zones, the transition zone- this accounts for 5% of the prostatic volume and is located around the proximal urethra as two lateral lobes, the central zone- this accounts for 25% of the prostatic volume and is located around the ejaculatory ducts from apex to prostatic base, and the peripheral zone- this accounts for 70% of the prostatic volume and is located around the other zones and the distal urethra.

The prostate gland is said to have a capsule, however this is not a true capsule but a condensation of fibromuscular stroma. It covers the majority of the prostate gland, but not at the bladder neck, here the prostatic stroma blends into the smooth muscle of the bladder neck.

The prostate gland receives its blood supply from the internal iliac artery via the inferior vesical and middle rectal branches. The prostatic veins drain into the prostatic plexus that surrounds the gland and then drains into the internal iliac veins. There is an extensive venous network in both the capsule and peri-capsular connective tissue of the prostate. The lymphatic drainage of the prostate gland is to the internal iliac nodes

mainly, via intra and peri-prostatic lymphatics. Some however do drain directly into the external iliac and sacral lymph nodes. The prostate gland has a rich nerve supply located in the neurovascular bundles that are situated on the supero-lateral borders of the prostate [Young 1998].

2.2. Histo-pathology of the Prostate Gland.

The prostate gland consists of both stromal and glandular elements as shown in Fig 2.2. It is surrounded by a fibro-elastic capsule, (a pseudocapsule), that is made up of numerous smooth muscle fibres. This capsule extends fibres into the stroma of the prostate gland, in doing so the gland is separated into approximately 50 poorly defined lobules. The glandular tissue has three groups of glands that are arranged around the urethra. These are compound tubulo-acinar glands, and they drain into either the distal urethra via long ducts (main glands), into the urethral sinuses via short ducts (submucosal glands), or directly into the urethra (mucosal / peri-urethral glands). The ducts are lined with transitional epithelium near their entry points into the urethra. The glandular epithelium has a pseudostratified columnar form, with the majority of cells being either tall cuboidal or columnar. Their nuclei are uniform and located basally, they also have abundant apical cytoplasm that tends to be pale and granular, rarely being vacuolar. The cell type depends on the degree of activity of the prostate gland and the androgenic stimulation to the prostate. The epithelial cells produce the prostatic secretions.

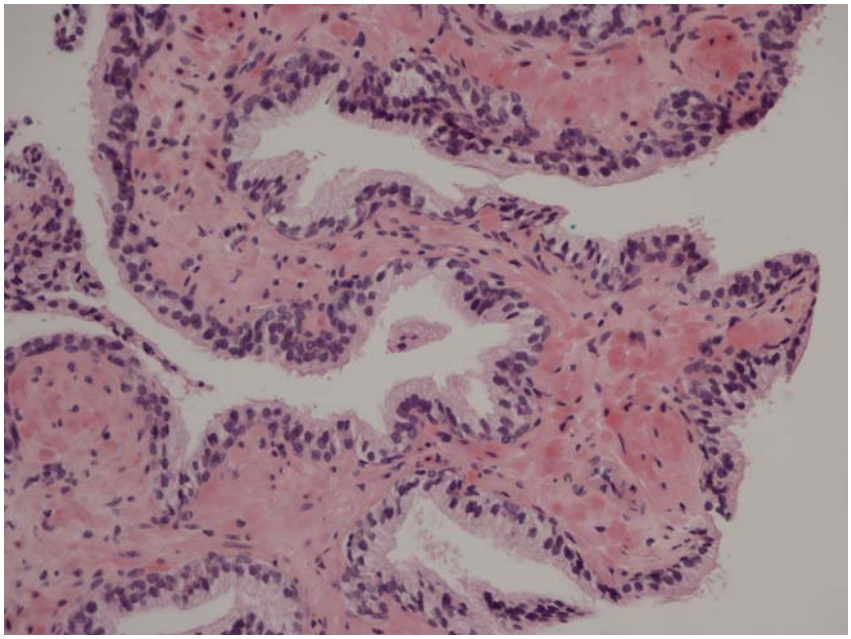

Fig 2.2: Histology of the normal prostate gland. Prostatic acini are interspersed between striated muscle prepared at Gloucestershire Royal Hospital.

There is zonal variation to the normal histology of the prostate gland. The transitional and peripheral zones both contain glands that have simple, rounded contours, with some gentle undulation of the luminal borders. The central zone however contains glands that are larger and tend to be arranged in lobules around central ducts. Also the epithelial cells of the central zone tend to be more granular than those of the other zones. The stroma in the peripheral zone is randomly arranged with smooth muscle bundles that are loosely woven, whereas that of the transitional zone interlaces with the smooth muscle bundles and is more compact. The central zone however has a less abundant stroma with compact smooth muscle fibres [Young 1998].

2.3. The Function of the Prostate Gland.

The function of the prostate gland is to produce a secretion that mixes with the semen and contributes approximately 25% of the volume of semen. The secretion consists of a mildly acidic fluid with a pH of approximately 6.5. This fluid contains zinc, citrate (which provides ATP to the sperm), acid phosphatase, PSA, prostate binding protein, hormones, growth factors, pepsinogen, fibrinolysin (liquefies coagulated semen after deposition in the female genital tract) [Burkitt 1993], lysozyme, amylase, and hyaluronidase [Zaneveld 1981, Tortora 1996]. The function of the secretion is therefore to contribute to the motility and viability of the sperm, as well as provide a medium for the transport of sperm [Tortora 1996, Foley 2002]. The prostatic fluid also acts to affect the female reproductive tract and prevent the activation of the female immune response to the foreign sperm antigens [Foley 2002].

2.4. PSA (Prostate specific antigen).

PSA is a component of the prostatic secretion (seminal fluid) that is present in high concentrations. It is produced by epithelial cells lining the prostatic ducts and acini and secreted directly into the lumen of the prostatic ducts [Eble 2004, Goldfarb 1986]. It has a half-life of 2.2-3.2 days. PSA is a protein that is responsible for the liquefaction of seminal fluid, and is not produced until puberty [Goldfarb 1986]. It is also present in the serum of male patients in much lower concentrations, and this concentration is dependent on age, race and prostate volume. In some diseases of the prostate gland, the

concentration of PSA within the serum can be markedly raised. CaP is one of these diseases and in view of this, it is utilised as a serum marker for both detecting CaP and monitoring CaP. The problem with using PSA as a marker for CaP is that although it is highly sensitive, it is not very specific. Therefore many men undergo unnecessary invasive procedures to rule out CaP.

A number of studies have shown that measuring the ratio of free to total PSA in the serum can reduce the number of unnecessary biopsies, as there is a difference between the ratio in patients with CaP as compared to those with Benign prostatic hyperplasia (BPH) [Eble 2004, Catalona 1998]. The ratio < 15% is suggestive of cancer, >25% is suggestive of BPH, and 15-25 is unknown [Campbell 2002]. This can be utilised as the majority of serum PSA is bound to antiproteases, but up to a third may be present as free PSA [Stenman 1991]. It is felt that the level is useful in patients with a PSA of between 4 and 10ng/ml [Campbell 2002].

Prostate density is the serum PSA level divided by the volume of the prostate gland. Therefore by measuring prostate density with the aid of TRUS, you can distinguish between the prostate gland with a raised PSA secondary to CaP, and that due to BPH. A PSA density of >0.15 has been proposed as a cut off threshold for undertaking biopsies [Campbell 2002].

Another means of avoiding unnecessary invasive procedures is to look at the PSA velocity. This is the rate of change of serum PSA over a period of time. Those patients

with CaP will have a higher PSA velocity than those with normal prostate glands or BPH. There have been studies suggesting that the PSA velocity improves the pickup of men with CaP and borderline PSA levels, but this does result in multiple serum PSA measurements over a minimum of 18 months [Smith 1994]. It is felt that a rise of >0.75ng/ml in a year is a cause for concern for prostate cancer [Campbell 2002].

The other diseases in which the serum PSA can be raised are: BPH, prostatitis, acute urinary retention (AUR), and urinary tract infection (UTI). The PSA will also be raised with recent urethral instrumentation, catheterisation, prostatic biopsy and DRE. The PSA level in the serum can also be affected by certain operations as well as by medications the patient is taking. The operations are transurethral resection of prostate (TURP), radical prostatectomy, radiotherapy to the prostate gland and orchidectomy. The medications are Finasteride and gonadatrophin releasing hormone agonists. Finasteride has been shown to reduce the group mean PSA levels by approximately 50% however individual serum PSA responses are highly variable. As serum PSA is used in the detection of CaP it is suggested that a baseline PSA level is taken prior to commencing patients on Finasteride [Campbell 2002].

2.5. Diseases of the Prostate Gland.

2.5.1. Benign prostatic hyperplasia.

Benign prostatic hyperplasia (BPH), is a very common disease of the prostate gland. It is present in approximately 20% of males by the age of 40 years [Kumar 1997] and approximately 70% of men aged 70 – 80 years are affected by BPH and suffer with variable symptoms [Underwood 1996]. BPH is however very rare under the age of 30 years [Berry 1984].

Garraway (1991) has shown with prevalence studies in one community of men aged between 40 and 79 years that 'the prevalence rate of BPH, defined as enlargement of the prostate gland of equivalent weight greater than 20 g in the presence of symptoms of urinary dysfunction and/or a urinary peak flow rate less than 15 ml/s and without evidence of malignancy, was 253 (95% CI 221-285) per 1000 men in the community, rising from 138 per 1000 men aged 40-49 years to 430 per 1000 men aged 60-69 years'. There are racial differences as well in the prevalence of BPH in that it is low in Orientals in China, Hong Kong and Japan [World Health Organisation 1985], and also low in some African countries such as Sudan [Young 1998], but higher in the American black population [Moore 1943].

The aetiology of BPH is thought to be related to an imbalance in the hormones, but the exact mechanism is uncertain. It is thought that androgens and oestrogens play a synergistic role in its development. It is known that BPH will not develop in males castrated prior to puberty, and therefore an intact testis is necessary for its development

[Kumar 1997]. Oestrogen increases the expression of dihydroxytestosterone (DHT), receptors on the parenchymal cells within the prostate gland. Therefore the effects of DHT are enhanced. DHT is an androgen derived from testosterone through the actions of 5 α- reductase, and is the major hormonal stimulus for glandular and stromal proliferation. The oestrogen in males is produced by the peripheral conversion of testosterone and androstenedione [Young 1998].

Morphologically the hyperplastic process involves the lateral lobes and the peri-urethral glands / the transitional zone. Macroscopically, the prostate is enlarged and weights greater than 200g have been reported. The cut surface of the gland shows multiple nodules that are yellow in colour, and cysts that are well circumscribed (Fig 2.3).

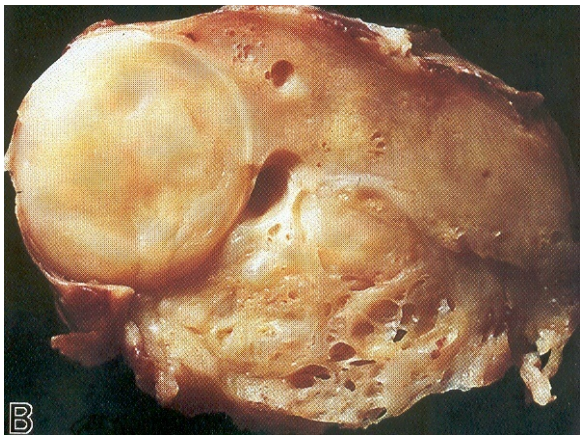

Fig 2.3: The cut section of a prostate gland showing the variable solid and cystic nodules associated with BPH.
Reproduced from the Atlas of Tumor Pathology, Tumours of the Prostate Gland, Seminal Vesicles, Male Urethra, and Penis, 3rd series [Young 1998].

Microscopically, there is hyperplasia of the glandular and / or stromal components of the prostate gland. The hyperplastic glands have a lining of tall epithelial cells that are columnar in nature (Fig 2.4). They resemble the glands of the normal prostate but have little or no secretory activity. There is a peripheral layer of flattened basal cells, and the overcrowding can result in papillary infoldings. Proliferating stromal elements are always present between the glands and differ from that of the normal prostate. The stroma in BPH has more smooth muscle and there is an absence of elastic tissue. Also there are often areas of squamous metaplasia within the prostatic ducts adjacent to areas of necrosis, but BPH is not a pre malignant condition. Corpora amylacea are also present, but less so than in a normal prostate gland. These are deposits of proteinaceous secretory material within the acini that may have phosphates and oxalates deposited around them to form prostatic calculi.

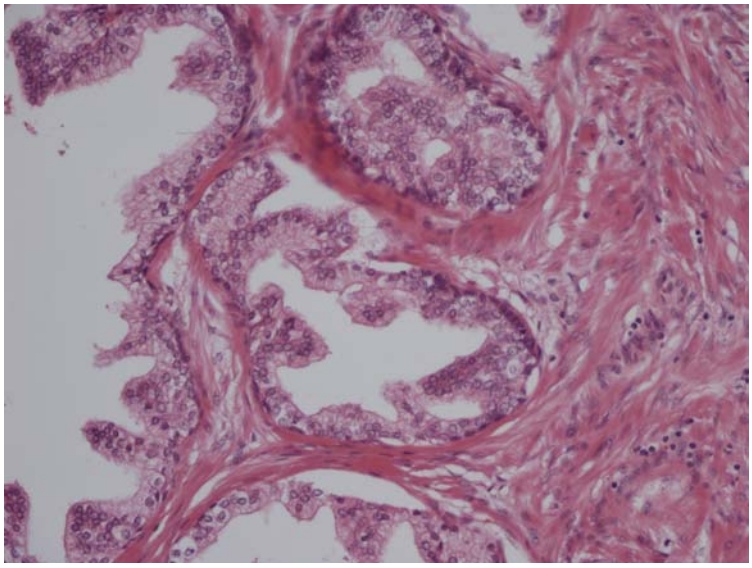

Fig 2.4: A needle biopsy showing the hyperplastic glands of varying size and shape, associated with BPH prepared at Gloucestershire Royal Hospital.

The clinical presentation of BPH varies, and some men although they have the disease will not suffer with any of the symptoms associated with it. As the peri-urethral glands / transitional zone are commonly affected then the presentation tends to be of lower urinary tract obstruction. The symptoms associated with this consist of hesitancy, poor / reduced urinary flow, post micturition dribbling (PMD), nocturia, and haematuria may occur. In severe cases there is incomplete emptying of the bladder that leads to stagnant residual urine. This predisposes the patient to cystitis and UTI's. In longstanding BPH this results in bladder dilatation, hypertrophy and trabeculation, with the potential for further complications with hydroureter, hydronephrosis and pylenephritis [Young 1998].

The signs tend to be of an enlarged prostate gland on DRE that is firm but rubbery to touch. Patients may suffer with chronic urinary retention (CUR), which is painless, or go into acute urinary retention (AUR), which is painful.

Treatment of BPH can be either medical or surgical. Medical treatment is by means of α- blockers- these act to relax the prostate gland and therefore open up the urethra, relieving the obstruction. They do this by specifically blocking the smooth muscle $\alpha 1$-adrenoceptors of the prostate and bladder. 5 α- reductase inhibitors can also be used - these down regulate the DHT receptors and help halt the hyperplasia and shrink the prostate gland to an extent (approximately 18%). The 5 α- reductase inhibitors block the enzyme that converts testosterone to the more active DHT. Surgical treatment is either by ablation or enucleation of the prostate gland or by open or endoscopic methods. These all act to open up the urethra by making a channel through the prostate gland.

2.5.2. Prostatitis.

Prostatitis is the inflammation of the prostate gland that can be either acute or chronic in nature. It is rarer than BPH or CaP, but is responsible for more urology clinic visits. It tends to affect younger men between the ages of 25 and 55 years, and can have a significant impact on their quality of life [Foley 2002].

The aetiology of prostatitis can be any cause of an increase in inflammatory cells within the prostatic parenchyma, and depends on the type of prostatitis. There are four main groups for the classification of prostatitis, as are shown below (the National Institutes for Health Classification) [Foley 2002]:

1) Acute bacterial prostatitis
2) Chronic bacterial prostatitis
3) a. Chronic prostatitis / pelvic pain syndrome 'inflammatory'
   b. Chronic prostatitis / pelvic pain syndrome 'non-inflammatory'
4) Asymptomatic inflammatory prostatitis

Each of these has differing aetiologies and prevalence.

Acute bacterial prostatitis is rare and is caused by bacteria, whereby the spread of infection can be via the prostatic ducts secondary to urethritis or cystitis, haematogenous, or via the lymphatics. Typical bacteria include, Escherichia Coli (80%), Proteus spp, Klebsiella spp and Serratia spp.

Chronic bacterial prostatitis accounts for only 5 – 10% of cases of prostatitis, and the aetiology is the same as that for acute bacterial prostatitis. The infection however, is thought to persist due to prostatic calculi, or the bacteria have an exo-polysaccharide coat that is poorly penetrated by either antibiotics or the host's defences.

Chronic non-bacterial prostatitis, 'inflammatory' is the most common form of prostatitis. It is thought to be caused by either, an autoimmune response to host prostatic proteins, or a chemical cell mediated inflammatory immune response to refluxed urine.

Chronic non-bacterial prostatitis, 'non-inflammatory' is a difficult diagnosis to make, and the aetiology is unknown. However there does appear to be a strong psychological factor and videourodynamics suggest a neurological or neuromuscular cause [Foley 2002].

Morphologically the groups differ. The acute prostatitis is microscopically characterised by a neutrophilic infiltrate, congestion and stromal oedema (Fig 2.5). Without treatment the glandular epithelium is destroyed and micro-abscesses are formed. The chronic prostatitis however shows a variable amount of lymphoid infiltrate and glandular injury. There is stromal fibrosis, plasma cell and acinar atrophy. There must be evidence of tissue destruction and proliferation of fibroblasts, along side other inflammatory cells for a diagnosis of chronic prostatitis. The presence or absence of bacteria separates the second and third groups in terms of classification.

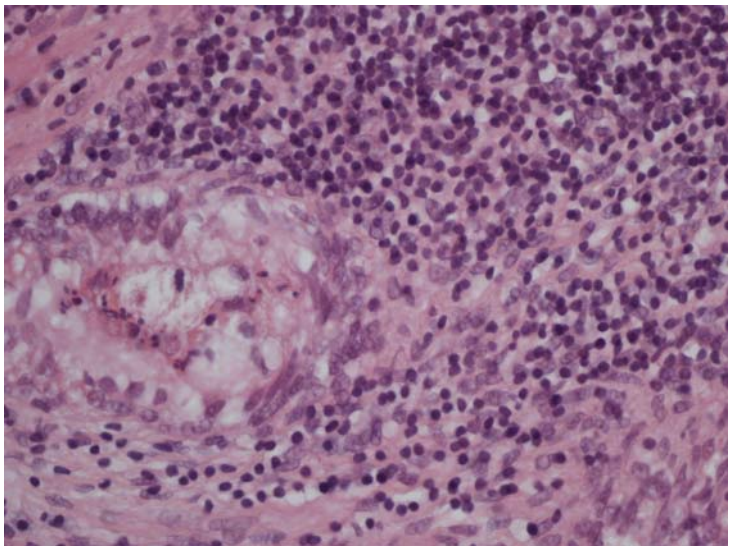

Fig 2.5: A histological section showing the inflammatory atypia and the amphophilia of the cytoplasm in prostatitis prepared at Gloucestershire Royal Hospital.

The clinical presentation of prostatitis can vary, however symptoms include; dysuria, urinary frequency, lower back pain, poorly localised pelvic pain and prostadynia. As well as symptoms of fever and feeling generally unwell. Signs include a tender prostate gland that may be enlarged, and the presence of a urinary tract infection.

Diagnosis is made via clinical examination and the classic Meares and Stamey 4 glass technique. This was first described in 1968 by Meares and Stamey and remains the gold standard test used to distinguish between urethral, prostate and bladder infections in men with chronic prostatitis. It consists of the following 4 samples -

VB1 (voided bladder 1) - the first 10 ml of urine representing the urethral specimen.

VB2 (voided bladder 2) - similar to a midstream urine collection and represents the bladder urine.

EPS (expressed prostatic secretions) – collected directly in a container during prostatic massage.

VB3 (voided bladder 3) - the first 10 ml of urine voided after prostatic massage, includes any EPS trapped in the prostatic urethra.

The three urine specimens are centrifuged for 5 minutes and then the sediment is examined under high power for leukocytes macrophages, oval fat bodies, erythrocytes, bacteria, and fungal hyphae. A wet mount of a drop of EPS is examined under a coverslip in a similar manner. All four specimens are also cultured [Campbell 2002].

Treatment of prostatitis will depend on its cause. Acute bacterial prostatitis is usually easily treatable with a long course of high dose antibiotics, i.e. ciprofloxacin 500mg twice a day for four to six weeks. The other types of prostatitis tend to be refractory to treatment, although antibiotics are tried. Other treatments that can be tried include, allopurinol- thought to lower urinary urate levels therefore reducing inflammation when reflux occurs, repeated prostatic massage or regular ejaculation- thought to encourage emptying of the prostatic ducts therefore reducing congestion, and non-steroidal anti-inflammatory drugs may ease the pain.

For the rest of the thesis the histological diagnosis of acute prostatitis will be referred to as opposed to the clinical diagnosis of prostatitis, as the details of individual patients' symptoms were unknown.

2.5.3. Prostatic intra-epithelial neoplasia.

Prostatic intra-epithelia neoplasia (PIN), can either be low or high grade, with high grade PIN (HGPIN), being thought to be a pre-malignant condition. Figure 2.6 shows the increasing cytological atypia corresponding to the different grade of PIN. It has a high predictive value as a marker for CaP, and in a Norwegian prospective study of HGPIN over 8 years, it was found to have a 38% progression rate to CaP [Harvei 1998]. There is a lot of controversy over the association of PSA and HGPIN, in that some feel that the rise in PSA found with HGPIN is due to the CaP that has not been found yet [Alexander1996] whereas others feel that HGPIN itself will raise the PSA level of a patient [Brawer 1994].

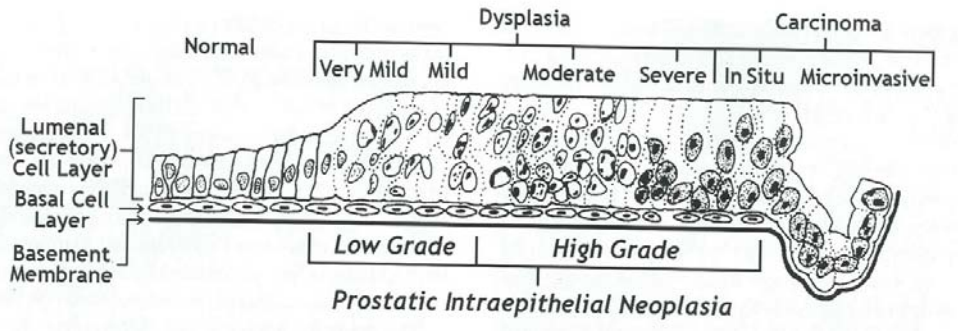

Fig 2.6: A schematic diagram showing the increasing cytological atypia corresponding to the different grades of PIN.
Reproduced from Pathology of the Prostate [Bostwick 1998].

The incidence of high grade PIN, in prostate biopsies has been shown to be between 0.7 and 20%, and it increases with age. It is thought to predate CaP by more than 5 years, thereby reinforcing the idea that it is a pre-malignant condition [Kovi 1988]. HGPIN like CaP tends to be found in the peripheral zone, with only 5 % being seen in the transitional zone [Gaudin 1997].

The morphology of PIN is a continuum between benign and dysplasia. Microscopically HGPIN is a cellular proliferation within medium to large glands, with cytological atypia. It tends to be multifocal and is characterised by large prominent nucleoli that are hyperchromatic. There are an increase number of mitoses and there is a partial loss of the basal layer. There may also be occasional foci of luminal bridging therefore giving it a cribiform appearance. This is one of the four major architectural patterns described. The others are tufted- whereby stratified groups of secretory cells protrude into the lumen of the glands (Fig 2.7), micropapillary- this has slender filiform structures, and flat- this is the least common type that is characterised by an absence of significant stratification [Young 1998, Eble 2004].

The follow up of HGPIN found at prostatic biopsy is controversial, some feel that the biopsy has missed the CaP, whereas others feel that there is a high risk of it progressing over the years into CaP. It has been shown that the mean incidence of CaP on re-biopsy following a diagnosis of HGPIN is 30% whereas that following a diagnosis of BPH or low grade PIN is 20% [Eble 2004].

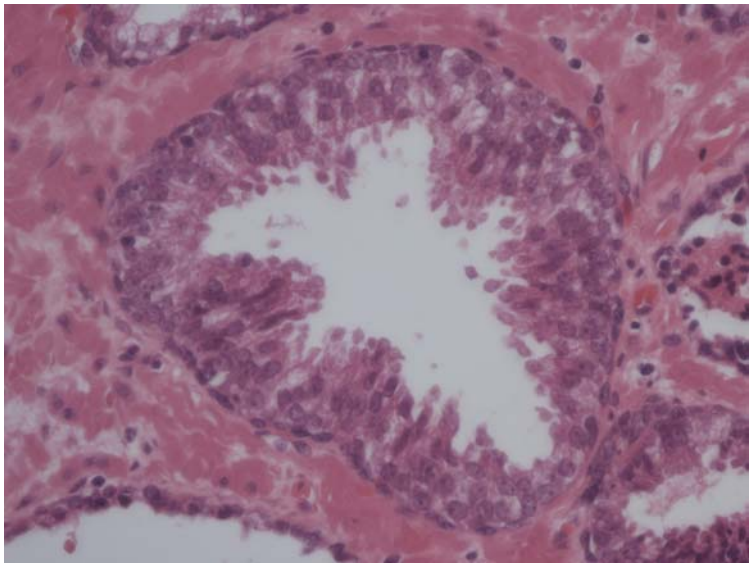

Fig 2.7: A needle biopsy showing the tufted and micropapillary patterns of HGPIN prepared at Gloucestershire Royal Hospital.

Bostwick et al (1992) suggested biannual prostatic biopsies should be taken until the CaP was found. The consensus tends to be of close follow up with PSA testing and DRE biannually, and if there is a significant rise in the PSA or the DRE is suspicious then a repeat biopsy should be recommended. Although many urologists tend to re-biopsy at between 0 – 6 months irrespective of PSA or DRE [Eble 2004].

2.5.4. Adenocarcinoma of the Prostate gland.

Adenocarcinoma of the prostate gland (CaP), is the most frequently diagnosed non-cutaneous cancer affecting Western men, and is the second most common cause of cancer related death in Western men [Foley 2002, Kurth 1998]. It represents 95% of the cancers affecting the prostate gland, with the other 5% being made up of the following;

transitional cell carcinoma, neuroendocrine carcinoma, sarcoma and lymphoma [Foley 2002].

The incidence of CaP increases with age, and as the life expectancy of the population increases so does the prevalence of CaP. In the year 2000, 27,149 men in the UK were newly diagnosed with CaP and in the year 2002 there were 9,937 deaths in the UK from CaP. The 1997 the incidence rate for England and Wales was shown to be 34 per 100,000 population and the crude rate in the UK in 2000 was 95.3 per 100,000 population [Cancer research UK 2004].

However a diagnosis of CaP is not the death sentence, as the following Figures that were illustrated in Mims [Foley 2002] suggest:

> There is a 30% lifetime risk of microscopic prostate cancer in a Western male.
>
> There is a 10% lifetime risk of clinical disease.
>
> There is a 3% lifetime risk of death from CaP.

There is a marked difference between the incidence of CaP at autopsy as compared to the clinical manifestation of the disease [Sheldon 1980]. The prevalence of CaP at autopsy can be as high as 80% in the over 90 year olds [Bostwick 1992]. Many authors feel that these latent tumours are actually ones that behave in a benign fashion and therefore don't manifest themselves clinically [Dhom 1983, Flanders 1984, Franks 1956]. With the advent of PSA and TRUS and biopsy we are picking up more cases of CaP, some of which may never have manifested themselves clinically.

There is a lot of geographical variation in both the incidence rates and the mortality rates of CaP. For example China has the lowest mortality rates at 1 per 100.000

population, when compared to other parts of the world, and Switzerland has one of the highest at 25 per 100.000 population, whereas the USA has the highest incident rate at 104 per 100,000 population. This is thought to be secondary to screening [Boring 1992, Eble 2004, Cancer research UK 2004].

There is variation within the UK, with the 2000 crude rates of new cases being highest in Wales at 114.5 (86.5) per 100,000 population and lowest in Northern Ireland at 66 (67.5) per 100,000 population, (the Figures in brackets are for the European age standardised new case rate) [Cancer research UK 2004]. There has even been shown to be variation within England, with the 1997 incidence rates being higher in the South of England as compared to the North [Crow 2004].

The aetiology of CaP is unknown, but it is thought to be secondary to the hormonal changes that occur with advancing age. There is a decrease in the androgen levels due to the involution of the peripheral zone where the majority of tumours arise [Underwood 1996]. To verify this, it is well known that an orchidectomy can inhibit the growth of many tumours, as can the administration of oestrogens. Also patients who were castrated prior to puberty do not develop prostate cancer. There is thought to be genetic and racial influences as well, in that there is a well documented familial association, with 10% of CaP having a familial component, and by having a first degree relative with the disease you have a 2-3 fold increase in risk. If the relative is young this further increases the risk of developing CaP, with an estimated 45% of cases under the age of 55 years having a predisposing gene responsible [Cancer research UK 2004]. There are also significant geographical differences in the incidence of CaP suggesting that risk is

affected by ethnicity [Kumar 1997, Young 1998, Foley 2002, Cancer research UK 2004].

Other factors that have been related to CaP in some studies are a high fat diet, vitamin A and D deficiency, although data from the European prospective investigation into cancer and nutrition showed no association [Cancer research UK 2004]. Exposure to chemicals in the rubber, textile, fertilizer and atomic energy industries have also been implicated in certain studies [Young 1998].

As was previously discussed HGPIN and CaP are thought to be associated. It is present in biopsy samples near CaP, and is thought to be a pre-malignant condition, with a high predictive value as a marker [Mc Neal 1986]. A diagnosis of HGPIN should therefore alert you to the possibility of either a missed tumour, or the potential for its progression to CaP.

Macroscopically the tumours tend to be firm with a yellow or yellowy – orange colouration and also show mutifocality in approximately 85% of tumours (Fig 2.8) [Eble 2004]. Approximately 50% of radical prostatectomy specimens were found to have multifocal CaP, although a lot of these were very small [Eble 2004, Young 1998]. They tend to arise more predominantly in the peripheral zone (75%) (Fig 2.9), with approximately 15% originating in the transitional zone and 10% in the central zone [Mc Neal 1968, 1969, Eble 2004].

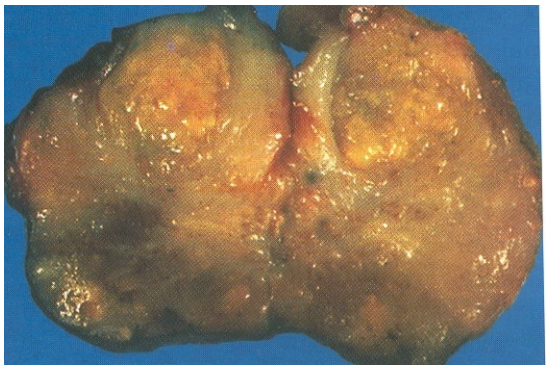

Fig 2.8: A cut section of the prostate gland showing multiple tan- yellow nodules of CaP. Reproduced from the Atlas of Tumor Pathology, Tumours of the Prostate Gland, Seminal Vesicles, Male Urethra, and Penis, 3rd series [Young 1998].

Microscopically they are, as the name implies, adenocarcinomas with a varying degree of differentiation. Those tumours that are well differentiated show a glandular arrangement that infiltrates the adjacent stroma. The glands are not encircled by collagen or stromal cells but lie next to each other. The glands are lined with a single layer of cuboidal cells, which have irregular nucleoli with a high nuclear to cytoplasm ratio. There is no basal layer seen and the glandular cells have varying degrees of anaplasia. As differentiation progresses the cells resemble their original structure less and less. Although many histological grading systems have been proposed, the one widely used by pathologists is the Gleason grading system [Eble 2004, Cancer research UK 2004, Kumar 1997].

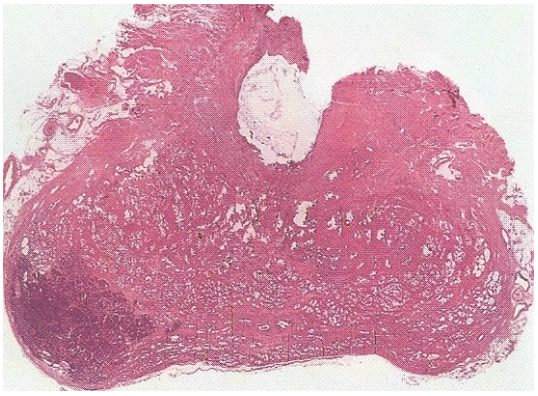

Fig 2.9: A whole mount section of the prostate gland showing a carcinoma in the left peripheral zone.

Reproduced from the Atlas of Tumor Pathology, Tumours of the Prostate Gland, Seminal Vesicles, Male Urethra, and Penis, 3rd series [Young 1998].

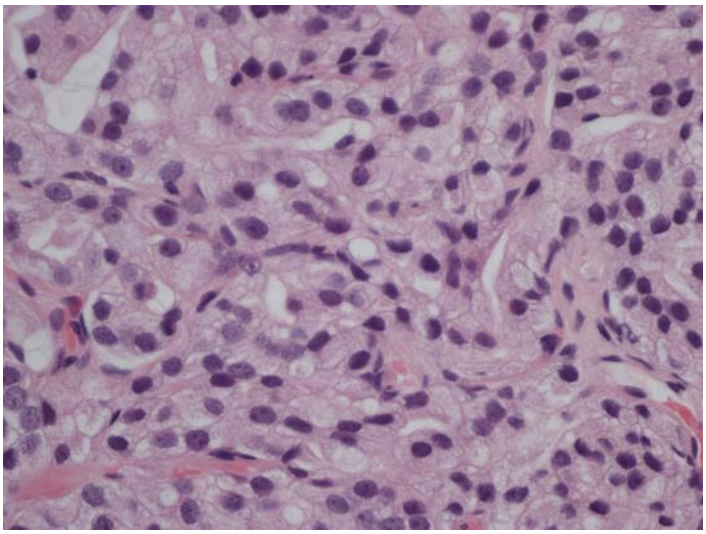

Fig 2.10: A histology section from the prostate gland showing prominent fusion of epithelial elements, seen in CaP (Gleason 4a) prepared at Gloucestershire Royal Hospital.

The Gleason grading system for CaP correlates well to its prognosis. The Gleason grade is a grade between 1 and 5 that is given to specific histological appearances. Figure 2.10 shows an example of a Gleason 4a adenocarcinoma of the prostate gland and Fig 2.11

shows the histological appearences of the other grades. The Gleason score is utilised by the pathologists and urologists to help with the determination of the prognosis of CaP. It is the sum of the first and second most common grades seen within the tumour. The score can be anywhere between 2 and 10 (e.g. 4+3 = 7), where a score between 2 and 4 show a well differentiated tumour, 5 and 7 a moderately differentiated tumour and between 8 and 10 show a poorly differentiated tumour [Foley 2002].

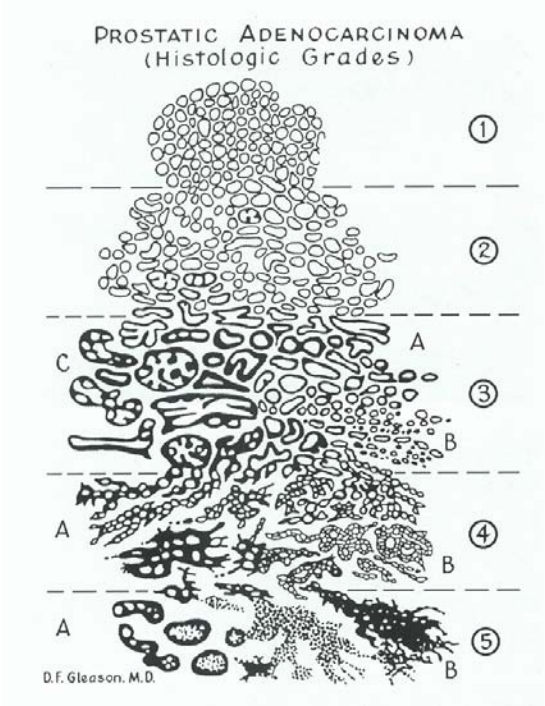

HISTOLOGIC CRITERIA FOR GLEASON GRADING*

1	Single, separate, uniform glands closely packed, with definite edge
2	Single, separate uniform glands loosely packed, with irregular edge
3A	Single, separate, uniform glands, scattered
3B	Single, separate, very small glands, scattered
3C	Papillary/cribriform masses, smoothly circumscribed
4A	Fused glands, raggedly infiltrating
4B	Same, with large pale cells ("hypernephroid")
5A	Almost solid, rounded masses, necrosis ("comedocarcinoma")
5B	Anaplastic, raggedly infiltrating

*Original wording of Dr. D. F. Gleason.

Fig 2.11: Histological grades of CaP as schematically depicted by Dr D. F. Gleason, (left). Description of the Gleason grades (right). Reproduced from the Atlas of Tumor Pathology, Tumours of the Prostate Gland, Seminal Vesicles, Male Urethra, and Penis, 3rd series [Young 1998].

The staging of CaP is done by means of clinical and pathological findings. The system that is widely used by Urologists is the TNM (tumour-nodes-metastases) system. This is

a system that looks at the size and site of the tumour (T), whether the local regional lymph nodes are involved (L), and whether there are any distant metastases (M). The 2002 edition of the TNM classification for CaP is shown below.

T – Primary tumour:

Tx Primary tumour can't be assessed.

T0 No evidence of primary tumour.

Tis In situ cancer (PIN).

T1 Clinically inapparent tumour not palpable or visible by imaging.

- **T1a** Tumour found in < 5% of tissue resected at TURP.
- **T1b** Tumour found in > 5% of tissue resected at TURP.
- **T1c** Tumour identified by a needle biopsy.

T2 Tumour confined within the prostate.

- **T2a** Tumour involves less than half of one lobe.
- **T2b** Tumour involves more than half of one lobe.
- **T2c** Tumour involves both lobes.

T3 Tumour extends through the prostatic capsule.

- **T3a** Extracapsular extension (unilateral or bilateral).
- **T3b** Tumour invades the seminal vesicle(s).

T4 Tumour is fixed or invades adjacent structures other than the seminal vesicles, i.e. bladder neck, external sphincter, rectum, levator muscles or the pelvic wall.

N – Regional lymph nodes:

Nx Regional lymph nodes can't be assessed.

N0 No regional lymph node metastases.

N1 Regional lymph node metastases.

M – Distant metastases:

Mx Distant metastases can't be assessed.

M0 No distant metastases.

M1 Distant metastases.

M1a Spread to non- regional lymph nodes.

M1b Spread to bone(s).

M1c Spread to other site(s).

[Foley 2002, Eble 2004]

Both the grade and the stage of the tumour are important in guiding the treatment of CaP, as well as in determining the prognosis.

The mode of spread of CaP can be:

Direct – this occurs both within the gland (urethra, bladder neck and stromal invasion), and to extracapsular structures such as the seminal vesicles. The rectal wall is rarely involved.

Lymphatic spread – These provide a good route for dissemination. Initially the sacral and iliac nodes are involved and later the para-aortic nodes.

Haematogenous – Invasion of the blood vessels results in distant metastases. This is commonly to the bone(s), lungs and liver. The bones commonly involved are the proximal femurs, pelvis and the lumbo-sacral spine.

The clinical presentation of CaP can range from being asymptomatic and an incidental finding, to being because of either obstruction or symptoms of metastases. The incidental finding of CaP tends to be in patients who have either had a raised PSA level or an abnormal DRE that prompted a TRUS and biopsy, or patients who have undergone a TURP for BPH and the CaP has been found in the resection chips.
Symptomatic patients can complain of a variety of symptoms. These include the following:

Obstructive bladder symptoms due to the compression of the urethra by the tumour. These symptoms consist of hesitancy, decreased flow, intermittent stream, incomplete voiding and post micturition dribbling.

Irritative bladder symptoms due to either an obstruction of the outflow or invasion of the trigone or pelvic nerves. These symptoms consist of dysuria, urgency and nocturia.

If the tumour invades the urethra, nerves sphincters or seminal vesicles then you may get the following symptoms; haematuria, suprapubic pain, perineal pain, impotence incontinence or haematospermia.

Ureteric obstruction by the tumour can result in loin pain and renal failure.

If the tumour invades the rectum then you may get tenesmus or rectal bleeding.

Metastatic symptoms can be due to spread to the bones (bone pain, pathological fractures or spinal cord compression), spread to the lymph nodes, (enlarged nodes leading to lymphoedema), or general symptoms of metastases, (weight loss and lethargy).

[Eble 2004, Cancer research UK 2004, Foley 2002]

The treatment of CaP is very controversial and is determined by the grade and stage of the disease, as well as the age of the patient.

Localised disease.

Patients with a low grade and stage disease or localised disease, may be offered curative treatment or active monitoring. Active monitoring is where the patient undergoes regular review in terms of DRE and PSA testing. This is because well-differentiated

tumours have a disease specific survival of 87% over 10 years [Foley 2002, Eble 2004, Cancer research UK 2004]. Curative treatment involves one of the following; radical prostatectomy, radical external beam radiotherapy, or brachytherapy. Hormone therapy may be used with all of these treatments and there have been many papers looking at the effectiveness of this [Schulman 1997, Soloway 1997, Klotz 1997, Candas 1997]. Adenocarcinoma of the prostate has been shown to be androgen dependent and hormone therapy acts to medically castrate the patient and halt or slow the tumours progression. This effect however is not permanent and clinical progression will eventually occur [Huggins 1941].

Locally advanced disease.

Patients with locally advanced disease (there is extracapsular spread but no evidence of metastasis to regional lymph nodes or distant sites) will be offered treatment to try and halt or slow the progression of the CaP. This is either by external beam radiotherapy with or without adjuvant hormonal therapy, or hormonal therapy alone. Bolla et al (2002) showed that there was both a disease free and overall survival advantage in those patients who were given hormone therapy during radiotherapy treatment and following treatment 3 years. In patients who are up staged following a radical prostatectomy it has been shown that not only does adjuvant anti-androgen therapy (medically or surgically) confer a survival advantage but also adjuvant radiotherapy has been shown to improve PSA relapse free survival in those patients at high risk of local recurrence [Eble 2004, Cancer research UK 2004].

Metastatic disease.

Patients with metastatic disease tend to be treated either palliatively or by halting or slowing the disease progression. This is by means of hormonal therapy. Hormonal therapy acts on the principle that 70 – 80% of tumours respond to androgen ablation [Campbell 2002]. This ablation can be either by bilateral subcapsular orchidectomy, antiandrogens or gonadotrophin releasing hormone analogues. Second line therapies are used when the tumour becomes hormone resistant (HRPC). This normally occurs between 18 and 36 months with an overall mean survival of 30 months and with 80% of patients achieving symptomatic relief [Cancer research UK 2004]. The second line therapies can include oestrogens and anti-oestrogens which act on the principle that oestrogen receptors may be unregulated in HRPC. Diethylstilboestrol has been shown to have a response rate of 43% [Smith 1998]

Recently there have been two randomised controlled phase III trials (TAX327 and SWOG) that have effectively shown that HRPC is chemotherapy sensitive. These trials have shown that overall and disease free survival times were significantly longer (2 / 3 months) when patients were given docetaxal – a taxane They also showed that patients quality of life was improved. Taxanes are cytotoxic drugs that polymerize tubulin into stable microtubules, leading to cell death due to mitotic arrest [Tannock 2004, Petrylak 2004].

Other treatments employed in CaP are for the symptoms associated with it.

Obstruction and urinary retention can be treated by a channel TURP. Ureteric obstruction and renal failure can be treated by nephrostomy or ureteric stents.

Spinal cord compression is treated by steroids, external beam radiotherapy to the lesion or by surgical decompression.

Bone pain is also treated by external beam radiotherapy or intravenous strontium radioisotope. Also by giving bisphosphonates the osteoclast activity can be inhibited which may help. Any fractures that occur are treated by surgical fixation with external beam radiotherapy to the fracture site.

Patients may also become **anaemic** requiring either blood transfusions or supplementation with iron and vitamins.

3. The normal Urinary bladder.

3.1. Anatomy of the bladder.

The bladder is a hollow organ that is found deep in the pelvic cavity (Fig 3.1). It lies posterior to the symphysis pubis and anterior to the rectum in males, and in females it is anterior to the vagina and inferior to the uterus [Murphy 1993, Tortora 1996, Underwood 1996]. The bladder is a mobile organ that is held in place by peritoneal folds, and is covered by peritoneum only over the superior surface of the bladder.

The bladder forms as a result of different embryological events, which accounts for its shape and portions. There is the trigone, which is on the base of the bladder. This as the name suggests is a triangular area, which at its two posterior corners receives the ureters from the kidneys. The anterior corner opens into the internal urethral orifice or the bladder neck. The posterior walls, dome and lateral walls of the bladder are formed from mesenchyme, and the anterior wall and portions of the lateral walls are formed when the infraumbilical portion of the abdominal wall closes [Meyer 2003].

The shape of the bladder varies depending on how much urine is within it. The female bladder will hold less than the male bladder, as the uterus is just superior to it. The average capacity of the bladder is between 500-800ml of urine, although most people will normally void when there is between 200 and 400ml within the bladder.

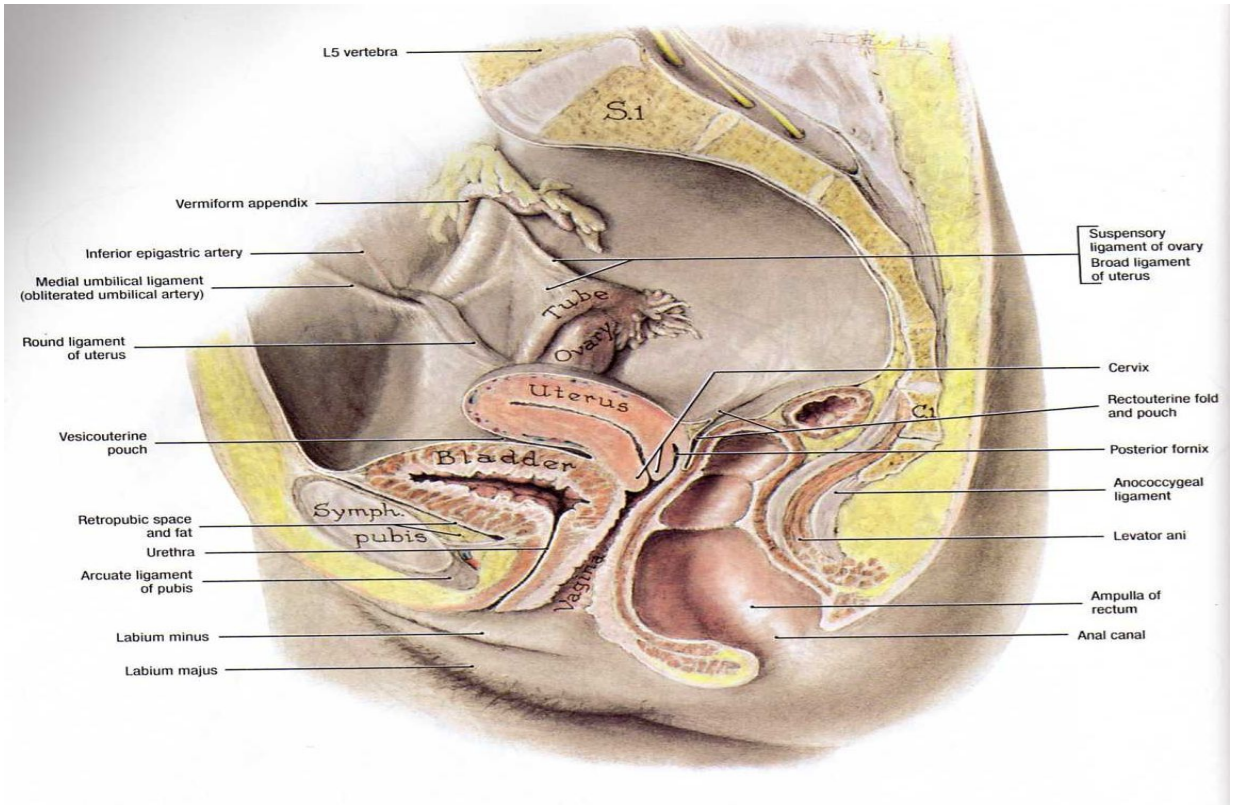

Fig 3.1: Anatomy of the female lower urinary tract.

Reproduced from Grant's Atlas of Anatomy, 10th edition [Agur 1999].

The blood supply to the bladder is in the form of superior, middle and inferior vesical arteries, these are branches of the anterior trunk of the hypogastric artery. Small branches to the bladder also come from the obturator artery and the inferior gluteal artery, as well as from uterine and vaginal arteries in women.

The venous drainage of the bladder is via a plexus that ultimately drains into the hypogastric vein.

The nerve supply to bladder is from fine medullated fibres from the third and fourth sacral nerves, and non-medullated fibres from the hypogastric plexus. These are connected with ganglia in the outer and submucous coats and are finally distributed to the muscular layer and epithelial lining.

3.2. Histo-pathology of the bladder.

Macroscopically the bladder is made up of three main layers. The innermost layer or the deepest layer is the mucosa, next is the muscularis and the outermost layer is the adventitia.

The mucosa is made up of transitional epithelium lying on a layer known as the lamina propria. Transitional epithelium, also known as urothelium, is made up of transitional cells, so named as their shape changes as you go through its layers (Fig 3.2). It is approximately 7-8 cells thick and can be divided into 3 zones – basal, intermediate and superficial. The cells in the basal and intermediate zones are small and uniform with very well defined borders. The cytoplasm within these cells is rich in glycogen. The cells in the superficial layer are much more specialised. These cells have larger nuclei although the nuclear to cytoplasm ratios are low. The cells also secrete mucin and act to maintain the integrity of the mucosa during the constant changes in the bladder's shape as it fills and expels urine. The mucin also acts to prevent urine transport.

The lamina propria is made up of loose connective tissue which carries a network of blood vessels to the epithelium.

The muscularis layer consists of a muscle known as the detrusor muscle. This consists of three layers of smooth muscle bundles – an inner and outer longitudinal layer and a middle circular layer. These layers aid the ability for the change in shape that occurs during filling and expelling of urine, and also ensures complete voiding of urine on contraction.

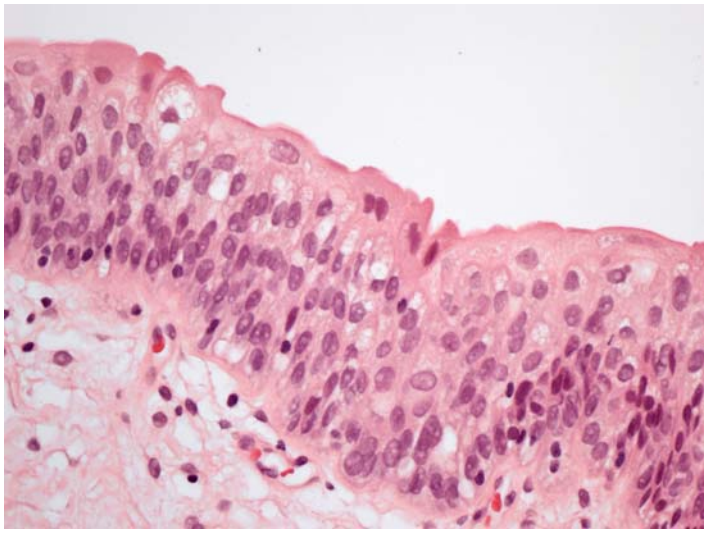

Fig 3.2: A histological section showing normal urothelium prepared at Gloucestershire Royal Hospital.

There is an internal urethral sphincter that is composed from the layer of circular muscle; this relaxes as the bladder contracts so that urine can be expelled.

The adventitia is the most superficial layer of the bladder. It is made up of areolar connective tissue that is continuous with the superficial layer of the ureters, and is only present on the posterior and inferior surfaces of the bladder. The dome or superior superficial surface of the bladder is made up of a layer of peritoneum known as serosa. [Tortora 1996, Kumar 1997].

3.3. The Function of the Bladder.

The bladder is designed to store and expel urine that is produced by the kidneys. Micturition occurs secondary to a combination of voluntary and involuntary activities. When a bladder is full, or at micturating capacity, the stretch receptors present in the

bladder wall transmit impulses to the spinal cord. These impulses commence the micturition reflex as well as initiating the conscious desire to void. The reflex is controlled by the parasympathetic nervous system and causes contraction of the detrusor muscle and relaxation of the internal urethral sphincter.

Micturition is not able to occur however until the external urethral sphincter that is made up of skeletal muscle is relaxed. The relaxation of this sphincter is controlled voluntarily. Therefore although the micturition reflex is involuntary, micturition can be controlled and stopped due to cerebral cortical control of the external urethral sphincter [Tortora 1996].

3.4. Investigations for diseases of the bladder.

The main investigations for the diseases of the bladder covered by this thesis are urine microscopy looking for organisms, cystoscopy and biopsy, and urine cytology. The latter two are subject to inter and intra – observer variation.

3.4.1 Cystoscopy.

Cystoscopy involves passing either a rigid or flexible scope into the bladder via the urethra, filling the bladder full of saline or glycine and having a look around the bladder using white light. Any abnormal areas can then be biopsied and sent for histology.

It can however be very difficult to distinguish between areas of cystitis and malignancy. De Dominicis et al showed that the sensitivity and specificity of white light cystoscopy was 18% and 82% respectively. They also showed that by instilling 5-aminolevulinic acid into the bladder an hour before cystoscopy and using a blue light to detect areas of fluorescence (photodynamic diagnosis) the sensitivity of cystoscopy could be increased to 87%. The specificity does decrease to 63% however, due to inflammatory or hyperplastic tissue also fluorescing.

3.4.2 Urine cytology.

The gold standard, non-invasive test for urothelial tumours (found anywhere in the urinary tract that is lined with urothelium) is urine cytology. This is stained with a Papanicolaou stain and has 95% specificity. However the test is only 40 – 60% sensitive (the sensitivity increases with the grade of the tumour). This is because of the significant inter- and intra-observer variability, as well as the fact that urine cytology is altered by UTI, bladder instrumentation, indwelling catheters, radiotherapy and intravesical chemotherapy.

It is ideal to obtain the urine sample from the first morning voided sample.

3.5. Diseases of the Bladder.

3.5.1. Cystitis.

Cystitis is the inflammation of the bladder.

The commonest cause of cystitis is infective, and the majority of causative pathogens are the Gram negative facultative anaerobes usually present in the bowel flora.

The majority of patients suffering with infective cystitis are women, with 30% of women between the ages of 20 and 40 having at least one episode and 12% of men between the ages of 14 and 61 reporting symptoms of kidney, bladder or urine infection. 85% of women in the community-acquired setting have cystitis secondary to Escherichia coli, 5-10% are caused by other Gram negative Enterobacteriacae including Proteus spp. and Klebsiella spp. Gram positive organisms such as Staphylococcus saprophyticus occur in 10-30% of women. Infection is much commoner in women, and this is thought to be due to the length of the female urethra which is short. The male urethra on the other hand is much longer and is thought to help to prevent bacterial colonisation.

The means by which the majority of bacteria reach the urinary tract is by the ascending route, although infection can also occur haematogenously. Bacteria tend to be normal flora within the bowel and they ascend from the bowel, into the vagina and then up through the urethra, into the bladder. It is within the bladder that they then adhere to the urothelial surface, this is done by the bacterial adhesins produced by the bacterial pili

interacting with receptors on the urothelial surface. The bacteria then have to overcome host defences such as urinary flow to be able to colonise and cause cystitis.

The macroscopic features are of an erythematous oedematous mucosa with hyperaemia at cystoscopy. Pyuria may also be noted, and there may be debris within the bladder. Microscopically there is an inflammatory infiltrate with neutrophils; this is characteristically in the submucosal layers. If the cystitis is chronic then the infiltrate also contains fibroblasts and mononuclear cells (Fig 3.3).

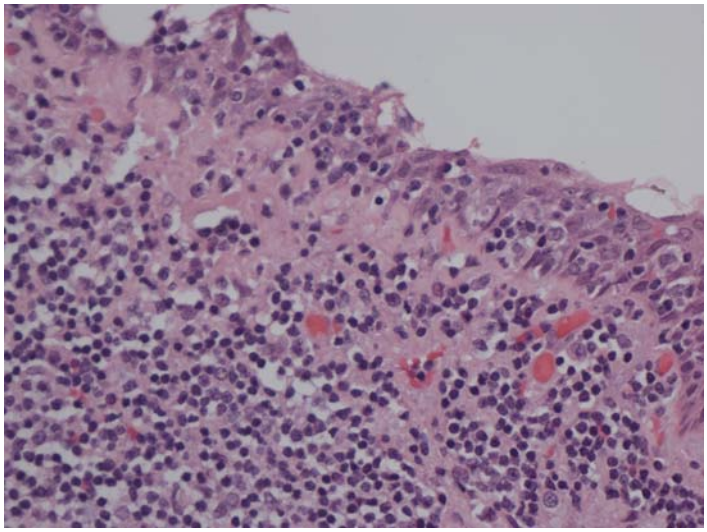

Fig 3.3: A histological section showing cystitis prepared at Gloucestershire Royal Hospital.

The presentation of cystitis can be asymptomatic but the majority of cases suffer with any or all of the following; frequency, urgency, urge incontinence, dysuria, haematuria,

pungent urine, malaise and suprapubic pain. It is diagnosed by urine culture where it tests positive for blood leucocytes and nitrites, and definitively contains > 10^5 bacteria per ml of urine. [Campbell 2002]

Treatment of cystitis secondary to simple infection involves antibiotics aimed at the offending pathogen and treatment of any other cause i.e. bladder stones, bladder neck stenosis. Patients also need to be advised on prevention. This involves the following; drinking plenty of fluid, avoiding dehydration, ensuring that the bladder empties properly, voiding post sexual intercourse, showering rather than having baths and wiping front to back with moist tissue.

3.5.2. Bladder Cancer.

Transitional cell carcinoma (TCC), of the bladder is the commonest form of cancer arising in the bladder. It accounts for 90% of all bladder tumours [Anderson 1996, Campbell 2002]. Other carcinomas of the bladder make up 10% of tumours within the bladder and consist of squamous cell carcinomas, mixed carcinomas, adenocarcinomas, sarcomas and poorly differentiated carcinomas.

The incidence of bladder cancer has reduced since the 1980s and it is now the fourth and eighth most common cancer in men and women respectively, in the UK, with 9000 men and 3600 women diagnosed each year [Meyer 2003]. In the United States, bladder cancer accounts for 4% of all male cancers and 2% of all female cancers [Anderson 1996]. As you can see from these Figures there is a greater incidence in men and this is thought to be due to its aetiology.

Another encouraging statistic is that the population based survival rates have increased from 40% in the 1970s to greater than 60% in the early 2000s [Cancer research UK 2004]. Unusually men have higher survival rates than women both in the UK and in Europe. The UK mortality statistics for 2001/2002 show that 4% and 2% of cancer related deaths in men and women respectively are due to bladder cancer [Meyer 2003, Cancer research UK 2004].

There is also geographical variation in bladder cancer types and mortality. For example the highest incidence of squamous cell carcinomas of the bladder are found in areas that are endemic for Schistosoma haematobium and it is also the commonest cause of cancer related death in these areas, whereas the highest incidence of transitional cell carcinomas are found in Western Europe, North America and Australia [Murphy 1993, Eble 2004, Anderson 1996].

The aetiology of bladder cancer is multifocal, and many toxins are now well recognised. Cigarette smoking and occupational exposure to aromatic amines are the most important. There is now a list of industrial occupations that have an increased risk of developing bladder cancer, these are as follows:

Manufacture of rubber or rubber products.

Manufacture of cable.

Manufacture of dyestuffs.

Manufacture of organic chemicals.

Gas works and coke ovens.

Rodent extermination.

Sewage works.

Manufacture of firelighters or patent fuels.

Laboratory work.

The toxic chemicals responsible are the metabolic products of α- and β-naphthylamine, benzidine, and 4-aminodiphenyl. Other toxins associated with bladder cancer are cigarette smoke, phenacetin containing analgesics, cyclophosphamide and chlornaphazin. Pelvic radiation and trauma to the urothelium are also known risk factors for bladder cancer.

The occupational cancers do tend to occur at an earlier age than those tumours that appear to be spontaneous, but there is thought to be a latent period of 15 – 20 years post initial exposure.

Smoking tobacco is the major risk factor in the development of bladder cancer, with the estimated risk being attributed to tobacco being 66% and 30% for men and women respectively [Eble 2004]. This risk increase with the duration of smoking so that the risk increases from a 2 fold increase to a 6 fold increase for those who have smoked for more than 60 years. The risk also increase with the number of cigarettes smoked per day with a maximum of 40 or more cigarettes. Unusually some studies have shown that there is a higher risk in women for the equivalent level of exposure [Eble 2004].

Recurrent infection is also a risk factor for developing bladder cancer but it tends to be squamous cell carcinoma as with infection by Schistosoma haematobium.

As TCC is the commonest form of bladder cancer I am going to refer only to this in the following sections.

Macroscopically TCC of the bladder can be uni- or multifocal, they can be finely or coarsely fronded, papillary, sessile, nodular, solid or ulcerative. Adjacent areas may be normal, erythematous or may have associated CIS present. They can occur anywhere within the bladder, but they do have a predilection for the trigone, around the ureteric orifices and the posterolateral walls [Murphy 1993 Eble 2004, Anderson 1996].

Microscopically they are, as the name implies, transitional cell carcinomas with a varying degree of differentiation. TCC is divided into three grades depending on this degree of differentiation.

Grade 1 or well differentiated tumours have densely packed, evenly distributed, uniform cells with indistinct borders and little or no cytoplasm. The nuclei are enlarged, slightly pleomorphic and have irregular borders. There is also an increase in mitoses. They are noticeably transitional cell in origin but have an increase in the number of layers (Fig 3.4).

Grade 2 or intermediately differentiated tumours are also able to be recognised as being of transitional cell origin, but they have even more layers of cells with a more pronounced hyperchromicity and increase in mitotic activity than those cells in the grade 1 tumours.

Grade 3 or poorly differentiated tumours are not recognisable as being transitional cell in origin. The cells tend to cluster and their borders may be sharply defined or indistinct. Nuclei are markedly pleomorphic and mitoses are common and may be abnormal (Fig 3.5). Calcification has also been noted in tumours that are poorly differentiated. [Murphy 1993, Eble 2004, Anderson 1996].

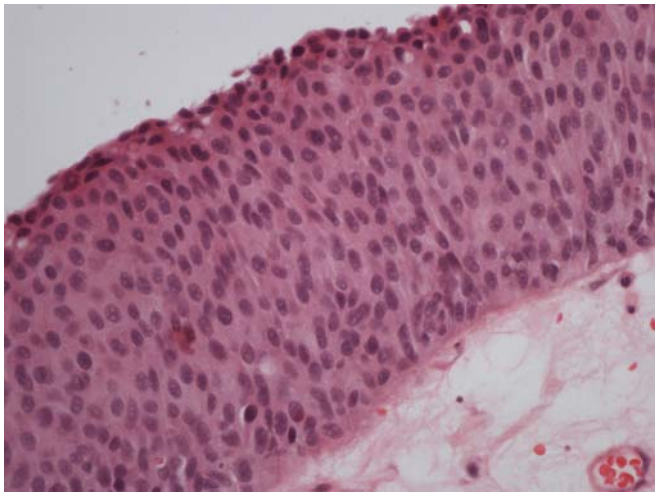

Fig 3.4: A histological section showing grade 1 TCC of the bladder prepared at Gloucestershire Royal Hospital.

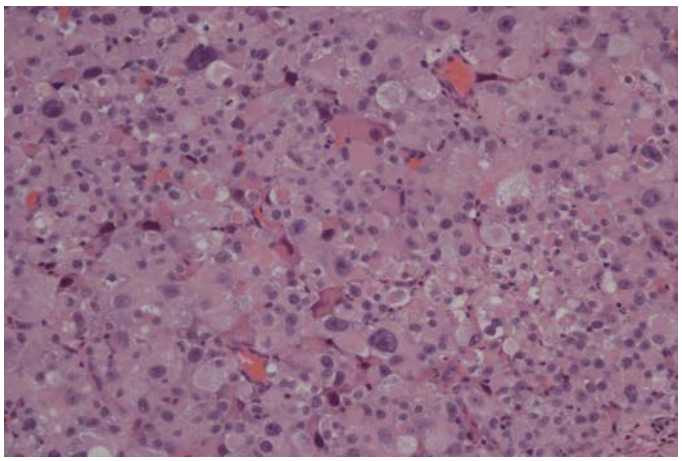

Fig 3.5: A histological section showing grade 3 TCC of the bladder prepared at Gloucestershire Royal Hospital.

The staging of TCC is done by means of clinical and pathological findings. The system that is widely used by Urologists is the TNM (tumour-nodes-metastases) system. This is a system that looks at the size and site of the tumour (T), whether the local regional lymph nodes are involved (L), and whether there are any distant metastases (M). The 2002 edition of the TNM classification for bladder transitional cell carcinoma is shown below.

T – Primary tumour:

Tx Primary tumour can't be assessed.

T0 No evidence of primary tumour.

Ta Non invasive papillary carcinoma

Tis Carcinoma in situ

T1 Tumour invades subepithelial connective tissue.

T2 Tumour invades muscle.

- **T2a** Tumour invades superficial muscle (inner half).
- **T2b** Tumour invades deep muscle (outer half).

T3 Tumour invades perivesical tissue.

- **T3a** Microscopically.
- **T3b** Macroscopically.

T4 Tumour invades adjacent structures, i.e. prostate, uterus, vagina, pelvic wall, abdominal wall.

- **T4a** Tumour invades prostate, or uterus, or vagina.
- **T4b** Tumour invades pelvic wall or the abdominal wall.

N – Regional lymph nodes:

Nx Regional lymph nodes can't be assessed.

N0 No regional lymph node metastases.

N1 Single lymph node < 2cm.

N2 Single lymph node 2 - 5cm or multiple lymph nodes < 5cm.

N3 Lymph node > 5cm.

M – Distant metastases:

Mx Distant metastases can't be assessed.

M0 No distant metastases.

M1 Distant metastases.

[Hermanek 1997, Sobin 2002].

Diagrammatic representation of the T part of the TNM classification is shown on the following page in Fig 3.6.

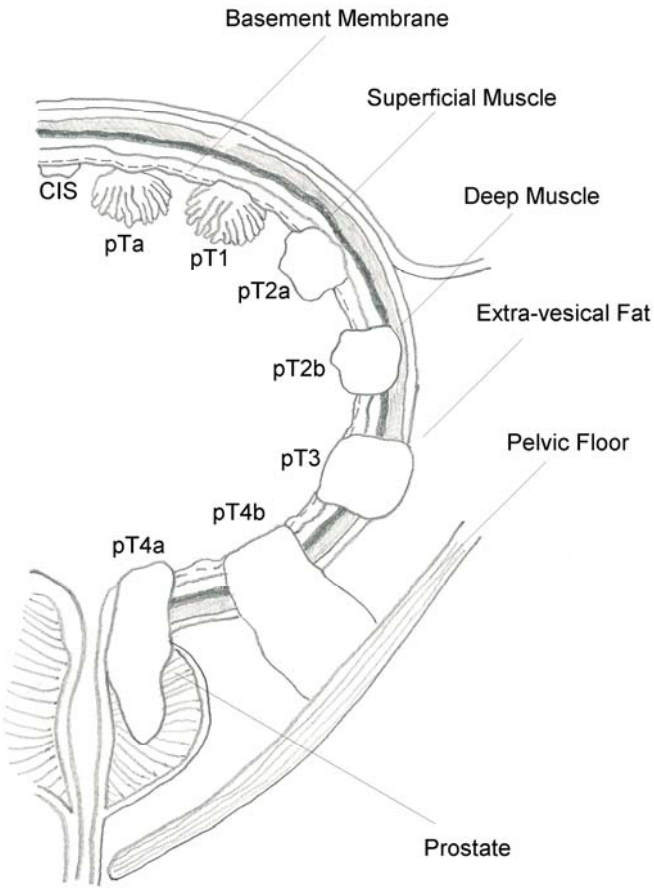

Fig 3.6: Diag ɔn, modified from TNM classification of malignant tumours: Urinary bladder, 6th ed. [Sobin 2002]

Both the grade and the stage of tumour are important in guiding the treatment of TCC, as well as in determining the prognosis.

The mode of spread of TCC of the bladder can be:

Direct – this occurs via invasion of the muscular wall of the bladder. It can be to the prostatic urethra, distal ureters and the prostatic ducts. In advanced disease it can also involve the pelvic wall, tethering the bladder to it.

Lymphatic spread – These provide a good route for dissemination. Initially the sacral and iliac nodes are involved and later the para-aortic nodes.

Haematogenous – Invasion of the blood vessels results in distant metastases. This is commonly to the lungs, liver and then to the bone(s), in order of declining frequency. Other recorded sites include the adrenals, heart, brain and kidney.

[Murphy 1993, Anderson 1996].

The presentation of TCC and other forms of bladder cancer is the same. Patients may be asymptomatic and the tumour can be an incidental finding. Otherwise patients may have microscopic or macroscopic haematuria, especially if the tumour is epithelial, 85% of patients present with painless haematuria [Eble 2004]. With extensive haematuria the patient may present with anaemia of unknown cause or in clot retention.

Some patients will experience dysuria, frequency or suprapubic pain depending on the site of the tumour. Patients may also present with a mass or symptoms of metastases, such as general lethargy and weight loss, or enlarged nodes leading to lymphoedema.

If the tumour blocks one or both of the ureters then obstruction may occur resulting in loin pain and renal failure.

The definitive treatment of TCC will depend on the grade and stage of the disease and the age of the patient.

The mainstay for diagnosis and establishing the grade and stage of TCC is cystoscopy (Fig 3.7) and biopsy / transurethral resection of bladder tumour (TURBT). Patients will

also have undergone an intravenous urogram (IVU) and/or an ultrasound scan (USS) of the abdomen and pelvis, however these are not good for staging the disease. USS has a high false negative rate with less than 70% accuracy for staging. This is due to both patient factors i.e. obesity and tumour factors i.e. site of tumour. Magnetic resonance imaging (MRI) is the modality of choice for assessing the primary tumour and searching for metastases however it still only reaches 83% accuracy for staging. Computerised tomography CT can also be used where MRI is not available and tends to be used in a lot of centres due to its ease of accessibility and cost. CT however only has a 55% accuracy for bladder tumours due to their size (small tumours are hard to visualise on CT) and an understaging of lymph node metastases in 40-70% [Eble 2004, Campbell 2002].

Fig 3.7: An example of a small papillary tumour found at white light cystoscopy. Reproduced from the Fluorescence diagnosis of bladder tumour using 5 Aminolevulinic Acid – fundamentals and results [Baumgartner 1999].

Assuming the patient is able to undergo any form of treatment and has no medical reasons preventing any of the treatment options. The definitive treatment for the different stages of TCC are as follows:

Superficial tumours (Ta/T1): (Follow up with cystoscopy at intervals determined by history and pattern of recurrence).	Single	TURBT/Cystodiathermy/Laser
	Multifocal	As above with adjuvant chemotherapy – Intravesical BCG or Mitomycin C.
	Recurrence	As for multifocal
T2 tumours:		TURBT → Radiotherapy/ cystectomy.
T3 tumours:	Controversial.	Possibilities include; radiotherapy, chemotherapy, cystectomy and radiotherapy, cystectomy alone with either an ileal conduit or a neo-bladder.
T4 tumours:	**T4a**	Cystectomy.
	T4b	Palliative radiotherapy.

The cystectomies are cystoprostatectomy or cystectomy and hysterectomy.

Superficial bladder cancer (Ta / T1) as can be seen above is treated differently to invasive bladder cancer (T2 – T4). The superficial tumours can be managed

endoscopically and with intravesical therapy. Parmar et al (1989) postulated the notion of risk stratification to help to assess the risk of recurrence in these tumours as it has been shown that 70-88% of superficial tumours will recur following treatment endoscopically [Sobin 2002].

Superficial tumours are separated into 3 groups depending on the number of tumours at presentation and the presence of recurrent tumour at the first check cystoscopy. Group 1 is a single tumour with no recurrence at first check and Group 3 is multiple tumours with recurrence at first check. Group 3 are at a high risk for recurrences and therefore require more frequent cystoscopies and further intravesical treatment whereas group 1 is very low risk and can go straight to annual check cystoscopies. Stromal invasion (T1) and the grade of the tumour are not good indicators of recurrence but are good indicators of progression with grade 1 / 2 and Ta disease having a lower risk of progression than grade3 T1 disease.

Invasive bladder cancer is a different entity in that it is aggressive and therefore requires aggressive treatment modalities to prevent and treat metastatic disease. Treatment will depend on the individual patient and is in the form of either cystectomy with urinary diversion or formation of a neo-bladder or radiotherapy. Both have similar overall 5 year survival rates of 40 – 60% although a Cochrane report suggested that cystectomy conferred an overall survival benefit [Shelley 2002]. In select patients neo- adjuvant and adjuvant chemotherapy can be considered with either cystectomy or radiotherapy. It is used as up to 50% of patients with muscle invasive disease may develop metastases as they already had micrometastatic disease [Sternberg 2002].

3.5.2.1 Carcinoma in situ.

Carcinoma in situ (CIS) is defined as a flat, non-invasive urothelial lesion composed of cells with significant anaplasia. Lesions often termed as severe dysplasia are also included in this definition [Murphy 1993], these involve cellular maturation toward the surface and can be difficult to distinguish from mild or moderate dysplasia, or atypical hyperplasia in morphologic terms. Richards et al showed that there is significant inter and intra-observer error between pathologists when diagnosing degrees of dysplasia and CIS [Richards 1991].

CIS can be found adjacent to a tumour within the bladder or in a bladder with no evidence of bladder tumour, and is thought to be a premalignant condition. Droller et al (2000) found that CIS could be associated with a high risk of progression in the context of a concomitant or prior neoplasm. However when diagnosed as a primary or unifocal lesion it could represent a non-progressive lesion or even one that had terminally de-differentiated rather than one that may progress.

The aetiology and true prevalence of CIS is unknown. However Cheng et al have shown that urothelial dysplasia is believed to be the putative precursor of CIS [Cheng 1999]. Patients diagnosed with CIS tend to be in their fifth to sixth decade of life, and the incidence of primary CIS is thought to count for less than 1 – 3% of urothelial neoplasms. CIS is however seen in between 45 and 65% of invasive neoplasms and 7 – 15% of papillary neoplasms [Eble 2004].

The clinical features vary from patients being asymptomatic to those suffering with any or all of the following; dysuria, frequency, urgency and/or haematuria.
Morphologically CIS of the bladder on cystoscopic examination can look normal, and it is not picked up until random biopsying is undertaken [Richards 1991]. Alternatively it can appear as defined, a flat lesion that may be erythematous. It tends to be multifocal involving areas other than the bladder base.

Microscopically CIS (Fig 3.8) is characterised by some or all of the following:

An increase in the number of cell layers.

Crowding of the nuclei.

Loss of the regular arrangement and polarity of the cells.

Hyperchromatic nuclei.

Increased mitotic activity.

Presence of mitoses above the basal layer of cells.

Lack of cohesion of the superficial layers of cells, which may desquamate into the lumen of the bladder [Andersons 1996, Eble 2004].

The presentation of CIS can be of irritative symptoms, e.g. dysuria, frequency and suprapubic pain, or haematuria, or some patients may be asymptomatic.

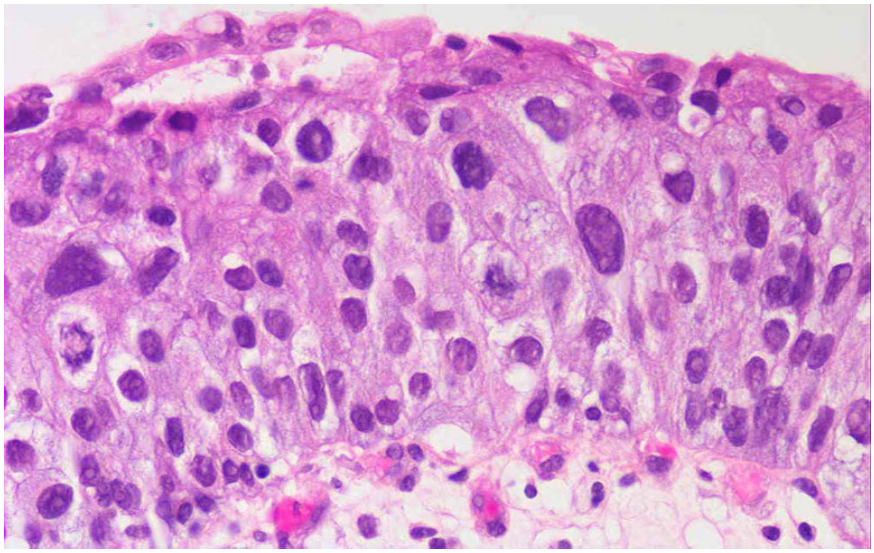

Fig 3.8: A histological section showing CIS undermining adjacent urothelium. Reproduced from Campbell's urology 8th edition [Campbell 2002].

Treatment of CIS when confined to the urinary bladder is currently treated with local ablation and instillation of intravesical immunotherapy such as bacillus Calmette-Guerin (BCG) [Herr 1986, Campbell 2002] this is due to the presumed aggressive nature of the disease. 30% of patients do not respond to BCG, but 53% of these will respond to a second course. Also 30% of responders will relapse at 5 years [Campbell 2002].

Photodynamic therapy has also been suggested to treat CIS, however as yet it has not gained much acceptance throughout the urological community [Kriegmair 1994]. Patients are closely followed up and if invasion or progression is found on repeat biopsy, then radical treatment in the form of a radical cystoprostatectomy / cystectomy is advocated [Cheng 1999, Herr 1989].

4. Biomedical applications of Raman spectroscopy: A critical review of the literature.

Raman spectroscopy is rapidly becoming popular in the field of research due not only to its potential ability to provide real time diagnosis of tissue *in vivo*, but also due to the evolution of lasers and detectors/spectrometers. It wasn't until the late 1980s / early 1990s that Raman spectroscopy really took off in terms of looking at biological tissues. This was because it wasn't until this time that the Raman spectra obtained from tissue were of adequate quality to allow the identification of the different components within them.

In this chapter the latest literature on the biomedical applications of Raman spectroscopy will be discussed as a discussion on the development and evolution of Raman spectroscopy and its instrumentation was had in chapter 1.

4.1 Raman spectroscopy of the prostate gland and bladder

There has been little in the way of literature looking at the use of Raman spectroscopy in the bladder and prostate that hasn't originated from our own group.

There has been no previous work done on the prostate gland except that done by our group. Crow et al (2003a, 2003b, 2004) showed that we were not only able to

distinguish between different pathologies within the prostate gland *in vitro* but also between different grades of adenocarcinoma of the prostate. However the sample size for each pathology was small and I have substantially improved upon this in my thesis.

Recent work on the bladder by De Jong et al (2002, 2003) looked at the identification of bladder wall layers and the changes in the molecular composition of bladder muscle caused by outlet obstruction. Both of these papers looked at spectra taken from the bladders of guinea pigs. They showed that Raman spectroscopy could be used to identify different layers of the bladder *in vitro* and also that the urothelium had a high fatty acid concentration on comparison with oleic acid showing peaks at 1081,1261, 1299, 1439 and 1659 cm^{-1}. The group showed that the lamina propria and muscle layer spectra also compared well to the spectra of their major constituents (collagen and actin respectively). They used a Visionex Gaser 10 forward viewing fibreoptic probe to obtain spectra from the bladders of guinea pigs during urodynamic studies and were able to estimate the proportion that each layer attributed to the overall spectrum. The authors showed by means of mapping that there was a difference between the normal and damaged bladder in that there appeared to be clusters of glycogen within the damaged tissue. The authors hope that they will be able to determine the degree of damage to the bladder wall (*in vivo*) secondary to bladder outflow obstruction without the need to take biopsies.

Prior to this, some work was performed by Feld et al (1995) looking at spectra from bladder samples. They showed that there was an increase in nucleic acid and a decrease in lipid contributions to the spectra from bladder cancer samples as opposed to normal

bladder sample spectra. The authors however do not seem to have taken this work any further.

The most recent work done on the bladder was by our group. Crow et al (2003a, 2004)[Stone 2002] showed that we were not only able to distinguish between different pathologies within the bladder *in vitro* but also to stage and grade the transitional cell carcinoma of the bladder. However the sample size for each pathology was small and cross validation testing was the best that could be achieved. Greater numbers would allow more vigorous testing.

4.2 Raman spectroscopy of other tissues.

Early work on the biomedical applications of Raman spectroscopy were confined to analysis of urinary calculi [Daudon 1983, Sudlow 1991,Hong 1992] and calcification of the aorta [Klug 1992]. As instrumentation and techniques improved groups started looking at the ability of Raman spectroscopy to differentiate between normal and malignant tissue. There have been many authors over the years who, have looked at the progress made in this field resulting in some very comprehensive review articles [Hanlon 2000, Mahadevan-Jansen 1996, Manoharan 1996]. The main aspects of work done in other tissues will be highlighted focusing on those dealing with the spectroscopic analysis of pre malignant and malignant tissue, and those tissues where the majority of work has been done.

4.2.1. The gastrointestinal tract.

There have been several studies looking at the use of Raman spectroscopy in the oesophagus. Most recently Stone et al (2002) has shown that by measuring spectra from eight pathological groups of oesophageal samples and constructing a diagnostic algorithm they were able to achieve between 73 and 100% sensitivity and specificity for the correct classification of each spectrum. This was the first study to spectrally separate so many pathological groups therefore indicating the ability of Raman spectroscopy to classify pathologies as well as simply detecting disease.

Georgakoudi et al (2001) showed that by combining fluorescence, reflectance and light-scattering spectroscopy they were able to improve upon the sensitivity and specificity of using just one of the techniques. Their numbers however were very small having only looked at 16 patients with known Barrett's oesophagus and there is the need for complex software with the ability to analyse all three types of spectroscopic information. This makes its use as a real time diagnostic tool more complicated.

Barr et al (1998) reviewed different optical spectroscopic techniques in the early diagnosis of gastrointestinal malignancy and they concluded that Raman spectroscopy had the potential for the diagnosis of malignancy in the gastrointestinal tract, but that there were still a number of technical problems such as the fibre probes generating a Raman signal, to overcome before *in vivo* measurements become routine.

Work is ongoing in this field to develop an *in vivo* probe. Initial work done by Shim et al (2000) showed that their probe was able to sample to an estimated depth of 500μm thereby enabling the detection of early stage lesions. There was no detectable increase in temperature when ex vivo experiments were done and they concluded that the near

infrared light was non-mutagenic. They were the first to use an *in vivo* fibre optic probe down an endoscope during a routine endoscopy. They are planning to take this further with a multi-centre clinical trial to further assess the probes ability to detect and diagnose disease thereby enabling its use in both surgical and therapeutic guidance.

4.2.2. Gynaecological tissue.

There has been a lot of work done over the years on cervical pre malignancies. Like the oesophagus, cervical malignancy has an intermediary condition between normal and cancer. This is known as cervical intraepithelial neoplasia. The incidence of this is rising and women over the age of 20 years are screened for this.

Mahadevan – Jansen et al (1998a) investigated the potential of Raman spectroscopy to differentiate between different pathologies within the cervix. They used two pathologists gaining a consensus opinion on the histology. They found that they were able to get a sensitivity of 100% and specificity of 73% with the Raman system as compared to histology when differentiating between intraepithelial lesions and non-intraepithelial lesions. They suggest that Raman spectroscopy is potentially superior to colposcopy and cytology and also observed that peaks at 1246 and 1656 cm-1 were also found in other epithelial tissues (colon and bladder). They did point out that their *in vitro* system was not applicable for *in vivo* use due to the long integration times.

Mahadevan- Jansen et al (1995, 1998b, 2002) also compared Raman with fluorescence and looked at an *in vivo* probe for detecting cervical malignancy. They showed the following advantages that Raman spectroscopy had over fluorescence – they achieved

better sensitivity and specificity when differentiating intraepithelial lesions from normal tissue, and also enabled further differentiation of the pathologies. The *in vivo* probe consisted of a portable system with a diode 785nm, 80mW laser. They showed that by using the probe they were able to achieve sensitivities and specificities similar to that of colposcopy, which unfortunately did not mimic the *in vitro* results, which were much better than colposcopy. The authors felt that this may be due to the probe geometry and interference from sunlight. They did however show that the use of Raman spectroscopy *in vivo* had potential in the diagnosis of cervical dysplasia, the pre malignant condition.

More recently Mahadevan – Jansen et al have looked at the different sources of intra and inter-patient variability such as menopausal status, smoking history, overall patient diagnosis and the application of acetic acid. They looked at 35 patients undergoing a hysterectomy for reasons other than cervical disease. A portable spectroscopy system was used with a 785nm diode laser and fibre optic probe to obtain the spectra from the patients prior to their hysterectomy. They found that the intra-patient variability due to different locations on the cervix was negligible however there was greater variability due to inter – patient variation such as menopausal status. The authors demonstrated a difference in the intensity at 1324cm^{-1} which has also been shown to be one of the key difference between cervical dysplasia and normal ectocervix. Therefore they concluded that future studies were needed to separate classification algorithms depending on menopausal status. They also clarified the optimum integration time of 5 seconds by analysing the signal to noise ratio of different times. This also minimised probe movement during spectra acquisition that could lead to user error. The authors also found that although there was no statistical difference between the spectral difference before and after application of acetic acid, the difference is enhanced between normal

and diseased tissue. Therefore the authors inferred that the application of acetic acid would actually be advantageous in the detection of dyplasia [Robichaux-Viehoever (to be published)].

Utzinger et al (2001) also looked at the *in vivo* detection of cervical pre malignant conditions. They used a diode 789nm laser coupled to a fibre optic delivery and collection probe. They also found that they had trouble with long integration times and interference from the lighting in the room. However they did conclude that it was a promising technique that needed to evolve.

Ovarian tissue has also been looked at with Raman spectroscopy, this is because ovarian tumours are rarely detected early on, as the main means of detection is a pelvic examination and a finding of an enlarged ovary. Lieber et al (2002) revealed that there were a number of significant Raman peaks that were observed only in some pathologies, but there sample size was very small having only looked at nine samples. They found that the following peaks were seen in the non- normal tissue; 1250, 1282, 1364, 1543, 1594 and 1634cm^{-1}. The authors were hoping to go onto *in vivo* testing with the completion of this study and the development of the probe.

4.2.2. Breast tissue.

There have been several studies in the literature that have looked at the diagnosis of breast cancer by using Raman spectroscopy. Alfano et al (1991) utilised near infrared Fourier transform Raman spectroscopy in medicine to obtain spectra from normal breast tissue and benign and malignant breast tumours. The authors showed that there were

four distinct peaks seen in normal tissue (1078, 1300, 1445, and 1651cm^{-1}), and these differed in malignant tissue in terms of the intensity ratios between wavenumber 1445 and 1651cm^{-1}, and loss of the peaks at 1078 and 1300cm^{-1}. They concluded that the spectral measurements could be used as a diagnostic tool however the sample numbers were small and needed increasing.

Frank et al (1994) noted that near infrared wavelengths in the 691 – 832nm range yield high signal to noise ratio spectra with moderate power. The peaks noted were predominately from lipid and carotenoids, but that the carotenoid peaks at 1006, 1157, and 1525cm^{-1} wavenumbers were only picked up at laser wavelengths of 488nm where they were enhanced. They also noted that of the major lipid peaks in normal breast tissue, oleic acid appeared to be the major component. The group were also able to show that there was no qualitative difference between normal breast tissue taken from breasts that were being re-contoured and normal breast tissue adjacent to a cancer.

Frank et al (1995) went on to show that at 784nm, sample to sample and patient to patient variations in normal breast tissue was less than 5% for the ratios between the major peaks. The authors also showed a difference between the spectra obtained from normal tissue, fibrocystic (benign) tissue and infiltrating ductal carcinoma were different. They noted the absence of the carotenoid peaks due to the lack of enhancement at 784nm, and also showed that by using a fibre optic needle they could obtain spectra from tissue and still get a difference between the pathologies. Using a wavelength of 784nm however did require long integration times, therefore necessitating further evolution of the probe prior to its use as an *in vivo* probe.

Manoharan et al (1998) were able to distinguish spectral differences between even more pathologies within breast tissue. They looked at normal fatty tissue, normal glandular

tissue, fibrocystic disease, adenosis, carcinoma in situ and infiltrating ductal carcinoma, although they then grouped them into pairs resulting in three groups; normal, benign and malignant. The authors compared Raman spectroscopy and fluorescence photon migration imaging, concluding that Raman spectroscopy was better for the histochemical analysis of the breast lesions. It was felt that the sample numbers were too small to be able to distinguish between all the pathologies and a larger database was planned for the future.

More recently Shafer – Peltier et al (2002) have taken things in the breast a step further. They looked at the contributions of fat, collagen, cell nucleus, cytoplasm, cholesterol-like, Beta carotene and calcium hydroxyapatite, to the spectra from different pathologies in the breast. In this way they were able to not only show that there were spectral differences between the pathologies but also to give a morphological understanding to the spectra obtained.

5. Materials and Methodology.

5.1. Constituents.

The aim of measuring constituents was to assess the biochemical properties of each of the pathologies within the bladder and the prostate gland. In this way it was hoped that I would be able to quantify the differences between the pathologies.

This thesis was limited to those constituents that were thought to be in sufficient concentrations in the tissue for the Raman spectrometer to be able to measure, ie gross molecules that change with pathology as opposed to subtle genetic changes such as p53. After consultation with available literature and discussions with pathologists in Gloucestershire Royal Hospital and Bristol Royal Infirmary the following constituents were picked. They were thought to be representative of different areas within a cell and this was confirmed by the literature [Shafer-Peltier 2002]. Unfortunately we are unable to completely validate the exact composition of tissue which is heterogenous. Berger et al [1996, 1997, 1999] have shown however that Raman spectroscopy can accurately determine concentration measurements of aqueous biological analytes and blood glucose. DNA is representative of the cell nucleus as the other constituents of the nucleus (ribosomes, RNA) have previously been shown to have a minor effect on the spectrum from the nucleus [Shafer-Peltier 2002]. Actin is thought to be representative of the cell cytoplasm and β-carotene is thought to be decreased in malignant tissue [Hata 2000, Toniolo 2001, Czeczuga-Seminiuk 2003]. Cholesterol is representative of necrosis [Shafer-Peltier 2002], choline is thought to be abundant in malignant tissue

[Anon 2003] and collagen is representative of the extracellular matrix / basement membrane. Glycogen is reduced in rapidly dividing cells such as malignant tissue, and only mature cells store glycogen. Lycopene is thought to be decreased in malignant tissue and oleic acid is thought to be abundant in urothelium.

PSA is known to be produced by the prostate gland and triolein is representative of triglicerode lipids.

Given the above directed approach, the following constituents were purchased from Sigma – Aldrich;

Actin-	from bovine muscle, (A3653).
β-carotene-	type 1, synthetic, approx 95%, (C9750).
Cholesterol-	sigma grade, 99%+, (C8667).
Choline-	base, approx 50% (w/w) aqueous solution, (C9154).
Collagen-	**type 1**, from human placenta, acid soluble, (C7774).
	type 3, from human placenta, acid soluble, (C4407).
	type 4, from human placenta, acid soluble, (C7521).
DNA-	from human placenta, (D7011).
Glycogen-	from bovine liver, (G0885).
Lycopene-	from tomato, (L9879).
Oleic Acid-	water soluble, (O1257).

Prostate Specific Antigen-	from human seminal fluid, minimum 95%, (P3338).
Triolein (C18:1,(cis)-9)-	sigma grade, approx 95%, (T7140).

5.2. Tissue collection.

The experiments carried out that form the basis of the research were all undertaken at either the Gloucestershire Royal Hospital or at the Rutherford Appleton Laboratories. Local ethics committee approval was obtained for the collection of tissue [Appendix 1] and patients were given an information leaflet and asked to sign a consent form if they agreed for us to take some samples [Appendix 2].

5.2.1. Collection of prostate tissue.

The aim of tissue collection from the prostate was to obtain samples from the following pathologies; Gleason grade 1 – 5 adenocarcinoma, HGPIN, prostatitis, and benign prostatic hyperplasia. Due to the variety of pathologies needed the prostate tissue was collected from patients undergoing routine TURP using a resectoscope, (Stortz 27040 DH). Figure 5.1 shows a sample of prostate being taken during a standard TURP. The irrigating fluid during the TURP procedure was glycine. Once removed from the patient the sample was placed on a piece of acetate paper to facilitate its handling and preparation.

Once the tissue had been placed on the acetate paper it was placed into a 2.0ml cryovial, (Corning Incorporated) and dropped into liquid nitrogen, thereby snap freezing the tissue. The tissue was then stored at -80°C.

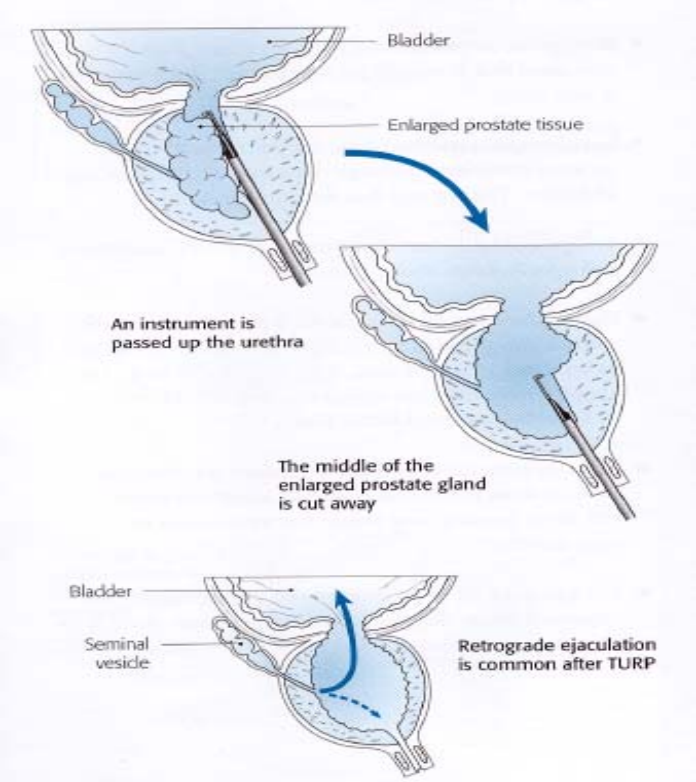

Fig 5.1: Sample of prostate taken during a TURP.

Reproduced with kind permission from Health Press.

5.2.2. Collection of bladder tissue.

The aim of tissue collection from the bladder was to obtain samples from the following pathologies; Grades 1 – 3 TCC, CIS, Cystitis, and normal urothelium. Due to the variety of pathologies needed the bladder tissue was collected from patients undergoing routine

TURP, TURBT, and cystoscopy procedures, using either a resectoscope, (Stortz 27040 DH), or cold cup biopsy forceps. The normal urolthelium was taken from the TURP and cystoscopy procedures to avoid any potential field changes that may be found in a bladder undergoing TURBT.

Figure 5.2 shows a sample of TCC being taken using the resectoscope. The irrigating fluid during the procedure was glycine. Once removed from the patient the sample was orientated on to a piece of acetate paper to facilitate its handling and preparation. The orientation of the sample on to the acetate paper is crucial to the cutting of the sample using a cryotome. This is shown in Figure 5.3 and as you can see, is orientated so that the slices taken for H&E staining include both urothelium and muscle, otherwise the urothelium may potentially have been stripped.

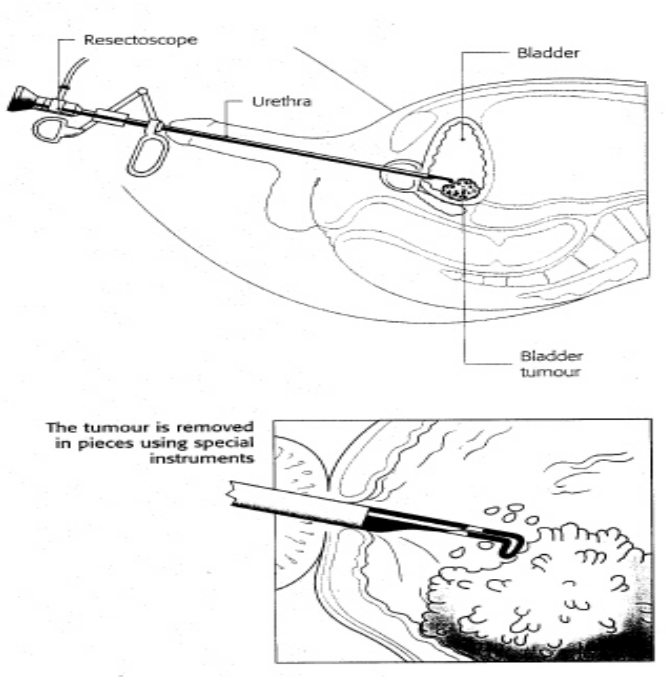

Fig 5.2: Resection of a sample of TCC using a resectoscope.

Reproduced with kind permission from Health Press.

Once the tissue had been placed on the acetate paper it was placed into a 2.0ml cryovial, (Corning Incorporated) and dropped into liquid nitrogen, thereby snap freezing the tissue. The tissue was then stored at -80°C.

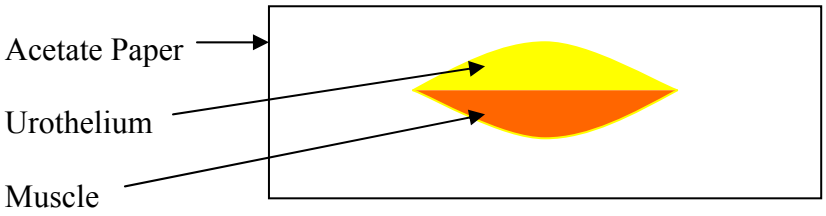

Fig 5.3: Orientation of the bladder tissue on the acetate paper.

5.2.3. Snap freezing tissue.

The rationale behind snap freezing the tissue in liquid nitrogen is as follows;

1. There is no contamination to the tissue from formalin or other chemicals that may be used to fix the tissue.
2. Tissue fixation halts metabolism and stabilises tissue structure but also produces chemical changes that will alter the spectra obtained [Bancroft 1996].
3. Slow freezing can distort and damage to tissue due to ice crystal artefact.
4. Snap freezing gives us an in vitro model that is as close as possible to in vivo spectroscopy.

5.3. Histopathological process and analysis.

5.3.1. The prostate tissue.

The prostate tissue was cut into histological sections using a cryotome. The top layer was discarded to level out the sample, and then a 7μm section was cut for H&E staining, and placed on to a histology slide (Snowcoat X-tra, Surgipath). The next section cut was 30 μm and this was placed on a calcium fluoride slide which was stored at -80°C. Another 7μm section was cut for H&E staining below this so that the histology could be accurately identified. The remainder of the tissue was placed back into the cryovial and stored at -80°C.

The use of the acetate paper made it possible for the tissue to be adhered to the cryotome chuck without the use of cutting agents. Therefore potential chemical contamination of the tissue was avoided.

The H&E slides were viewed by a consultant histopathologist and the pathology in the sample was identified. As the prostate tissue is heterogenous, there was often more than one pathology present on the slide, therefore each of these needed to be accurately identified so that the diagnosis for the spectra taken was correct. This was done by marking the H&E slides and then finding the corresponding position on the 30 μm section used for spectral acquisition. The spectra were then acquired and each spectrum was given a corresponding pathology code.

5.3.2. The bladder tissue.

The bladder tissue was cut into histological sections using a cryotome. The top layer was discarded to level out the sample, and then a 7μm section was cut for H&E staining, and placed on to a histology slide (Snowcoat X-tra, Surgipath). The remainder of the tissue was placed back into the cryovial and stored at -80°C.

The use of the acetate paper made it possible for the tissue to be adhered to the cryotome chuck without the use of cutting agents. Therefore potential chemical contamination of the tissue was avoided.

The H&E slides were viewed by a consultant histopathologist and the pathology of the sample was identified. Bladder tissue is usually homogenous and therefore easier than prostate to obtain a specific pathological diagnosis.

5.4. Raman spectroscopy.

5.4.1. Instrumentation – The Raman spectrometer.

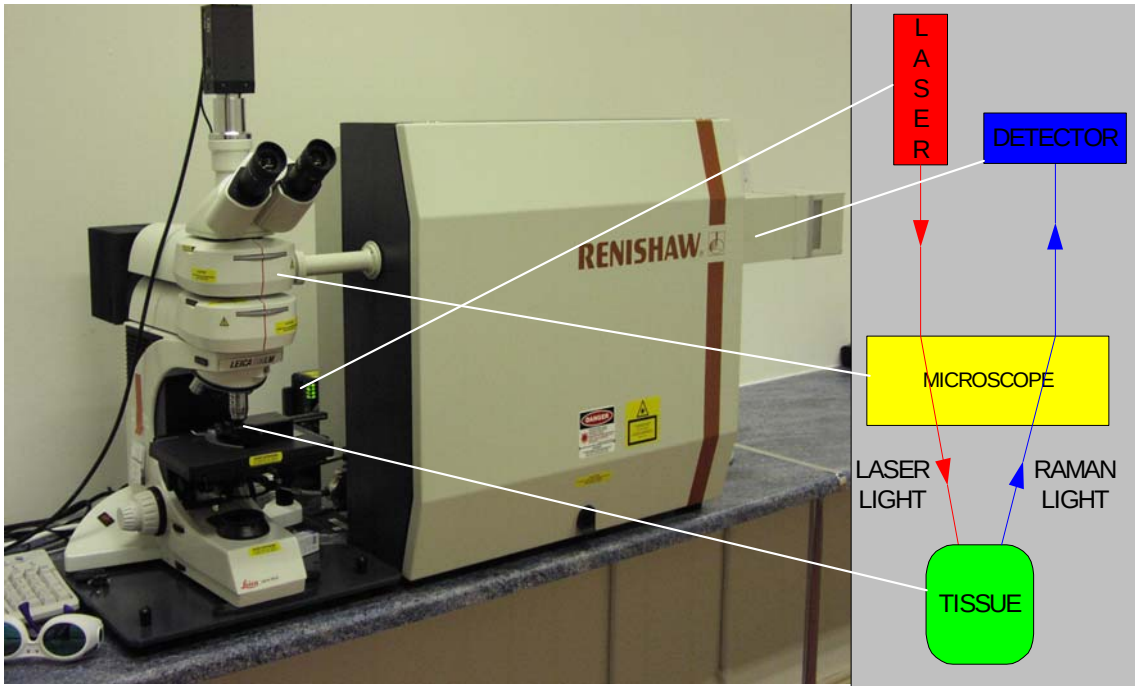

Fig 5.4: The Renishaw diode laser spectrometer. Reproduced from Crow (2004).

Figure 5.4 shows the Raman spectrometer (Renishaw plc**,** New Mills, Wotton under Edge, Gloucestershire, GL12 8JR.) used to obtain spectra from the tissue samples and the constituents. The system has been optimised for use on human tissue through the work of Dr Nick Stone (2001).

The laser used is a Renishaw high power near infrared diode laser, which supplies the excitation light at a wavelength of 830nm and generates 300mw of power. This is then focused through the microscope lens onto the tissue sample or the constituent. The spectrometer then collects the scattered light from the tissue/constituent and detects it.

The detected spectrum is recorded on the p.c. Figure 5.5 below shows the components of the Renishaw spectrometer in greater detail.

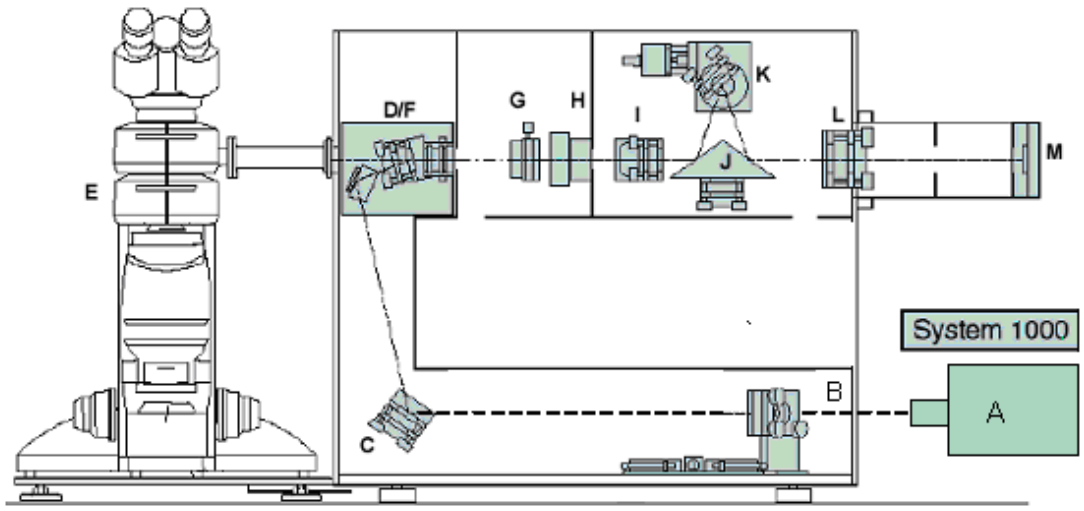

Fig 5.5: The components of the Renishaw spectrometer.

A – Diode laser, B/C – Steering mirrors, D/F – Laser line rejection apparatus, E – Microscope, G – Focusing lens, H – monochromator entry slit, I – Beam expanding lens, J – Prism mirror, K – Grating, L – CCD focusing lens, M – CCD detector.

When a spectrum is measured from some tissue or a constituent the following occurs. The diode laser (A) acts as the excitation light source. This is directed to the laser line rejection apparatus by the steering mirrors (B/C). The laser line rejection apparatus, reflects light at the laser's wavelength, but allows other wavelengths to pass through. D reflects the incident laser light via the Leica DML polarised light microscope (E) onto the sample. Due to the power density and signal to noise ratio achieved, as well as Raman and fluorescence signals from the microscope lens a x80 MIRPLAN ultra-long working distance (Olympus) lens was used for the prostate a x20 MIRPLAN ultra-long working distance (Olympus) lens was used for the bladder and a x50 MIRPLAN ultra-

long working distance (Olympus) lens was used for the constituents. These were actually selected to provide the sampling volume we wanted in the tissue. Following interaction with the sample, the light passes back, via the collection optics, to the laser line rejection apparatus (F). Light at the laser wavelength (Rayleigh scattering which is elastic) is reflected away, whereas the remainder of the scattered light, including the Raman scattering, passes through and is focused onto the monochromator entry slit (H) by the focusing lens (G). The slit (H) is used to reject scattered light from the out-of-focus sample volume, this acts to improve spatial resolution and reduce fluorescence. The monochromator has a 300 line / mm grating which had been previously selected by Dr Stone (2001) to give the best compromise between range and resolution. The light then passes via the beam expanding lens (I) to the prism mirror (J). The prism mirror deflects the light so that it passes to the grating (K), which separates the light into its constituent wavelengths, (The grating can be adjusted to allow a variable range of wavelengths to be selected for detection). Following separation at the grating, the light is again redirected by the prism mirror, so that it passes through the CCD focusing lens (L). The light is thereby focused onto the CCD detector (M), this consists of pixels that pick up different wavelengths of light on the vertical axis. The intensity at each wavelength is calculated by summing the charge on the pixels in the horizontal axis, and a spectrum is formed. The CCD used is a deep depletion charge-coupled-device detector (Renishaw RenCam) that comprises an array of 576 by 384 detector elements. The area on the array was reduced so that background noise could be reduced. The number of pixels on the array ultimately used to detect the spectrum has been reduced to twenty at each wavelength to give the best signal to noise ratio [Stone 2001].

5.4.2. Renishaw spectrometer software.

The Renishaw spectrometer is controlled by means of Hewlett Packard Pentium II Vectra personal computer (P.C.). This P.C. runs the Renishaw WiRE software (Windows 98 based Raman environment, version 1.3.15). This meant that the experimental set up, conFiguration, calibration of the spectrometer and data acquisition could occur. Also the GRAMS/32 software (Galactic Industries) enabled some initial basic analysis to occur. The vast majority of the analysis however was done on an office P.C. using Matlab, which will be discussed later.

The system also contains a motorised XYZ stage that is controlled by the software and allows movement of the sample in three dimensions for spectra acquisition. This enables spectra to be obtained from an area or volume of tissue and therefore allows for mapping of the tissue.

5.4.3. Optimisation of the Raman system.

As well as ensuring that the system is optimised in terms of the excitation source, edge filter, monochromator and objective lens, it is also necessary to be aware of potential causes of noise within the system and to reduce the noise as much as possible.

To measure a Raman spectrum from a biological tissue you need to maximise the signal to noise ratio as much as possible. This ratio is determined by the Raman intensity divided by the noise intensity. If you have too much noise the Raman signal will be swamped and meaningless.

There are two types of noise within the system, these are determinant noise (inherent within the system) and random noise (secondary to environmental changes).

The main determinant noises are shot noise (reduced by minimising acquisition time and laser intensity) and detector noise (dark current reduced by cooling the detector).

The main random noises are from variation in temperature and ambient light as well as cosmic rays. To minimise fluctuations in temperature an air conditioning system is used to provide a constant temperature of 22° C and to minimise ambient light fluctuations spectra are either taken in the dark or with a standard 60W light bulb which has previously been shown to have no detectable effects on the spectra [Stone 2001]. Cosmic rays cause sharp spikes to appear in the Raman spectrum, these are very obvious and can be removed from the spectra using the customised analysis programme in Matlab.

5.4.4. Calibration of the system.

As well as minimising factors that cause noise so as to improve the signal to noise ratio of our spectra, we also have to ensure the reproducibility of our spectra and the ability to transfer the information obtained from the spectra to other systems. In this way they can be used for medical applications. A means of doing this is by accurately calibrating the system and the importance of this has been discussed in the literature in the past [Mann 1999].

The system has to be calibrated for wavenumber as well as intensity. The wavenumber is calibrated by obtaining spectra from a neon argon lamp source with known emission

lines. Day to day checks are made by taking spectra of silicon. The spectra are taken using the x50 Leica objective with the static scans centred at 1150 cm^{-1}. One accumulation at 0.1seconds is taken. The system is then re-calibrated if the silicon peak was not at 520 cm^{-1} wavenumbers. The intensity is calibrated using a white light source lamp that has been calibrated against a standard by the National Physical Laboratory which provides the user with a spectrum of absolute intensities over wavenumbers at a fixed distance from the light source. The system was tested using the following 3 objectives to collect the light – x20 MIRPlan Olympus, x50 Leica and the x80 MIRPlan Olympus. The spectra were obtained to give an intensity count of 500000 arbitrary units.

5.4.5. Spectra acquisition.

All spectra were acquired following daily calibration of the spectrometer using silicon.

5.4.5.1. Spectra acquisition from the constituents.

The solid constituents were placed on a calcium fluoride slide, and the liquid constituents were placed in a cell plate. An x50 MIRPlan ULWD Olympus microscope objective was then used to focus in on the substance and to measure the spectra. Different acquisition times were used for each constituent, but the laser was always at full power with the monochromator slit set to 50μm. The spectra were centred at 1150cm^{-1} and stored on the system's P.C following acquisition. All of the spectra were

then white light corrected, baseline corrected and truncated to 450 – 1850cm^{-1} as outlined in Stone (2001).

5.4.5.2. Spectra acquisition from the prostate samples.

The TURP chip that was cut to 30µm and placed on a calcium fluoride slide, was passively warmed to room temperature. Initially an x2.5 NPlan Leica objective was used to take a white light image of the area to be mapped. Then an x80 MIRPlan ULWD Olympus microscope objective was used to focus on the prostate and to record the prostate spectra. Once focused for the white light, the focus was moved in to the tissue by 10µm and the system was set up for a map. The autofocus was left off and the acquisition time was set to 60 seconds at full laser power, for 1 acquisition. The spectra were taken in a line fashion from a mark on the calcium fluoride slide with 50 steps between each spectral acquisition. The monochromator slit was set at 50µm, and the recorded spectra were centred at 1150 cm^{-1} and stored on the system's P.C. All of the spectra were then white light corrected, baseline corrected and truncated to 450 – 1850cm^{-1} as outlined in Stone (2001).

5.4.5.3. Spectra acquisition from the bladder samples.

The remaining bladder tissue (either TURBT sample or biopsy) following sectioning for histological grading, was removed from its backing acetate, placed on a calcium

fluoride slide or glass slide and passively warmed to room temperature. The bladder biopsy samples, which had been orientated with the epithelial surface on the side, were re-orientated with the urothelial/epithelial surface facing upwards. Therefore the spectra obtained were from the urothelium, which mimics an in vivo setting.

An x20 MIRPlan ULWD Olympus microscope objective was used to measure bladder spectra, with an acquisition time of 10secs at full laser power. The monochromator slit was set to 50µm and spectra were centred at 1150cm^{-1} and stored on the system's P.C. Approximately 10 spectra were taken from each sample in a random fashion. All of the spectra were then white light corrected, baseline corrected and truncated to 450 – 1850cm^{-1} as outlined in Stone (2001).

5.5. Kerr - gated Raman spectroscopy.

Raman spectroscopy of tissue is usually limited to sampling of the first 1 – 200 microns from its surface. Furthermore dark tissue fluoresces in such a way that the important Raman information is buried within the noise of the fluorescence spectral background. It was thought that both these problems may be overcome by combining Raman spectroscopy and the Kerr - gated technique.

The following experiments were performed at the Rutherford Appleton laboratory (a UK national science facility) and were therefore allocated limited laboratory time for system optimisation and measurements. This restricted much of the following studies to

proof of principle, with the expectation that further beam time would be gained to extend the study in the future. This unfortunately is beyond the time available for this body of work.

5.5.1. Instrumentation

The Kerr gating system is based on the high throughput 4 picosecond optical Kerr shutter that has been described in previous publications by Matousek et al (1999, 2001). The Kerr gate is made up of two crossed polarisers (41x 41mm, Glan Taylor polarisers) and a Kerr medium consisting of a 2mm optical cell that is filled with CS_2.

When the gate is closed, the light from the sample is blocked as the polarisers are in cross orientation. When the gate is open the light collected from the sample has its polarisation rotated to allow it to pass through the cross polariser. The gate is opened by a short 1 picosecond gating pulse at 800nm. This bypasses the polarisers and creates a transient anisotropy within the Kerr medium, this then acts to rotate the polarisation of the light from the sample, (Figure 5.6), this effect lasts for about 4 picoseconds.

The spectra were collected using a conventional Raman spectrometer (Spex, Triplemate). To prevent residual elastically scattered light from the 488nm probe laser entering the spectrometer a Kaiser holographic notch filter was used. To also prevent the residual 800nm gating beam scatter from entering, a saturated copper sulphate solution in a 1cm thick optical cell was placed in front of the spectrometer slit.

The Raman scattered light was collected in 180º geometry using a lens with f-number 2. A liquid nitrogen cooled, back illuminated NIR CCD (Andor Technology) was used to record the Raman spectra from the tissue.

The probe wavelength used was 488nm, and the pulse duration was 1 picosecond. The pulse energy at the sample was 5 μJ (1 kHz) corresponding to 5 mW of average power. The beam was focused down to 300 μm diameter spot.

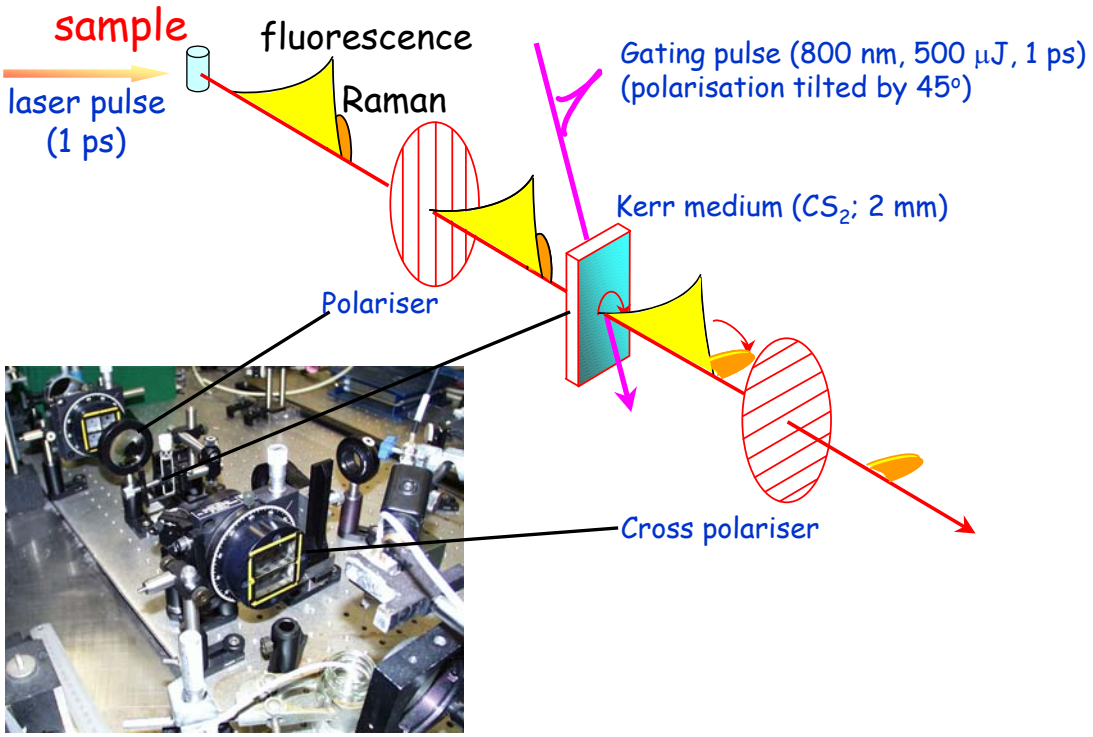

Fig 5.6: A diagram and picture showing the Kerr gating Raman system.

5.5.2. Spectra acquisition.

All spectra were acquired following daily calibration of the spectrometer using acetylnitrile.

5.5.2.1. Spectra acquisition from the prostate sample.

Prostate samples were obtained by taking a chip at TURP. The samples were then snap frozen in liquid nitrogen and transferred to a -80°C freezer for storage.

At the time of the experiment the tissue was passively warmed to room temperature and placed on a cell containing urea crystals. Urea is very strongly Raman active, and was chosen to allow a demonstration of probing of Raman spectra at depth through the prostate tissue. The spectra were obtained for 20 seconds and 5 accumulations at varying distances through the tissue, i.e. at various time delays following the laser probe excitation pulse.

A simple approximation as to the distance traveled by the incident photons in the tissue can be made (the refractive index of the tissue was taken to be 1.4). In a time of 1ps the photons will have traversed approximately 0.2mm of the tissue. This will not necessarily be in a straight line as the tissue is highly scattering.

By taking the scattering coefficient, μ_s to be 48 mm^{-1} and the absorption coefficient, μ_a to be 1.9 mm^{-1} (for epithelial tissue at 577nm) [Smithies 1995] an optical depth (OD) can be calculated from

$$OD = \frac{1}{\mu_s + \mu_a}$$

The approximate optical depth in prostate tissue for 488nm is 0.02mm.

5.5.2.2. Spectra acquisition from the bladder sample.

Bladder samples were collected at cystoscopic procedures including TURP (normal biopsies) and TURBT. The samples were then snap frozen in liquid nitrogen and transferred to a -80°C freezer for storage.

At the time of the experiment the tissue was passively warmed to room temperature and placed on a cell containing uric acid. Uric acid is very strongly Raman active, and was chosen to allow a demonstration of probing of Raman spectra at depth through the bladder tissue. The spectra were obtained for 20 seconds and 5 accumulations at varying distances through the tissue, i.e. at various time delays following the laser probe excitation pulse.

As calculated for the prostate gland in section 5.5.2.1, the approximate optical depth in bladder tissue for 488nm is 0.02mm.

5.5.2.3. Spectra acquisition from dark tissue (kidney and liver).

Pig's liver and kidney were purchased from a local supermarket and kept refrigerated until used. When needed the tissue was cut into thin slices and placed on a glass slide ready for sampling with the laser. Obviously human tissue would have been more favourable for this experiment. However this was a first line experiment to assess the Kerr gate technique on fluorescing tissue and with the time constraints it would have been difficult to get ethical approval or to recruit patients for the use of human tissue. The animal tissue will still exhibit similar fluorescence and Raman properties, within the range of those necessary to perform this specific study.

To demonstrate the ability to obtain Raman spectra from dark tissue without fluorescence we performed two sets of measurements; the first involved obtaining spectra from the liver and kidney without the use of the Kerr gate, and the second involved obtaining spectra with the Kerr gate. The spectra were obtained at different wavelengths to assess whether different components would be resonantly enhanced.

5.6. Analysis of the spectra.

5.6.1. Empirical analysis (univariate / bivariate analysis).

Empirical analysis was the method used by Alfano et al (1991), to analyse the difference between spectra taken from normal breast tissue, benign breast tumour and malignant breast tumour. He found that by looking at the ratio of the peak intensities at

1445 cm^{-1} and 1651 cm^{-1}, that there was a difference between the pathological groups and this could be used to differentiate between them spectrally.

This type of analysis is widely used to initially construct diagnostic algorithms. It is a supervised method in that it can be used to differentiate between pathological groups purely on spectral variance when the pathology is known. It is also useful when prior knowledge of the tissue is not available (in this circumstance it is an unsupervised method) or patterns in multiple spectra are under investigation. Empirical analysis is extremely good when being used for simple solutions or single constituents, as by comparing the ratios of relevant peak intensities, concentrations can be calculated.

Biological tissue however is a lot more complicated. Empirical analysis can be used with tissue by measuring the peak intensities of selected random peaks within the tissue spectrum to give a peak intensity ratio. Then by comparing this with the same peak intensity ratios in each pathological group it may be possible to differentiate between the groups. Alfano et al (1991) found that the peak intensity ratios between 1445 and 1651 cm^{-1} was 1.23, 0.93 and 0.87 respectively for normal breast tissue, benign breast tumour and malignant breast tumour.

The disadvantage of this method of analysis is that only a small proportion of the measured data is being used in the analysis. As biological tissue is complex a method of analysis therefore that incorporates as much of the measured data as possible is more likely to provide a more vigorous method of detection and diagnosis of biological pathologies [Shim 2000].

Multivariate analysis is the name for analytical methods that try to achieve this by utilising large numbers of variables.

5.6.2. Multivariate analysis.

Multivariate analysis allows virtually all of the data contained within a measured spectrum to be used in the analysis. This is much better for biological tissue due to the subtle changes that occur between the pathological groups being classified and the complexity of the tissue spectra.

The techniques used can be either supervised or unsupervised. Unsupervised techniques identify natural clusters or groupings and can be used to differentiate between pathological groups purely on spectral variance. This is useful when prior knowledge of the spectra is not available or patterns in multiple spectra are under investigation. Supervised techniques require prior knowledge of the origins of the spectra within the training set, i.e. class / pathological identity.

There are a number of software packages that are commercially available for multivariate analysis. PLS-toolbox® for use with Matlab® (Eigenvector Technologies, Manson, Washington, USA) is one of these and was adapted for use with the data in these studies [Stone 2001]

5.6.2.1.Principal component analysis.

Principal component analysis (PCA) is an orthogonal technique that is unsupervised. Therefore it does not take into account the pathology of the tissue measured. It involves the calculation of principal components (PC's) that describe the greatest variance from the mean. They accurately characterise the entire range of spectral variations.

A PC is a product of the load and the score of the spectrum whereby the load describes progressively decreasing amounts of variance from the mean of the dataset being analysed and the score is the value by which the load must be multiplied by to reconstruct the original spectrum from the mean. We tend to use up to 25 PC's in our analysis.

PCA is a technique that is used as a means of data reduction / compression. Therefore the data to be processed is reduced without actually losing any of the functional information. It allows collinear spectral variations to be considered together. Many spectral features have the same source of variation and are therefore said to be collinear i.e. the same information is found at more than one peak in the spectrum.

Constituent spectra within the tissue spectra have multiple peaks, therefore a change in concentration of the constituent between the pathologies will change the peaks in the total spectrum. This collinear variation can be picked up by PCA in the form of the loads. If a load reflects a significant change in the concentration we can gain some insight into the molecular differences between pathologies. Also the loads for all the spectra in a spectral dataset or pathology are the same, therefore a tissue spectrum can be represented by just a small set of numbers, the PC scores. In this way the amount of data to be processed can be reduced without actually reducing the amount of functional data available.

The problems with PCA tend to be due to systematic errors within the spectra such as unfiltered cosmic rays, inconsistent background removal and drift in wavenumber or intensity axes. Diagnostically significant PC's are those that show a significant difference in value between the pathological groups. These are determined by analysis of variance (ANOVA) which will be described later in the section.

5.6.2.2.Linear discriminant analysis.

Linear discriminant analysis (LDA) is a supervised technique whereby the identity of the class / pathological group is required. Therefore prior knowledge about the samples in the training set is required. LDA selects the linear combination vectors / direction in spectral space that provide the maximum value for the ratio between inter group variance and intra group variance for the optimal separation of 2 groups. Therefore you get linear discriminant functions that maximise the variance in the data between the pathological groups and minimise the variance between the members of the same pathological group. If there are more than 2 groups the multivariate discriminant analysis is used. This is the multi-group extension of LDA using (n-1) orthogonal directions than best separates (n) groups. For this thesis however I will use the umbrella term LDA. LDA is a technique therefore that is used to accentuate the clustering of different pathological groups.

The disadvantage of LDA however is that the input variable (spectral wavenumbers) in this technique should be less than the number of spectra in the dataset. To overcome this PCA led LDA is used.

5.6.2.3. **Principal component analysis led linear discriminant analysis.**

PCA led LDA is a technique whereby the PCA is performed first to obtain PC's and the PC scores are then used as the input variables instead of the spectral wavenumbers. In

this way the input variable number is reduced. Like LDA, PCA led LDA is a supervised technique. The LDA goes through each of the PC's to ascertain whether they are useful in providing the maximum value for the ratio between inter group variance and intra group variance for the optimal separation of the pathological groups. Each PC is given a weight as to its ability to discriminate. It is then used to construct diagnostic algorithms for different pathological groups. Once constructed the diagnostic algorithm needs to be tested to ascertain its accuracy in predicting the confirmed histological diagnosis for each spectrum. The disadvantage of this type of analysis is that if there are too many PCs compared to a small sample size then you can overfit the data as there is not enough variation described in the dataset to cover a patient population.

Also given that the gold standard Gleason scoring system and the histopathological grading for bladder are subject to both inter and intra observer error therefore the prediction madel may be incorrectly trained which may lead to groups that are misclassified to a greater extent than others.

5.6.3. **Analysis of variance.**

Analysis of variance (ANOVA) can be used with any of the previously described techniques. It is a technique that is used to investigate the relationship between a

response variable (the measurement) and one or more independent variables.

In the case of the empirical analysis ANOVA works by compiling a matrix of all the possible combinations of peaks therefore all the peak intensity ratios are calculated. The

matrix compiled is a (n x m) matrix whereby the spectra are represented by (n) and the intensity value by the (m). Therefore in the case of the PCA led LDA it is used on the PC's to ascertain which of the PC's are significantly able to differentiate between the pathologies.

ANOVA extends the two sample t-test to a more general null hypothesis comparing the equality of more than two means versus them all not being equal. The t-test is used for testing the equality of two population means [Kendall 2002].

ANOVA results in F values whereby the greater the F value the greater the difference between the pathological groups. When the F value is above a critical value (F-crit), there is a statistical difference between the groups. The F-crit value in this study is set at 99.9% or $p<0.001$. Two of the high F values can be plotted against each other to show how efficiently the variables (PC's / peak ratios) differentiate between the pathological groups.

5.6.4. Testing the diagnostic algorithm.

The diagnostic algorithms can be tested by two means. The first method is the 'leave one spectrum / sample out' cross validation method. This method involves leaving a spectrum or all spectra from a sample out of the test data, performing PCA led LDA on the test data to produce an algorithm and then testing the algorithm with the left out spectrum / sample. The process is then repeated using all of the spectra / samples in the original dataset. The 'leave one spectrum out' method is what was previously used in

urology as there was only one dataset and sample numbers were limited. The disadvantage of this is that the algorithm was constructed using spectra from the same sample as the spectrum that was left out. This can therefore result in bias and an inaccurate result in terms of sensitivity and specificity of the algorithm. A more rigorous means of testing is by using a completely different dataset to test the diagnostic algorithm. However with a limited number of samples this can be an acceptable way of testing the data

5.6.5. Least squares analysis.

To date the spectral fingerprints have only been used for classification of pathology groups. However, one of the objectives of this study was to attempt a first approach at elucidating the biochemical origins of spectral differences seen in the signals between pathologies. This involved the use of ordinary least squares fitting of the spectral data with spectra taken from the pure standards listed in section 5.1.

Regression is a process that is used to estimate the mean outcome of a population by analysing the relationship between variables. In this way it can help us to understand the relationship between the given variables.

For example if you assume that there are two continuous variables (X and Y) measured on each subject and an explanation as to how changes in variable Y are predicted by

changes in variable X is required, then Y is the dependent variable and X the independent variable [Altman].

To achieve the understanding for the changes a line (which can be linear (straight) or non-linear (curved)) is formed between the variables whereby the line is fitted so that each point (variable) is as close to line as it can be. In this way a line of 'best fit' is formed. This is achieved by using a regression equation [Altman].

The most widely used means of 'fitting' a regression equation is by using a computer based mathematical method known as least squares. As was explained earlier the line fits well if it passes close to each point therefore the least squares regression line is the line for which the sum of the squared distances from the points to the line is minimised.

If the variables are unrelated then the line formed will have a gradient of zero (a horizontal straight line) and this is known as the regression coefficient which will also be zero.

The PLS-toolbox® (Eigenvector Technologies, Manson, Washington, USA) for use with Matlab® was adapted for use with the data in these studies [Stone 2001]. The mean spectra for the pathologies and the constituents were ascertained allowing for further analysis to occur. The fitting of the mean spectra of the constituents to the mean spectra of the different pathologies in the bladder and the prostate gland was done by using 'ordinary least squares' analysis. This is explained simply below:

$$X = cS + E$$

Where S is the matrix of spectral components, c is the matrix of concentrations to be predicted, and X is the measured spectra. This can be used to provide a 'best fit' of the spectral components or basis spectra found within the measured spectra. The assumption is made that the residual is minimised and that the spectral components selected are the main components of the spectra.

$$c = \frac{(X - E)}{S}$$

The disadvantage with this technique is that any co linearity in the components selected will skew the fit. An example being amino acids and the proteins containing them being used in the model. Observation of the residual E (E=X-cS) enables the quality of the fit to be observed and any remaining features of the spectra to be included in the next iteration of the model.

6. Results.

6.1. Constituent spectra.

The constituent spectra were obtained as was described in section 5.4.5.1. The mean of the spectra from each constituent was then obtained by using Matlab® which was adapted for use with the data in these studies [Stone 2001]. The mean spectra are shown below in Figures 6.1 to 6.12.

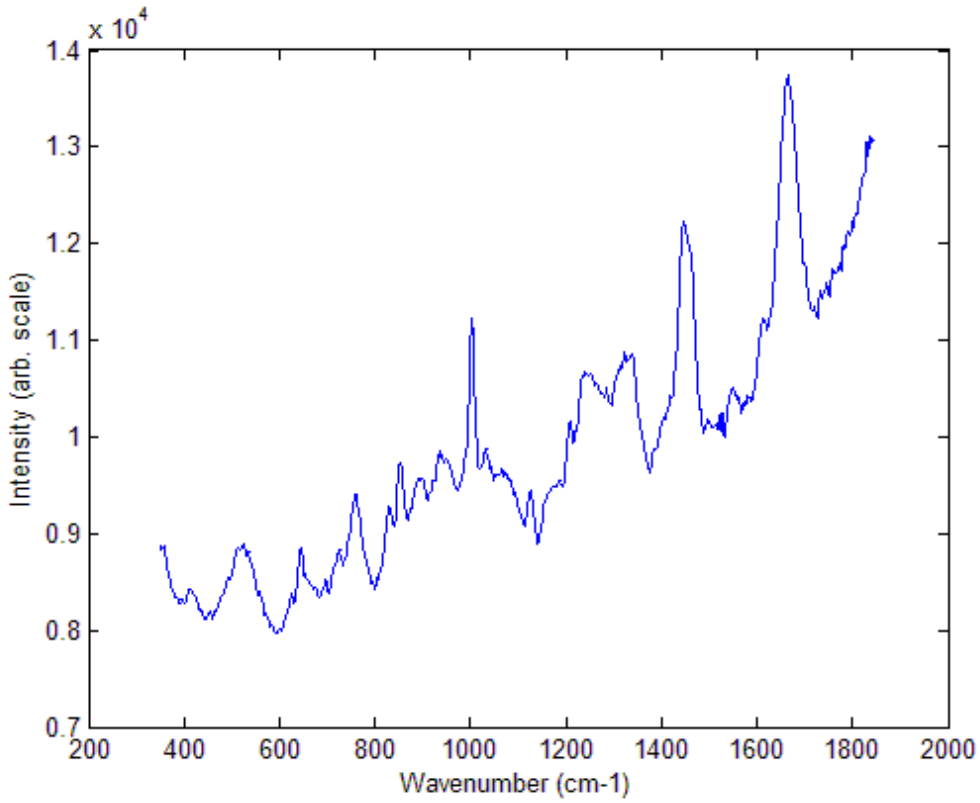

Fig 6.1. The mean spectrum of actin.

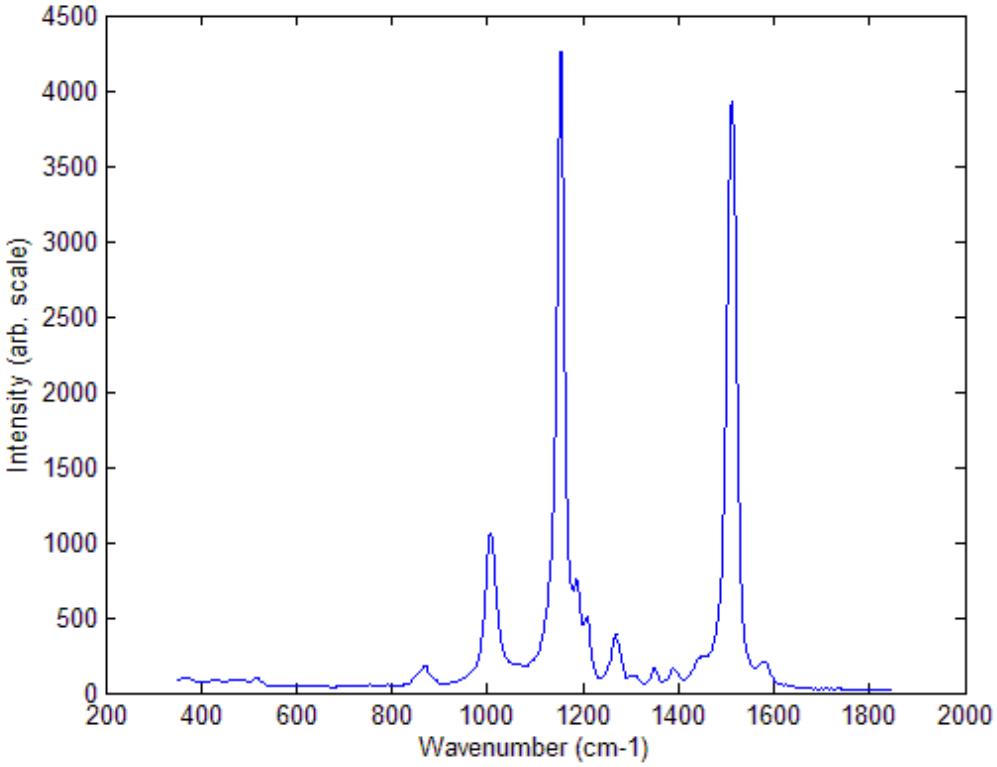

Fig 6.2. The mean spectrum of ß carotene.

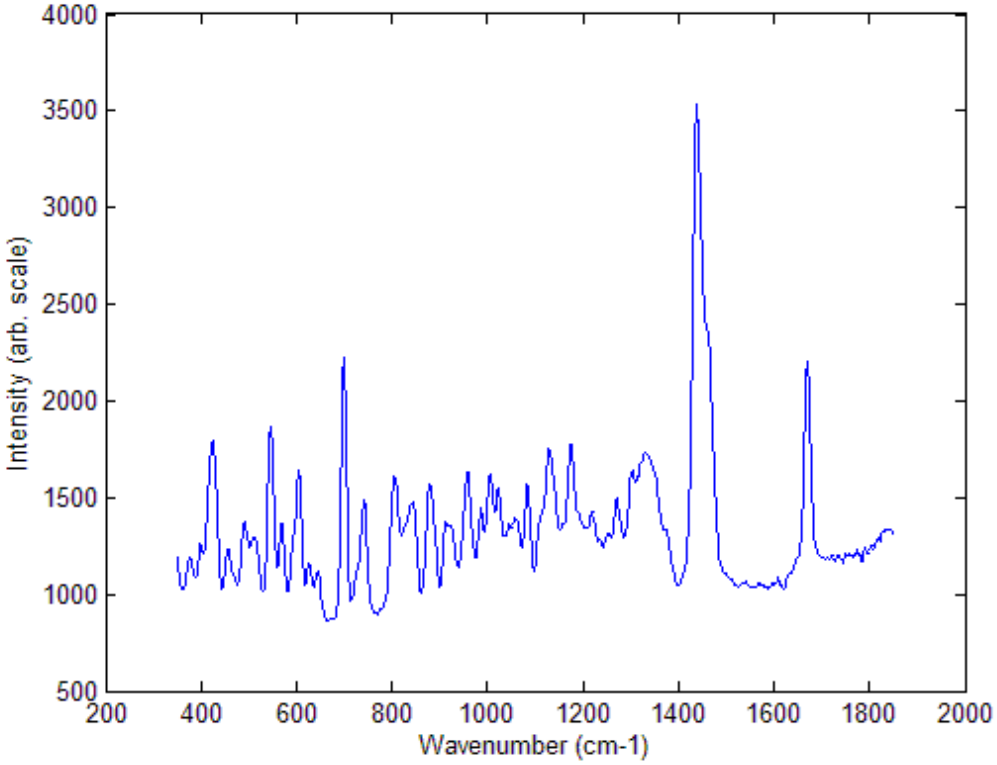

Fig 6.3. The mean spectrum of cholesterol.

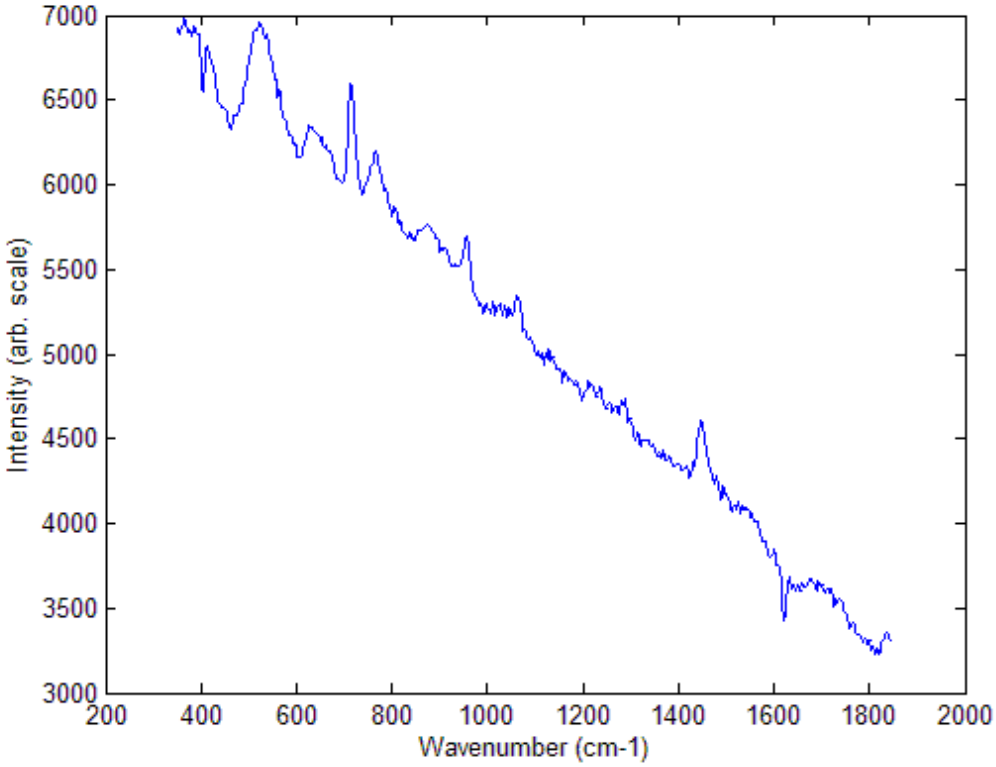

Fig 6.4. The mean spectrum of choline.

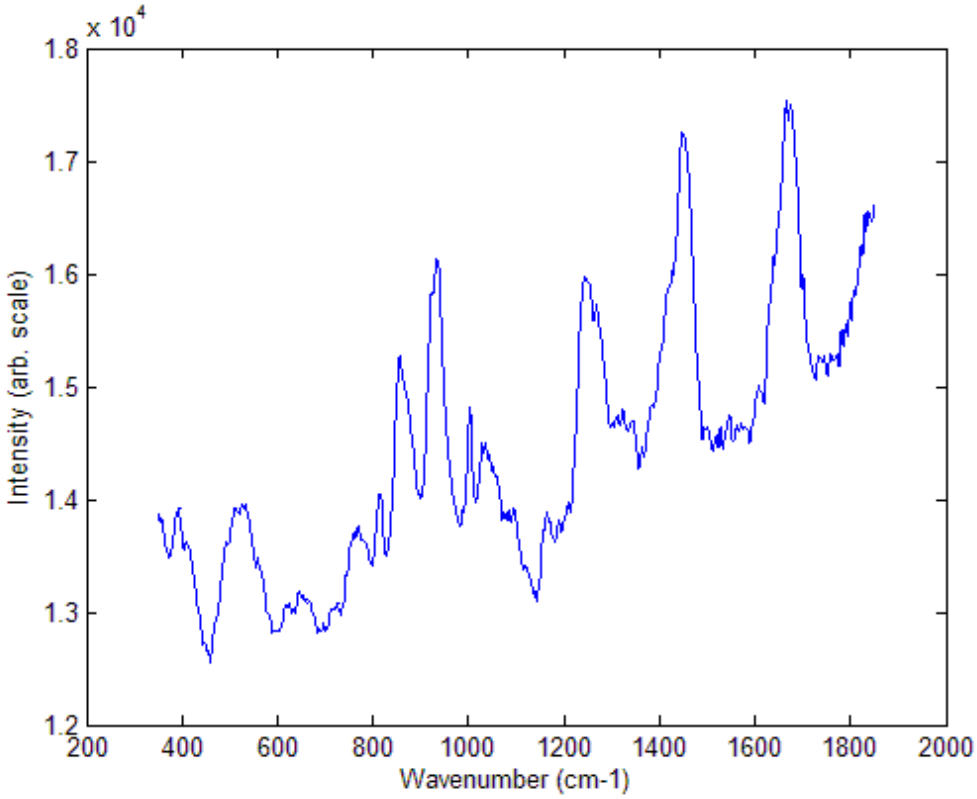

Fig 6.5. The mean spectrum of collagen type 1 (col1).

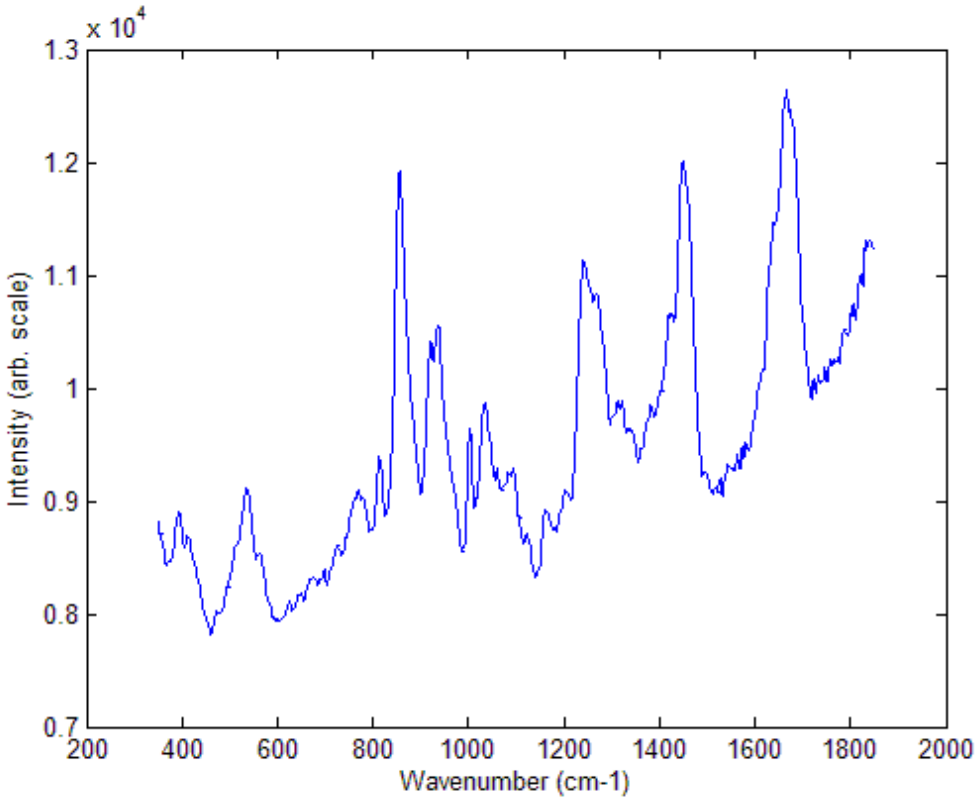

Fig 6.6. The mean spectrum of collagen type 3 (col3).

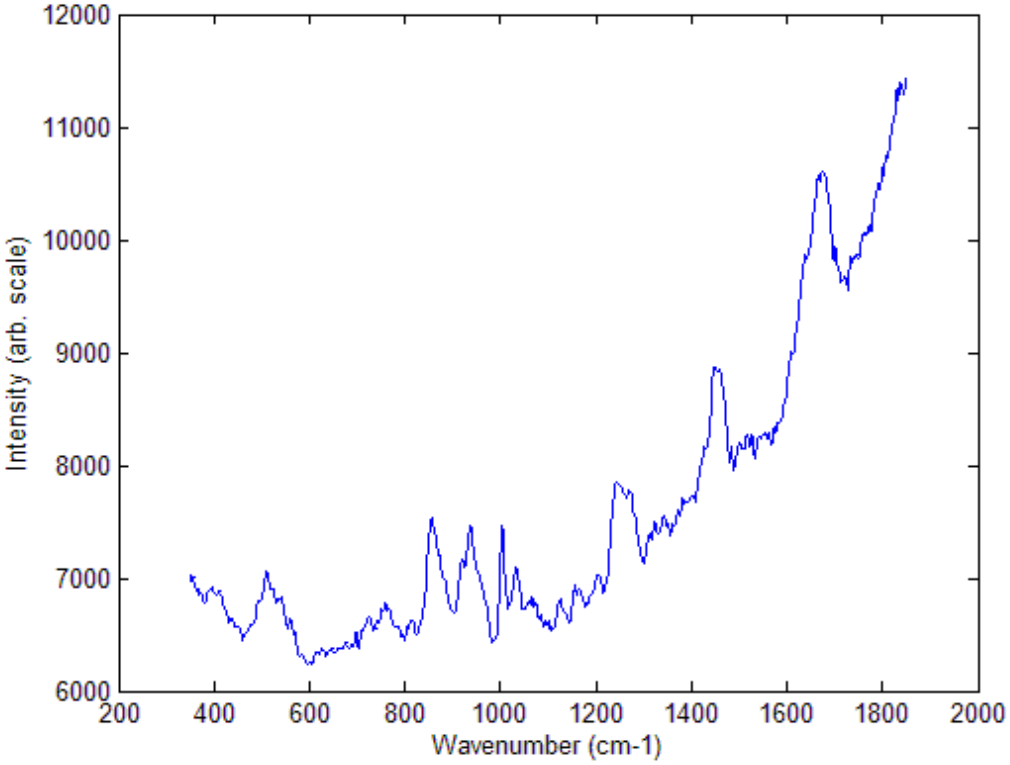

Fig 6.7. The mean spectrum of collagen type 4 (col4).

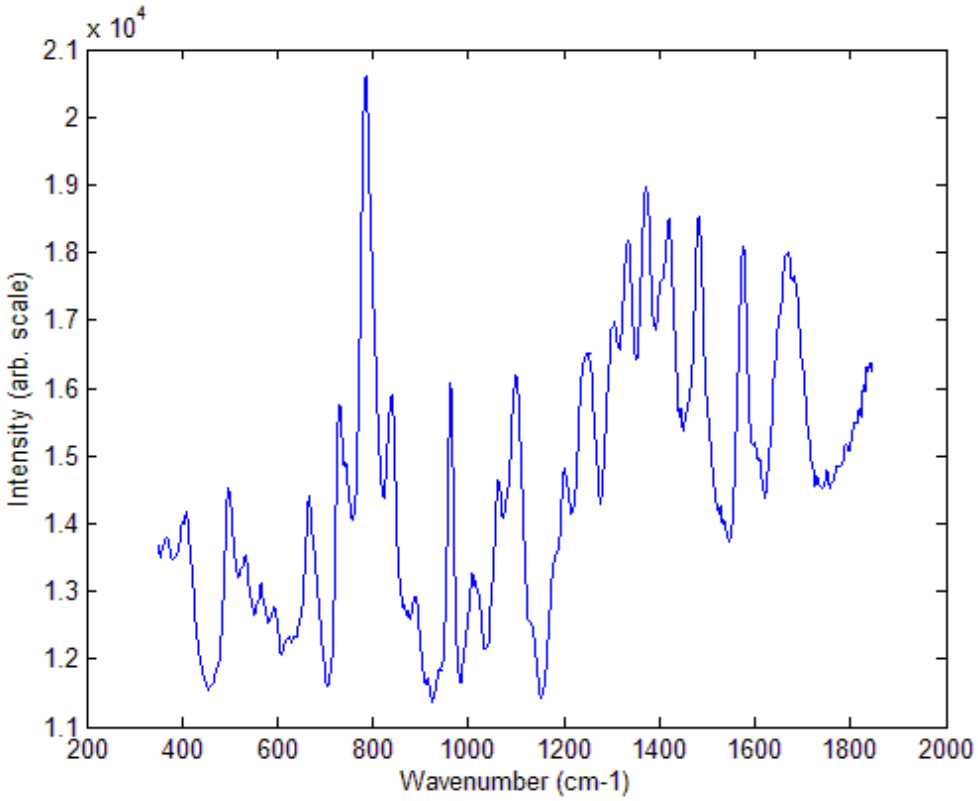

Fig 6.8. The mean spectrum of DNA.

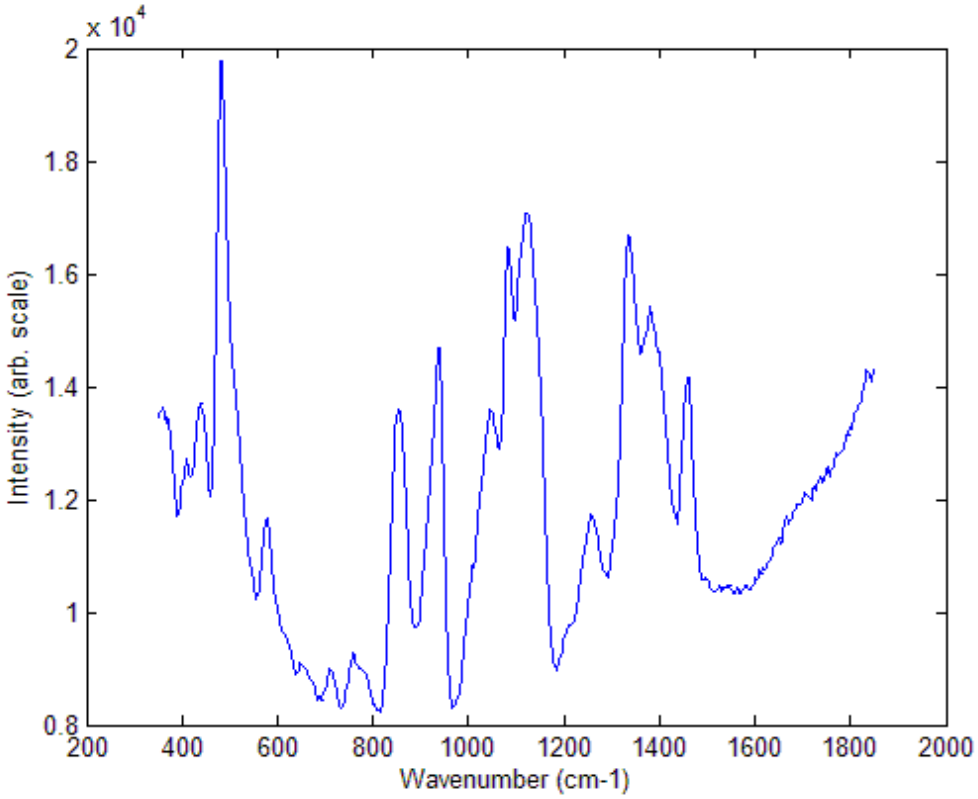

Fig 6.9. The mean spectrum of glycogen.

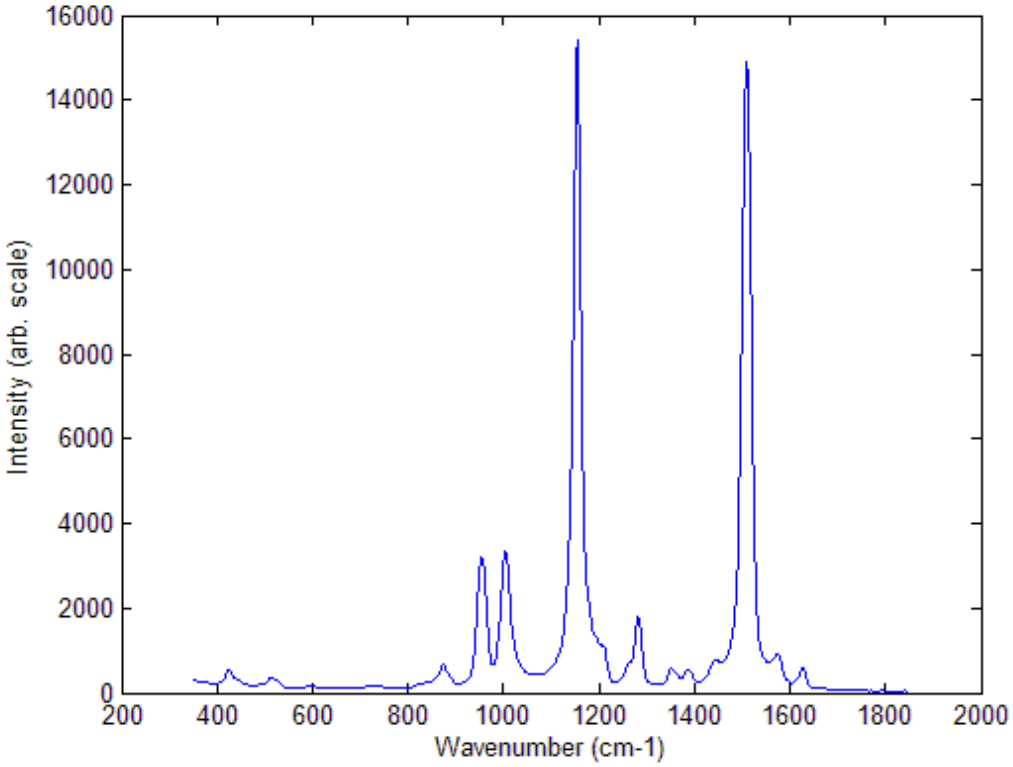

Fig 6.10. The mean spectrum of lycopene.

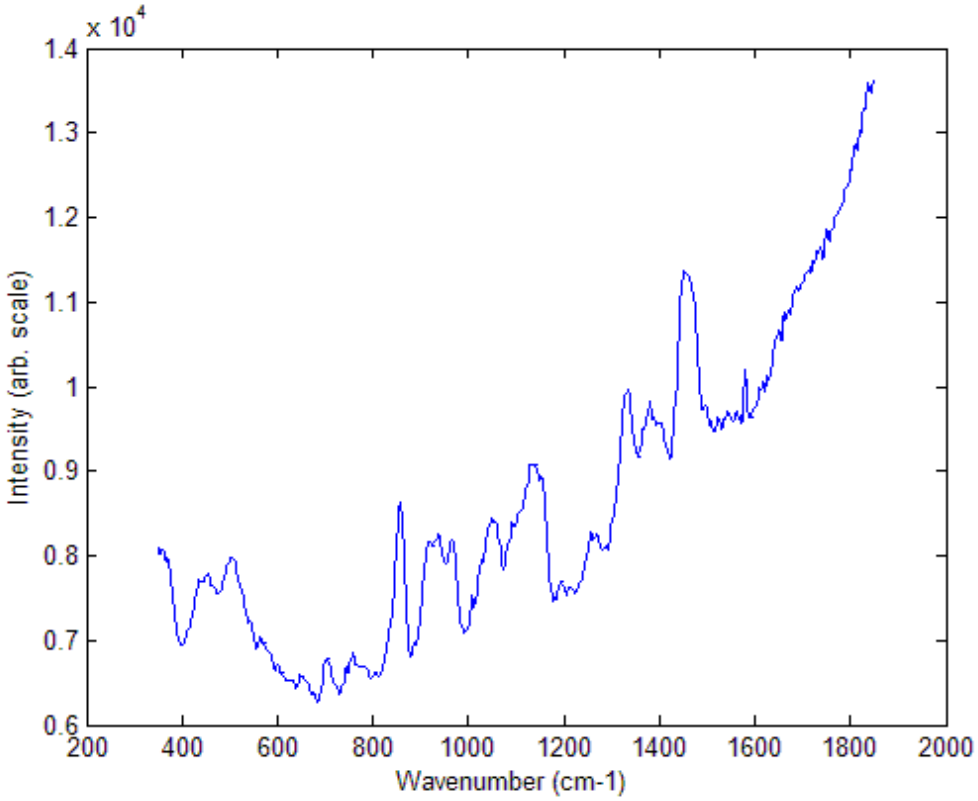

Fig 6.11. The mean spectrum of oleic acid.

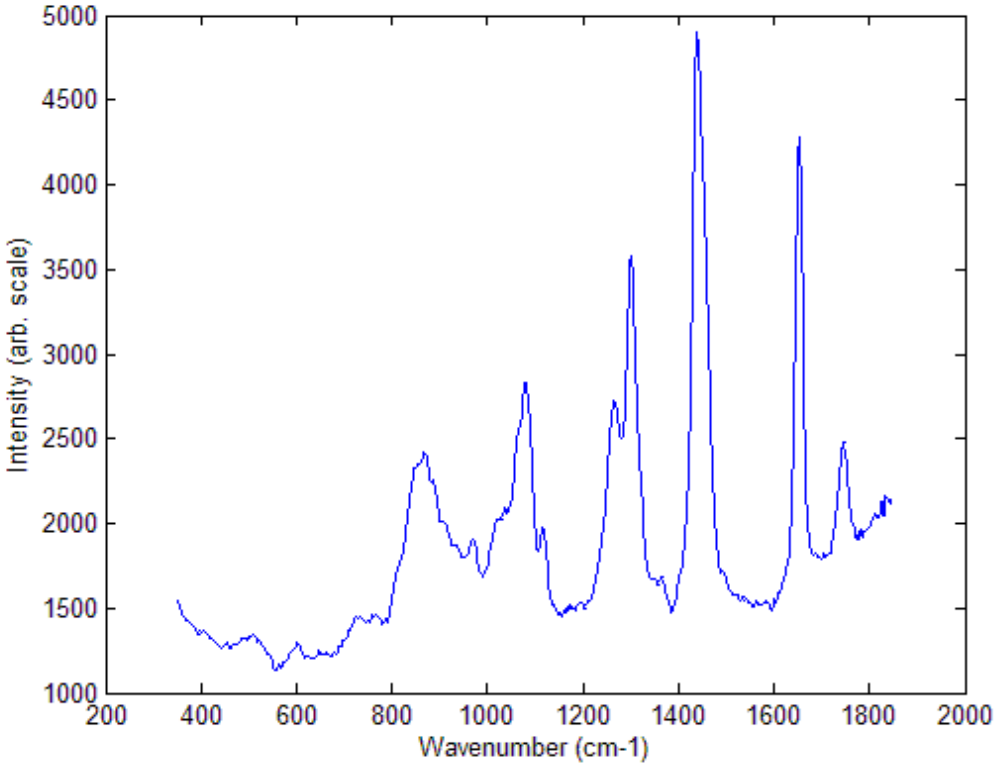

Fig 6.12. The mean spectrum of triolein.

6.2. Analysis of tissue spectra.

Prostate and bladder tissue were obtained as outlined in sections 5.2.1 and 5.2.2. Raman spectra were then obtained from each of the tissue samples (following procedures outlined in section 5.4.5) and were grouped according to the histopathology of the sample as determined by a consultant histopathologist. The spectra were then analysed as discussed later in the chapter.

Figure 6.13 shows a mean spectrum taken from a prostate sample and Figure 6.14 one taken from a bladder sample. The principal peaks have been labelled and the tentative assignments for these peaks are shown in table 6.1. These principal peaks are used in the empirical analysis of the spectra.

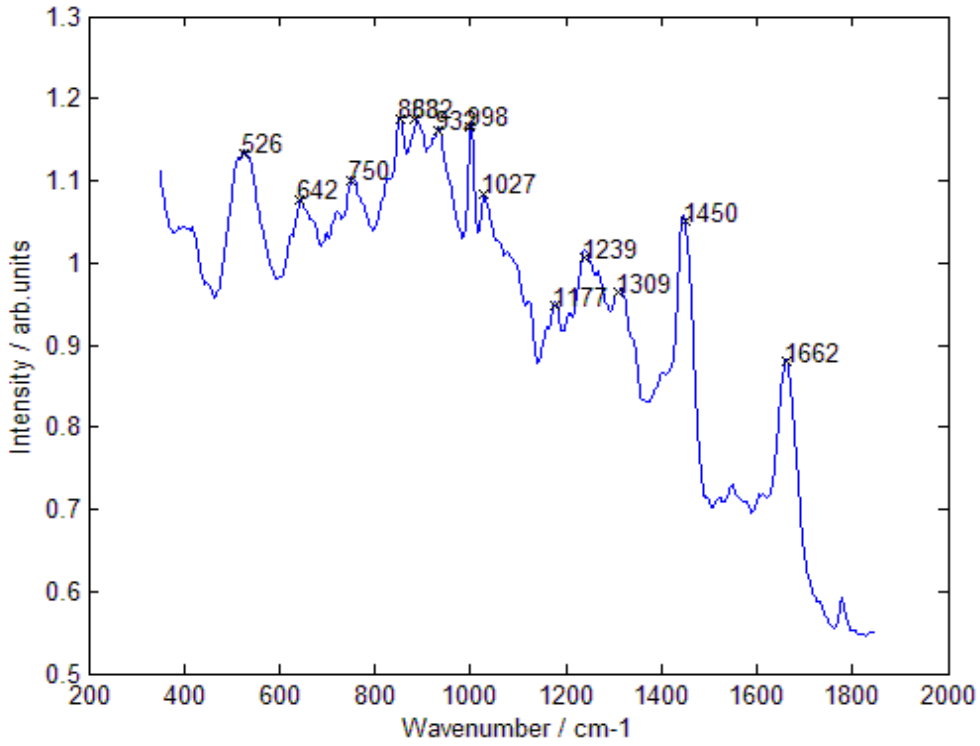

Fig 6.13. A mean spectrum taken from a prostate sample.

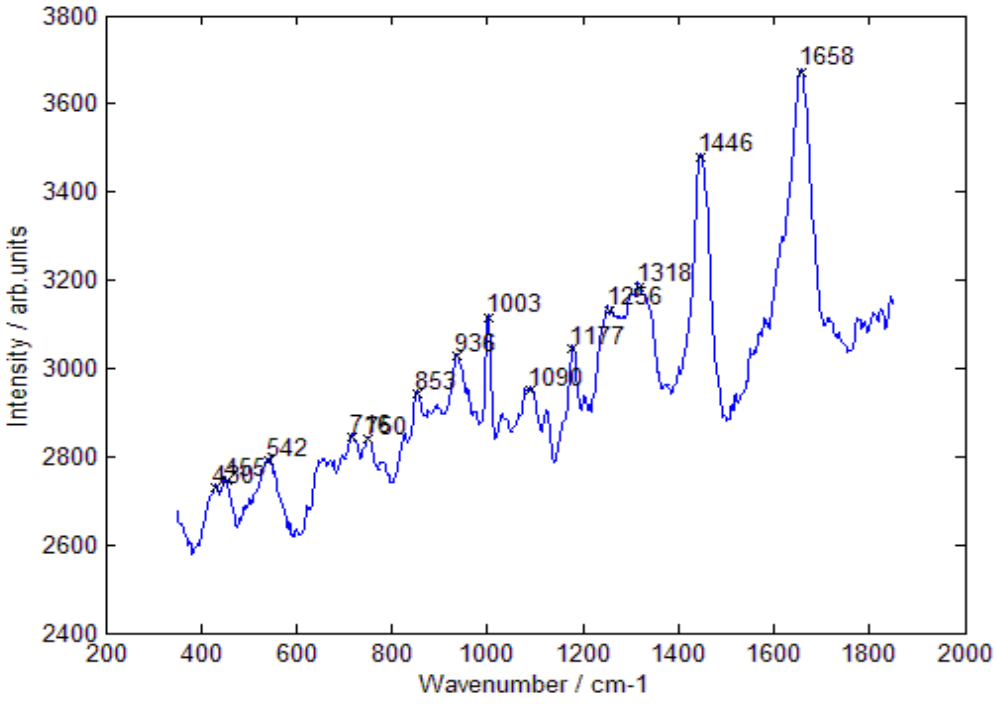

Fig 6.14. A mean spectrum taken from a bladder sample.

Peak Position (cm-1)	Major peak assignments
430	Cholesterol
455	Unassigned
526	Disulphide (C-S-S-C gauche-gauche-gauche)
542	Disulphide (C-S-S-C gauche-gauche-trans)
642	Tyrosine
716	Nucleotide peak
750	Symmetric breathing of thymine
853	Tyrosine
882	Tryptophan
932	Skeletal C-C: α -helix
936	Hydroxyproline & C-C collagen backbone
998	Phenylalanine
1003	Phenylalanine
1027	Proline
1090	PO_2^- (DNA)
1177	Tyrosine, phenylalanine
1239	Amide III: β- sheet
1256	Cytosine
1309	CH_2 twist/wag (lipids)
1318	CH_2 symmetric wagging (lipids)
1446	CH_2 bending mode of proteins and lipids
1450	C-H deformation
1662	Nucleic acids

Table 6.1. Table showing the tentative assignments for the principal peaks of the spectra [Stone 2001].

6.2.1. Analysis of the prostate samples and their spectra.

Table 6.2 shows the number of prostate samples obtained (section 5.2.1), their pathology as assessed using the technique described in section 5.3.1 and the number of

spectra obtained (using the technique described in section 5.4.5.2) for each pathology. The spectra were then analysed using the analytical methods described in section 5.6 and the mean spectrum for each pathological group was obtained. All the prostate spectra measured are shown in Figure 6.15. There are a number of random cosmic ray events superimposed over the tissue spectra. It can be seen that these have little effect on the mean of all the spectra from benign prostatic hyperplasia (BPH), adenocarcinoma Gleason score less than 7 (GS<7) and Gleason score greater than 7 (GS>7) are shown in Figure 6.16. From Figure 6.16 it can be seen that the differences between the pathological groups are very subtle. On first glance they appear very similar with only subtle variations in peak height and positions noted between the groups.

	BPH	CaP (GS<7)	CaP (GS>7)
No. of Samples	51	4	3
No. of Spectra	1071	84	63

Table 6.2. The number of prostate samples obtained for each pathology and the number of spectra measured for each pathology.

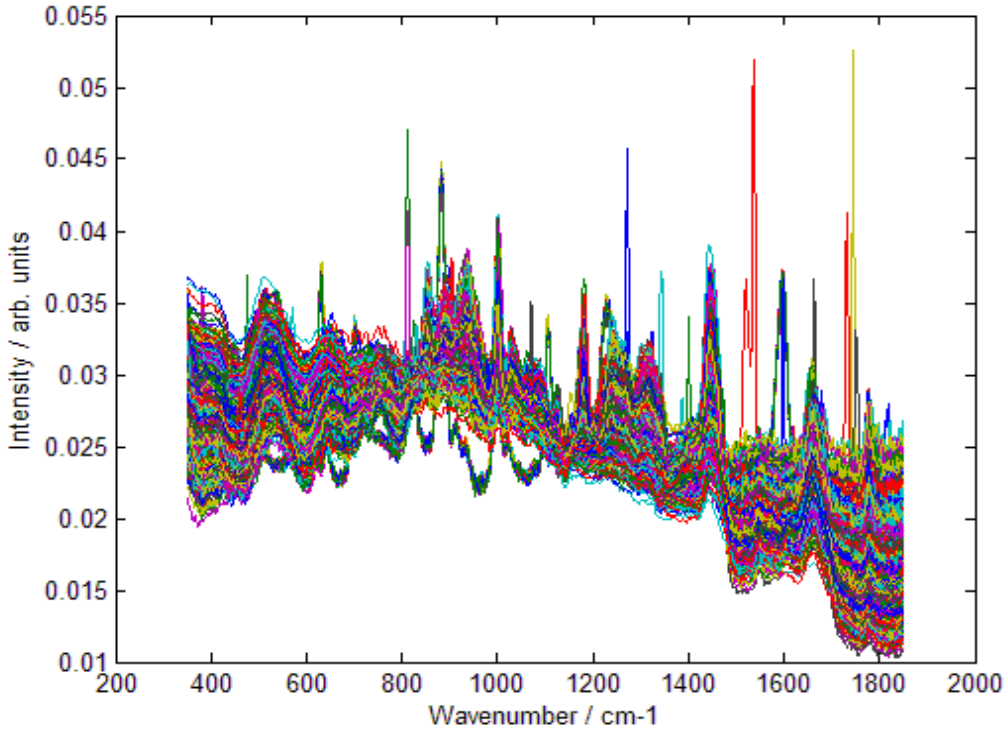

Fig 6.15. The spectra obtained for the prostate samples.

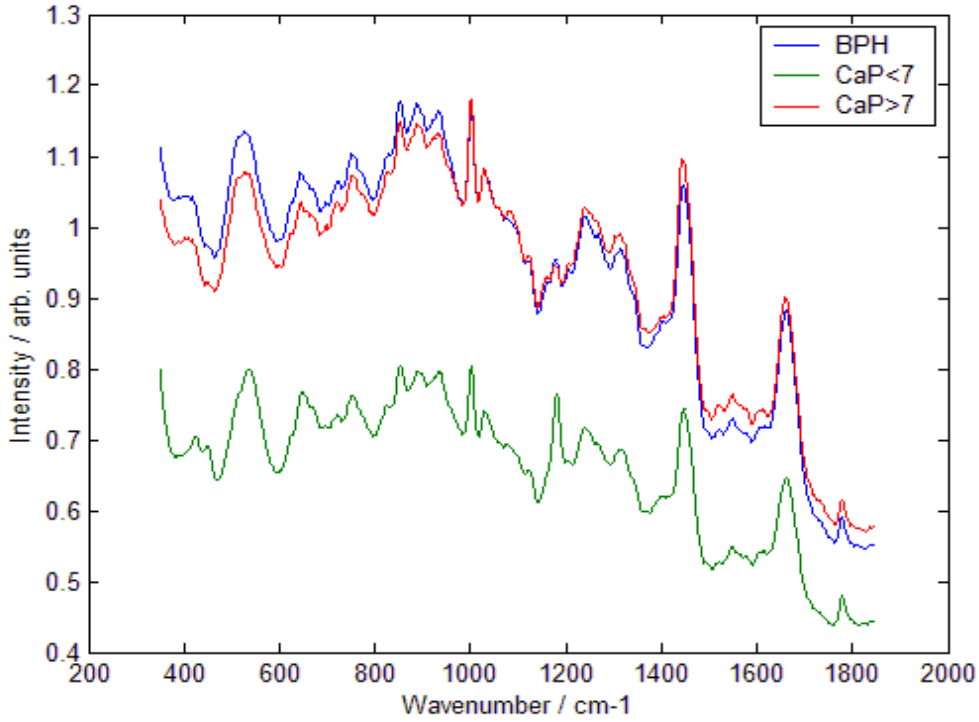

Fig 6.16. The mean spectra obtained for each prostate pathology.

Linear discriminant analysis was then used on the spectra to produce cross validation classification results. This uses a 'leave one out' method described in chapter 5.6.4. 80% of cross validated grouped spectra are correctly classified using this method. The results of this method are shown in table 6.3.

Table 6.4 shows the specificity and sensitivity of Raman spectroscopy as a diagnostic test to classify the pathology in the prostate. This was calculated from the cross validation results obtained from the linear discriminant model. This table has been included purely to help in understanding how well the preliminary model is working and also to ensure that it is comparable to work done previously in the group. The spectra from these samples were added to the bank of those already collected and will be used in future experiments.

		Raman Prediction		
		BPH	CaP <7	CaP >7
Histology	BPH	**558**	44	91
	CaP <7	10	**31**	1
	CaP >7	17	0	**46**

Table 6.3. A table showing the cross validation of the Raman prediction compared to the actual histology for the prostate samples.

	BPH	CaP <7	CaP >7
Sensitivity	81	74	73
Specificity	74	93	87

Table 6.4. A table showing the sensitivity and specificity of Raman spectroscopy as a diagnostic test to classify pathology in the prostate.

6.2.2. Analysis of the bladder samples and their spectra.

Table 6.5 shows the number of bladder samples obtained using the technique described in section 5.2.2, their pathology as assessed using the technique described in section 5.3.2 and the number of spectra obtained using the technique described in section 5.4.5.3 for each pathology. These were then analysed using the analytical methods described in section 5.6 and the mean spectrum for each pathological group was obtained. All the bladder spectra measured are shown in Figure 6.17 and the mean of all the spectra from normal, cystitis, transitional call carcinoma (TCC) grades 1, 2 and 3 and squamous differentiation are shown in Figure 6.18. It can be seen from Figure 6.18 that the differences between the pathological groups are very subtle. On first glance they appear very similar with only subtle variations in peak height and positions noted between the groups.

	Normal	Cystitis	TCC			
			G1	G2	G3	Sq. Dys
No. of Samples	39	61	6	18	3	6
No. of Spectra	390	610	60	180	30	60

Table 6.5. The number of bladder samples obtained for each pathology and the number of spectra measured for each pathology.

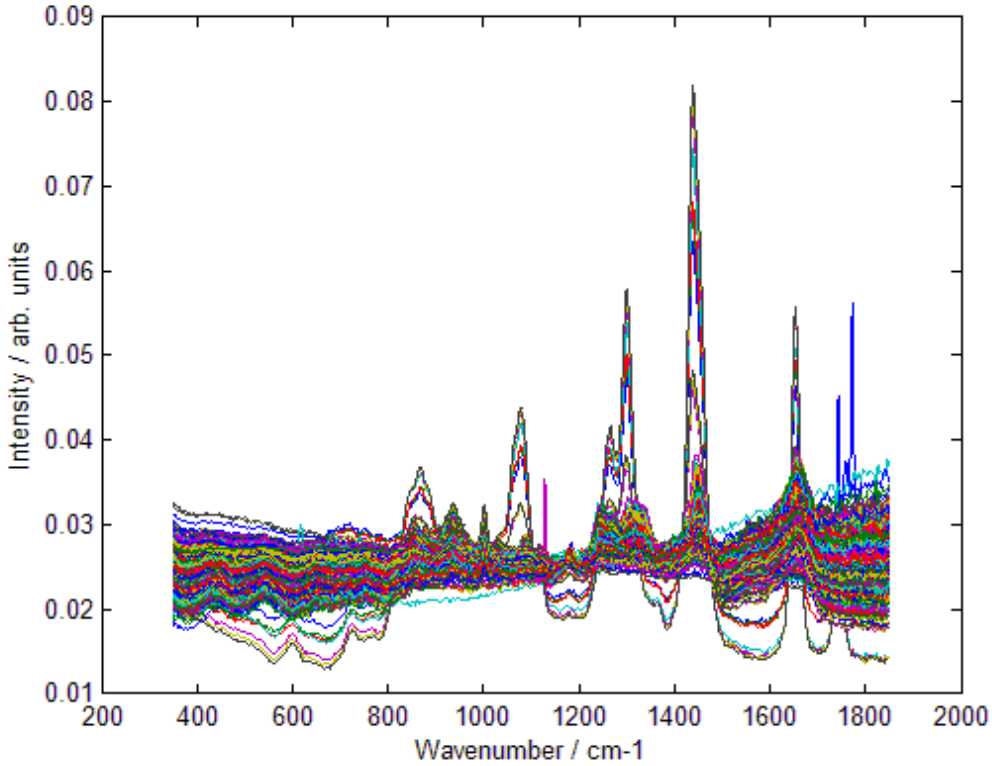

Fig 6.17. The spectra obtained from the bladder samples.

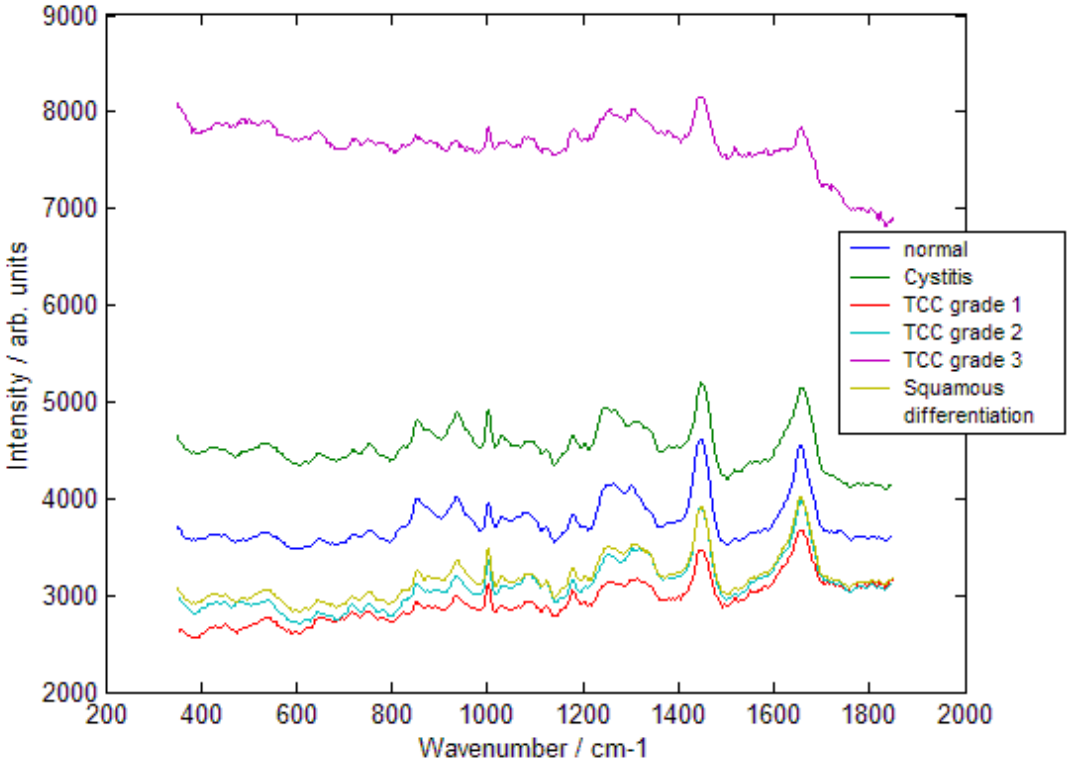

Fig 6.18. The mean spectra obtained for each bladder pathology.

Linear discriminant analysis was then used on the spectra to produce cross validation classification results. This uses a 'leave one out' method described in chapter 5.6.4. 72% of cross validated grouped spectra are correctly classified using this method. The results of this are shown in table 6.6.

Table 6.7 shows the specificity and sensitivity of Raman spectroscopy as a diagnostic test to classify the pathology in the bladder. This was calculated from the cross validation results obtained from the linear discriminant model. As was discussed for the prostate gland this table has been included purely to help in understanding how well the preliminary model is working (ie the likely prediction mis-classification will be highlighted here). Furthermore these values allowed comparison with the equivalent

work done previously in the group. The spectra from these samples were added to the bank of those already collected and will be used in future experiments.

Raman Prediction								
Histology			Normal	Cystitis	TCC			Squamous differentiation
					Grade1	Grade2	Grade3	
	Normal		**157**	54	21	0	2	7
	Cystitis		50	**175**	8	0	3	0
	TCC	Grade1	0	0	**10**	0	0	0
		Grade2	0	0	1	**27**	2	0
		Grade3	0	1	0	0	**29**	0
	Squamous differentiation		1	10	0	0	0	**19**

Table 6.6. A table showing the cross validation of the Raman prediction compared to the actual histology for the bladder samples.

	Normal	**Cystitis**	**TCC Grade 1**	**TCC Grade 2**	**TCC Grade 3**	**Squamous differentiation**
Sensitivity	65	74	100	90	96	63
Specificity	84	81	95	100	99	99

Table 6.7. A table showing the sensitivity and specificity of Raman spectroscopy as a diagnostic test to classify pathology in the bladder.

6.3. Constituent analysis of the tissue spectra.

6.3.1. Constituent analysis of the prostate spectra.

Over 1000 spectra were obtained from the prostate samples and these were analysed to give mean spectra for each of the following pathologies, Adenocarcinoma (Gleason score <7, 7 and >7, prostatitis, and normal prostate tissue. As the bank of spectra collected by the research group obtained a greater mix of pathology, this was used rather than just the spectra from the prostate samples collected by the author. The constituent spectra were fitted to the mean spectra measured (Fig 6.19) and an approximate value for the constituent concentration was obtained (Fig 6.20). In this way the biochemical basis for each pathology within the prostate was elucidated. Table 6.8 shows the relative percentages of each constituent present in each of the pathologies.

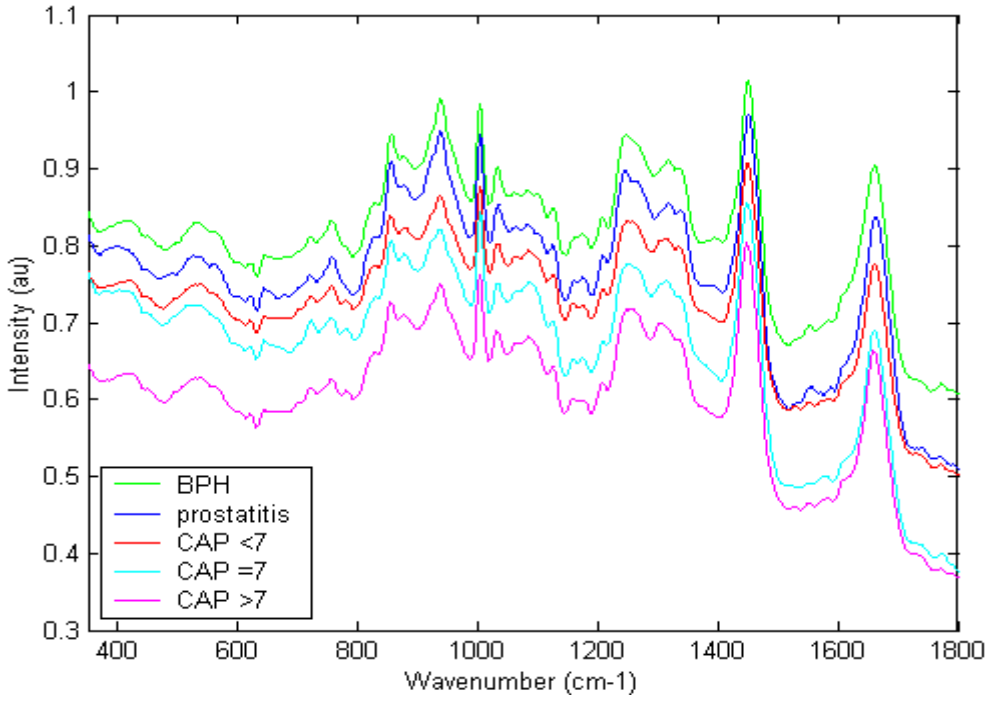

Fig 6.19. The mean spectra obtained for each prostate pathology.

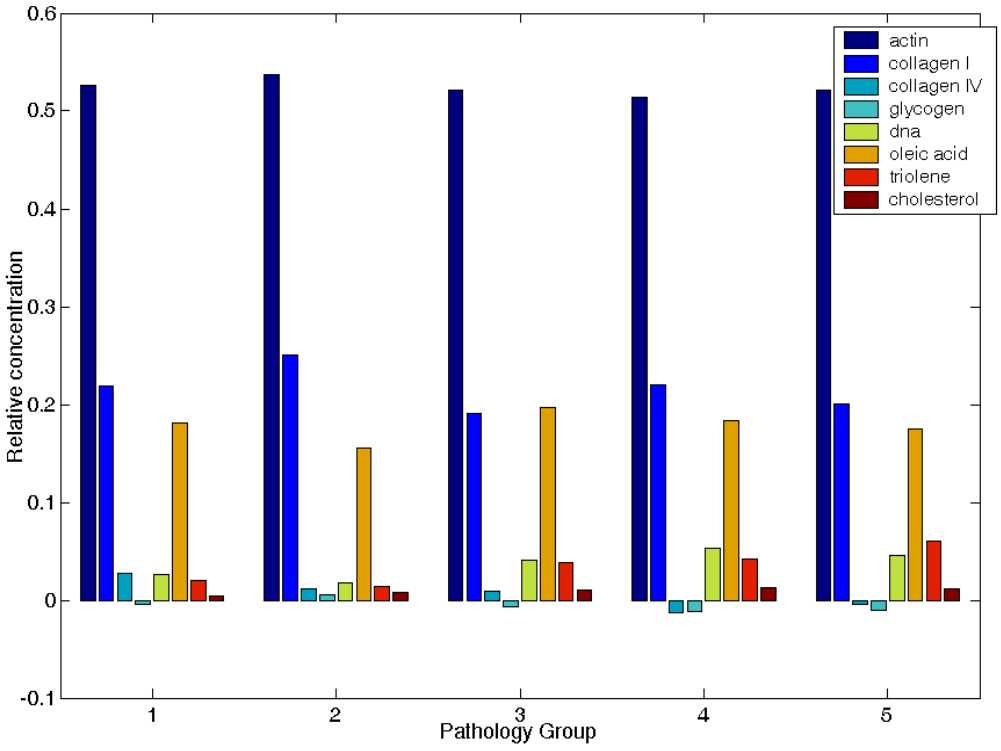

Fig 6.20. A bar graph showing the relative concentration of each constituent for each prostate pathology (the pathology relating to the groups are specified in the table 6.8).

Pathology	No	Actin (%)	Col1 (%)	Col4 (%)	Glycogen (%)	DNA (%)	Oleic acid (%)	Triolein (%)	Cholesterol (%)
BPH	1	52.6	21.9	2.7	-0.4	2.6	18.1	2.0	0.4
Prostatitis	2	53.7	25.1	1.2	0.6	1.8	15.5	1.4	0.7
Gleason <7	3	52.1	19.1	0.9	-0.7	4.1	19.6	3.8	1.1
Gleason 7	4	51.4	22.1	-1.2	-1.2	5.3	18.3	4.2	1.2
Gleason >7	5	52.1	20.1	-0.4	-1.1	4.6	17.5	6.1	1.2

Table 6.8. The relative percentages of each constituent present in each prostate pathology. Normalised to a total of unity.

6.3.2. Constituent analysis of the bladder spectra.

Over 1000 spectra were obtained from the bladder samples and these were analysed to give mean spectra for each of the following pathologies, TCC grades 1 to 3, cystitis, CIS, adenocarcinoma (adenoCa) and normal urothelium. As the bank of spectra collected by the group obtained a greater mix of pathology, this was used rather than just the spectra from the bladder samples collected by the author. The constituent spectra were then fitted to the mean spectra measured (Fig 6.21) and an approximate value for the constituent concentration was obtained (Fig 6.22). In this way the biochemical basis of each pathology within the bladder was elucidated. Table 6.9 shows the relative percentages of each constituent present in each of the pathologies.

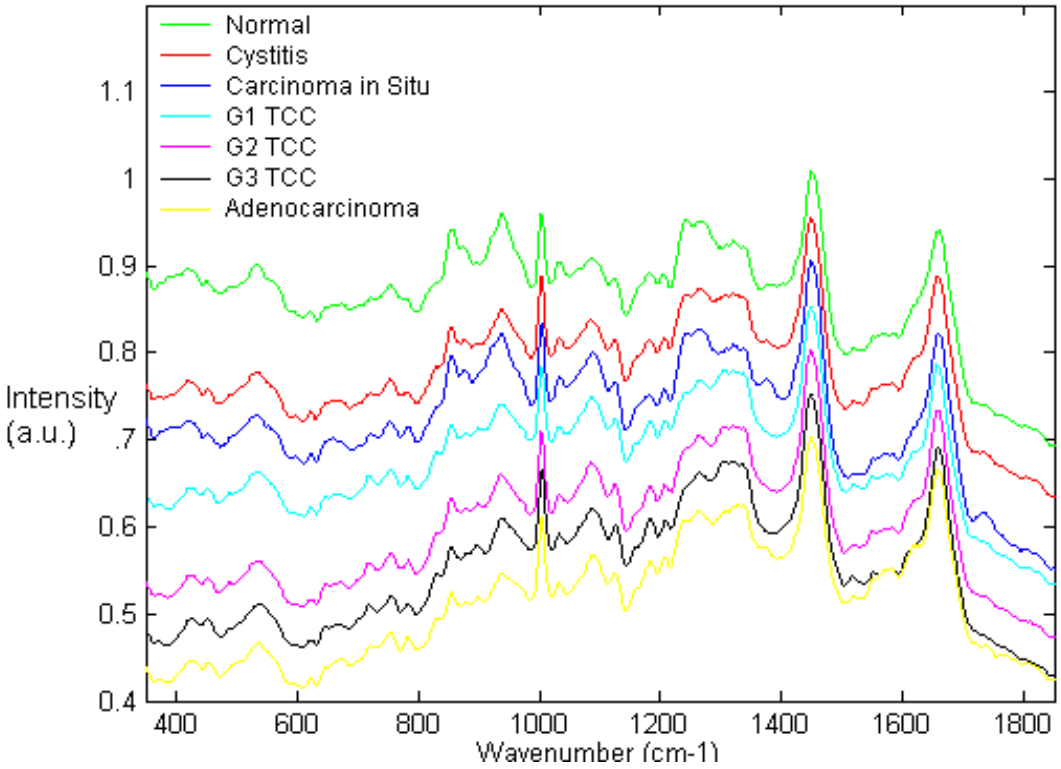

Fig 6.21. The mean spectra obtained for each bladder pathology.

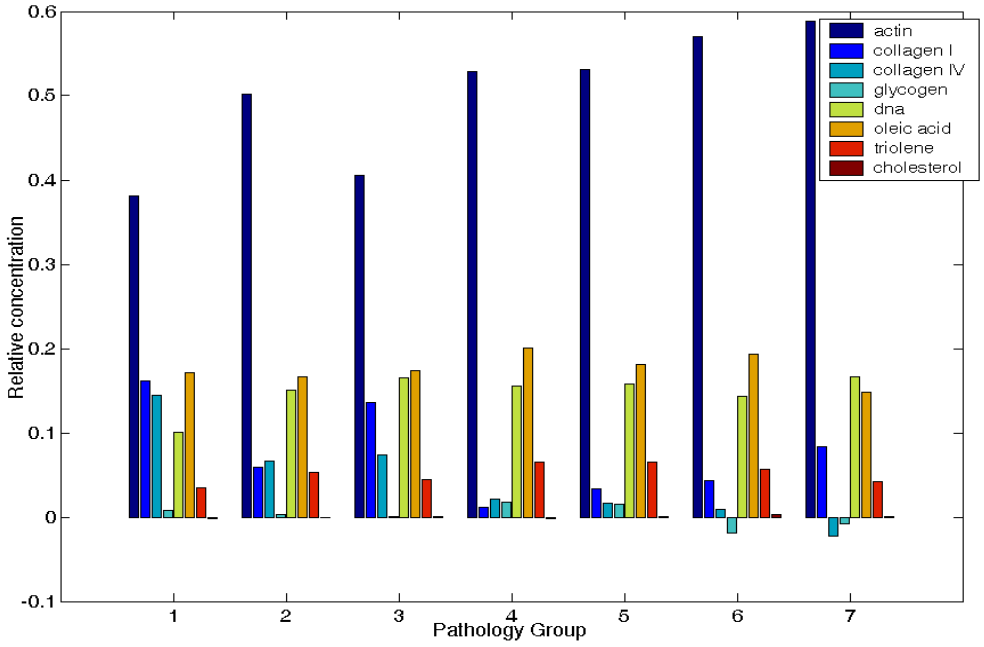

Fig 6.22. A bar graph showing the relative concentration of each constituent for each bladder pathology. Normalised to a total of unity. (the pathology relating to the groups are specified in the table 6.9).

Pathology	No	Actin (%)	Col1 (%)	Col4 (%)	Glycogen (%)	DNA (%)	Oleic acid (%)	Triolein (%)	Cholesterol (%)
Normal	1	42.2	17.9	5.4	0.8	11.1	19.0	3.9	-0.2
Cystitis	2	52.5	6.1	2.3	0.4	15.8	17.4	5.6	-0.0
CIS	3	42.6	14.2	2.6	0.1	17.4	18.3	4.7	0.1
G1 TCC	4	53.7	1.2	0.7	1.9	15.8	20.3	6.7	-0.2
G2 TCC	5	53.8	3.4	0.6	1.5	15.9	18.3	6.6	0.0
G3 TCC	6	57.4	4.4	0.3	-2.0	14.5	19.5	5.7	0.3
AdenoCa	7	58.0	8.2	0.7	-0.7	16.4	14.6	4.2	0.0

Table 6.9: The relative percentages of each constituent present in each bladder pathology.

6.4. The Kerr gated Raman spectroscopy.

6.4.1 Depth profiling of the prostate.

Figure 6.23 shows the spectra obtained as we go through the prostate gland tissue and on to the urea cell. As you can see the peak intensities change as the temporal position of the Kerr gate is varied. This relates to increasing depth with longer time delays and hence suggests that you are moving through the prostate. You can see the first 3 spectra are clearly tissue spectra with peaks at 1240 cm^{-1}, 1445 cm^{-1} and 1650 cm^{-1} consistent with protein peaks. The 4^{th} spectrum has lost a lot of the signal and then the following spectra yield the urea peaks clearly seen at 1003 cm^{-1} and 1170 cm^{-1}.

Figure 6.24 shows the spectra obtained from the urea cell to highlight the peaks. The peaks in Figure 6.23 at 662 cm^{-1} and 803 cm^{-1} are consistent with the CS_2, and peaks at 1079 cm^{-1}, 1339 cm^{-1} and 1533 cm^{-1} are consistent with hot pixels from the detector and are consistent throughout all of the spectra.

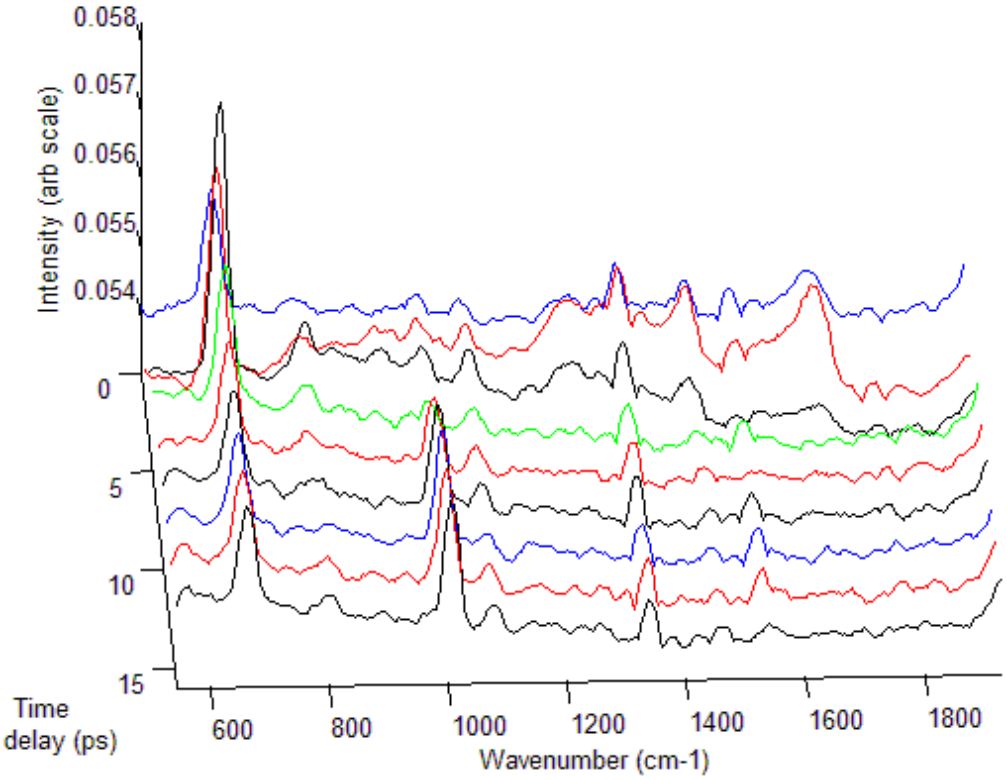

Fig 6.23. Raman spectra taken from different depths (by adjusting the delay in opening the Kerr-gate) through a sample of prostate gland on a quartz cell containing urea. See text for explanation of peak contributions from the experimental system.

6.4.2. Depth profiling of the bladder.

Figure 6.25 shows the Raman spectra measured from the bladder on top of the cell containing uric acid. As you can see the peak intensities change as the temporal position

of the Kerr gate is varied. This relates to increasing depth with longer time delays and hence suggests that you are moving through the urothelium and into the basement membrane and then on into the muscle layer. Eventually the signal from the tissue is lost, with peaks coming up at ~1400 cm^{-1} and 1650 cm^{-1} which are consistent with the main uric acid peaks as shown in Figure 6.26. The peaks in Figure 6.25 at 662 cm^{-1} and 803 cm^{-1} are consistent with the CS_2 of the Kerr-gate, and peaks at 1079 cm^{-1}, 1339 cm^{-1} and 1533 cm^{-1} are caused by hot pixels from the CCD detector.

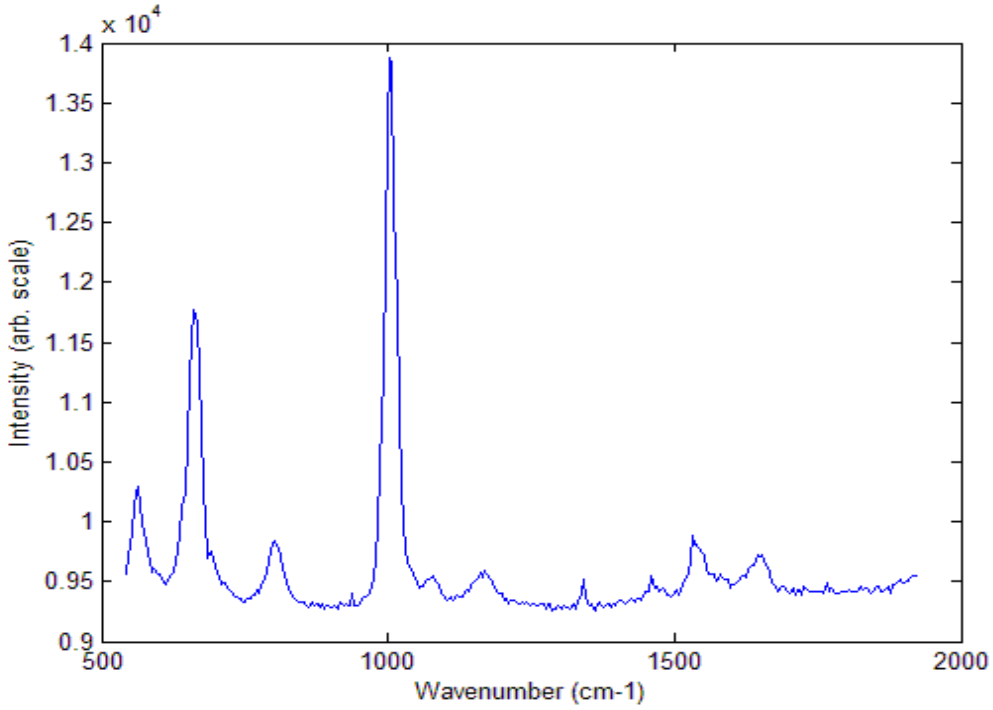

Fig 6.24. Raman spectra, at a wavelength of 488nm, taken from a quartz cell containing urea.

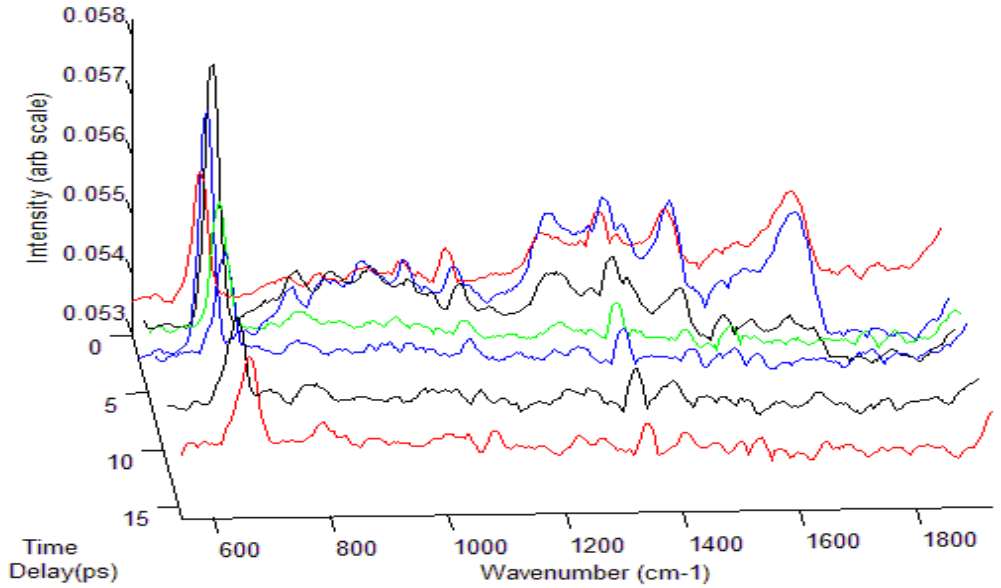

Fig 6.25. Raman spectra taken from different depths (by adjusting the delay in opening the Kerr-gate) through a sample of bladder on a quartz cell containing uric acid. See text for explanation of peak contributions from the experimental system.

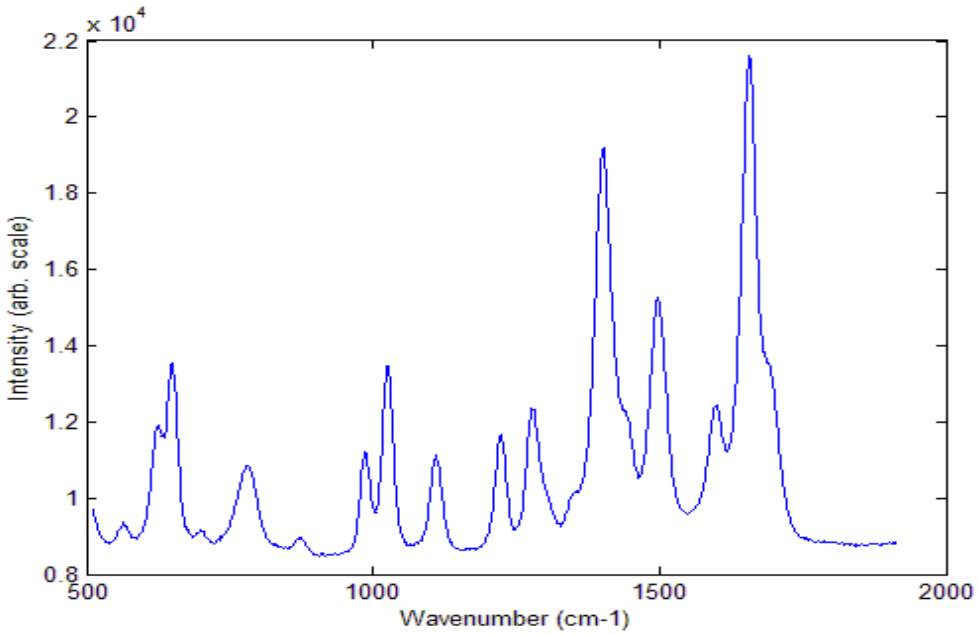

Fig 6.26. A Raman spectrum, at a wavelength of 488nm, taken a quartz cell containing uric acid.

6.4.3. Suppression of fluorescence and resonant enhancement of dark tissue.

Figures 6.27, 6.29 and 6.31 show the significant improvement in the obtained spectral quality from kidney and liver when using the Kerr-gate. As you can see there is a marked difference in the overall intensities of the spectra as well as the relative quality of the Raman components of the spectra. This is more enhanced between the spectra measured from the kidney medulla. The difference in the intensities has caused the remaining Raman tissue spectrum to be flattened in Figures 6.27 and 6.31. This demonstrates the significant affect of the Kerr-gate in suppressing the fluorescence. The true quality of the resonant Raman spectra at both wavelengths with the Kerr-gate on can be seen in Figures 6.28, 6.30 and 6.32. These Figures also show that you get improved enhancement of the haemoglobin and carotenoids at a wavelength of 488nm when compared to a wavelength of 532nm. The peaks for the haemoglobin are at approximately 1356 cm^{-1}, 1547 cm^{-1} and 1605 cm^{-1}, whereas the main peak from the carotenoids is at 1003 cm^{-1}.

The peaks in Figures 6.27, 6.28, 6.29, 6.30, 6.31, and 6.32 at 665 cm^{-1} and 795 cm^{-1} are consistent with the CS2, and the peaks in Figures 6.28, 6.29, 6.30, and 6.32 at 915 cm^{-1}, 974 cm^{-1}, 1250 cm^{-1}, 1318 cm^{-1}, 1410 cm^{-1}, 1510 cm^{-1}, 1612 cm^{-1} are caused by hot pixels from the detector.

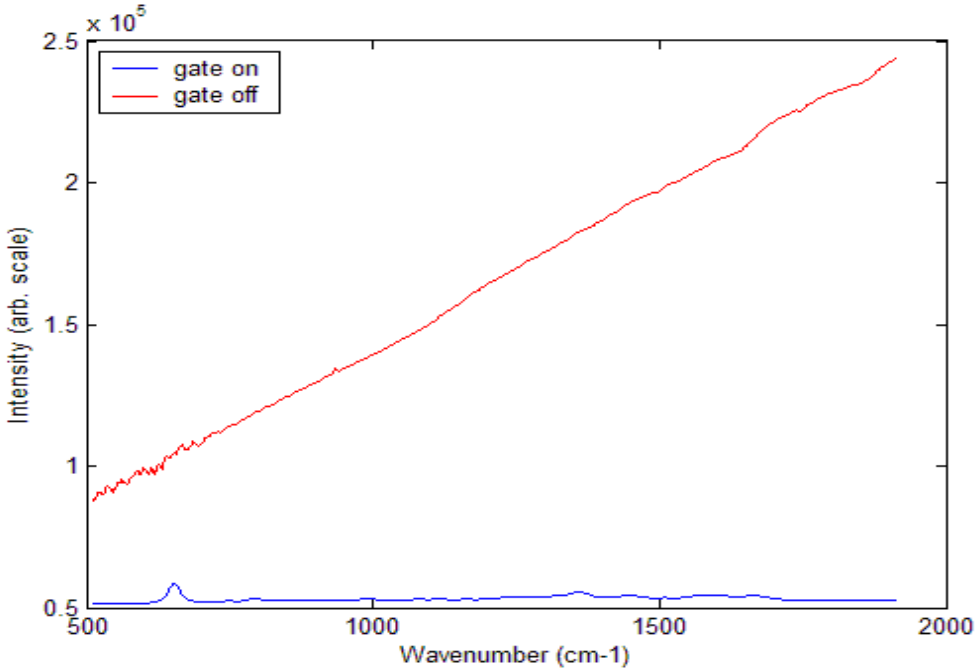

Fig 6.27. Spectra from the cortex of a pig's kidney at a wavelength of 488nm with the Kerr-gate on (20s x 30 accumulations) and off (5s x 30 accumulations).

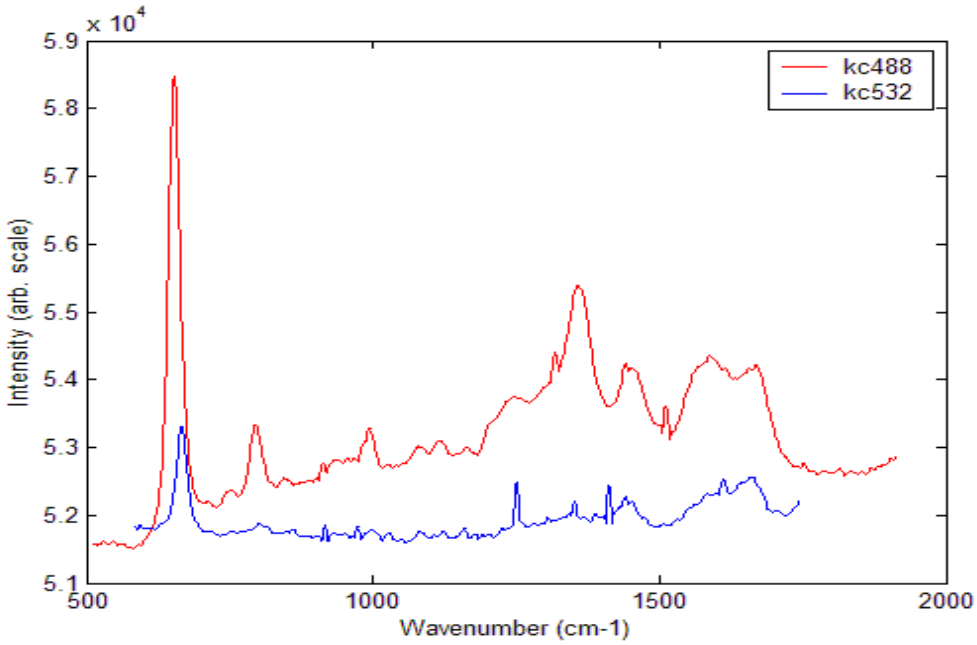

Fig 6.28. Spectra from the cortex of a pig's kidney at wavelengths of 488nm (20s x 30 accumulations) and 532nm (30s x 60 accumulations) with the Kerr-gate on.

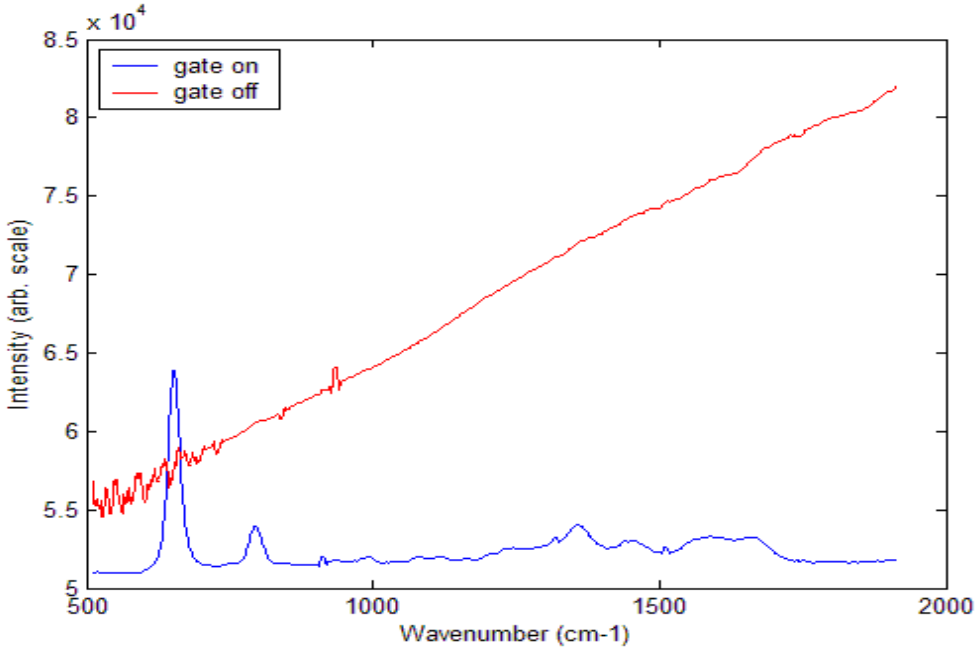

Fig 6.29. Spectra from the medulla of a pig's kidney at a wavelength of 488nm with the Kerr-gate on (20s x 30 accumulations) and off (5s x 30 accumulations).

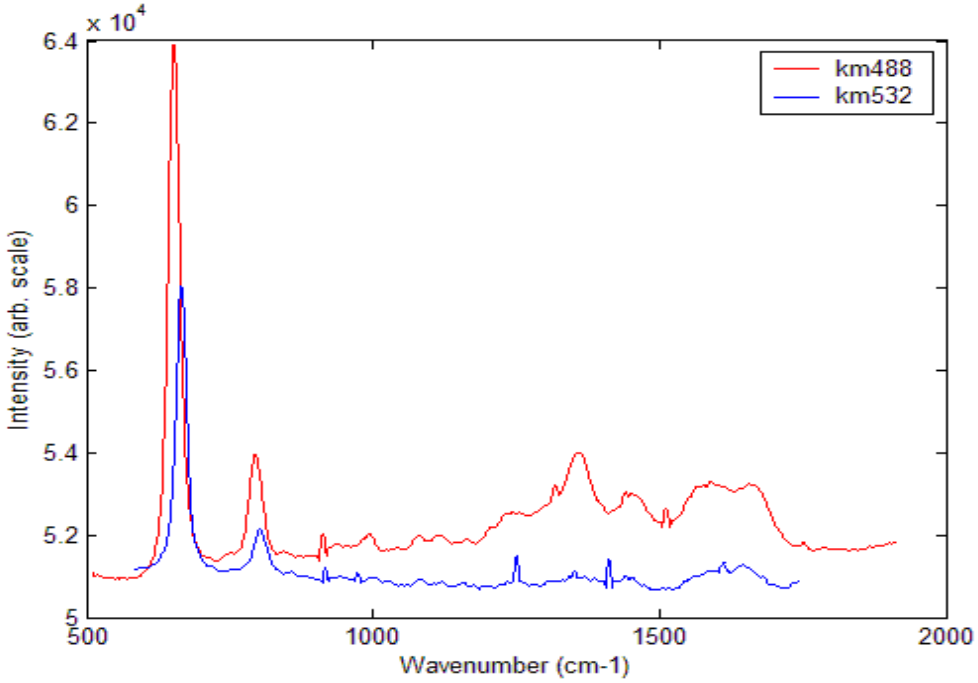

Fig 6.30. Spectra from the medulla of a pig's kidney at wavelengths of 488nm (20s x 30 accumulations) and 532nm (30s x 60 accumulations) with the Kerr-gate on.

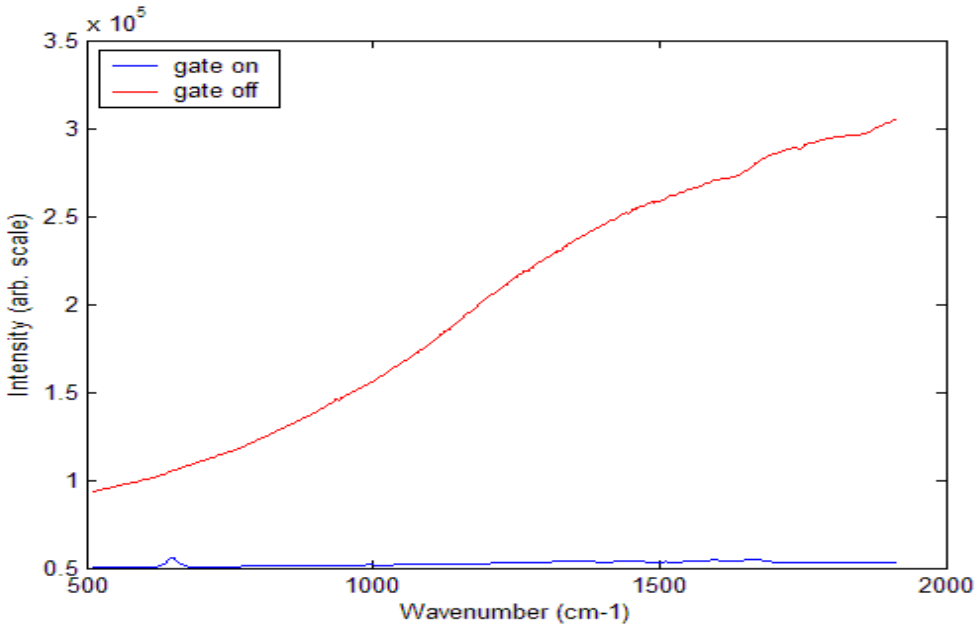

Fig 6.31. Spectra from pig's liver at a wavelength of 488nm with the Kerr-gate on (10s x 30 accumulations) and off (5s x 30 accumulations).

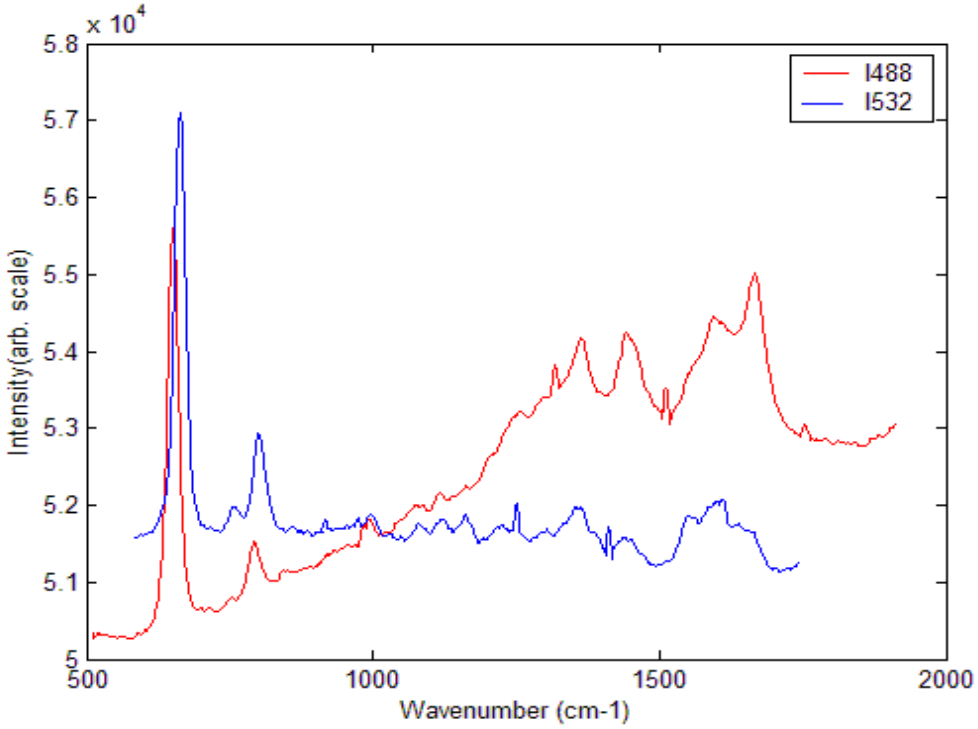

Fig 6.32. Spectra from pig's liver at wavelengths of 488nm (10s x 30 accumulations) and 532nm (20s x 30 accumulations) with the Kerr-gate on.

7. Discussion of results.

7.1. Raman spectroscopy of the bladder and the prostate gland.

Raman spectroscopy has been shown to be of use in distinguishing between pathologies within the bladder and the prostate [Crow 2003, 2004, 2005, Hart Prieto 2004]. This study has not only reiterated this but also shown that it is possible using slightly different techniques by sectioning the prostate tissue and carefully localising glands within the tissue as opposed to sampling a whole TURP chip (section 5.4.5.2).

Unfortunately the histology mix collected solely by the author was not diverse enough for the determination of the biochemical basis of pathologies within each of the tissues, however they could be added to the bank of spectra collected by the group.

The sensitivities and specificities that were calculated following cross validation (leave one spectrum out) for each of the pathologies measured showed ranges of 63% - 100% and 81% - 93% for bladder and prostate respectively and were equivalent to not only those obtained by Crow (2003) but also to sensitivities and specificities obtained by Gazi et al (2006) using FTIR spectroscopy on prostate cancer biopsies (70%-78% and 81%-89% repectively), and De Dominicis et al (2001) using fluorescence spectroscopy in the bladder (87% and 63% respectively).

The sensitivities and specificities were included purely to help in understanding how well the preliminary model was working and also to ensure that it was comparable to work done previously in the group. The spectra from these samples were added to the bank of those already collected and will be used in future experiments.

The sensitivities and specificities enabled an indication of the system performance in terms of correlation with the gold standard histopathology. The numbers of samples however were small even though large numbers of spectra were measured, therefore the 'leave one spectrum out method' is potentially flawed as 9 – 21 spectra (depending on the tissue) within the diagnostic algorithm would be from the same tissue as the test spectrum. Therefore spectra from the same patient remain in the model when it is testing the left out spectrum. Unfortunately given the low number of samples in the malignant pathological groups we were unable to use a 'leave one sample out' method which would have ensured a more robust model.

Using PCA led LDA in the analysis of the spectra has the disadvantage that if there are too many PCs compared to a small sample size then you can overfit the data as there may not be enough variation described in the dataset to cover a patient population.

Also given that the gold standard Gleason scoring system and the histopathological grading for bladder are subject to both inter and intra observer errors [Allsbrook 2001] then there may be groups that are misclassified to a greater extent than others.

The numbers for both the adenocarcinoma of the prostate gland and the transitional cell carcinoma of the bladder were small due to a number of factors. These included the fact that Gloucestershire Royal Hospital is not a large cancer centre, fresh tissue collection was required to represent repeatable biochemical changes likely to be found *in vivo* (we are working towards the development of an *in vivo* probe) and there isn't the facility available to us to use retrospective specimens held in a large bank of snap frozen tissue. Time constraints for the thesis and a single person doing the tissue collection limited the

number of samples collected. Furthermore the pathologists preferred samples not to be taken from whole prostate and bladder specimens as it was felt that the pathology would be distorted. Prostate biopsies were taken at a neighbouring hospital and due to logistics and time constraints the author was unable to collect these samples. Also unfortunately a few of the samples had diathermy artefacts and could not be utilised.

For these reasons the spectra measured were added to the bank of spectra already obtained by the group to try to alleviate any bias from the small numbers. This is something the group will continue to improve upon over time.

Another source potentially skewing the results could have come from there only being one consultant histopathologist to view the histology, with the potential intra – observer variation with the subjective Gleason scoring system and the identification of bladder histology. Ideally more than one histopathologist should have viewed the samples, a number of attempts were made to recruit others, but this proved difficult. Therefore only one urology histopathologist available to help with this work.

Table 6.3 showing the cross validation (leave one spectrum out) of the Raman prediction compared to the actual histology for the prostate samples does have a reasonably high number of both false positives and false negatives. This is possibly a consequence of the heterogeneity of the prostate samples. Although the samples were checked and the areas for spectra acquisition were noted, some sampling errors may have occurred within the BPH section of the tissue. If this occurred then the algorithm would have been trained with some inaccurate data. The other theory for the false negatives and positives is that there are biochemical changes within the tissue that could

not have been seen by the method of histopathology used but that were picked up by Raman spectroscopy which is molecularly specific.

Table 6.4 showing the cross validation (leave one spectrum out) of the Raman prediction compared to the actual histology for the bladder samples also has a few false negatives and false positives. Given the homogenous nature of the tissue samples these could not be secondary to spectra sampling error but are more likely due to biochemical or field changes that were not visible to the histopathologist. More samples were falsely predicted as cancer which would reinforce this hypothesis. The normal bladder samples were taken from cystoscopy or TURP procedures and not from TURBT procedures.

To conclude we have shown that we are able to obtain usable spectra by using previously described techniques (section 5.4.5.2). This has enabled spectra obtained from tissue collected at a later date to be added to a bank of spectra. In this way our group will be able to achieve a bank of spectra for future analysis and to build a more robust model.

As was discussed above the diagnostic algorithm contained spectra from the same tissue as the test spectrum therefore reducing the power of the test. The aim would be for the group to obtain a bank of spectra large enough that a ‘leave on sample out’ cross validation test could be done thereby making the model more robust.

7.2. The biochemical basis of pathologies within the bladder and the prostate gland.

Raman spectroscopy has been in use for chemical analysis in industry for many years now. It wasn't however until recently due to advances in technology that we have been able to apply it to biological tissues.

Shafer – Peltier et al (2002a/b) have been the only other group in the literature to have looked at the chemical basis of disease. However this was done in breast tissue, not always with pure standards and has never been done before in urology.

This study was performed to determine the biochemical basis of pathologies within the bladder and the prostate gland in order to attain a better understanding of pathogenesis and disease progression.

Firstly the main building blocks or constituents of biological tissue were considered. This was done by reviewing those collected by Shafer – Peltier et al (2002a/b) and on discussion with histopathologists in both the Gloucestershire Royal Hospital and the Bristol Royal hospital. This unfortunately was limited to building blocks that were thought to be in concentrations that could be measured by Raman spectroscopy, i.e. gross molecules that change with pathology as opposed to subtle genetic changes such as p53. Also unfortunately this thesis was unable to completely validate the composition of tissue due to it's molecular complexity. Other methods that could potentially help with this would be the use high pressure liquid chromotography (HPLC) or gas chromotography mass spectroscopy (GCMS). However these are expensive and would be very time consuming, leading to results that would still likely be a best guess.

Spectra were obtained from these constituents and the mean spectrum for each one was derived using empirical analysis. The first derivatives of these were used with 'ordinary least squares' analysis to formulate a biochemical spectral model (a full explanation of the analysis is given in chapter 5.6). In formulating a spectral model containing the main biochemical building blocks (constituents) for tissue we were able to apply it to the mean spectra of different pathologies within the bladder and the prostate gland. In doing so we were able to extract information about the microscopic composition of tissue in different pathologies. Note that the resulting concentrations have been calculated with ordinary least squares, which can be subject to some errors if significantly collinear constituent spectra are used or if the data is of poor quality, i.e. noisy. Great care was taken to minimise these possible issues.

Also as 'ordinary least squares' analysis was used, we obtained negative percentages with some constituents. The 'ordinary least squares' analysis was used so that we were left with a residual spectrum and ensured that the author didn't over fit the data. A way to overcome the negative values would be to use 'non negative least squares' analysis [Sowa 2006]. This is a similar method, but with the constraint that only positive concentrations can be obtained. Using this methodology it is feasible to overfit the data by still fitting the residual of the fit with the basis spectra. When 'ordinary least squares' is used, it is easier to see when things go wrong with the fit, by picking up the occurrence of big negative concentrations and large residuals.

The results have shown that for pathologies within the bladder and the prostate gland, the DNA content increases as the tissue progresses from normal to malignant, and the

collagen content decreases. This is as expected as the nuclear to cytoplasm (actin) ratio increases from normal to malignant tissue and DNA is abundant in the nucleus. Also the cells become more abundant and therefore the extracellular matrix is reduced which is abundant in collagen. Until the tumour becomes larger and then you would usually expect more collagen. We found that using collagen types 1 and 4 gave a better spectral fit than by including collagen type 3 suggesting that types 1 and 4 are more abundant in the bladder and prostate tissue. Cholesterol was used in the model as a potential component of necrosis. As a tumour becomes bigger there tends to be necrotic areas within it where it is too big for its blood supply. Interestingly there is no cholesterol in the bladder spectra but it is increased in that of the prostate tissue that is malignant. This may be because a lot of the tumours in the bladder undergoing TURBT are papillary and very vascular; therefore they do not show necrotic areas. The glycogen content appears to increase with malignancy suggesting a higher metabolic rate in malignant tissue which is understandable, although different to that found in some other epithelial tissues such as the oesophagus. The actin level however increases in the bladder but decreases in the prostate gland. This may be because the bladder tumours tend to be papillary and therefore have a larger surface area, however the actin represents the cytoplasm and as the nuclear to cytoplasm ratio increase with malignancy you would expect the relative actin level to decrease.

Both lycopene and β carotene were thought to be decreased in malignant tissue [Hata 2000, Toniolo 2001, Czeczuga-Seminiuk 2003], however we found that there was none detected using our spectral analysis. This may be because they are in such small concentrations that the other spectra hide them. Also we were unable to measure the

PSA for our model as the only samples we could obtain were in such small quantities that we were unable to measure a usable spectrum.

To conclude we have shown for the first time that we are able to utilise Raman spectroscopy in determining the biochemical basis, to a first approximation, to the different pathologies within the bladder and prostate gland. In this way we may achieve a better understanding of disease process and carcinogenesis. This could have major implications in the future of the diagnosis of pathologies within the bladder and the prostate gland. Histopathology is at present the 'gold standard' for diagnosis, by utilising Raman spectroscopy and the knowledge we have gleaned from the biochemical studies performed, we potentially will be able to eliminate the intra and inter – observer error that is seen in histopathology. Further to this it is likely that biochemical signatures once understood will lead to readily available prognostic information.

7.3. Depth profiling of bladder and prostate tissue.

In view of previous studies, Raman spectroscopy is thought to have the potential for minimally invasive detection of malignancies and pre-malignancies within the bladder and the prostate gland. A problem with this is the inability to obtain spectra from significantly beneath the surface (more than of the order of 100μm) [Caspers 2001]. This is needed to ascertain whether there has been any local invasion of the disease in the case of the bladder, or to find a focus of adenocarcinoma in an otherwise benign prostate gland.

There have been studies utilising the Kerr-gating technique to improve upon Raman spectra obtained from bone interiors [Morris 2004] as well as test experiments demonstrating the depth resolving power of the Raman Kerr gating concept on artificially prepared samples [Matousek 2005]. This study was designed to expand on this work by studying the facility of Kerr-gated Raman spectroscopy to measure biochemical data from depths of a few millimetres in soft tissue. To make certain that signal has been detected from beneath the tissue layer; specimens with strong and distinct Raman signals have been used. These were also selected for their relevance in urology.

As can be seen from the results, the Raman spectra measured from the bladder on top of the cell containing uric acid, show how the peak intensities change as the temporal position of the Kerr gate is varied. This relates to increasing depth with longer time delays and hence suggests that you are moving through the urothelium and into the basement membrane and then on into the muscle layer. Eventually the signal from the tissue is lost, with peaks coming up at ~1400 cm^{-1} and 1650 cm^{-1} which are consistent with the main uric acid peaks.

The Raman spectra obtained as we go through the prostate gland tissue and on to the urea cell show that the first 3 spectra are clearly tissue spectra with peaks at 1240 cm^{-1}, 1445 cm^{-1} and 1650 cm^{-1} consistent with protein peaks. The 4^{th} spectrum has lost a lot of the signal and then the following spectra yield the urea peaks clearly seen at 1003 cm^{-1} and 1170 cm^{-1}.

To summarise we have shown for the first time that we are able to obtain spectra from different depths through prostate and bladder tissues, by utilising Kerr-gated Raman spectroscopy. Modeling of the time-dependent photon pathway would provide an enhanced understanding of the depth profiling process. This could have major implications in the future of Raman spectroscopy as a tool for diagnosis. Up until now we have been able to distinguish between different pathologies within the bladder and the prostate gland by sampling the tissue *in vitro*. This has involved looking at only the surface of the sample.

The prostate gland is usually biopsied via the rectum. This is a painful procedure and can give false negatives. With the help of Raman spectroscopy and Kerr gating we would potentially be able to pick up the spectral differences from a small focus of adenocarcinoma of the prostate gland in an otherwise benign gland.

The bladder would also potentially benefit from Raman spectroscopy combined with Kerr-gating. We would not only be able to diagnose the presence of a transitional cell carcinoma but would also be able to assess the stage of the tumour in terms of its extension through the basement membrane and beyond (i.e. greater than a few hundred microns below the surface).

We have demonstrated the first principals for the use of Kerr-gated Raman spectroscopy in the diagnosis of biological pathologies. Presently however the instrumentation at the Rutherford Appleton Laboratory (RAL) fills two rooms. Therefore, the use of this

technique will require technical evolution and advancement before it will be ready for use *in vivo*.

Further studies are planned to demonstrate the facility of the technique to discriminate between normal and diseased tissue at depths of a millimetre or more.

7.4. Suppression of fluorescence and resonant enhancement of dark tissue.

Dark tissues such as kidney and liver have always caused problems for Raman spectroscopy because they are highly absorbing and fluorescent at most visible and NIR wavelengths. Therefore it has proved difficult to obtain spectra with anything more than the most significant peaks. Because of this the use of Raman spectroscopy in the diagnosis of renal and liver disease has been largely ignored. There has been some work however on near infrared Fourier transform Raman spectroscopy and the liver [Keller 1994, Crupi 2004]. These showed characteristic differences between the spectra from different pathological tissues but analysis was not performed to evaluate the extent of these differences.

Hawi et al (1996) also looked at hepatocytes and liver tissue at an excitation wavelength of 632nm and they concluded that there were spectral differences between the pathologies but that also at 632nm there was enhancement of the haem component of the tissue that resulted in marked spectral difference between the tissue and the hepatocytes.

One way to try and overcome the problem with fluorescence is by using picosecond Kerr-gating. This technique utilises impulsive excitation with a picosecond pulsed laser and fast temporal gating of instantaneous Raman scattered light. In this way the signal to noise ratio is increased and the slow emitting fluorescence is minimised.

There have been studies utilising the Kerr-gating technique to improve upon Raman spectra obtained from bone interiors [Morris 2004] but there is no published work on utilising this technique to obtain spectra from dark biological tissues.

This study was performed to as a first principals study to investigate the use of Kerr-gating for fluorescence suppression at different wavelengths in the kidney and the liver. Obviously it would have been better to use human tissue however we were limited with our time in Rutherford Appleton Laboratories and we were unable to get ethical approval at such short notice fresh tissue was used.

As can be seen from the results we have shown that by utilising the Kerr - gated technique on the liver and kidney samples, we have been able to obtain useable Raman spectra from dark tissue.

Given our positive results the group will be able to apply for more time at the Rutherford Appleton Laboratories to take these experiments forward. As this is done on a yearly basis I was unable to take this forward myself. Further work may enable the use of Raman for disease diagnosis in these fluorescent dark tissues, furthermore resonance Raman can be utilised and the accompanying fluorescence suppressed using this technique. Resonance Raman can be utilised to specifically enhance molecular constituents, such as carotenoids, nucleic acids or amino acids, depending on the wavelength of illumination used. As can be seen in Figures 6.28, 6.30 and 6.32 there is

improved enhancement of the haemoglobin and carotenoids at a wavelength of 488nm when compared to a wavelength of 532nm.

To conclude due to the fluorescence of tissues that are extremely vascular, and therefore dark, we have traditionally been unable to obtain good quality spectra. We have shown for the first time, that by incorporating the Kerr-gating technique into the spectral analysis of tissue using Raman spectroscopy, we have been able to suppress the fluorescence and obtain spectra of adequate quality to enable further studies on biological tissue.

Other excitation wavelengths can be used, and by tuning these to specific electronic absorption bands, particular species can be resonantly enhanced. With the use of Kerr-gated fluorescence suppression there is the potential for the detection of subtle changes in resonance Raman spectra likely to accompany pathological changes in tissue.

Raman spectroscopy is already being used to distinguish between different pathologies in other tissues such as the bladder [Crow 2004, Hart Prieto 2004]), prostate [Crow 2003, 2004], cervix [Liu 1992, Mahadevan – Jansen 1996], breast [Alfano 1991] and oesophagus [Shim 2000, Stone 2001, Kendall 2003]. Now we will be able to potentially distinguish between different pathologies in more vascular tissue such as the liver and kidney by utilising Kerr-gated Raman spectroscopy.

8. Future research prospects of Raman spectroscopy in urology.

The future of Raman spectroscopy in urology holds no bounds.

It has already been shown that *in vitro* diagnosis of pathologies within the bladder and the prostate gland is possible with good sensitivity and specificity when compared to the gold standard method of diagnosis – histopathology [Crow 2003, 2004]. Using this technique a histopathology tool can be produced. This has implications not only for the patient in terms of an objective diagnosis of the tissue but also for the workload of the histopathologist who will not need to look down a microscope to obtain a diagnosis.

The next step is to show that these results are reproducible when diagnosing pathologies *in vivo*.

Our group is in the process of perfecting a probe that will be able to go down an endoscope. This probe will potentially be able to take real time spectra from suspicious areas within the bladder. The first step however will be to form a diagnostic algorithm with the probe by taking spectra using the probe in an *in vitro* setting. This will involve an experimental technique similar to those used for the studies in this thesis and that of Crow (2004). Once a diagnostic algorithm has been formulated it will then need to be tested *in vivo*.

To test a probe *in vivo*, real time spectra will be taken of specific areas within the bladder and then that area will be biopsied. The spectroscopic diagnosis will then need to be compared to the histopathology of that sample. In this way the diagnostic algorithm will also be tested.

Once vigorous testing of the probe *in vivo* has been undertaken, the need for biopsy will potentially be obviated. This will not only improve the time to diagnosis in patients with suspected cancer of the bladder but will reduce the risks associated with diagnosis (the spectral test will be able to be done under a local anaesthetic with a smaller diameter cystoscope, whereas to take a biopsy, a general anaesthetic is needed with a larger diameter cystoscope) and the time to definitive treatment.

Not only will this be advantageous to the patient but also to the surgeon who will be able to diagnose more patients in a specific period of time, and the histopathologist who will not need to be assessing as many biopsies.

A probe is already being used experimentally with the cervix and in the oesophagus and therefore is a very real potential for the bladder [Boere 2003, Mahadevan-Jansen 1998 Motz 2004, Shim 2000,Utzinger 2003,]

The use of the Kerr gating technique in conjunction with Raman spectroscopy has widened our potential prospects even further. The studies in the thesis have shown the potential to depth profile through prostate and bladder samples *in vitro*. If this can be combined with the probe it will be possible not only to assess the stage of a tumour by seeing how deeply through the bladder tissue it goes but also to assess surgical margins following resection of a tumour. When a tumour in the bladder is resected endoscopically it is done so using essentially a hot wire that cuts through the tissue. This has the effect of diathermising or burning the tissue that is left behind. When a Raman spectrum is taken of this diathermised area, all you get is fluorescence and no tissue spectrum. In utilising the Kerr gating technique a spectrum can be obtained from below the diathermised area and potentially will be able to be identified as normal tissue

or tumour. If tumour is still seen then the surgeon will know that more tissue needs to be taken and if the tissue beneath is normal then the surgeon will know that the surgical margins are clear of tumour. This has the potential to improve cure rates in patients with bladder cancer.

The same can be applied to the prostate gland. In utilising the Kerr gating technique in conjunction with Raman spectroscopy and a probe, a small focus of adenocarcinoma within a large benign prostate gland can be localised using depth profiling. This initially will lead to more accurate biopsying of the prostate gland and ultimately to guided ablation of the tumour. In this case the probe will need to be tested *in vivo* by taking guided biopsies and comparing the spectral diagnosis to the histopathology of that sample. This will act to test the *in vitro* diagnostic algorithm that will have needed to have been formulated.

The potential with this will not only obviate the need for biopsy and therefore have implications to the patient, surgeon and histopathologist as was mentioned with the bladder but will also potentially lead to spectroscopic guided ablation of the tumour and then surveillance resulting in reduced numbers of patients undergoing major operations such as a radical prostatectomy.

As with the bladder this combination will also potentially result in the ability to assess surgical margins following a radical prostatectomy. A spectrum can be obtained from the surgical site or below the diathermised area if diathermy has been used and potentially will be able to be identified as normal tissue or tumour. If tumour is still seen then the surgeon will know that more tissue needs to be taken and if the tissue is normal then the surgeon will know that the surgical margins are clear of tumour. This has the

potential to improve cure rates in patients with prostate cancer post radical prostatectomy.

Studies in this thesis have also shown the ability for Kerr-gated Raman spectroscopy to suppress fluorescence and resonantly enhance spectra from dark tissue such as the liver and the kidney. In urology there are a few dark tissues that have been neglected in terms of Raman spectroscopy because they fluoresce. These are the kidney and the testes. In utilising the Kerr-gated Raman spectroscopy to analyse these tissues we have the potential to diagnose pathologies within the kidney and the testes both *in vitro* and *in vivo*. The studies that have been carried out so far (as well as the potential future studies) on bladder and prostate tissue will be able to be performed on kidney and testicular tissue. This has major implications for the future of diagnosis in urology. The histopathologists workload will potentially be reduced and patients will be diagnosed and treated quickly with less invasive techniques.

The use of Kerr – gated Raman spectroscopy will need further development and research. At present the instrumentation takes up a room in the Rutherford Appleton Laboratory, however given how far Raman spectroscopy has come since the Raman effect was first described in Nature by Chandrasekhara Venkata Raman [Raman 1928] this is a very real prospect.

As was said at the beginning of this chapter 'The future of Raman spectroscopy in urology holds no bounds'. Urology has the potential to move into a spectroscopic era that will improve upon our knowledge of pathogenesis, will provide a streamlined pathway to diagnosis and treatment and will improve the lives of surgeons, histopathologists and patients in terms of workload and quality of care.

References.

Agur, A.M.R., Lee, M.J., Boileau Grant, J.C. (1999). Grant's Atlas of Anatomy, 10th ed. Lippincott, Williams and Wilkins.

Alberts, B., Bray, D., Lewis, J., Raff, M., Roberts, K., Watson, J.D. (1994). Molecular biology of the cell., Garland Publishing.

Alexander, E.E., Qian, J.Q., Wollan, P. C., Myers, R. P., Bostwick, D. G.(1996). "Prostatic intraepithelial neoplasia does not appear to raise serum prostate-specific antigen concentration." Urology **47**(5): 693-698.

Alfano, R.R., Liu, C.H., Sha, W.L., Zhu, H.R., Akins, D.L., Cleary, J., Prudente, R., Cellmer, E. (1991). "Human breast tissues studied by IR Fourier Transform Raman spectroscopy." Lasers in the life Sciences **4**(1): 23-28.

Alfano, R.R., Tomaselli, V.P., Beuthan, J., Feld, M. S., Flotte, T. J., Fujimoto, J., G.Thomsen, S (1998). Advances in optical biopsy and optical mammography - Panel discussion - Review and summary of presentations. Advances in Optical Biopsy and Optical Mammography. **838:** 194-196.

Altman, D.G. Practical statistics for medical research, 2nd ed. Chapman and Hall.

Anderson, W.A.D., Linder, J. (1996). Anderson's Pathology, 10th ed. C.V. Mosby.

Anidjar, M., Ettori, D., Cussenot, O., Meria, P., Desgrandchamps, F., Cortesse, A., Teillac, P., LeDuc, A., Avrillier, S. (1996). "Laser induced autofluorescence diagnosis of bladder tumors: Dependence on the excitation wavelength." Journal of Urology **156**(5): 1590-1596.

Anonymous (2003). "MRI technique could replace breast cancer biopsies." Biophotonics international **dec 10** (11): 13.

Avrillier, S., Tinet, E., Ettori, D., Anidjar, M. (1997). "Laser-induced autofluorescence diagnosis of tumors." Physica Scripta **T72**: 87-92.

Bancroft, J.D., Stevens, A. (1996). Fixation and Fixatives. Theory and practice of histological techniques., Churchill, Livingstone.

Baraga, J.J., Feld, M.S., Rava, R.P. (1992). "Rapid near-infrared Raman spectroscopy of human tissue with a spectrograph and CCD detector." Applied Spectroscopy **46**(2): 187-190.

Barr, H., Dix, T., Stone, N. (1998). "Optical spectroscopy for the early diagnosis of gastrointestinal malignancy." Lasers in Medical Science **13**(1): 3-13.

Baumgartner, R., Kriegmair, M., Hofstetter, A. (1999). Flourescence diagnosis of bladder tumor. Using 5-Aminolevulinic Acid - fundamentals and results., Karl Storz.

Beljebbar, A., Romijn, J.C., Puppels G. L. (2000). Investigation of androgen effects on prostate cancer cell lines by near infrared Raman microspectroscopy. Biomedical Spectroscopy: Vibrational Spectroscopy and Other Novel Techniques. **1:** 161-165.

Berger, A.J., Itzkan, I., Feld, M. S. (1997). "Feasibility of measuring blood glucose concentration by near- infrared Raman spectroscopy." Spectrochimica Acta Part a-Molecular and Biomolecular Spectroscopy **53**(2): 287-292.

Berger, A.J., Koo, T.W., Itzkan, I., Horowitz, G., Feld, M. S. (1999). "Multicomponent blood analysis by near-infrared Raman spectroscopy." Applied Optics **38**(13): 2916-2926.

Berger, A.J., Wang, Y., Feld, M. S. (1996). "Rapid, noninvasive concentration measurements of aqueous biological analytes by near-infrared Raman spectroscopy." Applied Optics **35**(1): 209-212.

Berry, S.J., Coffey, D.S., Walsh, P. C., Ewing, L. L. (1984). "The Development of Human Benign Prostatic Hyperplasia with Age." Journal of Urology **132**(3): 474-479.

Bhargava, R., Levin, I.W. (2001). "Fourier transform infrared imaging: theory and practice." Analytical chemistry **73:** 5157-5167.

Bindig, U., H. Winter, Wasche, W., Zelianeos, K., Muller, G. (2002). "Fiber-optical and microscopic detection of malignant tissue by use of infrared spectrometry." Journal of Biomedical Optics **7**(1): 100-108.

Boere, I.A., Schut, T.C.B., van den Boogert, J., de Bruin, R. W. F., Puppels, G. J. (2003). "Use of fibre optic probes for detection of Barrett's epithelium in the rat oesophagus by Raman spectroscopy." Vibrational Spectroscopy **32**(1): 47-55.

Bolla, M., Collette, L., Blank L, Warde P, Dubois JB, Mirimanoff RO, Storme G, Bernier J, Kuten A, Sternberg C, Mattelaer J, Lopez Torecilla J, Pfeffer JR, Lino Cutajar C, Zurlo A, Pierart M. (2002). "Long term results with immediate androgen suppression and external irradiation in patients with locally advanced prostate cancer (an EORTC study): a phase III randomised trial." Lancet **360** (9327): 103-6.

Boring, C.C., Squires, T.S., Yong, T. (1992). "Cancer Statistics, 1992." Ca-a Cancer Journal for Clinicians **42**(1): 19-38.

Bostwick, D.G. (1990). Pathology of the prostate. 1st ed. New York, Churchill Livingstone.

Bostwick, D.G., Cooner, W.H., Denis, L., Jones, G. W., Scardino, P. T., Murphy, G. P. (1992). "The Association of Benign Prostatic Hyperplasia and Cancer of the Prostate." Cancer **70**(1): 291-301.

Brawer, M.K., Deering, R.E., Brown, M., Preston, S. D., Bigler, S. A. (1994). "Predictors of Pathological Stage in Prostatic-Carcinoma - the Role of Neovascularity." Cancer **73**(3): 678-687.

Brennan, J.F., Romer, T.J., Lees, R. S., Tercyak, A. M., Kramer, J. R., Feld, M. S. (1997). "Determination of human coronary artery composition by Raman spectroscopy." Circulation **96**(1): 99-105.

Brennan, J.F., Wang, Y., Dasari, R. R., Feld, M. S. (1997). "Near-infrared Raman spectrometer systems for human tissue studies." Applied Spectroscopy **51**(2): 201-208.

Burkitt, H.G., Young, B., Heath, J.W. (1993). Wheater's functional Histology - A text and colour atlas., Churchill Livingstone.

Campbell, M.F., Walsh, P.C., Retik, A.B. (2002). Campbell's Urology, 8th ed. W.B. Saunders.

Cancer Research UK (2004). Cancerstats monograph.

Candas, B., Gomes, J.L., Cusan, L., Diamond, P., Laverdiere, J., Labrie, F. (1997). "Effects of neoadjuvant and adjuvant combined androgen blockade associated to radiation therapy on serum PSA." British Journal of Urology. **80**(suppl 2): 259.

Carmona, P., Bellanato, J., Escolar, E. (1997). "Infrared and Raman spectroscopy of urinary calculi: A review." Biospectroscopy **3**(5): 331-346.

Caspers, P.J., Lucassen, G.W., Puppels, G.J. (2003). "Combined *in vivo* confocal Raman spectroscopy and confocal microscopy of human skin." Biophysical Journal **85**(1): 572-580.

Caspers, P.J., Lucassen, G.W., Wolthius, R., Bruining, H.A, Puppels, G. L. (1998). "*In vitro* and *in vivo* Raman spectroscopy of human skin." Biospectroscopy **4**(5): S31-S39.

Caspers, P.J., Lucassen, G.W., Carter, E.A., Bruining, H.A., Puppels, G.J. (2001). "*In vivo* confocal Raman microspectroscopy of the skin: Noninvasive determination of molecular concentration profiles." Journal of Investigative Dermatology **116**(3): 434-442.

Catalona, W.J., Partin, A.W., Slawin, K. M., Brawer, M. K., Flanigan, R. C., Patel, A., Richie, J. P., deKernion, J. B., Walsh, P. C., Scardino, P. T., Lange, P. H., Subong, E. N. P., Parson, R. E., Gasior, G. H., Loveland, K. G., Southwick, P. C. (1998). "Use of the percentage of free prostate-specific antigen to enhance differentiation of prostate cancer from benign prostatic disease - A prospective multicenter clinical trial." Jama-Journal of the American Medical Association **279**(19): 1542-1547.

Cheng, L., Cheville, J.C., Neumann, R.M., Bostwick, D.G. (1999). "Natural history of urolthelial dysplasia of the bladder." American Journal of surgical pathology. **23**(4): 443-447.

Choo-Smith, L.P., Edwards, H.G.M., Endtz, H. P., Kros, J. M., Heule, F., Barr, H., Robinson, J. S., Bruining, H. A., Puppels, G. J. (2002). "Medical applications of Raman spectroscopy: From proof of principle to clinical implementation." Biopolymers **67**(1): 1-9.

Cothren, R.M., Sivak, M.V., Petras, R., Rava, R., Feld, M. S. (1993). "Insitu Diagnosis of Colonic Adenomas by Autofluorescence Spectroscopy." Gastrointestinal Endoscopy **39**(2): 295-295.

Crow, P. (2003). The use of Raman spectroscopy to differentiate between benign and malignant pathologies of the bladder and prostate *in vitro*. MD Thesis. Bristol University.

Crow, P., Barrass, B., Hart Prieto, M., Kendall, C., Wright, M., Stone, N. (2004). "The use of Raman spectroscopy to differentiate between different cultured prostate cancer cell lines *in vitro*." Journal of Urology **171**(4): 114-114.

Crow, P., Kendall, C., Uff, J., Gilbert, H., Persad, R., Wright, M (2003). "Optical diagnostics in prostate cancer: The use of Raman spectroscopy to differentiate between different prostatic pathologies *in vitro*." Journal of Urology **169**(4): 1618.

Crow, P., Molckovsky, A., Uff, J., Stone, N., Wilson, B., Wongkeesong, L. M (2004). "Fibre-optic raman spectrsocopy: The prospects for *in vivo* diagnosis of bladder and prostate cancer." Journal of Urology **171**(4): 68-68.

Crow, P., Stone, N., Kendall, C., Uff, J., Ritchie, A., Wright, M. (2003). "Optical diagnostics in bladder cancer: The use of Raman spectroscopy to differentiate between bladder pathologies *in vitro*." Journal of Urology **169**(4): 871.

Crow, P., Stone, N., Kendall, C. A., Persad, R. A., Wright, M. P. J (2003). "Optical diagnostics in urology: current applications and future prospects." Bju International **92**(4): 400-407.

Crow, P., Stone, N., Kendall, C. A., Uff, J. S., Farmer, J. A. M., Barr, H., Wright, M. P. J. (2003). "The use of Raman spectroscopy to identify and grade prostatic adenocarcinoma *in vitro*." British Journal of Cancer **89**(1): 106-108.

Crow, P., Uff, J.S., Farmer, J. A., Wright, M. P., Stone, N. (2004). "The use of Raman spectroscopy to identify and characterise transitional cell carcinoma *in vitro*." BJU International **93**(9): 1232-1236.

Crow, P., Barrass, B., Hart Prieto, M., Kendall, C., Wright, M., Stone, N (2005). "The use of Raman spectroscopy to differentiate between different prostatic adenocarcinoma cell lines." British Journal of Cancer **92**(12): 2166-2171.

Crupi, V., Majolino, D., Migliardo, P., Mondello, M.R., Pergolizzi, S., Venuti, V. (2004). "FT-IR spectroscopy for the detection of liver damage." Spectroscopy **18**: 67-73.

Czeczuga-Semeniuk, E., Wolczynski, S., Markiewicz, W. (2003). "Preliminary identification of carotenoids in malignant and benign neoplasms of the breast and surrounding fatty tissue." Neoplasma **50**(4): 280-286.

Daudon, M., Protat, M.F., Reveillaud, R. J., Jaeschkeboyer, H (1983). "Infrared Spectrometry and Raman Microprobe in the Analysis of Urinary Calculi." Kidney International **23**(6): 842-850.

Dawson, C., Whitfield, H. (2002). ABC of Urology, 3rd ed. BMJ Publishing group.

De Dominicis, C., Liberti, M., Perugia G. De Nunzio C. Sciobica F. Zuccala A. Sarkozy A. Iori F. *l* (2001). "Role of 5-aminolevulinic acid in the diagnosis and treatment of superficial bladder cancer: Improvement in diagnostic sensitivity." Urology. **57**(6): 1059-1062.

De Jong, B.W.D., Schut, T.C.B., Coppens, J., Wolffenbuttel, K. P., Kok, D. J., Puppels, G. J (2003). "Raman spectroscopic detection of changes in molecular composition of bladder muscle tissue caused by outlet obstruction." Vibrational Spectroscopy **32**(1): 57-65.

De Jong, B.W.D., Schut, T.C.B., Wolffenbuttel, K. P., Nijman, J. M., Kok, D. J., Puppels, G. J. (2002). "Identification of bladder wall layers by Raman spectroscopy." Journal of Urology **168**(4): 1771-1778.

Demul, F.F.M., Buiteveld, H., Lankester, J., Mud, J., Greve, J. (1984). "Raman Microspectroscopy in Human Pathology." Human Pathology **15**(11): 1062-1068.

Dhom, G. (1983). "Epidemiologic Aspects of Latent and Clinically Manifest Carcinoma of the Prostate." Journal of Cancer Research and Clinical Oncology **106**(3): 210-218.

Droller, M.J. and Malmstrom P.U. (2000). "Premalignant lesions and carcinoma in situ in bladder neoplasia - Introduction and overview." Scandinavian Journal of Urology and Nephrology **34**: 62-66.

Eardley, I., Fitzpatrick, J., Foley, C, Jefferson, K, Kirby, R, MacDonagh, R, Mahendra, V, Nambirjan, T, Persad, R, Taylor, C, Walsh, I (2002). Mims handbook of urology.

Eble, J.N., Sauter, G., Epstein, J.I., Sesterhenn, I.A. (2004). World Health Organisation Classification of Tumours. Pathology and Genetics of Tumours of the Urinary System and Male Genital Organs. Lyon, IARC Press.

Feld, M.S., Manoharan, R., Salenius, J., Orensteincarndona, J., Romer, T. J., Brennan, J. F., Dasari, R., Wang, Y. (1995). Detection and characterization of human tissue lesions with near infrared Raman spectroscopy. Advances in Fluorescence Sensing Technology Ii. **2388:** 99-104.

Fitzmaurice, M., Wallace, M.B., Perelman, L. T., Backman, V., Crawford, J. M., Seiler, M., Badizadegan, K., Shields, S. J., Itzkan, I., Dasari, R., Van Dam, J., Feld, M. S.. (1999). "Endoscopic diagnosis of dysplasia in Barrett's esophagus (BE): A novel light scattering-reflectance spectroscopy technique." Laboratory Investigation **79**(1): 428.

Flanders, W.D. (1984). "Review - Prostate-Cancer Epidemiology." Prostate **5**(6): 621-629.

Foley, C., Bott, S., Kirby, R., Fitzpatrick, J. (2002). Mims guide to prostate health.

Frank, C.J., McCreery, R.L., Redd, D. C. B. (1995). "Raman-Spectroscopy of Normal and Diseased Human Breast Tissues." Analytical Chemistry **67**(5): 777-783.

Frank, C.J., Redd, D.C.B., Gansler, T. S., McCreery, R. L. (1994). "Characterization of Human Breast Biopsy Specimens with near-Ir Raman-Spectroscopy." Analytical Chemistry **66**(3): 319-326.

Franks, L. (1956). "Latency and progression in tumours; the natural history of prostatic cancer." Lancet **2**: 1037-1039.

Fulljames, C., Stone, N., Bennett D., Barr H. (1999). "Beyond white light endoscopy - the prospect for endoscopic optical biopsy." Italian Journal of Gastroenterology and Hepatology **31**(8): 695-704.

Garraway, W.M., Collins, G.N., Lee, R.J. (1991). "High prevalence of benign prostatic hypertrophy in the community." Lancet. **338**(8765): 469-71.

Gaudin, P.B., Sesterhenn, I.A., Wojno, KJ; Mostofi, FK; Epstein, JI. (1997). "Incidence and clinical significance of high-grade prostatic intraepithelial neoplasia in TURP specimens." Urology **49**(4): 558-563.

Gazi, E., Dwyer, J., Lockyer, N., Gardner, P., Vickerman, J. C., Miyan, J., Hart, C. A., Brown, M., Shanks, J. H., Clarke, N. (2004). "The combined application of FTIR microspectroscopy and ToF-SIMS imaging in the study of prostate cancer." Faraday Discussions **126**: 41-59.

Gazi, E., Baker, M., Dwyer J. Lockyer NP. Gardner P. Shanks JH. Reeve RS. Hart CA. Clarke NW. Brown MD.. (2006). "The correlation of FTIR spectra derived from prostate cancer biopsies with gleason grade and tumour stage." European urology **50**: 750-761.

Georgakoudi, I., Jacobson, B.C., Van Dam, J., Backman, V., Wallace, M. B., Muller, M. G., Zhang, Q., Badizadegan, K., Sun, D., Thomas, G. A., Perelman, L. T., Feld, M. S. (2001). "Fluorescence, reflectance, and light-scattering spectroscopy for evaluating dysplasia in patients with Barrett's esophagus." Gastroenterology **120**(7): 1620-1629.

Goetz, M.J., Cote, G.L., Erckens, R., March, W., Motamedi, M. (1995). "Application of a Multivariate Technique to Raman-Spectra for Quantification of Body Chemicals." Ieee Transactions on Biomedical Engineering **42**(7): 728-731.

Goldfarb, D.A., Stein, B.S., Shamszadeh, M., Petersen, R. O. (1986). "Age-Related-Changes in Tissue-Levels of Prostatic Acid- Phosphatase and Prostate Specific Antigen." Journal of Urology **136**(6): 1266-1269.

Grimbergen, M.C.M., Van Swol, C.F.P., Van Moorselaar, R.J.A., Mahadevan-Jansen, A., Stone, N. (2006). "Feasibility of Raman spectroscopy *in vitro* after 5-ALA-based fluorescence diagnosis in the bladder. " Photonic therapeutic and diagnostics II. **6078:**

Hanlon, E.B., Manoharan, R., Koo, T. W., Shafer, K. E., Motz, J. T., Fitzmaurice, M., Kramer, J. R., Itzkan, I., Dasari, R. R., Feld, M. S. (2000). "Prospects for *in vivo* Raman spectroscopy." Physics in Medicine and Biology **45**(2): R1-R59.

Hart Prieto, M.C., Crow, P., Kendall, C., Uff, J., Wright, M., Ritchie, A., Stone, N. (2004). "Urological applications of Raman spectroscopy for improved malignant diagnostics." Biomedical Vibrational Spectroscopy and Bohazard Detection Technologies. **5321:** 57-68.

Harvei, S., Skjorten, F.J., Robsahm, T. E., Berner, A., Tretli, S. (1998). "Is prostatic intraepithelial neoplasia in the transition/central zone a true precursor of cancer? A long-term retrospective study in Norway." British Journal of Cancer **78**(1): 46-49.

Hata, T.R., Scholz, T.A., Ermakov, I. V., McClane, R. W., Khachik, F., Gellermann, W., Pershing, L. K (2000). "Non-invasive Raman spectroscopic detection of carotenoids in human skin." Journal of Investigative Dermatology **115**(3): 441-448.

Hawi, S.R., Campbell, W.B., Kajdacsy-Balla, A., Murphy, R., Adar, F., Nithipatikom, K. (1996). "Characterisation of normal and malignant hepatocytes by Raman microspectroscopy." Cancer **110**: 35-40.

Hermanek, P., Hutter, R.V.P., Sobin, L.H., Wagner, G., Wittekind, C.H. (1997). TNM Atlas: Illustrated guide to the Tnm/Ptnm classification of malignant tumours., Springer-Verlag Telos.

Herr, H.W. (1989). "When is a cystectomy necessary in carcinoma in situ?." Progress in Clinical & Biological Research. **303**: 511-515.

Herr, H.W., Pinsky, C.M., Whitmore, W.F. Jr., Sogani, P.C., Oettgen, H.F., Melamed, M.R. (1986). "Long-term effect of intravesical bacillus Calmette-Guerin on flat carcinoma in situ of the bladder." Journal of Urology. **135**(2): 265-7.

Hong, T.D., Phat, D., Plaza, P., Daudon, M., Dao, N.Q. (1992). "Identification of urinary calculi by Raman laser fiber optics spectroscopy." Clinical chemistry **38**(2): 292-298.

Hopwood, D. (1996). Fixation and fixatives. Theory and practice of histological techniques. S. A. Bancroft JD, Churchill livingstone.

Huggins, C., Hodges, C.V. (1941). "Studies on prostate cancer. I. The effect of castration, of estrogen and of androgen injection on serum phosphatases in metastatic carcinoma of the prostate. " Cancer Research **1:** 293-7.

Ishida, H., Kamoto, R., Uchida, S, Ishitani, A, Ozaki, Y, Iriyama, K, Tsukie, E, Shibata, K, Ishihara, F, Kameda, H. (1987). "Raman microprobe and Fourier Transform infrared microsampling studies of the microstructure of gallstones." Applied Spectroscopy **41**: 407-412.

Keller, S., Schrader, B., Hoffman, A, Schrader, W, Metz, K, Rehlaender, A, Pahnke, J, Ruwe, M, Budach, W. (1994). "Application of near infrared fourier transform Raman spectroscopy in medical research." Journal of Raman Spectroscopy **25**: 663-667.

Kendall, C. (2002). A study of Raman spectroscopy for the early detection and classification of malignancy in oesophageal tissue. School of engineering, Cranfield University.

Kendall, C., Barr, H., Shepherd, N., Stone, N. (2002). Optimum procedure for construction of spectral classification algorithms for medical diagnosis. Biomedical Vibrational Spectroscopy Ii. **3:** 152-158.

Kendall, C., Schut, T.B., Stone, N., Stravroulaki, P., Puppels, G., Barr, H. (2000). Raman spectroscopy for the diagnosis of dysplasia in columnar and squamous epithelium. Optical Biopsy and Tissue Optics. **1:** 131-137.

Kendall, C., Stone, N., Shepherd, N., Barr, H. (2003). Raman spectral mapping for the illumination of biochemical changes associated with malignancy in the oesophagus. Diagnostic Optical Spectroscopy in Biomedicine Ii. **5141:** 237-248.

Kendall, C., Stone, N., Shepherd, N., Geboes, K., Warren, B., Bennett, R., Barr, H. (2003). "Raman spectroscopy, a potential tool for the objective identification and classification of neoplasia in Barrett's oesophagus." Journal of Pathology **200**(5): 602-609.

Klotz, K.L., Goldenberg, S.L., Bullock, M., Srigley, J., Jewett, M., Mador, D., Fradet, Y., Barkin, J., Chin, J., Paquin, J. M., Lapalante, J. (1997). "Neoadjuvant androgen ablation prior to radical prostatectomy (CUOG P-92): 24 month post treatment PSA resuls." British Journal of Urology. **80**(suppl 2): 266.

Klug, D. D., Singleton, D.L, Walley, V. M.. (1992). "Laser Raman-Spectrum of Calcified Human Aorta." Lasers in Surgery and Medicine **12**(1): 13-17.

Kneipp, J., Schut, T.B., Kliffen, M., Menke-Pluijmers, M., Puppels, G. (2003). "Characterization of breast duct epithelia: a Raman spectroscopic study." Vibrational Spectroscopy **32**(1): 67-74.

Koenig, F., McGovern, F.J., Enquist, H., Larne, R., Deutsch, T.F., Schomacher, K.T. (1998). "Autofluorescence guided biopsy for the early diagnosis of bladder carcinoma." Journal of Urology **159**: 1871-1875.

Kovi, J., Mostofi, F.K., Heshmat, M. Y., Enterline, J. P. (1988). "Large Acinar Atypical Hyperplasia and Carcinoma of the Prostate." Cancer **61**(3): 555-561.

Kriegmair, M., Baumgartner, R., Knuechel, R, Steinbach, P, Ehsan, A, Lumper, W, Hofstadter, F, Hofstetter, A. (1994). "Fluorescence photodetection of neoplastic urothelial lesions following intravesical instillation of 5-aminolevulinic acid." Urology. **44**(6): 836-41.

Kumar, V., Cotran, R.S., Robbins, S.L. (1997). Basic Pathology, W.B. Saunders.

Kurth, K. H., Mickisch, G.H., Schroder, F.H. (1998). Renal, bladder and prostate cancer - an update, Parthenon Publishing.

Lawson, E.E., Barry, B.W., Williams, A. C., Edwards, H. G. M. . (1997). "Biomedical applications of Raman spectroscopy." Journal of Raman Spectroscopy **28**(2-3): 111-117.

Lewis, I. R., Edwards, H.G. (2001). Handbook of Raman spectroscopy - from the research laboratory to the process line., Marcel Dekker.

Lieber, C.A., Mahadevan-Jansen, A. (2003). "Automated method for subtraction of fluorescence from biological Raman spectra." Applied Spectroscopy **57**(11): 1363-1367.

Liu, C. H., Das, B.B., Sha Glassman, W.L, Tang, G.C, Yoo, K.M, Zhu, H.R, Akins, D.L, Lubicz, S.S, Cleary, J, Prudente, R, Celmer, E, Caron, A, Alfano, R.R. (1992). "Raman, flourescence and time-resolved light scattering as optical diagnostic techniques to separate diseased and normal biomedical media." Journal of Photochemistry and Photobiology B-Biology **16**: 187-209.

Mahadevan, A., N. Ramanujam, Mitchell, M. F., Malpica, A., Thomsen, S., Richardskortum, R. (1995). Optical techniques for the diagnosis of cervical precancers: A comparison of Raman and fluorescence spectroscopies. Advances in Fluorescence Sensing Technology Ii. **2388:** 110-120.

Mahadevan-Jansen, A., M. F. Mitchell, Ramanujam, N., Malpica, A., Thomsen, S., Utzinger, U., Richards-Kortum, R. (1998). "Near-infrared Raman spectroscopy for *in vitro* detection of cervical precancers." Photochemistry and Photobiology **68**(1): 123-132.

Mahadevan-Jansen, A., W. F. Mitchell, Ramanujam, N., Utzinger, U., Richards-Kortum, R. (1998). "Development of a fiber optic probe to measure NIR Raman spectra of cervical tissue *in vivo*." Photochemistry and Photobiology **68**(3): 427-431.

Mahadevan-Jansen, A., Richards-Kortum R. (1996). "Raman spectroscopy for the detection of cancers and precancers." Journal of Biomedical Optics **1**: 31-70.

Mann, C. K., Vickers, T.J. (1999). "Instrument-to-Instrument Transfer of Raman Spectra." Applied Spectroscopy **53**(7): 856-861.

Manoharan, R., J. J. Baraga, Feld, M. S., Rava, R. P. (1992). "Quantitative Histochemical Analysis of Human Artery Using Raman-Spectroscopy." Journal of Photochemistry and Photobiology B-Biology **16**(2): 211-233.

Manoharan, R., K. Shafer, Perelman, L., Wu, J., Chen, K., Deinum, G., Fitzmaurice, M., Myles, J., Crowe, J., Dasari, R. R., Feld, M. S. (1998). "Raman spectroscopy and fluorescence photon migration for breast cancer diagnosis and imaging." Photochemistry and Photobiology **67**(1): 15-22.

Manoharan, R., Y. Wang, Feld, M. S. (1996). "Histochemical analysis of biological tissues using Raman spectroscopy." Spectrochimica Acta Part a-Molecular and Biomolecular Spectroscopy **52**(2): 215-249.

Manoharan, R., Wang, Y, Boustany, N, Brennan III, J.F, Baraga, J.J, Dasari, R.R, Van Dam , J, Singer, S, Feld, M.S. (1994). "Raman Spectroscopy for Cancer Detection: Instrument Development and Tissue Diagnosis." Proc. SPIE: Biomedical Optoelectronic Devices and Systems II, **2328**: 128-132.

Matousek, P., Everall, N, Towrie, M, Parker, A.W. (2005). "Depth profiling in diffusely scattering media using Raman spectroscopy and picosecond Kerr gating." Applied Spectroscopy **59**(2): 200-5.

Matousek, P., Towrie, M, Ma, C, Kwok, W.M, Phillips, D, Toner, A.W, Parker, A.W. (2001). "Fluorescence suppression in resonance Raman spectroscopy using a high-performance picosecond Kerr gate." Journal of Raman Spectroscopy **32**: 983-988.

Matousek, P., Towrie, M, Stanley, A, Parker, A.W. (1999). "Efficient rejection of fluorescence from Raman spectra using picosecond Kerr gating." Applied Spectroscopy **53**(12): 1485-1489.

McNeal, J. E. (1968). "Regional morphology and pathology of the prostate." American Journal of clinical pathology. **49**: 347-357.

McNeal, J. E. (1969). "Origin and development of carcinoma of the prostate." Cancer **23**: 24-34.

McNeal, J. E. (1988). "Normal Histology of the Prostate." American Journal of Surgical Pathology **12**(8): 619-633.

McNeal, J. E. and D. G. Bostwick (1986). "Intraductal Dysplasia - a Premalignant Lesion of the Prostate." Human Pathology **17**(1): 64-71.

Meyer, J. P., Gillat, D. (2003). "What's new in bladder cancer." Trends in urology, gynaecology and sexual health. **8**(6): 25-29.

Molckovsky, A., L. Song, Shim, M. G., Marcon, N. E., Wilson, B. C (2003). "Diagnostic potential of near-infrared Raman spectroscopy in the colon: differentiating adenomatous from hyperplastic polyps." Gastrointestinal Endoscopy **57**(3): 396-402.

Moore, R. A. (1943). "Benign hypertrophy of the prostate - a morphologic study." Journal of Urology **50**: 680-710.

Morris, M. D., A. E. Goodship, et al. (2004). Kerr-gated picosecond Raman spectroscopy and Raman photon migration of equine bone tissue with 400-nm excitation. Biomedical Vibrational Spectroscopy and Bohazard Detection Technologies. **5321:** 164-169.

Motz, J. T., M. Hunter, Galindo, L. H., Gardecki, J. A., Kramer, J. R., Dasari, R. R., Feld, M. S, (2004). "Optical fiber probe for biomedical Raman spectroscopy." Applied Optics **43**(3): 542-554.

Mulvaney, S. P. and C. D. Keating (2000). "Raman spectroscopy." Analytical Chemistry **72**(12): 145R-157R.

Murphy, W. M., Beckwith, J.B, Farrow, G.M. (1993). Tumours of the kidney, bladder and related urinary structures., AFIP.

Nie, S. M., D. C. B. Redd, Li, Y. Z., Yu, N. T. (1992). Near-Ir Fourier-Transform Raman-Spectroscopy in Surgery and Medicine - Detection of Renal Stones and Bladder-Cancer. Proceedings of Laser Surgery : Advanced Characterization, Therapeutics, and Systems Iii. **1643:** 60-66.

Pacifico, R., K. Wang, Molckovsky, A., Buttar, N. S., Wong, L. M., Song, K., Carpenter, H., Lutzke, L. (2002). "Biopsy strategies in Barretts esophagus: Which is the best to detect high-grade dysplasia?" Gastroenterology **122**(4): 485.

Parmar, M.K.D., Friedman, L.S., Hargreave, T.B., Tolley, D.A. (1989) "Prognostic factors for recurrence and follow up policies in the treatment of superficial bladder cancer. A report from the Medical Research Council Subgroup on superficial bladder cancer."Journal of Urology. **142:** 284.

Partin, A. W., L. A. Mangold, Lamm, D. M., Walsh, P. C., Epstein, J. I., Pearson, J. D. (2002). "Contemporary update of prostate cancer staging nomograms (Partin tables) for the new millennium." Journal of Urology **168**(1): 374-375.

Partin, A. W., J. Yoo, Carter, H. B., Pearson, J. D., Chan, D. W., Epstein, J. I., Walsh, P. C. (1993). "The Use of Prostate-Specific Antigen, Clinical Stage and Gleason Score to Predict Pathological Stage in Men with Localized Prostate-Cancer." Journal of Urology **150**(1): 110-114.

Pestaner, J. P., F. G. Mullick, Johnson, F. B., Centeno, J. A. (1996). "Calcium oxalate crystals in human pathology - Molecular analysis with the laser Raman microprobe." Archives of Pathology & Laboratory Medicine **120**(6): 537-540.

Petrylak, D.P., Tangen, C.M., Hussain MH, Lara PN Jr, Jones JA, Taplin ME, Burch PA, Berry D, Moinpour C, Kohli M, Benson MC, Small EJ, Raghavan D, Crawford ED. (2004). "Docetaxel and estramustine compared with mitoxantrone and prednisone for advanced refractory prostate cancer." New England Journal of Medicine. **351:** 1513-1520.

Puppels, G. J. (2000). "*In vivo* Raman spectroscopy." Microbeam Analysis 2000, Proceedings**:** 63-64.

Raman, C., Krishnan, K. (1928). "A new type of secondary radiation." Nature **121**(3048): 501-502.

Richards, B., M. K. B. Parmar, Anderson, C. K., Ansell, I. D., Grigor, K., Hall, R. R., Morley, A. R., Mostofi, F. K., Risdon, R. A., Uscinska, B. M. (1991). "Interpretation of Biopsies of Normal Urothelium in Patients with Superficial Bladder-Cancer." British Journal of Urology **67**(4): 369-375.

Richards Kortum, R. and E. SevickMuraca (1996). "Quantitative optical spectroscopy for tissue diagnosis." Annual Review of Physical Chemistry **47**: 555-606.

Robichaux, A., C. Lieber, Shappell, H., Huff, B., Jones, H., Mahadevan-Jansen, A. (2002). *In vivo* detection of cervical dysplasia with near infrared Raman spectroscopy. Biomedical Vibrational Spectroscopy Ii. **3:** 145-151.

Robichaux-Viehoever, A., Shappell, H, Billheimer, D, Jones, III, H, Mahadevan-Jansen, A. (2005). "Characterization of variability in Raman spectra of the cervix." Awaiting publication.

Romer, T. J., Brennan, J. F., Fitzmaurice, M., Feldstein, M. L., Deinum, G., Myles, J. L., Kramer, J. R., Lees, R. S., Feld, M. S. (1998). "Histopathology of human coronary atherosclerosis by quantifying its chemical composition with Raman spectroscopy." Circulation **97**(9): 878-885.

Salenius, J. P., J. F. Brennan, Miller, A., Wang, Y., Aretz, T., Sacks, B., Dasari, R. R., Feld, M. S. (1998). "Biochemical composition of human peripheral arteries examined with near-infrared Raman spectroscopy." Journal of Vascular Surgery **27**(4): 710-719.

Schulman, C.C., Debruyne, F.M.J., Forster, G., Van Cangh, P.J., Witjes, W.P.J. (1997). "Neoadjuvant combined androgen deprivation therapy in locally confined prostatic carcinoma. Three year follow up of a European multricentric randomized study" British Journal of Urology. **80**(suppl 2): 259.

Schut, T. C. B., N. Stone, Fulljames, C., Barr, H., Bruining, H. A., Puppels, G. J. (2000). Progress in the detection of neoplastic progress and cancer by Raman spectroscopy. Biomedical Spectroscopy: Vibrational Spectroscopy and Other Novel Techniques. **1:** 106-113.

Schut, T. C. B., Witjes, M. J. H., Sterenborg, Hjcm, Speelman, O. C., Roodenburg, J. L. N., Marple, E. T., Bruining, H. A., Puppels, G. J. (2000). "*In vivo* detection of dysplastic tissue by Raman spectroscopy." Analytical Chemistry **72**(24): 6010-6018.

Schut, T. C. B., R. Wolthuis, Caspers, P. J., Puppels, G. J. (2002). "Real-time tissue characterization on the basis of *in vivo* Raman spectra." Journal of Raman Spectroscopy **33**(7): 580-585.

Shafer, K., R. Manoharan, Dasari, R., Feld, M. S., Harrison, G. R., Myles, J., Crowe, J. (1998). "Modeling of nir Raman spectra of human breast tissue for breast cancer diagnosis." Abstracts of Papers of the American Chemical Society **216**: 344-PHYS.

Shafer-Peltier, K. E., A. S. Haka, Fitzmaurice, M., Crowe, J., Myles, J., Dasari, R. R., Feld, M. S. (2002). "Chemical basis for breast cancer diagnosis using Raman spectroscopy." Lasers in Surgery and Medicine: 3.

Shafer-Peltier, K. E., A. S. Haka, Fitzmaurice, M., Crowe, J., Myles, J., Dasari, R. R., Feld, M. S. (2002). "Raman microspectroscopic model of human breast tissue: implications for breast cancer diagnosis *in vivo*." Journal of Raman Spectroscopy **33**(7): 552-563.

Sheldon, C. A., Williams, R.D, Fraley, E.E. (1980). "Incidental carcinoma of the prostate: a review of the literature and critical appraisal of classification." Journal of Urology **124**: 626-631.

Shelley, M.D., Barber, J., Wilt, T., Mason, M.D. (2002). "Surgery versus radiotherapy for muscle invasive bladder cancer." Cochrane Database Systematic Review. **1:** CD002079.

Shim, M. G., Song, L., Marcon, N. E., Wilson, B. C, (2000). "*In vivo* near-infrared Raman spectroscopy: Demonstration of feasibility during clinical gastrointestinal endoscopy." Photochemistry and Photobiology **72**(1): 146-150.

Shrader, B., Keller, S, Lochte, T, Fendel, S, Moore, D.S, Simon, A, Sawatzki, I. (1995). "NIR FT Raman spectroscopy in medical diagnosis." Journal of molecular structure **348**: 293-296.

Smith, D.C., Redman, B.G., Flaherty L. E., Lang L. I, Strawderman M., Pienta K. J. (1998). "A phase II trial of oral diethylstilboesterol as a second line hormonal agent in advanced prostate cancer." Urology **52:** 257-260.

Smith, D. S. and W. J. Catalona (1994). "Rate of Change in Serum Prostate-Specific Antigen Levels as a Method for Prostate-Cancer Detection." Journal of Urology **152**(4): 1163-1167.

Smith, J., J. Christie-Brown, Sammon, A. M., Stone, N. (2004). Axillary lymph node analysis using Raman spectroscopy. Biomedical Vibrational Spectroscopy and Bohazard Detection Technologies. **5321:** 69-74.

Smith, J., C. Kendall, Christie-Brown, J., Sammon, A., Stone, N. (2003). Raman Spectroscopy in the assessment of breast cancer and axillary lymph node metastases. Diagnostic Optical Spectroscopy in Biomedicine Ii. **5141:** 305-309.

Smith, J., C. Kendall, Sammon, A., Christie-Brown, J., Stone, N. (2003). "Raman spectral mapping in the assessment of axillary lymph nodes in breast cancer." Technology in Cancer Research & Treatment **2**(4): 327-331.

Smith, J., N. Stone, Kendall, C., Christie-Brown, J., Shepherd, N., Sammon, A., Barr, H. (2003). "Raman spectroscopy: a novel optical technique for the diagnosis and management of carcinoma of the oesophagus and breast, and lymph node metastases." British Journal of Surgery **90**(5): 637-637.

Smithies, D. J., Butler, P.H. (1995). "Modelling the distribution of laser light in port-wine stains with the Monte Carlo method." Physics in Medicine and Biology **40**: 701-731.

Sobin, L. H., Wittekind, C.H. (2002). TNM classification of malignant tumours.

Soloway, M.S., Shairifi, R., Wajsman, Z., Mcleod, D., Wood, D., Puras-Baez, A. (1997) "Radical prostatectomy alone versus radical prostatectomy preceded by androgen blockade in cT2b prostate cancer – 24 month results" British Journal of Urology. **80**(suppl 2): 259.

Song, L., T. Y. Gao, Molckovsky, A., Burgart, L., Smyrk, T., Buttar, N., Lutzke, L., Wilson, B., Wang, K. (2003). "Accuracy of near-infrared Raman spectroscopy for differentiating adenocarcinoma from high-grade dysplasia in Barret's esophagus." Gastroenterology **124**(4): A71-A71.

Song, L., A. Molckovsky, Buttar, N., Hsieh, E., Riddell, R., Bassett, N., Cirocco, M., Marcon, N., Wilson, B., Wang, K. (2003). "Characterization of intestinal metaplasia by near-infrared Raman spectroscopy in patients with dysplastic and non- dysplastic Barrett's esophagus." Gastroenterology **124**(4): A644-A644.

Song, L., A. Molckovsky, Wang, K., Gao, T., Basset, N., Cirocco, M., Maroon, N., Shim, M., Wilson, B. (2002). "Near-infrared Raman spectroscopy for classification of colon polyps." Gastroenterology **122**(4): 259.

Song, L., A. Molckovsky, Wang, K., Gao, T. Y., Basset, N., Cirocco, M., Marcon, N., Hsieh, E., Riddell, R., Shim, M., Wilson, B. (2002). Raman Spectroscopy for *in vivo* classification of Barrett's tissue." Gastroenterology **122**(4): M1372.

Sowa, M. G, Smith, M. S. D, Kendall, C., Bock, E. R., Ko, L. A.C., Choo-Smith, I., Stone, N. (2006). "Compositional modeling of multicomponent systems using semi-parametric regression of Raman spectra." Applied spectroscopy **60**(8): 877-883.

Stenman, U. H., J. Leinonen, Alfthan, H., Rannikko, S., Tuhkanen, K., Alfthan, O. (1991). "A Complex between Prostate-Specific Antigen and Alpha-1- Antichymotrypsin Is the Major Form of Prostate-Specific Antigen in Serum of Patients with Prostatic-Cancer - Assay of the Complex Improves Clinical Sensitivity for Cancer." Cancer Research **51**(1): 222-226.

Sternberg, C.N. (2002). "Current perspectives in muscle invasive bladder cancer." European Journal of Cancer **38:** 460-467.

Stone, N. (2001). Raman Spectroscopy of biological tissue for the application in optical diagnosis of malignancy. PhD Thesis. Department of Environmental and Ordinance Systems R.M.C.S. and Cranfield post graduate medical school, Cranfield University.

Stone, N., C. Kendall, Chandratreya, N., Shepherd, N., Barr, H. (2002). "Near-infrared Raman spectroscopy for detection and classification of gastrointestinal disease." Biomedical Vibrational Spectroscopy . **3:** 117-126.

Stone, N., C. Kendall, Shepherd, N., Crow, P., Barr, H. (2002). "Near-infrared Raman spectroscopy for the classification of epithelial pre-cancers and cancers." Journal of Raman Spectroscopy **33**(7): 564-573.

Stone, N., C. Kendall, Smith, J., Crow, P., Barr, H. (2004). "Raman spectroscopy for identification of epithelial cancers." Faraday Discussions **126**: 141-157.

Stone, N., P. Stavroulaki, Fulljames, C. A., Birchall, M., Barr, H. (2000). Raman spectroscopy: A diagnostic tool for detection of early malignant changes in the larynx. Biomedical Spectroscopy: Vibrational Spectroscopy and Other Novel Techniques. **1:** 120-128.

Stone, N., Stavroulaki, P., Kendall, C., Birchall, M., Barr, H. (2000). "Raman spectroscopy for early detection of laryngeal malignancy: Preliminary results." Laryngoscope **110**(10): 1756-1763.

Sudlow, K. and Woolf, A. (1991). "Identification of Renal Calculi by Their Raman-Spectra." Clinica Chimica Acta **203**(2-3): 387-394.

Tannock, I.F., de Wit, R., etal. (2004). "Docetaxel plus prednisone or mitoxantrone plus prednisone for advanced prostate cancer." New England Journal of Medicine. **351:** 1502-1512.

Toniolo, P., A. L. Van Kappel, Akhmedkhanov, A., Ferrari, P., Kato, I., Shore, R. E., Riboli, E. (2001). "Serum carotenoids and breast cancer." American Journal of Epidemiology **153**(12): 1142-1147.

Tortora, G. J., Grabowski, S.R. (1996). Principles of Anatomy and Physiology, Harper Collins College.

Underwood, J. C. E. (2004). General and systematic pathology. 4th ed. Churchill Livingstone.

Utzinger, U., D. L. Heintzelman, Mahadevan-Jansen, A., Malpica, A., Follen, M., Richards-Kortum, R. (2001). "Near-infrared Raman spectroscopy for *in vivo* detection of cervical precancers." Applied Spectroscopy **55**(8): 955-959.

Utzinger, U. and R. R. Richards-Kortum (2003). "Fiber optic probes for biomedical optical spectroscopy." Journal of Biomedical Optics **8**(1): 121-147.

van de Poll, S. W. E., Buschman, H. P. J., Visser, M. J., van Bockel, J. H., van der Laarse, A., Bruschke, A. V. G., Puppels, G. J. (2000). "Raman spectroscopy provides characterization of human atherosclerotic plaque composition *in vivo*." Journal of the American College of Cardiology **35**(2): 52A-52A.

van de Poll, S. W. E., Puppels, G. J., van der Laarse, A. (2002). "Raman spectroscopy of atherosclerosis." Journal of Cardiovascular Risk **9**(5): 255-261.

VanDam, J., J. M. Crawford, Preisinger, E. A., Wang, Y., Feld, M. S. (1996). "Fluorescence endoscopic imaging of human colonic dysplasia *in vitro*." Gastroenterology **110**(4): A612-A612.

Wallace, M. B., S. J. Shields, Perelmen, L. T., Packman, B., Zonios, G., Manoharan, R., Badizadegan, K., Nusrat, A., Seller, M., Hamano, T., Itzkan, I., Lima, C., Fitzmaurice, M., Crawford, J. M., Van Dam, J., Feld, M. S. (1998). "Fiber-optic detection of low-grade dysplasia in patients with Barrett's esophagus using reflectance spectroscopy." Gastroenterology **114**(4): G1337.

Wang, J. S., Shi, J. S., Xu, Y. Z., Duan, X. Y., Zhang, L., Wang, J., Yang, L. M., Weng, S. F., Wu, J. G. (2003). "FT-IR spectroscopic analysis of normal and cancerous tissues of esophagus." World Journal of Gastroenterology **9**(9): 1897-1899.

Wang, J. S., Xu, Y. Z., Shi, J. S., Zhang, L., Duan, X. Y., Yang, L. M., Su, Y. L., Weng, S. F., Xu, D. F., Wu, J. G. (2003). "FTIR spectroscopic study on normal and cancerous tissues of esophagus." Spectroscopy and Spectral Analysis **23**(5): 863-865.

Wang, S. Y., Hasty, C.E, Watson, P.A, Wicksted, J.P, Stith, R.D, March, W.F. (1993). "Analysis of metabolites in aqueous solutions by using laser Raman spectroscopy." Applied Optics **32**(6): 925-929.

Wang, T. D., Crawford, J. M., Feld, M. S., Wang, Y., Itzkan, I., Van Dam, J. (1999). "*In vivo* identification of colonic dysplasia using fluorescence endoscopic imaging." Gastrointestinal Endoscopy **49**(4): 447-455.

Wang, T. D., VanDam, J., Crawford, J. M., Preisinger, E. A., Wang, Y., Feld, M. S. (1996). "Fluorescence endoscopic imaging of human colonic adenomas." Gastroenterology **111**(5): 1182-1191.

Weng, S. F., Lin, X. F., Yang, L. M., Soloway, R. D., Xu, Y. Z., Tian, W., Yang, Z. L., Kang, N., Yan, W. F., Hu, X. B., Fately, W. G., Wu, J. G. (2000). "Use of mid-infrared fiber optics to determine the extent of spread of gastric and colonic cancer." Gastroenterology **118**(4): 6436.

Weng, S. F., Ling, X.F, Song, Y.Y, Xu, Y.Z, Li, WH, Zhang, X, Yang, L, San, W, Zhou, X, Wu, J. (2000). "FTIR Fiber optics and FT Raman spectroscopic studies for the diagnosis of cancer." American Clinical Laboratories **19**(7): 20.

Young, R. H., Srigley, J.R, Amin, M.B, Ulbright, T.M, Cubilla, A.L. (1998). Tumours of the prostate gland, seminal vesicles, male urethra and penis., AFIP.

Yu, N. T., East, E.J. (1975). "Laser Raman spectroscopic studies of ocular lens and its isolated protein fractions." Journal of biological chemistry **250**: 2196-2202.

Zaneveld, L. J., Tauber, P.F. (1981). "Contribution of prostatic fluid components in the ejaculate." Progress in clinical biological research **75a**: 265-277.

Zonios, G. I., R. M. Cothren, Arendt, J. T., Wu, J., VanDam, J., Crawford, J. M., Manoharan, R., Feld, M. S. (1996). "Morphological model of human colon tissue fluorescence." Ieee Transactions on Biomedical Engineering **43**(4): 437-437.

Appendix 1.

Local ethical approval for the thesis work.

Gloucestershire Local Research Ethics Committee
Gloucestershire Royal Hospital
Great Western Road
Gloucester
GL1 3NN

Tel: 01452 395726
Fax: 01452 395720

Our Ref: 01_97(4_11)

November 4, 2003

Miss MC Hart Prieto
Research Fellow
Biophotonics Research Group
Gloucestershire Royal Hospital
Great Western Road
Gloucester
GL1 3NN

Dear Miss Hart Prieto

Study No 01/97G : Evaluation of Raman Spectroscopy to provide a real time, non-invasive method for the discrimination of normal and abnormal tissue in the bladder

I am writing further to receipt of your revised correspondence with regards to the above study, which include revisions that have previously been approved by Gloucestershire Local Research Ethics Committee, which also incorporate your contact details as the new lead researcher for this study.

The following documents have been received with thanks:

- Information Sheet *(undated)*
- Additional Information Sheet *(undated)*
- Consent Form *(undated)*
- Protocol for the Collection of Bladder Samples for Research *(undated)*
- Protocol for Evaluation of Raman Spectroscopy for Detection of Malignant Changes in the Bladder *(undated)*

Many thanks for forwarding your revised documentation to the committee.

Yours sincerely

Sue Starck
Administrator

An advisory committee to Avon, Gloucestershire and Wiltshire Strategic Health Authority

Gloucestershire Local Research Ethics Committee
Gloucestershire Royal Hospital
Great Western Road
Gloucester
GL1 3NN

Tel: 01452 395726
Fax: 01452 395720

Our Ref: 00_159(4_11)

November 4, 2003

Miss MC Hart Prieto
Research Fellow
Biophotonics Research Group
Gloucestershire Royal Hospital
Great Western Road
Gloucester
GL1 3NN

Dear Miss Hart Prieto

Study No 00/159G : Evaluation of Raman spectroscopy to provide a real time, non-invasive method for the discrimination of normal and abnormal tissue in the prostate

I am writing further to receipt of your revised correspondence with regards to the above study, which include revisions that have previously been approved by Gloucestershire Local Research Ethics Committee, which also incorporate your contact details as the new lead researcher for this study.

The following documents have been received with thanks:

- Information Sheet *(undated)*
- Additional Information Sheet *(undated)*
- Consent Form *(undated)*
- Protocol for the Collection of Prostate Samples for Research *(undated)*
- Protocol for Evaluation of Raman Spectroscopy for Detection of Malignant Changes in the Prostate *(undated)*

Many thanks for forwarding your revised documentation to the committee.

Yours sincerely

Sue Starck
Administrator

Appendix 2.

Patient information for obtaining prostate and bladder samples.

Patient consent form for obtaining prostate and bladder samples.

Patient information for obtaining bladder samples.

Patient consent form for obtaining bladder samples.

Gloucestershire Hospitals NHS
NHS Trust

Biophotonics Research Group
Gloucestershire Royal Hospital
Great Western Road
Gloucester
GL1 3NN

TAKING PART IN RESEARCH

Study Title: **Evaluation of Raman spectroscopy for the identification of normal and abnormal tissue within the prostate and bladder.**

You are being invited to take part in a research project. Here is some information to help you decide whether or not to take part. Please take time to read the following information carefully and discuss it with friends, family or members of staff if you wish. Ask us if there is anything you do not understand or if you would like more information. Take time to decide whether or not you wish to take part. Thank you for reading this sheet.

Background

The staff of Gloucestershire Royal Hospital and the Biophotonics research group are working together to find new ways of diagnosing and treating disease. Recent advances in laser technology has enabled us to develop new methods of detecting disease using light. By shinning light on tissue and studying the light given off we can measure the chemical makeup of the tissue using a technique called Raman spectroscopy. This technique should allow us to study changes that occur as part of the disease process. Future prospects include the measurement of the state of the prostate and / or bladder in the patient without the need for tissue removal. This may allow us to detect bladder and prostate disease earlier.

Initially in the laboratory we will study the changes that occur in the prostate and bladder during disease development. To do this we need a small amount of the prostate tissue that will be removed during a routine operation. We also ask if you would be willing to let us take a small sample from your bladder, if you are undergoing a trans-urethral resection of your prostate. This would not ordinarily be done as part of your operation, but as only a small sample is taken it should make no difference to your recovery. Once we have finished studying the tissue you have donated, it will be destroyed, and will not be used for any other research projects.

Your surgeon or doctor will discuss the clinical procedure with you. Being asked to be a part of this study does not mean you have an abnormal bladder or prostate. For involvement in this study we need bladder and prostate tissue ranging from normal to cancerous.

Thank you for your help and co-operation. Please read the additional information over the other side of the sheet.

Gloucestershire Hospitals NHS
NHS Trust

Biophotonics Research Group
Gloucestershire Royal Hospital
Great Western Road
Gloucester
GL1 3NN

ADDITIONAL INFORMATION

1. You may not receive any direct benefit from the study. However, information obtained during the course of the study will be used in medical scientific research.
2. It is up to you to decide whether to take part or not. If you decide to take part you will be given this information sheet and a consent form. If at any time you would like to withdraw from the study you are free to do so. This will not affect the standard of care you will receive. You doctor will not be upset if you decide not to take part.
3. All the information collected about you during the course of the research will be kept strictly confidential. Only the researcher collecting the tissue from you will know your identity.
4. Consumers for Ethics in Research (CERES) publish a leaflet entitled 'Medical Research and You'. This leaflet gives more information about medical research and looks at some questions you may want to ask. A copy may be obtained from CERES, PO Box 1365, London N16 0BW.
5. This study has been approved by the Gloucestershire Local Research Ethics Committee. They may be contacted at the following address: Gloucestershire Local Research Ethics Committee, Gloucestershire Health Authority, Pullman Court, Great Western Road, Gloucester, GL1 3NN.
6. Further information about this research study can be obtained from:

   Maria C Hart Prieto
   Biophotonics Research Group
   Gloucestershire Royal Hospital
   Tel: 01452 395714

(Oct 2003)

Gloucestershire Hospitals NHS
NHS Trust

Biophotonics Research Group
Gloucestershire Royal Hospital
Great Western Road
Gloucester
GL1 3NN

CONSENT FORM

Title of Project: **Evaluation of Raman spectroscopy for the indentification of normal and abnormal tissue within the prostate and bladder.**

Name of Researcher: Miss. Maria C Hart Prieto (Oct 2003)

Please initial box provided

1. I confirm that I have read and understood the information sheet dated 22/10/03 for the above study. ☐
2. I understand that my participation in the study is voluntary and that I am free to withdraw at any time without my medical care or legal rights being affected. ☐
3. I agree to take part in the above study. ☐

Name of patient	Date	Signature
Name of person taking consent (if different from researcher)	Date	Signature
Researcher	Date	Signature

Gloucestershire Hospitals NHS
NHS Trust

Biophotonics Research Group
Gloucestershire Royal Hospital
Great Western Road
Gloucester
GL1 3NN

TAKING PART IN RESEARCH

Study Title: **Evaluation of Raman spectroscopy for the identification of normal and abnormal tissue within the prostate and bladder.**

You are being invited to take part in a research project. Here is some information to help you decide whether or not to take part. Please take time to read the following information carefully and discuss it with friends, family or members of staff if you wish. Ask us if there is anything you do not understand or if you would like more information. Take time to decide whether or not you wish to take part. Thank you for reading this sheet.

Background

The staff of Gloucestershire Royal Hospital and the Biophotonics research group are working together to find new ways of diagnosing and treating disease. Recent advances in laser technology has enabled us to develop new methods of detecting disease using light. By shinning light on tissue and studying the light given off we can measure the chemical makeup of the tissue using a technique called Raman spectroscopy. This technique should allow us to study changes that occur as part of the disease process. Future prospects include the measurement of the state of the prostate and / or bladder in the patient without the need for tissue removal. This may allow us to detect bladder and prostate disease earlier.

Initially in the laboratory we will study the changes that occur in the prostate and bladder during disease development. To do this we need a small amount of the bladder tissue that may be removed during your routine operation. We also ask if you would be willing to let us take a small sample from your bladder. This would not ordinarily be done as part of your operation, but as only a small sample is taken it should make no difference to your recovery. Once we have finished studying the tissue you have donated, it will be destroyed, and will not be used for any other research projects.

Your surgeon or doctor will discuss the clinical procedure with you. Being asked to be a part of this study does not mean you have an abnormal bladder. For involvement in this study we need bladder tissue ranging from normal to cancerous.

Thank you for your help and co-operation. Please read the additional information over the other side of the sheet.

Gloucestershire Hospitals NHS
NHS Trust

Biophotonics Research Group
Gloucestershire Royal Hospital
Great Western Road
Gloucester
GL1 3NN

ADDITIONAL INFORMATION

1. You may not receive any direct benefit from the study. However, information obtained during the course of the study will be used in medical scientific research.
2. It is up to you to decide whether to take part or not. If you decide to take part you will be given this information sheet and a consent form. If at any time you would like to withdraw from the study you are free to do so. This will not affect the standard of care you will receive. You doctor will not be upset if you decide not to take part.
3. All the information collected about you during the course of the research will be kept strictly confidential. Only the researcher collecting the tissue from you will know your identity.
4. Consumers for Ethics in Research (CERES) publish a leaflet entitled 'Medical Research and You'. This leaflet gives more information about medical research and looks at some questions you may want to ask. A copy may be obtained from CERES, PO Box 1365, London N16 0BW.
5. This study has been approved by the Gloucestershire Local Research Ethics Committee. They may be contacted at the following address: Gloucestershire Local Research Ethics Committee, Gloucestershire Health Authority, Pullman Court, Great Western Road, Gloucester, GL1 3NN.
6. Further information about this research study can be obtained from:

   Maria C Hart Prieto
   Biophotonics Research Group
   Gloucestershire Royal Hospital
   Tel: 01452 395714

(Oct 2003)

Gloucestershire Hospitals NHS
NHS Trust

Biophotonics Research Group
Gloucestershire Royal Hospital
Great Western Road
Gloucester
GL1 3NN

CONSENT FORM

Title of Project: **Evaluation of Raman spectroscopy for the indentification of normal and abnormal tissue within the prostate and bladder.**

Name of Researcher: Miss. Maria C Hart Prieto (Oct 2003)

Please initial box provided

1. I confirm that I have read and understood the information sheet dated 22/10/03 for the above study. ☐
2. I understand that my participation in the study is voluntary and that I am free to withdraw at any time without my medical care or legal rights being affected. ☐
3. I agree to take part in the above study. ☐

Name of patient	Date	Signature
Name of person taking consent (if different from researcher)	Date	Signature
Researcher	Date	Signature

Appendix 3.

Papers published from this thesis work.

Raman spectroscopic biochemical mapping of tissues
N Stone, **M C Hart Prieto**, C A Kendall, G Shetty, H Barr.
Biomedical vibrational spectroscopy and biohazard detection technologies. SPIE Jan 2006

The use of picosecond Kerr gated Raman spectroscopy to suppress signals from both surface and deep layers in bladder and prostate tissue.
M. C. Hart Prieto, P. Matousek, M. Towrie, A. W. Parker, M. Wright, A. W. Ritchie, N. Stone.
Accepted for publication in the Journal of Biomedical optics.

Urological applications of Raman spectroscopy for improved malignant diagnostics.
M. C. Hart Prieto, P. Crow, C. Kendall, J. Uff, M. Wright, A. Ritchie, N. Stone.
Biomedical vibrational spectroscopy and biohazard detection technologies. SPIE Jan 2004: Vol 5321; 57-68

Papers submitted from this thesis work.

Kerr gated suppression of fluorescence in resonance Raman spectroscopy of tissue .
M. C. Hart Prieto, P. Matousek, M. Towrie, A.W. Parker, A. W. Ritchie, N. Stone.
Submitted to Lasers in medical science for consideration for publication.

The use of Raman spectroscopy to determine the biochemical basis of urological pathologies.
M. C. Hart Prieto, P. Crow, J. Uff, A. W. Ritchie, N.Stone.
Submitted to Analytical and bio-analytical chemistry for consideration for publication.

Raman spectroscopic biochemical mapping of tissues

Nicholas Stone, Maria Consuelo Hart Prieto, Catherine Ann Kendall, Geeta Shetty, Hugh Barr.

Biophotonics Research Group, Gloucestershire Royal Hospital, Great Western Road, Gloucester, GL1 3NN,
Email: n.stone@medical-research-centre.com

Abstract

Advances in technologies have brought us closer to routine spectroscopic diagnosis of early malignant disease. However, there is still a poor understanding of the carcinogenesis process. For example it is not known whether many cancers follow a logical sequence from dysplasia, to carcinoma in situ, to invasion. Biochemical tissue changes precede morphological and structural changes. These can be probed using Raman or FTIR microspectroscopy and the spectra analysed for biochemical constituents. Local microscopic distribution of various constituents can then be visualised.

Raman mapping has been performed on a number of tissues including oesophagus, breast, bladder and prostate. The biochemical constituents have been calculated at each point using basis spectra and least squares analysis. The residual of the least squares fit indicates any unfit spectral components. The biochemical distribution will be compared with the defined histopathological boundaries. The distribution of nucleic acids, glycogen, actin, collagen I, III, IV, lipids and others appear to follow expected patterns.

1. Background

To date Raman spectroscopy has been demonstrated for distinguishing between tissue pathologies by utilising the fingerprint of the spectra. This has usually involved the use of multivariate techniques to develop a discriminant model. However useful this may be, it gives a feeling of missed opportunity, considering that the fingerprint is based exclusively on the molecular constituents of the tissue probed. This paper outlines a first attempt at elucidation of the biochemical variation between and across oesophageal tissue specimens, ie microscopic biochemical distribution.

2. Methods

Epithelial specimens

Specimens were collected at routine endoscopy following informed written consent. They were mounted on acetate paper to and snap frozen in liquid nitrogen. Frozen sections were taken, one stained with haematoxylin and eosin, one mounted on calcium fluoride for Raman mapping and the rest of the biopsy block retained for study. The full pathological range from the oesophagus was included, following consensus histopathological opinion from three GI-registry pathologists. Specimens for point measurements were homogeneous to be certain of the pathology present, and for the mapping heterogeneous specimens were selected to enable distinct differences in spectral biochemistry between the pathologies to be visualised.

Point Raman spectra

Spectroscopy was performed using a customised Renishaw System 1000 Raman microspectrometer with electronic stage and control software. The laser used was a Renishaw high power near infrared diode laser, which supplies the excitation light at a wavelength of 830nm and generates 300mw of power. This is focused through the microscope lens onto the tissue sample or the constituent. The lens then collects the scattered light from the tissue/constituent which is then passed through the spectrometer. An 80x ultra-long working distance objective was used (Olympus MIRPLAN NA 0.75).

Raman tissue spectra were measured from the epithelial surface of the defrosted biopsy block. Each specimen had approximately 10 spectra taken from different positions, randomly determined. The time of acquisition was 30s.

Raman mapping

Raman spectral imaging was performed on 7 μm sections of snap frozen tissue. These were placed on calcium fluoride slides. Spectra were collected using an automated mapping function including autofocus steps, based upon maximising the Raman signal from the tissue at 1450cm^{-1}. Spectra were integrated for 60 seconds at each position, stepping 10-100μm between each position (depending on the map). Therefore each map can be thought of as a hyperspectral image, with each pixel representing the full Raman spectrum. Images of each section can be generated using false colour weighting of the principal component scores of the spectra acquired for the map. Further data analysis was performed to elucidate the microscopic biochemical variation across the samples.

Measurement of biochemical constituents

The aim of measuring likely constituents was to assess the biochemical properties of pathologies from a number of organs to enable some quantification of the differences between the pathologies. In addition the variation of the biochemistry across the sample and its relation to histopathological boundaries has been studied.

The following constituents were purchased from Sigma – Aldrich; Actin-from bovine muscle, (A3653). β-carotene- type 1, synthetic, approx 95%, (C9750). Cholesterol sigma grade, 99%+, (C8667). Choline- base, approx 50% (w/w) aqueous solution, (C9154). Collagen- type 1, from human placenta, acid soluble, (C7774), type 3, from human placenta, acid soluble, (C4407), type 4, from human placenta, acid soluble, (C7521). DNA- from human placenta, (D7011). Glycogen- from bovine liver, (G0885). Lycopene-from tomato, (L9879). Oleic Acid- water soluble, (O1257). Triolein (C18:1,(cis)-9)- sigma grade, approx 95%, (T7140).

The above constituents were picked to as they were thought to be representative of different areas within a cell. DNA is representative of the cell nucleus with the other constituents of the nucleus having previously been shown to have a small contribution on the spectrum from the nucleus (in the form of some protein signals). The other constituents and the region of the cell or sample that they represent is listed here: Actin- cell cytoplasm, β-carotene- thought to be decreased in malignant tissue,[1,2,3] cholesterol-necrosis,[4] choline- thought to be abundant in malignant tissue,[5] collagen- extracellular matrix/ basement membrane, glycogen- reduced in rapidly dividing cells such as malignant tissue. Only mature cells store glycogen. Lycopene- thought to be decreased in malignant tissue, oleic acid- abundant in epithelium and triolein- fat.

The same spectrometer configuration was used for the measurement of both the constituents and tissue spectra. The solid constituents were placed on a calcium fluoride slide, and the liquid constituents were placed in a well plate. A 20x (MIRPlan ULWD Olympus) microscope objective was then used to focus in on the substance and to measure the spectra. Different acquisition times were used for each constituent to optimise the signal and minimise the noise contribution. All the constituent spectra were corrected for time of acquisition, energy sensitivity of the spectrometer and concentration of substance measured. The spectra from the tissue and the constituents were pre-processed with a Savitsky-Golay 1st derivative filter to remove basic spectral offset values.

Biochemical evaluation

PLS-toolbox® for use with Matlab® (Eigenvector Technologies, Manson, Washington, USA) was adapted for use with the data in these studies. The 1st derivative mean spectra for the tissue and the constituents were ascertained facilitating further analysis. The fitting of the mean spectra of the constituents to the mean spectra of the different pathologies in the epithelial tissues was performed with ordinary least squares analysis.

This is explained simply below.

$$X = cS + E$$

Where S is the matrix of spectral components, c is the matrix of concentrations to be predicted, and X is the measured spectra. This can be used to provide a 'best fit' of the spectral components or basis spectra found within the measured spectra. The assumption is made that the residual is minimised (ie least square of the residual) and that the spectral components selected are the main constituents of the spectra.

$$c = \frac{(X - E)}{S}$$

The disadvantage with this technique is that any co linearity in the components selected will skew the fit. An example being amino acids and the proteins containing them being used in the model. Observation of the residual E (E=X-cS) enables the quality of the fit to be observed and any remaining features of the spectra to be included in the next iteration of the model.

3. Results and discussion

Biochemical fit of single tissue spectra

Figure 1 shows mean Raman spectra from nine pathology groups in the oesophagus, all measured from snap-frozen biopsy specimens. Previously linear discriminant models have been constructed demonstrating high levels of agreement with histopathology.[6,7] Further study of the data has been possible by fitting the mean spectra with constituent spectra using ordinary least squares, as explained above. Figure 2 shows some example spectra from the constituents measured. Note the many complex peaks that are often superimposed upon one another when the constituents are combined to form cells and tissues. One issue which must be bourn in mind is the fact that Raman spectra from pure chemicals can often be subtly different from those found within tissues, due to the local environment they are found in, i.e. the presence of other biomolecules. This is usually manifest in small shifts in spectral peaks.

Figure 3 demonstrates the relative concentrations of the constituents following the basis spectral fit of the mean oesophagus spectra. These were adjusted to provide a total concentration of unity (ignoring water contribution). The quality of the fit is demonstrated by the spectra in Figure 4. This displays the mean 1st derivative spectrum from normal oesophageal tissue and the residual, or spectral component not fit by the basis model. It can be seen that the fit is a good approximation, although not perfect. This is likely to be due to the need for further standard spectra to be included in the model, but may also be due to subtle shifts in the basis spectra due to microscopic environmental effects. The resulting relative concentrations for each pathology group, in Figure 3, follow changes expected during the carcinogenesis process. For example reducing glycogen from normal tissue onwards, increasing DNA to actin ratio as neoplasia progresses. This is one of the measures histopathologists use to grade the tissue. Varying levels of free fatty acids and triglycerides also appear to change with progression.

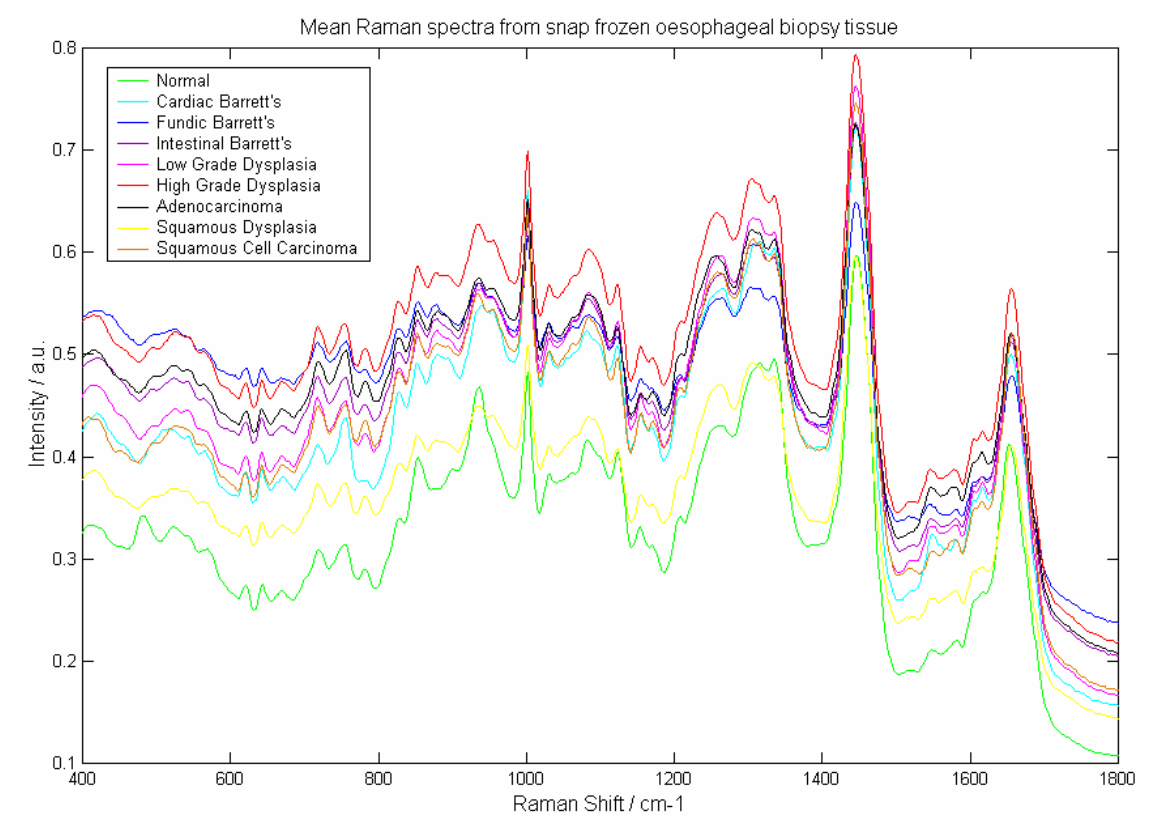

Figure 1: Mean spectra from snap-frozen oesophageal tissue.[6]

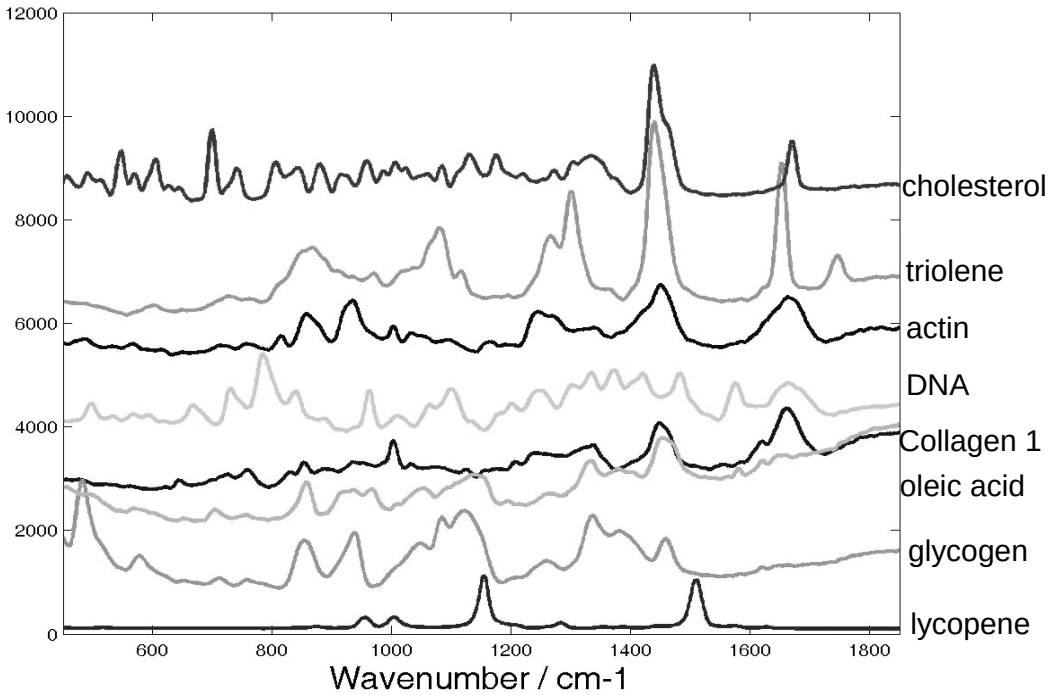

Figure 2: Example of basis spectra measured from pure chemical standards (Sigma).

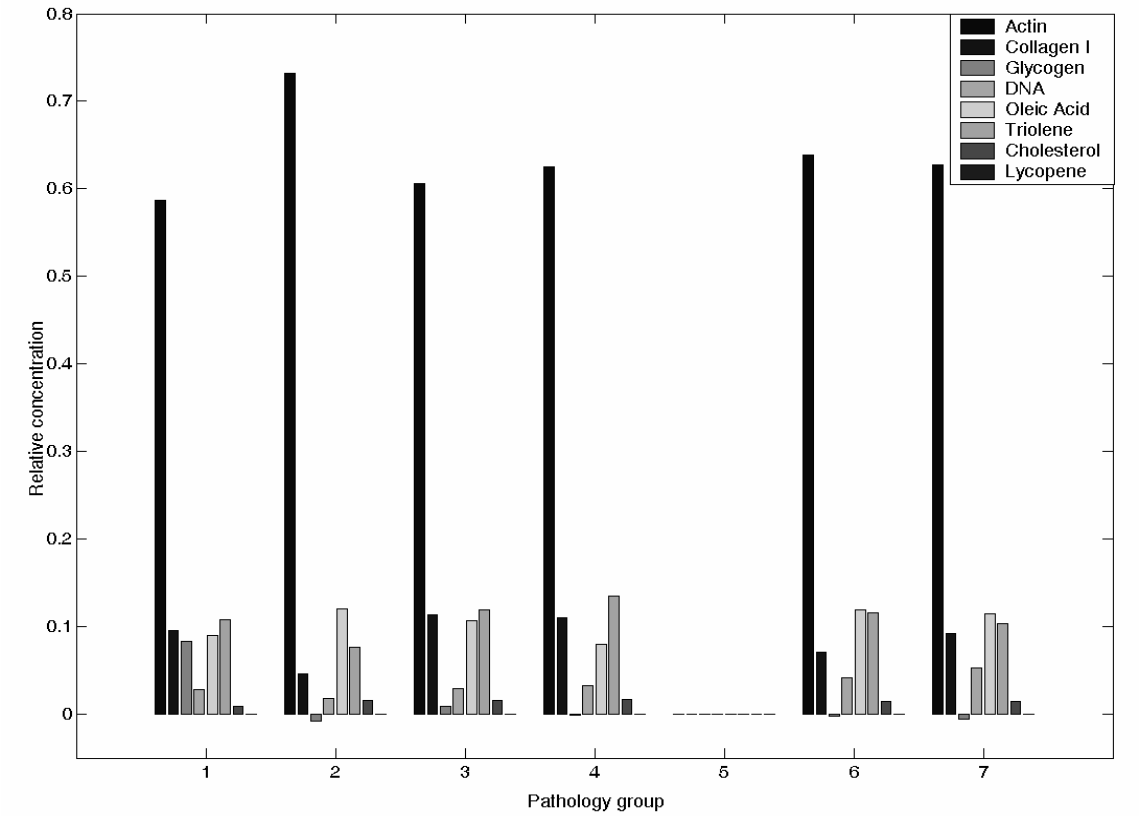

Figure 3: Biochemical fit for the mean spectra (1. Normal, 2. Fundic metaplasia, 3. Cardiac metaplasia, 4. Intestinal metaplasia, 6. Dysplasia, 7. Adenocarcinoma.).

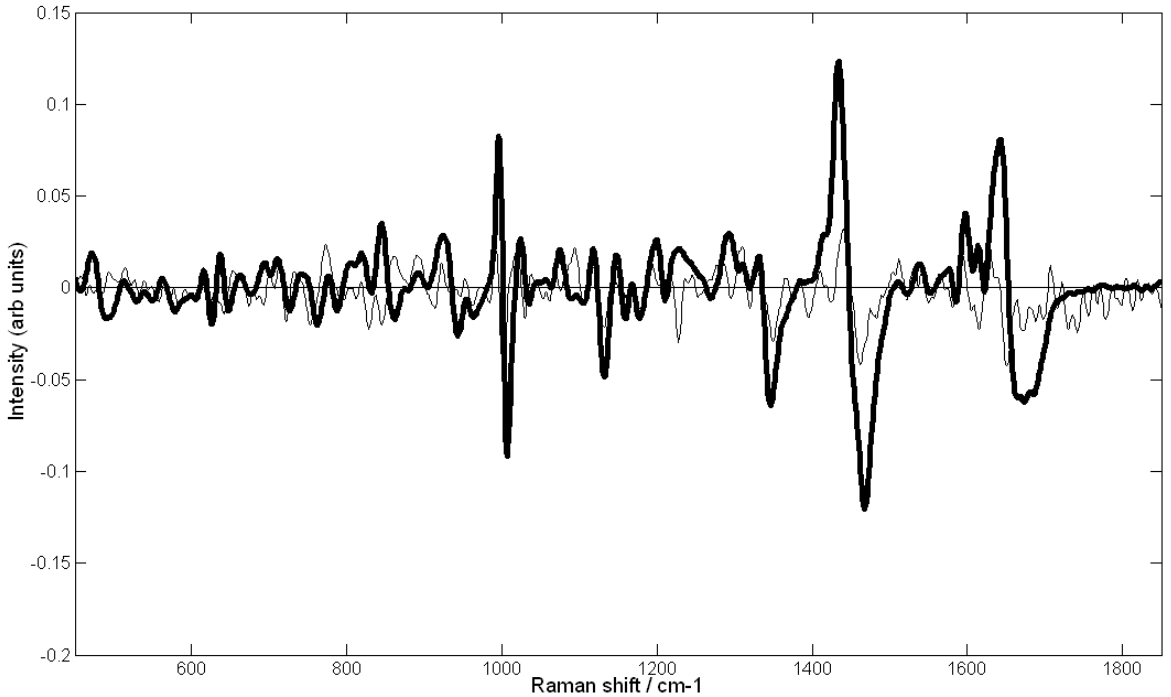

Figure 4: First derivative spectrum of mean normal oesophagus data (bold) with residual of fit (light).

Biochemical map of tissue sections

Mapping of tissue sections can identify the distribution of specific molecular constituents. This can be achieved with a spatial resolution using the Raman microprobe of around 3μm. The correlation between the biochemistry and boundaries between pathologies as defined by histology can be evaluated. Examples of Haematoxylin and Eosin stained sections from frozen sections measured for this study are shown in Figures 5 and 6.

The example shown in Figure 7 shows an oesophageal section with pre-cancerous Barrett's dysplasia at the top of the section and normal squamous tissue around the lower border. Note the raised nucleic acid to cytoplasmic ratio (DNA/actin) and choline in dysplasia and the high glycogen and triolein in normal squamous areas.

The example shown in Figure 8 shows an oesophageal section with adenocarcinoma around the left, right and top borders and at the bottom and middle of the section normal squamous epithelium. Note the raised nucleic acid to cytoplasmic ratio (DNA/actin) and oleic acid in adenocarcinoma and the high glycogen in normal squamous areas.

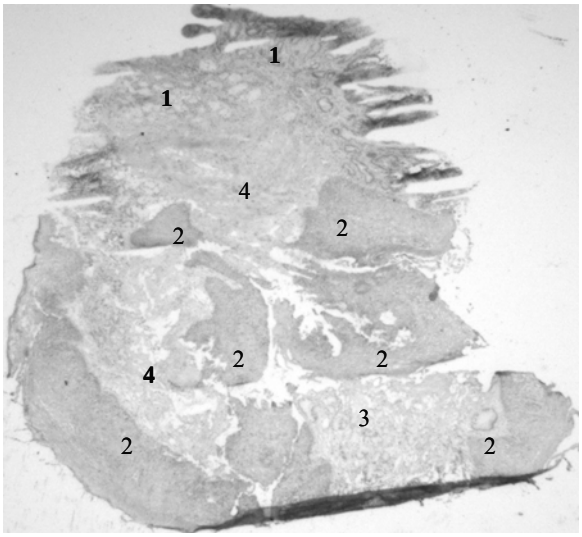

Figure 5: Haematoxylin and Eosin stained section of the oesophagus 1. HGD, 2. Normal Squamous, 3. Non dysplastic cardiac mucosa, 4. Submucosa / lamina propria / muscle.

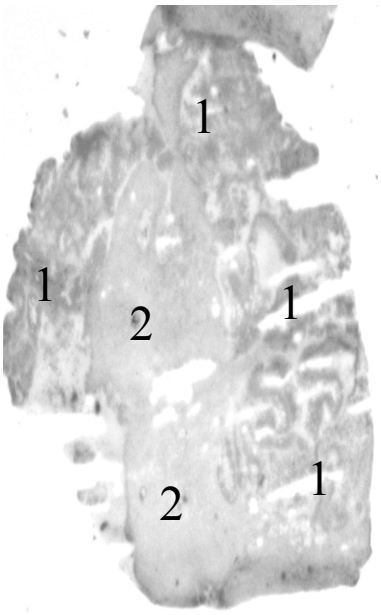

Figure 6: Haematoxylin and Eosin stained section of the oesophagus 1. Adenocarcinoma, 2. Normal Squamous.

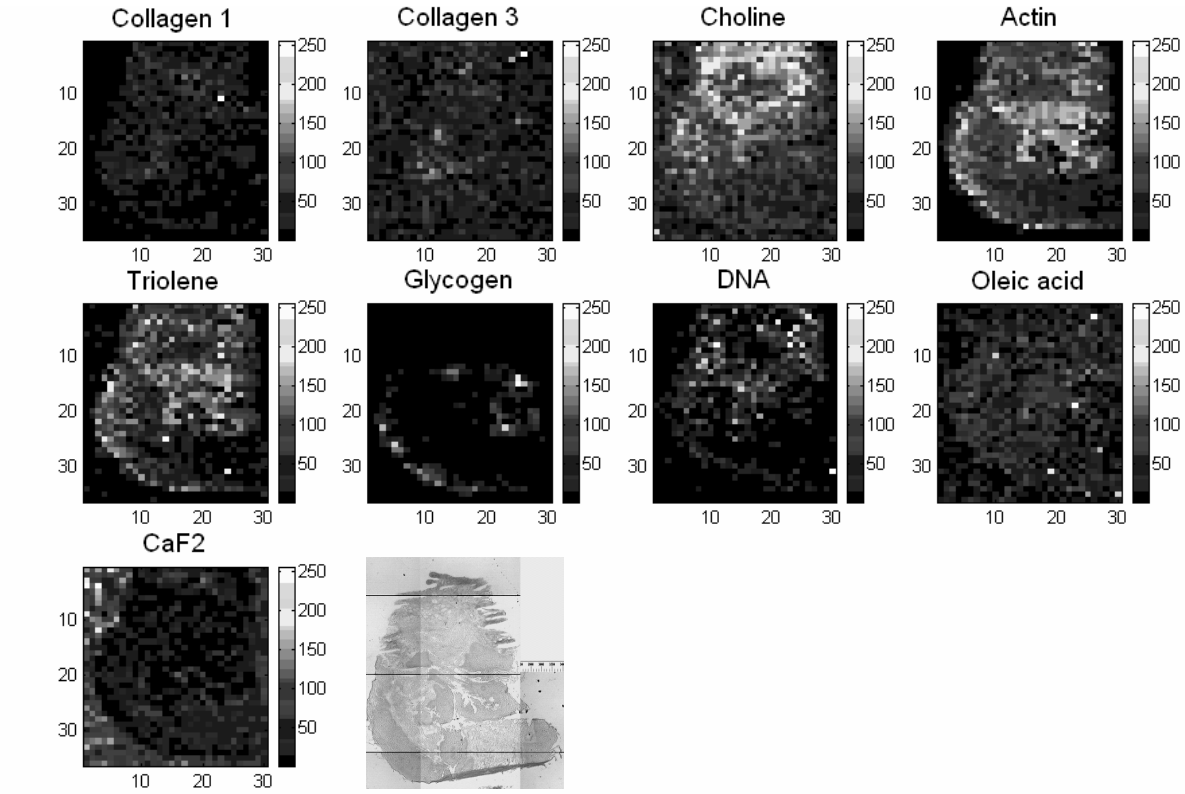

Figure 7: Normal squamous & high-grade dysplasia (HGD) oesophagus.

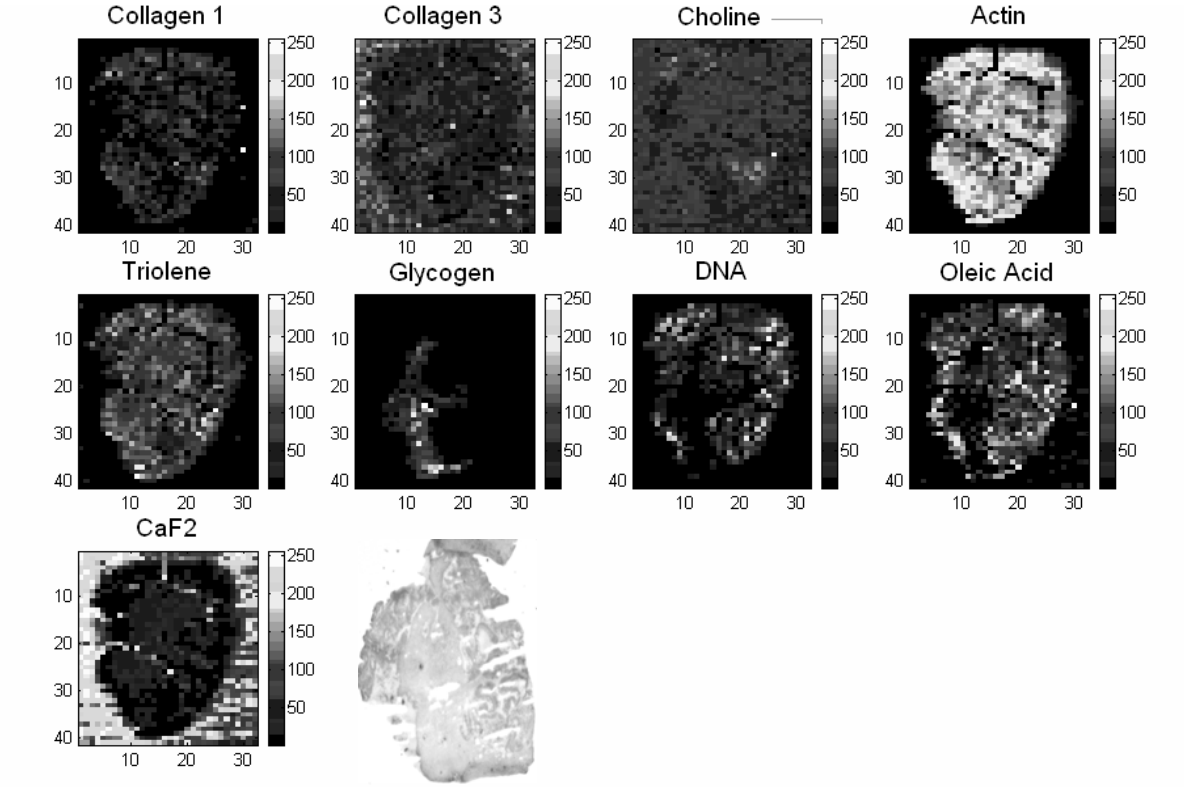

Figure 8: Normal squamous & adenocarcinoma oesophagus.

4. Conclusions

We have shown for the first time that we are able to utilise Raman spectroscopy to provide some biochemical basis for the different pathologies within the oesophagus. In this way we can achieve a better understanding of cacinogenesis and other disease processes. This could have major implications in the future of the diagnosis of pathologies within the oesophagus and other organs. Histopathology is at present the 'gold standard' for diagnosis, however, by utilising Raman spectroscopy and the knowledge we have gleaned from the biochemical studies performed, we may be able to provide analytical biochemical support. Thus working towards the objective of eliminating the intra and inter – observer error that is seen in histopathology.

5. References

[1] Hata, T.R., Scholz, T.A., *et al*. (2000). "Non-invasive Raman spectroscopic detection of carotenoids in human skin." *Journal of Investigative Dermatology* **115**(3): 441-448.

[2] Czeczuga-Semeniuk, E., Wolczynski, S., *et al*. (2003). "Preliminary identification of carotenoids in malignant and benign neoplasms of the breast and surrounding fatty tissue." *Neoplasma* **50**(4): 280-286.

[3] Toniolo, P., A. L. Van Kappel, et al. (2001). "Serum carotenoids and breast cancer." *American Journal of Epidemiology* **153**(12): 1142-1147.

[4] Shafer-Peltier, K. E, Haka, A. S, Fitzmaurice, M, Crowe, J, Myles, J, Dasari, R. R, Feld, M. S. (2002). 'Raman microspectroscopic model of human breast tissue: implications for breast cancer diagnosis in vivo,' *JRS.* **33**(7): 552-563.

[5] (2003). "MRI technique could replace breast cancer biopsies." Biophotonics international **dec**: 13.

[6] Kendall C, Stone N, Shepherd N, Geboes K, Warren B, Bennett R, Barr H. 'Raman spectroscopy a potential tool for the objective identification and classification of neoplasia in Barrett's oesophagus'. *J Pathology.* **200**, 602-609 (2003).

[7] Stone N, Kendall C, Shepherd N, Crow P, Barr H. 'Near-infrared Raman spectroscopy for the classification of epithelial pre-cancers and cancers.' *JRS.* **33,** 564-573 (2002).

Acknowledgements

The authors would like to thank the funders of this programme: the UK Department of Health (HTD), Gloucestershire Hospitals NHS Foundation Trust, and the PPP foundation and the Department of Health NHS R&D programme. Further support has been provided by Renishaw Spectroscopy Division, UK.

Use of picosecond Kerr-gated Raman spectroscopy to suppress signals from both surface and deep layers in bladder and prostate tissue

Maria Consuelo Hart Prieto
Gloucestershire Royal Hospital
Biophotonics Research Group
Pullman Court
Great Western Road
Gloucester GL 1 3NN
United Kingdom

Pavel Matousek
Michael Towrie
Anthony William Parker
CCLRC Rutherford Appleton Laboratory
Central Laser Facility
Didcot, Oxfordshire OX11 0QX
United Kingdom

Mark Wright
Bristol Royal Infirmary
Bristol BS2 8HW
United Kingdom

Alistair William Ritchie
Gloucestershire Royal Hospital
Great Western Road
Gloucester GL1 3NN
United Kingdom

Nicholas Stone
Gloucestershire Royal Hospital
Biophotonics Research Group
Pullman Court
Great Western Road
Gloucester GL1 3NN
United Kingdom
E-mail: n.stone@medical-research-centre.com

Abstract. Raman spectroscopy is an optical technique able to interrogate biological tissues, giving us an understanding of the changes in molecular structure that are associated with disease development. The Kerr-gated Raman spectroscopy technique uses a picosecond pulsed laser as well as fast temporal gating of collected Raman scattered light. Prostate samples for this study were obtained by taking a chip at the transurethral resection of the prostate (TURP), and bladder samples from a biopsy taken at transurethral resection of bladder tumor (TURBT) and TURP. Spectra obtained through the bladder and prostate gland tissue, at different time delays after the laser pulse, clearly show change in the spectra as depth profiling occurs, eventually showing signals from the uric acid cell and urea cell, respectively. We show for the first time, using this novel technique, that we are able to obtain spectra from different depths through both the prostate gland and the bladder. This has major implications in the future of Raman spectroscopy as a tool for diagnosis. With the help of Raman spectroscopy and Kerr gating, it may be possible to pick up the spectral differences from a small focus of adenocarcinoma of the prostate gland in an otherwise benign gland, and also stage the bladder cancers by assessing the base of the tumor post resection. [DOI: 10.1117/1.1991848]

Keywords: Raman spectroscopy; Kerr gating; prostate; bladder.

Paper 04257R received Dec. 22, 2004; revised manuscript received Mar. 20, 2005; accepted for publication Mar. 23, 2005; published online Aug. 1, 2005.

1 Introduction

1.1 *Bladder*

Each year there are 9000 cases of bladder cancer diagnosed in men and 3600 diagnosed in women in the United Kingdom. It is the fourth most common cancer in men and the eighth most common in women (the incidence is 8% in men and 3% in women[1]). There has, however, been a reduction in the age standardized incidence since the 1980s. This is thought to be due to the reduction in smoking and the banning of aromatic amines in the 1980s, both of which are known risk factors for the development of bladder cancer.

The vast majority of bladder cancers are transitional cell carcinomas of the bladder, and the majority of these are superficial. Bladder cancer is usually diagnosed by means of a cystoscopy and biopsy under general anaesthetic. Once diagnosed, patients are then staged using the tumor-nodes-metastases (TNM) classification and entered into a surveillance program, if no further treatment is required. The surveillance program involves six monthly to yearly cystoscopies for at least ten years.

Unfortunately, some of the bladder tumors, especially carcinoma *in situ* and flat superficial tumors, can look just like cystitis, or normal bladder.

1.2 *Prostate Gland*

The majority of men will suffer with symptoms related to diseases of the prostate gland at some point in their lives, with prostate cancer being the one of main concern. Adenocarcinoma of the prostate gland (CaP) is the most frequently diagnosed noncutaneous cancer affecting Western men.[2] Most (95%) of the cancers affecting the prostate gland are adeno-

Address all correspondence to Nicholas Stone, Gloucestershire Hospitals NHS Trust, Cranfield Postgrad Medical School-Great Western Rd., Gloucester, Gloucestershire GL1 3NN, Great Britain. Tel: 44 1452 395712; Fax: 44 1452 395713; E-mail: n.stone@medical-research-centre.com

1083-3668/2005/10(4)/044006/6/$22.00 © 2005 SPIE

carcinomas, the other 5% are made up of the following: transitional cell carcinoma, neuroendocrine carcinoma, sarcoma, and lymphoma. 40% of men aged between 60 and 70 years have microscopic foci of well-differentiated CaP. It is the second leading cause of cancer-related death in men in Western Europe and North America,[2] with 3 to 5% of men dying of CaP. It is also a major cause of morbidity and healthcare-related costs with 10% of men diagnosed with CaP developing clinical disease.[2]

CaP is diagnosed by means of an abnormal digital rectal examination (DRE) and/or a raised level of serum prostate-specific antigen (PSA). Either of these will lead onto transrectal ultrasonography (TRUS) and biopsy. The biopsies are taken randomly, with targeting if a lesion is suspected on TRUS. Unfortunately, the biopsies have a high number of false negatives, and therefore a cancer can remain undiagnosed. These false negatives are mainly due to sampling error (CaP is present as a small focus within the prostate gland and the biopsy has missed it). It has been shown that even if a man has two sets of negative biopsies with a persistently raised PSA, he has a 10% risk of having a cancer found on the third biopsy.

PSA measurement also comes with its own problems, in that although it is highly sensitive, it is not very specific. PSA can also be raised in the following: benign prostate hyperplasia (BPH), prostatitis, acute urinary retention (AUR), and urinary tract infection (UTI), as well as following recent urethral instrumentation, catheterization, prostatic biopsy, and DRE.

The ideal would be to diagnose CaP at an early stage when the PSA is within the range of 2.5 to 10 ng/ml; this would increase the chances of cure with radical treatment. The reality, given the low specificity of both the PSA, and the TRUS and biopsy, is that many of the cancers are diagnosed when a cure is not possible.

1.3 *Raman Spectroscopy*

Raman spectroscopy is an optical technique that can act to interrogate biological tissues with chemical specificity. In doing so, it gives us an understanding of the changes in the molecular structure that is associated with disease. With this in mind, it was felt that Raman spectroscopy could be used to distinguish between pathologies within the bladder and the prostate gland. By the start of the 1990s, various groups were using Raman spectroscopy to distinguish between normal and neoplastic tissue. The first studies looked at differentiating between normal tissue and advanced cancers in the breast[3] and gynecological organs.[4,5] As techniques were refined, interest moved to diagnosing neoplastic change at progressively earlier stages. To date, *in vitro* studies have also been undertaken to differentiate between different pathologies in a number of other tissues including colon,[6,7] esophagus,[8–10] brain,[11] skin,[12,13] lung,[14] and larynx.[15]

It has already been shown that Raman spectroscopy can be used to distinguish between different pathologies within the bladder and the prostate gland. This, however, has been exclusively *in vitro*.[16,17]

In view of previous studies, Raman spectroscopy is thought to have the potential for minimally invasive detection of malignancies and premalignancies within the bladder and the prostate gland. A problem with this is the inability to obtain spectra from significantly beneath the surface (more than of the order of 100 μm).[18] This is needed to ascertain whether there has been any local invasion of the disease in the case of the bladder, or to find a focus of adenocarcinoma in an otherwise benign prostate gland.

1.4 *Kerr Gating*

A Raman signal from depths within tissues tends to be diminished by elastic scattering, and therefore the surface signal is usually significantly stronger. A possible way to overcome this is by temporal gating techniques such as picosecond Kerr gating. The Kerr-gating technique uses excitation with a picosecond pulsed laser, in combination with a fast temporal gating of the Raman scattered light. The scattered light is collected at various time delays following the laser pulse.

The ability of depth probing using Raman is determined by two stages: 1. the laser photons have to be able to migrate to a given depth within the tissue; and 2. the Raman photons that have been produced have to migrate back to the surface.

In this way Raman spectra from differing depths within the tissue will emerge at different times, thereby making their separation feasible.[19]

There have been studies utilizing the Kerr-gating technique to improve on Raman spectra obtained from bone interiors,[20] as well as test experiments demonstrating the depth resolving power of the Raman Kerr-gating concept on artificially prepared samples.[19] This study is designed to expand on this work by studying the facility of Kerr-gated Raman spectroscopy to measure biochemical data from depths of a few millimeters in soft tissue. To make certain that a signal has been detected from beneath the tissue layer, specimens with strong and distinct Raman signals have been used. These were also selected for their relevance in urology.

2 Materials and Methods

2.1 *Subjects*

We obtained approval from the Gloucestershire Research Ethics Committee to obtain samples for experimentation using Raman spectroscopy. The samples used for this study were taken following fully informed consent.

2.2 *Tissue Collection and Preparation*

Prostate samples were obtained by taking an extra core at prostate biopsy procedures, or a chip at trans-urethral resection of the prostate (TURP). The prostate sample used in this study was assessed histopathologically to be benign prostatic hyperplasia. Bladder samples were collected at cystoscopic procedures including TURP (normal biopsies) and during trans-urethral resection of bladder tumor (TURBT). The bladder sample used was histologically normal and included the urothelial and subsurface layers. The samples were then snap-frozen in liquid nitrogen and transferred to an $-80\ ^{\circ}C$ freezer for storage.

At the time of the experiment, the tissue was passively warmed to room temperature and placed either on a cell containing urea, or on one containing uric acid. Urea and uric acid were chosen because they can be found within the bladder and prostate gland, and may also form crystals. Urea and

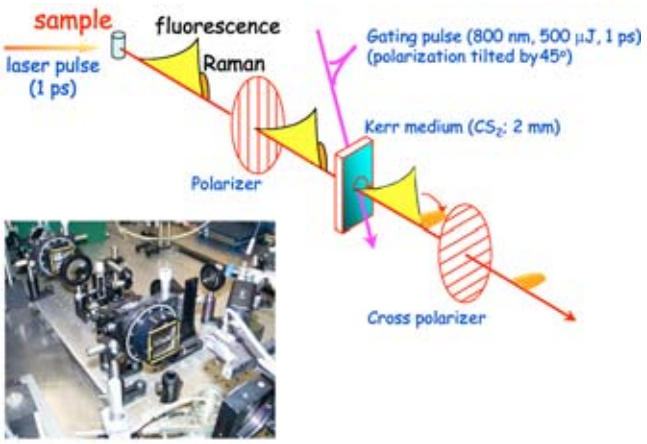

Fig. 1 A schematic diagram and photograph showing the Kerr-gated Raman system at the Rutherford Appleton Laboratory (RAL).

uric acid are also very strongly Raman active, and were chosen to allow a demonstration of probing of Raman spectra at depths through the tissue samples.

2.3 *Instrumentation*

The Kerr-gating system is based on the high throughput 4-ps optical Kerr shutter that has been described in previous publications by Matousek et al.[21,22] The Kerr gate is made up of two crossed polarizers (41 × 41 mm, Glan Taylor polarizers) and a Kerr medium consisting of a 2-mm optical cell that is filled with CS_2 (see Fig. 1).

When the gate is closed, the light from the sample is blocked as the polarizers are in cross orientation. When the gate is open, the light collected from the sample has its polarization rotated to allow it to pass through the cross polarizer. The gate is opened by a short 1-ps gating pulse at 800 nm. This bypasses the polarizers and creates a transient anisotropy within the Kerr medium, this then acts to polarize the light from the sample.

The spectra were collected using a conventional Raman spectrometer (Spex, Triplemate). To prevent residual elastically scattered light from the 488-nm probe laser entering the spectrometer, a Kaiser holographic notch filter was used. To also prevent the residual 800-nm gating beam scatter from entering, a saturated copper sulphate solution in a 1-cm-thick optical cell was placed in front of the spectrometer slit.

The Raman scattered light was collected in 180-deg geometry using a lens with f number of 2. A water heat-exchanger cooled, deep depletion near-infrared (NIR) CCD (Andor Technology, Belfast, UK, DU420BR-DD) was used to record the Raman spectra from the tissue.

The probe wavelength used was 488 nm, and the pulse duration was 1 ps. The pulse energy at the sample was 5 μJ (1 kHz) corresponding to 5 mW of average power. The beam was focused down to a 300-μm-diam spot.

To demonstrate the ability to obtain Raman spectra from deep layers, we performed two experiments: the first involved placing a bladder sample urothelium upward onto a uric acid cell, and the second involved placing the prostate sample onto a urea cell. Both tissue samples were 1 to 2 mm thick. The cells were made from UV-grade quartz 100 μm thick. The spectra were obtained for 20 s and 5 accumulations at varying distances through the tissue, i.e., at various time delays following the laser probe excitation pulse.

A simple approximation as to the distance traveled by the incident photons in the tissue can be made (the refractive index of the tissue was taken to be 1.4). In a time of 1 ps, the photons will have traversed approximately 0.2 mm of the tissue. This will not necessarily be in a straight line, as the tissue is highly scattering. By taking the scattering coefficient μ_s to be 48 mm^{-1} and the absorption coefficient μ_a to be 1.9 mm^{-1} (for epithelial tissue at 577 nm),[23] an optical depth (OD) can be calculated from

$$\mathrm{OD} = \frac{1}{\mu_s + \mu_a}.$$

The approximate optical depth in bladder tissue for 488 nm is 0.02 mm.

3 Results

Figure 2 shows the Raman spectra measured from the bladder on top of the cell containing uric acid. As you can see, the peak intensities change as the temporal position of the Kerr gate is varied. This relates to increasing depth with longer time delays, and hence suggests moving through the urothelium and into the basement membrane and then on into the muscle layer. Eventually, the signal from the tissue is lost, with peaks coming up at approximately 1400 and 1650 cm^{-1}, which are consistent with the main uric acid peaks, as shown in Fig. 3. The peaks in Fig. 2 at 662 and 803 cm^{-1} are consistent with the CS2 of the Kerr gate, and peaks at 1079, 1339, and 1533 cm^{-1} are caused by hot pixels from the CCD detector.

Figure 4 shows the spectra obtained going through the prostate gland tissue and on to the urea cell. As can be seen, the first three spectra are clearly tissue spectra with peaks at 1240, 1445, and 1650 cm^{-1} consistent with protein peaks. The fourth spectrum has lost a lot of the signal, and the following spectra yield the urea peaks clearly seen at 1003 and 1170 cm^{-1}.

Figure 5 shows the spectra obtained from the urea cell to highlight the peaks. The peaks in Fig. 4 at 662 and 803 cm^{-1} are consistent with the CS2, and peaks at 1079, 1339, and 1533 cm^{-1} are consistent with hot pixels from the detector and are consistent throughout all of the spectra.

4 Conclusions

We show for the first time that we are able to obtain spectra from different depths through prostate and bladder tissues by utilizing Kerr-gated Raman spectroscopy. Modeling of the time-dependent photon pathway would provide an enhanced understanding of the depth profiling process. This could have major implications in the future of Raman spectroscopy as a tool for diagnosis. Up until now, we have been able to distinguish between different pathologies within the bladder and the prostate gland by sampling the tissue *in vitro*. This has involved looking at only the surface of the sample.

The prostate gland is usually biopsied via the rectum. This is a painful procedure and can give false negatives. With the help of Raman spectroscopy and Kerr gating, we would po-

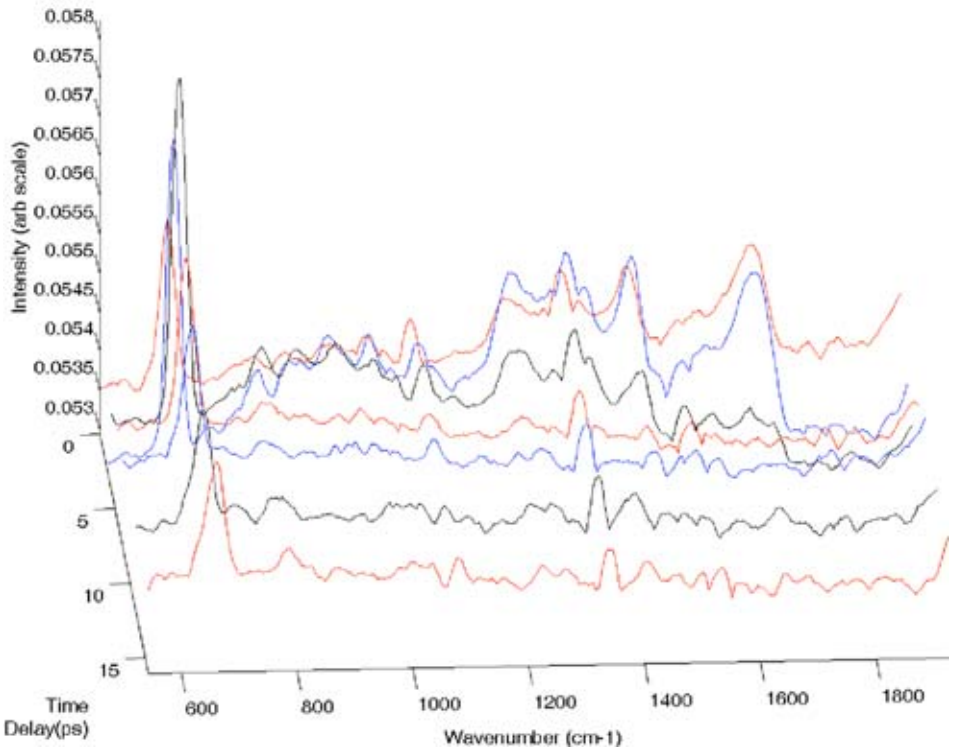

Fig. 2 Raman spectra taken from different depths (by adjusting the delay in opening the Kerr gate) through a sample of bladder on a quartz cell containing uric acid. See text for explanation of peak contributions from the experimental system.

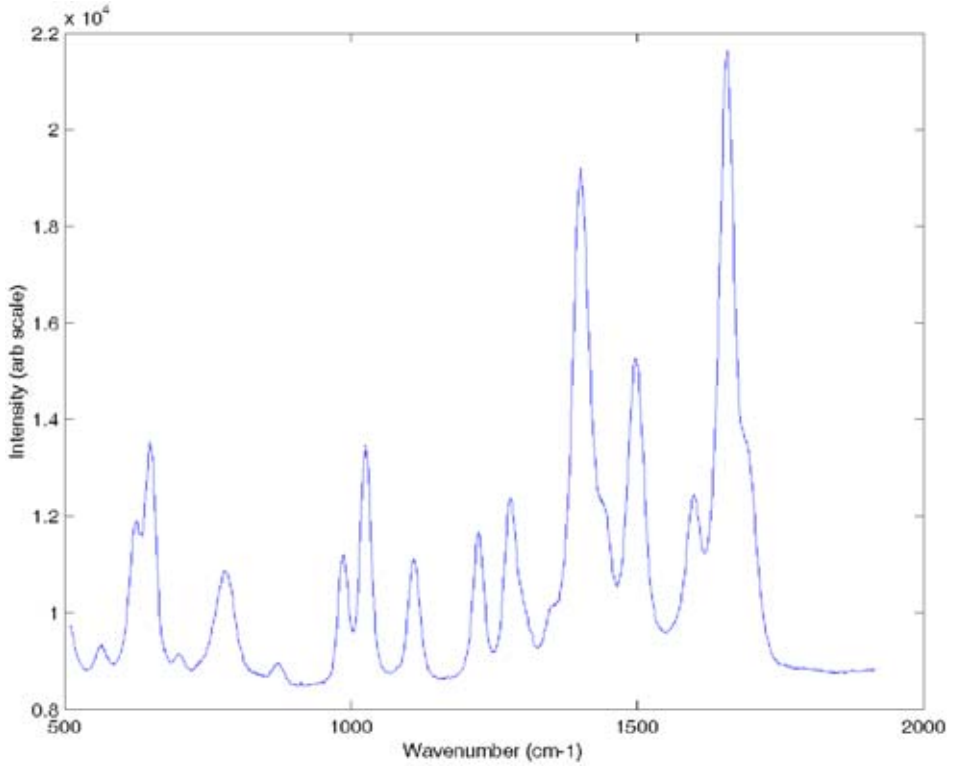

Fig. 3 A Raman spectrum, at a wavelength of 488 nm, taken from a quartz cell containing uric acid.

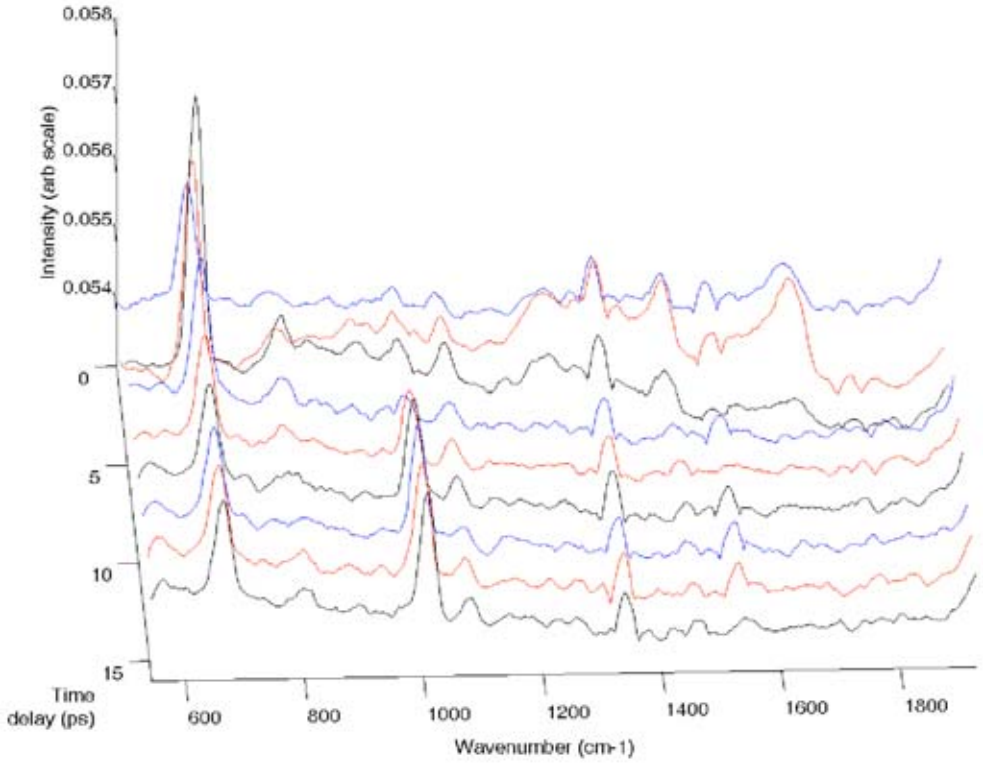

Fig. 4 Raman spectra taken from different depths (by adjusting the delay in opening the Kerr gate) through a sample of prostate gland on a quartz cell containing urea. See text for explanation of peak contributions from the experimental system.

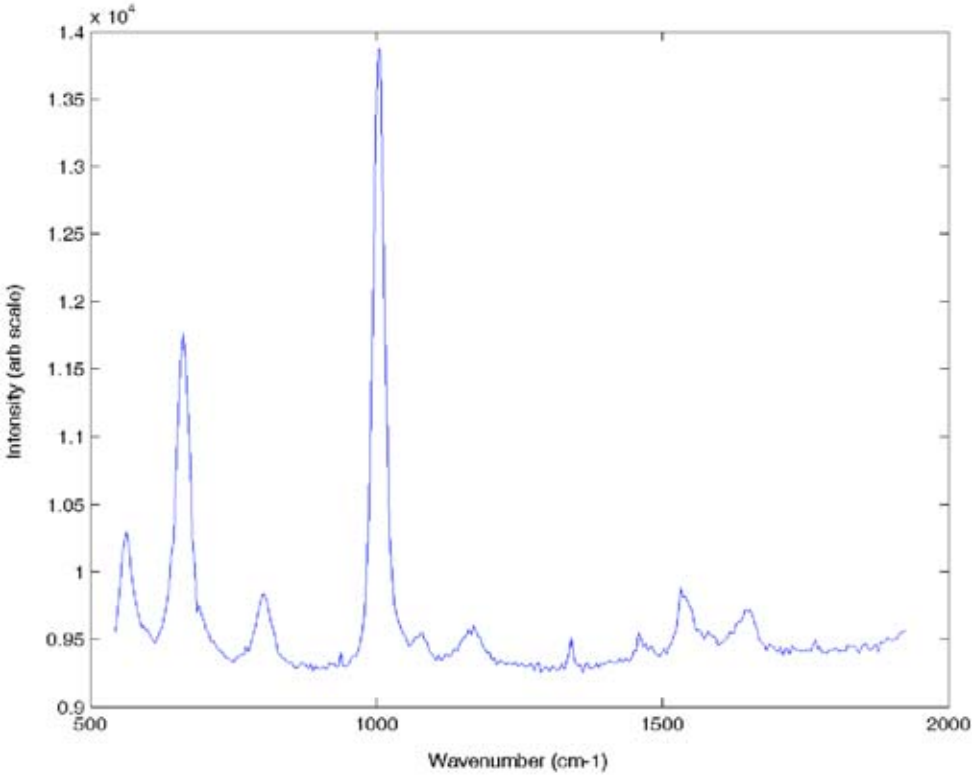

Fig. 5 Raman spectra, at a wavelength of 488 nm, taken from a quartz cell containing urea.

tentially be able to pick up the spectral differences from a small focus of adenocarcinoma of the prostate gland in an otherwise benign gland.

The bladder would also potentially benefit from Raman spectroscopy combined with Kerr gating. We would not only be able to diagnose the presence of a transitional cell carcinoma, but would also be able to assess the stage of the tumor in terms of its extension through the basement membrane and beyond (i.e., greater than a few hundred microns below the surface).

We demonstrate the first principals for the use of Kerr-gated Raman spectroscopy in the diagnosis of biological pathologies. Presently, however, the instrumentation at the Rutherford Appleton Laboratory (RAL) fills two rooms. Therefore, the use of this technique will require technical evolution and advancement before it will be ready for use *in vivo*.

Further studies are planned to demonstrate the facility of the technique to discriminate between normal and diseased tissue at depths of a millimeter or more.

Acknowledgments

We gratefully acknowledge the loan of a NIR deep-depletion CCD camera from Andor Technology. M. C. Hart Prieto is supported by the Cobalt Unit Appeal Fund and N. Stone is supported by the PPP foundation and the Department of Health NHS Research and Development program.

References

1. J. P. Meyer and D. Gillat, "What's new in bladder cancer?" *Trends Urol. Gynaecol. Sexual Health* **8**(6), 25–29 (2003).
2. J. Hugosson, "Early diagnosis: state of the art in clinical routine and screening studies," in *Renal, bladder, prostate and testicular cancer: an update: the proceedings of the VIth Congress and Controversies in Oncological Urology*, K. H. Kirth, G. H. Mickisch, and F. H. Schroder, Eds., Parthenon Publishing Group, New York (2001).
3. R. Alfano, C. H. Liu, W. L. Sha, H. R. Zhu, D. L. Akins, J. Cleary, R. Prudente, and E. Cellmer, "Human breast tissue studied by IR Fourier transform Raman spectroscopy," *Lasers Life Sci.* **4**(1), 23–28 (1991).
4. C. Liu, B. B. Das, W. L. Sha Glassmen, G. C. Tang, K. M. Yoo, H. R. Zhu, D. L. Akins, S. S. Lubicz, J. Cleary, R. Prudente, E. Cellmer, A. Caron, and R. R. Alfano, "Raman, fluorescence and time-resolved light scattering as optical diagnostic techniques to separate diseased and normal biomedical media," *J. Photochem. Photobiol., B* **16**(2), 187–209 (1992).
5. A. Mahadevan-Jansen and R. Richards-Kortum, "Raman spectroscopy for the detection of cancers and pre-cancers," *J. Biomed. Opt.* **1**, 31–70 (1996).
6. M. S. Feld, R. Manoharan, J. Salenius, J. Orenstein-Carndona, T. J. Roemer, J. F. Brennan, R. Dasari, and Y. Wang, "Detection and characterization of human tissue lesions with near infra-red Raman spectroscopy," *Proc. SPIE* **2388**, 99-104 (1995).
7. M. Shim, L. M. Song, N. E. Marcon, and B. C. Wilson, "*In vivo* near-infrared Raman spectroscopy: Demonstration of feasibility during clinical gastrointestinal endoscopy," *Photochem. Photobiol.* **72**, 146–150 (2000).
8. C. Kendall, N. Stone, N. Shepherd, K. Geboes, B. Warren, R. Bennett, and H. Barr, "Raman spectroscopy a potential tool for the objective identification and classification of neoplasia in Barrett's oesophagus," *J. Pathol.* **200**, 602–609 (2003).
9. N. Stone, "Raman spectroscopy of biological tissue for application in optical diagnosis of malignancy," PhD Thesis, Cranfield Univ., United Kingdom (2001).
10. T. C. Bakker Schut, M. J. H. Witjes, H. J. C. M. Sterenborg, O. C. Speelman, J. L. N. Roodenburg, E. T. Marple, H. A. Bruining, and G. J. Puppels, "*In vivo* detection of dysplastic tissue by Raman spectroscopy," *Anal. Chem.* **72**, 6010–6018 (2000).
11. B. Schrader, S. Keller, T. Lochte, S. Fendel, D. S. Moore, A. Simon, and I. Sawatzki, "FT Raman spectroscopy in medical diagnostics," *J. Mol. Struct.* **348**, 293–296 (1995).
12. H. Edwards, A. Williams, and B. Barry, "Potential applications of FT-Raman spectroscopy for dermatological diagnosis," *J. Mol. Struct.* **347**, 379–387 (1995).
13. P. Caspers, G. W. Lucassen, R. Wolthuis, H. A. Bruining, and G. J. Puppels, "*In vitro* and *in vivo* Raman spectroscopy of human skin," *Biospectroscopy* **4**, S31–S39 (1998).
14. S. Kaminaka, H. Yamazaki, T. Ito, E. Kohda, and H. Hamaguchi, "Near infrared Raman spectroscopy of human lung tissues: Possibility of molecular-level cancer diagnosis," *J. Raman Spectrosc.* **32**, 139–141 (2001).
15. N. Stone, P. Stravroulaki, C. Kendall, M. Birchall, and H. Barr, "Raman spectroscopy for early detection of laryngeal malignancy—preliminary results," *Laryngoscope* **110**, 1756–1763 (2000).
16. P. Crow, N. Stone, C. A. Kendall, J. S. Uff, J. A. Farmer, H. Barr, and M. P. Wright, "The use of Raman spectroscopy to identify and grade prostatic adenocarcinoma *in vitro*," *Br. J. Cancer* **89**(1), 106–108 (2003).
17. N. Stone, C. Kendall, N. Shepherd, P. Crow, and H. Barr, "Near-infrared Raman spectroscopy for the classification of epithelial precancers and cancers," *J. Raman Spectrosc.* **33**, 564–573 (2002).
18. P. J. Caspers, G. W. Lucassen, E. A. Carter, H. A. Bruining, and G. J. Puppels, "*In vivo* confocal Raman microspectroscopy of the skin: Noninvasive determination of molecular concentration profiles," *J. Invest. Dermatol.* **116**(3), 434–442 (2001).
19. P. Matousek, N. Everall, M. Towrie, and A. W. Parker, "Depth profiling in diffusely scattering media using Raman spectroscopy and picosecond gating," *Appl. Spectrosc.* **59**(2), 200–205 (2005).
20. M. D. Morris, A. E. Goodship, E. R. C. Draper, P. Matousek, M. Towrie, and A. W. Parker, "Kerr-gated picosecond Raman spectroscopy and Raman photon migration of equine bone tissue with 400-nm excitation," *Proc. SPIE* **5321**, 164–169 (2004).
21. P. Matousek, M. Towrie, A. Stanley, and A. W. Parker, "Efficient rejection of fluorescence from Raman spectra using picosecond Kerr gating," *Appl. Spectrosc.* **53**(12), 1485–1489 (1999).
22. P. Matousek, M. Towrie, C. Ma, W. M. Kwok, D. Phillips, A. W. Toner, and A. W. Parker, "Fluorescence suppression in resonance Raman spectroscopy using a high-performance picosecond Kerr gate," *J. Raman Spectrosc.* **32**, 983–988 (2001).
23. D. J. Smithies and P. H. Butler, "Modelling the distribution of laser light in port-wine stains with the Monte Carlo method," *Phys. Med. Biol.* **40**, 701–731 (1995).

Urological applications of Raman spectroscopy for improved malignant diagnostics.

M. Consuelo Hart Prieto, Paul Crow, Catherine Kendall, J. Uff, Mark Wright, Alistair Ritchie, Nicholas Stone.

Biophotonics Research Group, Gloucestershire Royal Hospital, Great Western Road, Gloucester. GL1 3NN.

ABSTRACT

The incidence of both prostate and bladder cancer is high; prostate cancer being the most frequently diagnosed non-cutaneous cancer affecting Western men. At present the gold standard for diagnosis of pathologies within the bladder and the prostate gland is by means of histological examination of biopsies. This is a subjective means of examining tissue and has an element of both inter and intra-observer variability.

A large number of specimens have been collected and analysed using both a NIR-Raman spectrometer and histopathology with H&E staining. Multivariate spectral prediction models have been constructed and tested. An evaluation of misclassification cost models and the use of cancer staging data to train the models has been made.

Keywords: Raman, bladder, prostate, cancer, prostatic intraepithelial neoplasia, carcinoma in situ, dysplasia.

1. INTRODUCTION

1.1 The bladder.

The incidence of bladder cancer in the UK is 8% in men and 3% in women.[1] It is the fourth most common cancer in men and the eighth in women. Each year there are 9000 cases diagnosed in men and 3600 diagnosed in women, but although the figures are high there has been a reduction in the age standardised incidence since the 1980's. It is thought that the reason for this is the reduction in smoking and the banning of aromatic amines in the 1980's, both of which are known risk factors for the development of bladder cancer.

The majority of bladder cancers are transitional cell carcinomas of the bladder, and most of these are superficial. The standard method for the diagnosis of bladder cancer is by means of a cystoscopy and biopsy, which ordinarily involves a general anaesthetic. Once diagnosed patients are staged by means of the TNM (tumour-nodes-metastases), classification and entered into a surveillance scheme, if no further treatment is required. The surveillance program involves 6 monthly – yearly cystoscopies for at least 10 years.

Unfortunately some of the bladder tumours, especially carcinoma in situ and flat superficial tumours can look just like cystitis, or normal bladder.

The gold standard, non-invasive test is urine cytology. This is stained with a Papanicolaou stain and has a 95% specificity. However the test is only 40 – 60% sensitive, (the sensitivity increases with the grade of the tumour). This is because of the significant inter and intra-observer variability.[2]

1.2 The prostate gland.

Recently the profile of the prostate gland has been raised in the media. This is because the vast majority of men will suffer with symptoms related to disease of the prostate at some point in their lives. The main concern however is of

prostate cancer. Adenocarcinoma of the prostate gland, (CaP), is the most frequently diagnosed non-cutaneous cancer affecting Western men.[3] It represents 95% of the cancers affecting the prostate gland, with the other 5% being made up of the following; transitional cell carcinoma, neuroendocrine carcinoma, sarcoma and lymphoma. As many as 40% of men aged between 60 and 70 years, have microscopic foci of well differentiated adenocarcinoma of the prostate gland, (CaP). It is the second leading cause of cancer related death in men in Western Europe and North America,[3] with 3-5% of men dying of CaP. It is also a major cause of morbidity and health care related costs with 10% of men diagnosed with CaP developing clinical disease.[3]

The diagnosis of CaP is dependent on an abnormal digital rectal examination, (DRE), and / or a raised level of serum prostate specific antigen (PSA). A finding of either of these in men will lead onto transrectal ultrasonography (TRUS) and biopsy. The biopsies are currently taken using a sextant sampling method, with targeting if a lesion is suspected on TRUS. Unfortunately the biopsies have a high number of false negatives, and therefore a cancer can remain undiagnosed. These false negative results are mainly due to sampling error, (in that the CaP may be present as a small focus within the prostate gland and the biopsy may have missed this).[3] It has been shown that even if a man has two sets of negative biopsies with a persistently raised PSA, he has a 10% risk of having a cancer found on the third biopsy.

Measuring the PSA comes with its own problems, in that although it is highly sensitive, it is not very specific. The other diseases in which the PSA can be raised are: BPH, prostatitis, acute urinary retention, (AUR), and urinary tract infection, (UTI). The PSA will also be raised with recent urethral instrumentation, catheterisation, prostatic biopsy and DRE.

CaP is graded using the Gleason system. This system recognises 5 grades representing a continuum of architectural patterns of CaP, with grade 1 being well differentiated and grade 5, poorly differentiated. The Gleason score is the primary and secondary growth pattern noted in the tissue, (i.e. 3+4). It has been noted that biopsy results may show inter and intra-observer error as they are subjective, and limit classification given the size of the sample.

The ideal would be to diagnose CaP at an early stage when the PSA is in the range of 2.5-10 ng/ml, as this would increase the chances of cure with radical treatment. The reality, given the low specificity of both the PSA, and the TRUS and biopsy, is that many of the cancers are diagnosed when a cure is not possible.

1.3 Raman Spectroscopy.

Raman spectroscopy is an optical technique that can act to interrogate biological tissues. In doing so it gives us an understanding of the changes in the molecular structure that is associated with disease. With this in mind it was felt that Raman spectroscopy could be used to distinguish between pathologies within the bladder and the prostate gland. By the start of the 1990s various groups were using Raman spectroscopy to distinguish between normal and neoplastic tissue. The first studies looked at differentiating between normal tissue and advanced cancers in the breast,[4] and gynaecological organs.[5,6] As techniques were refined, interest moved to diagnosing neoplastic change at progressively earlier stages. To date, in vitro studies have also been undertaken to differentiate between different pathologies in a number of other tissues including colon,[7,8]oesophagus, [9,10,11] brain,[12] skin,[13,14] larynx.[15] Raman spectroscopy is therefore thought to have the potential for minimally invasive detection of malignancies and pre-malignancies within the bladder and the prostate gland.

2. MATERIALS AND METHODS.

2.1 Subjects.

The protocol for this study was approved by the Gloucestershire Research Ethics Committee. All samples were taken following fully informed consent.

2.2 Tissue collection and preparation.

Prostate samples were obtained by taking an extra core at prostate biopsy procedures, or a chip at TURP. Bladder samples were collected at cystoscopic procedures including TURP (normal biopsies) and TURBT. The samples were then snap frozen in liquid nitrogen and transferred to a -80°C freezer for storage. A frozen section was then taken from

each sample and processed for standard histological examination. They were stained with haematoxylin and eosin, (H&E), and the remainder of the sample was retained at -80°C. The sections were then separately examined by two Consultant Pathologists and only included in the study where an agreement on histological diagnosis was reached. The area of interest on each section, was carefully mapped by the Pathologist, so that the region could subsequently be accurately targeted on the Raman system. Bladder samples were classified as normal, cystitis, carcinoma in situ, (CIS), transitional cell carcinoma, (TCC), and squamous cell carcinoma, (SCC). The TCCs were subdivided into grade 1, 2 or 3. Prostate biopsies were classified as Benign Prostatic Hyperplasia (BPH), prostatitis or adenocarcinoma, with the adenocarcinoma group further split into sub-groups depending on Gleason score The remainder of each sample, (from which the frozen section had been taken), was then passively warmed to room temperature and rinsed with a buffered normal saline solution.

2.3 Instrumentation.

The tissue samples were scanned on an Optimised Raman System (Renishaw System 1000), to obtain in vitro Raman spectra. The system employs a diode laser producing near infra-red light at 830nm, which is accurately targeted onto the tissue sample via a microscope objective lens. Bladder samples were orientated to mimic their in vivo orientation, (the epithelium was upward facing). Each Raman spectrum was then recorded on the spectrometer using an acquisition time of ten seconds for bladder (x20 objective) and twenty seconds for prostate (x80 objective). 10 to 20 spectra were acquired from random positions on each sample.

2.4 Analysis.

Raman spectra have been corrected for the energy sensitivity of the spectrometer by utilising a National Physical Laboratory calibrated tungsten filament lamp. Cosmic rays have been removed using a filter, otherwise spectra have not been baseline corrected or smoothed.

Spectral prediction models were constructed using the consensus histopathological data to provide the information for supervised classification using linear discriminant analysis following principal component analysis. The various histopathological groupings have been combined to produce models with differing clinical applications. Recent publications by the group have demonstrated excellent separation between the groups.[16,17] This analysis extends to studying the effects of misclassification costs and assesses whether the stage of cancer invasion can be detected in addition to the histological grade.

All models have been tested using leave one out cross-validation.

3. RESULTS

3.1 Bladder.

A total of 1525 spectra were recorded from 75 bladder samples. Table 1 shows the breakdown of samples and spectra measured. Mean Raman spectra from each of the groups are shown in Figure 1.

	Normal	Cystitis	CIS	TCC				Adeno-carcinoma
				G1	G2	G3	Sq. Dys	
No. of Samples	22	10	2	9	21	9	1	1
No. of Spectra	**266**	**206**	**49**	257	452	215	**30**	**50**
				924				

Table 1: Number of spectra measured and sample breakdown.

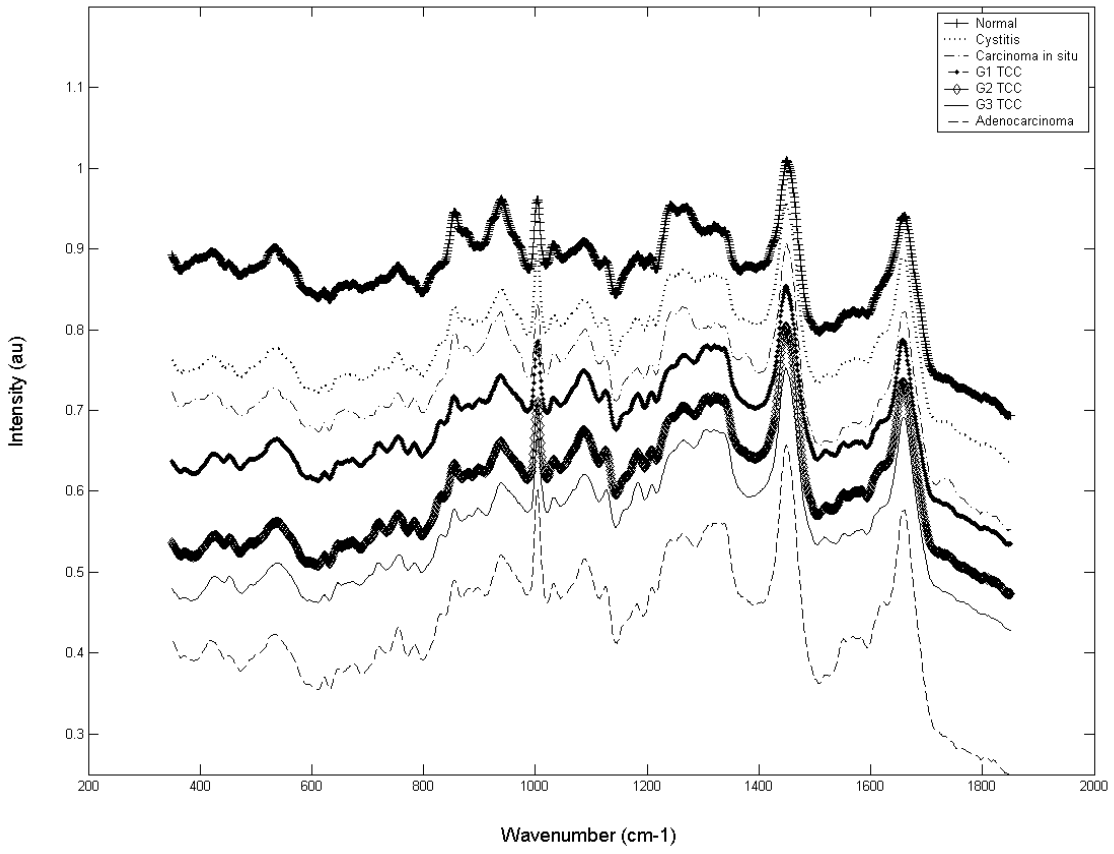

Figure 1: Mean Raman spectra from bladder tissue used in the spectral predictive models.

By combining the spectra into three groups that would be useful for biopsy selection, the model was constructed using two-linear discriminant functions. The resulting predictions following leave-one-out cross validation are shown in Table 2 and the outcome measures are shown in Table 3. Other models demonstrating discrimination between many more groups have been published elsewhere.[16]

Confirmed Histology		Raman Prediction		
		Normal	**Cystitis**	**TCC +CIS**
	Normal	**254**	12	0
	Cystitis	10	**186**	10
	TCC + CIS	29	54	**890**

Table 2: The cross-validated results of the three group diagnostic algorithm.

	Normal	**Cystitis**	**TCC + CIS**
Sensitivity	95%	90%	91%
Specificity	97%	95%	98%

Table 3: The sensitivities and specificities achieved by the three group diagnostic algorithm.

The spectral data described above was combined into two groups, benign and malignant. An evaluation of the use of misclassification costs was made to study the effects of changing these costs when constructing the model. Prior probabilities and misclassification costs can be included to better represent sampling populations and the impact of test outcome on patient care, i.e. radical treatment for a false positive measurement, versus death from non-treatment from a false negative outcome.[18] Figure 2 shows the distribution of the linear discriminant scores for the two-group model. Variation of the costs will in effect shift the decision line along the x-axis of the plot. A receiver operator curve (ROC) has been plotted to show the overall effect on the outcome of the model prediction when the costs of misclassification are varied from 1 to 491 for each group (Figure 3).

A comparison has been made between the outcome from using equal misclassification costs of unity and an optimum level defined by that achieving the maximum combined sensitivity and specificity for malignancy. This was achieved with misclassification costs of 71 and 141 for groups 1 and 2 respectively. Table 4 demonstrates these changes between the two models. The positive predictive values from the original to the optimised model change from 97% to 98%.

A further extension of previous work has been achieved by constructing a spectral predictive model of all the malignant spectra and training it with stage data, rather than histology grade data. See Figure 4 for a visual representation of this. The prediction results are shown in Table 5 and the outcome measures are shown in Table 5.

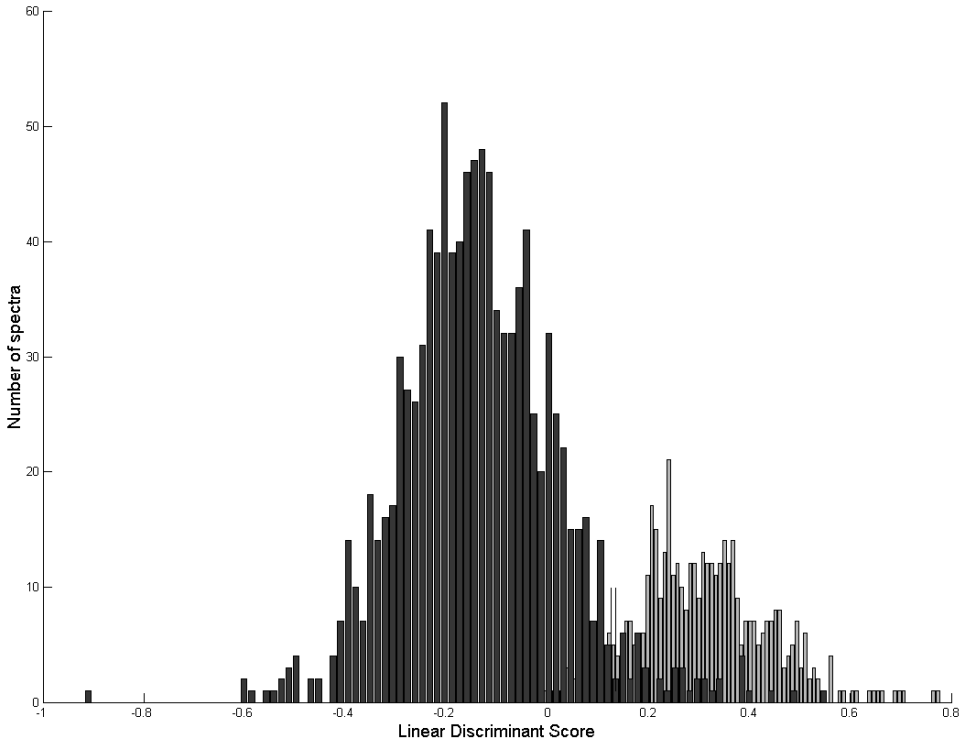

Figure 2: Histogram of linear discriminant scores for malignant versus benign bladder model. Malignant data are plotted in black, benign in grey.

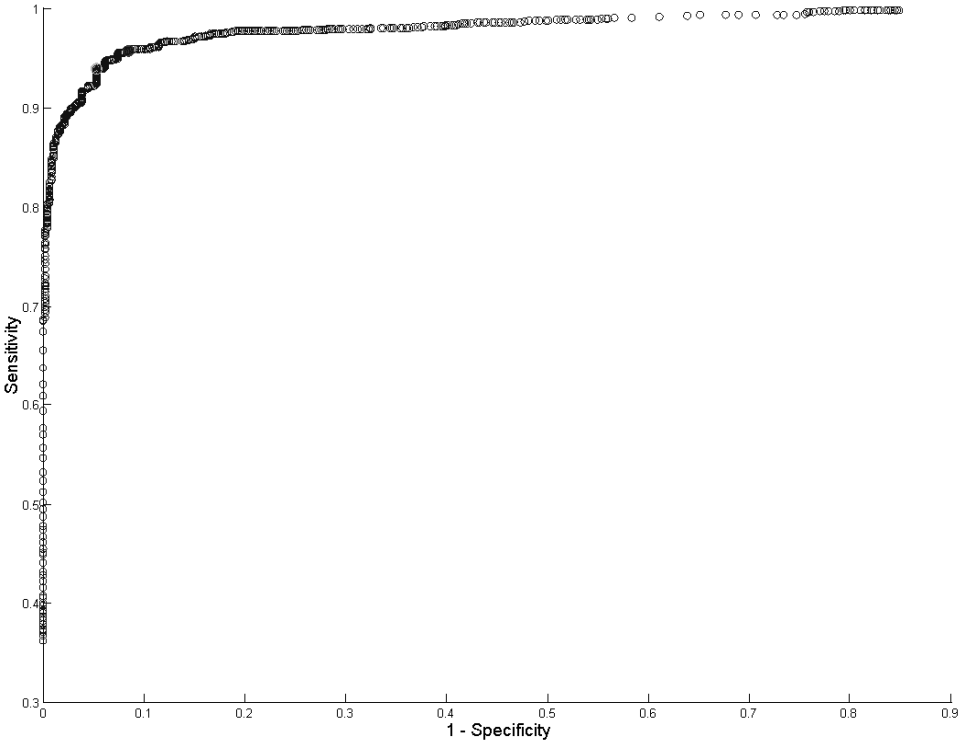

Figure 3: ROC of sensitivity versus 1-specificity for malignant group in the two-group bladder model. This has been achieved by varying the relative misclassification costs of the two groups.

			Raman Prediction		Total
			Benign	**Neoplastic**	
Equal costs (1:1)	**Pathology**	**Benign**	442 **(92%)**	30	472
		Neoplastic	46	1007 **(96%)**	1053
Optimum (141:71)		**Benign**	447 **(95%)**	25	472
		Neoplastic	70	983 **(94%)**	1053

Table 4: Table of results of Raman prediction of specimens defined by consensus, blinded histopathology. Changing of the misclassification costs has enabled adjustment of the outcome measures. The first model has equal misclassification costs of unity, the next has been modified to produce the maximum combined sensitivity and specificity to malignancy.

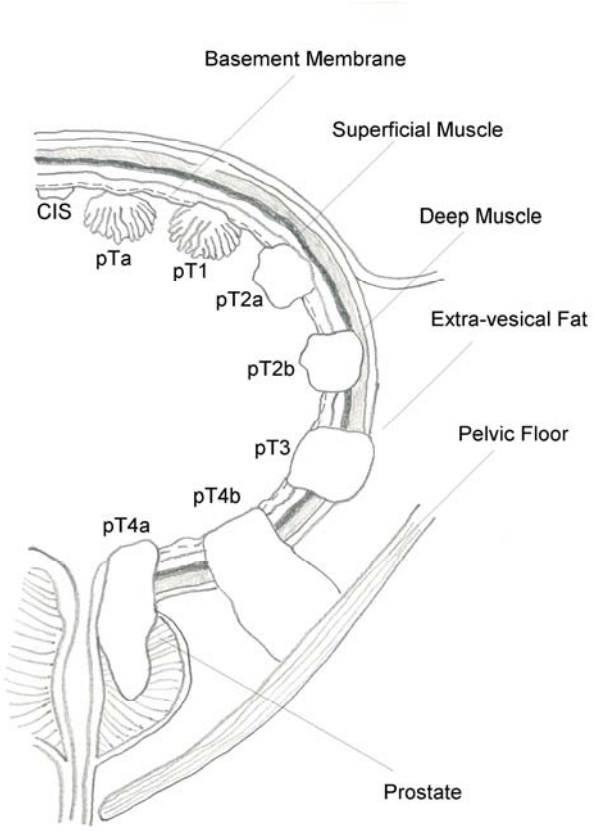

Figure 4: Schematic diagram of the relationship between stage of bladder carcinoma and depth of invasion. (modified from TNM classification of malignant tumours: Urinary bladder, 6th ed. Eds Sobin L.H, Wittekind C.H: John Wiley and Sons Inc.; 2002.)

Confirmed Stage		Raman Prediction		
		pTa	**pT1**	**pT2**
	pTa	**481**	23	1
	PT1	13	**266**	14
	pT2	0	12	**49**

Table 5: The cross-validated results of the three stage diagnostic algorithm.

	pTa	**pT1**	**pT2**
Sensitivity	95%	91%	80%
Specificity	96%	94%	98%

Table 6: Outcome measures from bladder stage model.

3.2 Prostate.

A total of 871 spectra were recorded from 56 prostate specimens. The breakdown is shown in Table 7. Mean spectra from each pathology group are shown in Figure 5.

	BPH	**Prostatitis**	**CaP (GS<7)**	**CaP (GS=7)**	**CaP (GS>7)**	**Totals**
No. of Samples	33	2	11	5	5	**56**
No. of Spectra	381	34	231	111	114	**871**

Table 7: The numbers of prostate biopsies and spectra for each pathological group studied.

A three-group model was constructed to demonstrate (with leave-one out cross validation) the ability of Raman spectroscopy to discriminate between clinically significant pathology groups. The prediction results and outcome measures are shown in Tables 8 and 9 respectively. There have been other models constructed to demonstrate discrimination between more pathological groups. These have been published by our group.[17]

The spectral data described above was combined into two groups, benign and malignant. An evaluation of the use of misclassification costs was made to study the effects of changing these costs when constructing the model. Figure 6 shows the distribution of the linear discriminant scores for the two-group model. Variation of the costs will in effect shift the decision line along the x-axis of the plot. A receiver operator curve (ROC) has been plotted to show the overall effect on the outcome of the model prediction (Figure 7).

A comparison has been made between the outcome from using equal misclassification costs of unity and an optimum level defined by that achieving the maximum combined sensitivity and specificity for malignancy. This was achieved with misclassification costs of 51 and 111 for groups 1 and 2 respectively. Table 10 demonstrates these changes

between the two models. The positive predictive values from the original to the optimised model change from 95% to 92%.

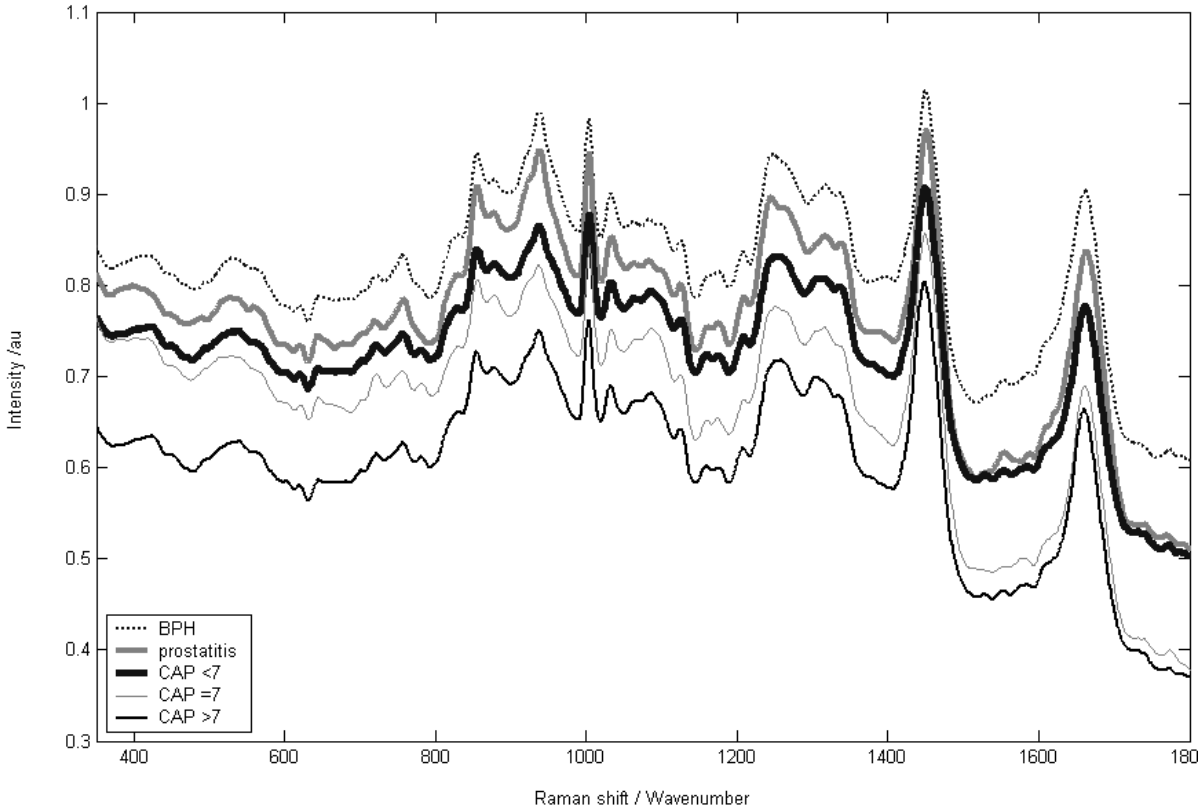

Figure 5: The mean Raman spectra measured from each of the pathological groups.

		Raman Prediction		
		BPH	**Prostatitis**	**Carcinoma**
Confirmed Histology	**BPH**	**350**	21	10
	Prostatitis	0	**34**	0
	Carcinoma	34	33	**389**

Table 8: The cross-validated results of the three group diagnostic algorithm.

	BPH	**Prostatitis**	**Carcinoma**
Sensitivity	92%	100%	85%
Specificity	94%	94%	98%

Table 9: The sensitivities and specificities achieved by the three group algorithm.

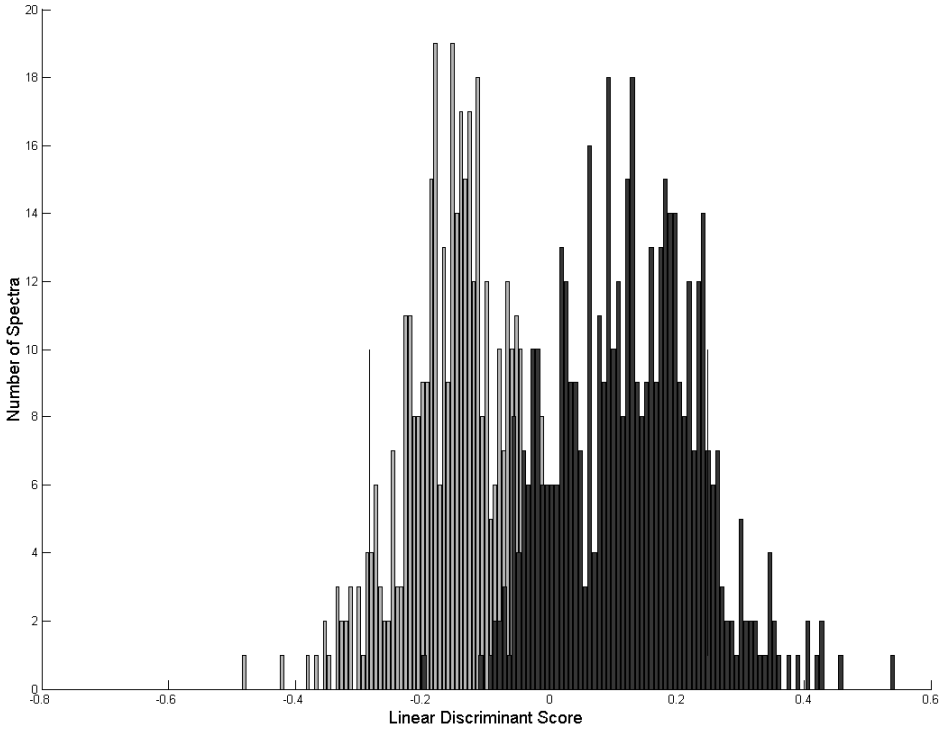

Figure 6: Histogram of linear discriminant scores for malignant versus benign bladder model. Malignant data are plotted in black, benign in grey.

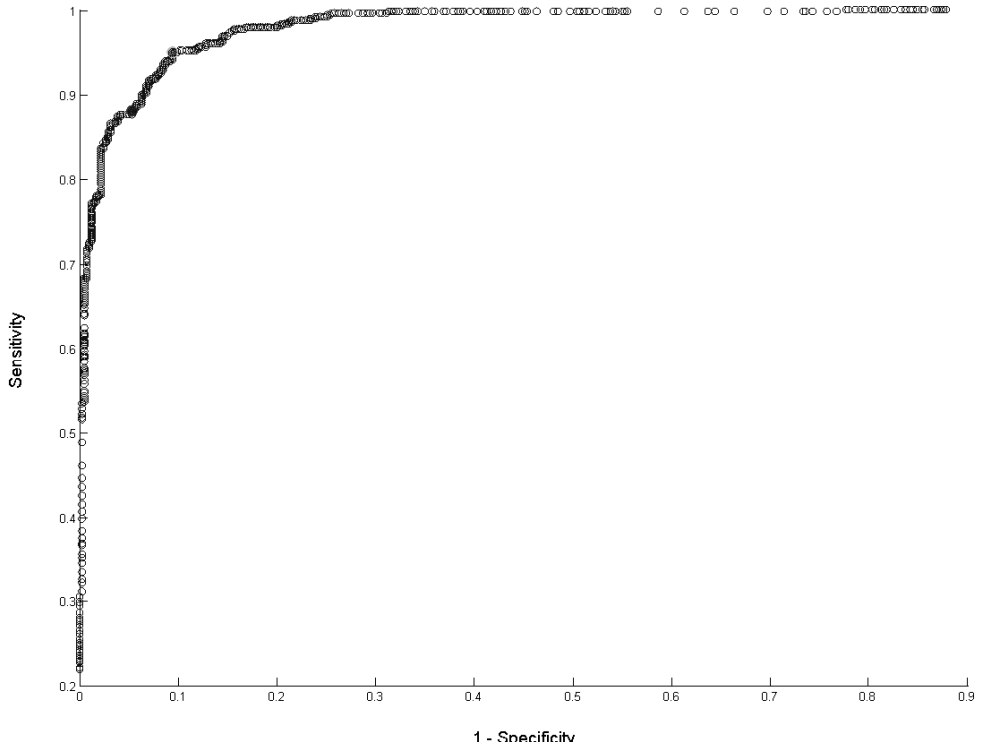

Figure 7: ROC of sensitivity versus 1-specificity for malignant group in the two-group prostate model. This has been achieved by varying the relative misclassification costs of the two groups.

			Raman Prediction		Total
			Benign	**Neoplastic**	
Equal costs (1:1)	**Pathology**	**Benign**	393 **(95%)**	22	415
		Neoplastic	57	420 **(88%)**	477
Optimum (51:111)		**Benign**	376 **(91%)**	39	415
		Neoplastic	24	453 **(95%)**	477

Table 10: Table of results of Raman prediction of specimens defined by consensus blinded histopathology. Adjustment of the misclassification costs has enabled adjustment of the outcome measures. The first model has equal misclassification costs of unity, the next has been modified to produce a higher sensitivity to malignancy, but without a significant increase in false positives.

4. DISCUSSIONS

Three group classification models have been constructed and exhibit good discrimination between pathology groups for the prostate and bladder. The use of misclassification costs has demonstrated that the prediction models could be adjusted to improve outcomes for a required application such as biopsy targeting, tumour margin detection, or in vivo diagnosis for immediate treatment. Each of these would require a different optimum model, either with low false negatives or low false positives.

For the first time Raman spectral models have been used to distinguish between stages of cancer in addition to grade, thereby demonstrating the potential to enhance the clinical decision process for optimum treatment. This may imply that the molecular constituents at the surface of the organ contain some biochemical marker of that occurring deeper in the lesion.

5. ACKNOWLEDGEMENTS

This work has been supported by the PPP Foundation and the DH NHS R&D Programme. Further funding has been provided by Gloucestershire Hospitals NHS Trust.

This work could not have been performed without the hard work of the histopathology technical team at Gloucestershire Royal Hospital and the pathology support of Dr Jill Farmer.

6. REFERENCES

[1] Meyer, J. P, et al. What's new in bladder cancer? *Trends in Urol Gynaecol and Sexual Health*, 2003. 8 (6): 25-29.

[2] Stewart, CS. *Novel detection strategies for transitional cell carcinoma.* In: Kirth, KH, Mickisch, GH, Schroder, FH, eds. Renal, bladder, prostate and testicular cancer: an update: the proceedings of the VIth Congress and Controversies in Oncological Urology. 2001. New York, Parthenon Publishing Group.

[3] Hugosson, J. *Early diagnosis: state of the art in clinical routine and screening studies.* In: Kirth, KH, Mickisch, GH, Schroder, FH, eds. Renal, bladder, prostate and testicular cancer: an update: the proceedings of the VIth Congress and Controversies in Oncological Urology. 2001. New York, Parthenon Publishing Group.

[4] Alfano, R, et al. Human breast tissue studied by IR Fourier transform Raman spectroscopy. *Lasers in Life Sciences*, 1991. **4**(1): 23-28.

[5] Liu, C, et al. Raman, fluorescence and time-resolved light scattering as optical diagnostic-techniques to separate diseased and normal biomedical media. *J Photochem Photobiol B: Biology*, 1992. **16**(2): 187-209.

[6] Mahadevan-Jansen, A, et al. Raman spectroscopy for the detection of cancers and pre-cancers. *J Biomed Optics*, 1996. **1**: 31-70.

[7] Feld, MS, et al. Detection and characterization of human tissue lesions with near infra-red Raman spectroscopy. *Advances in Fluorescence Sensing Technology*, 1995. **II** (SPIE 2388): 99-10.

[8] Shim, M, et al. In vivo near-infrared Raman spectroscopy: Demonstration of feasibility during clinical gastrointestinal endoscopy. *J Photochem Photobiol*, 2000. **72**: 146-150.

[9] Kendall C, et al. Raman spectroscopy a potential tool for the objective identification and classification of neoplasia in Barrett's oesophagus. *J Pathology* 2003. **200**: 602-609

[10] Stone, N. *Raman spectroscopy of biological tissue for application in optical diagnosis of malignancy*, PhD Thesis, Cranfield University. 2001.

[11] Bakker Schut TC, Witjes MJH, Sterenborg HJCM, et al. In vivo detection of dysplastic tissue by Raman spectroscopy. *Anal Chem* 2000;**72**:6010-6018.

[12] Schrader, B, et al. FT Raman Spectroscopy in medical diagnostics. *J Mol Struct*, 1995. **348**: 293-296.

[13] Edwards, H, et al. Potential applications of FT-Raman spectroscopy for dermatological diagnosis. *J Mol Struct*, 1995 .**347:**379-387.

[14] Caspers, P, et al. In vitro and in vivo Raman spectroscopy of human skin. *Biospectroscopy*, 1998. **4**: S31-S39.

[15] Stone, N, et al. Raman spectroscopy for early detection of laryngeal malignancy - preliminary results. *Laryngoscope*, 2000. **110**: 1756-1763.

[16] Crow, P., Kendall, C., Wright, M., Persad, R., Ritchie, A., Stone, N., 'The use of Raman spectroscopy to distinguish between normal tissue, carcinoma in situ and TCC within the bladder.', *British Journal of Urology*, 2002, **90(1)**, 71.

[17] Crow, P, Stone, N, Kendall, CA, Uff, JS, Farmer, JAM, Barr, H, Wright, MJP, 'The use of Raman spectroscopy to identify and grade prostatatic adenocarcinoma in vitro.', *British Journal of Cancer*, 2003, **89**, 1, 106-109.

[18] Stone, N, Kendall, C, Smith, J, Crow, P, Barr, H, 'Raman spectroscopy for identification of epithelial cancers.', *Faraday Discuss*., 2004, **126**, 141 –157.

Kerr-gated suppression of fluorescence in resonance Raman spectroscopy of tissue.

Maria Consuelo Hart Prieto[1], Pavel Matousek[2], Michael Towrie[2], Anthony William Parker[2], Alistair William Ritchie[1], Nicholas Stone[1]*.

1. Biophotonics Research Group, Pullman Court, Gloucestershire Royal Hospital, Great Western Road, Gloucester. GL1 3NN.
2. Central Laser Facility, CCLRC Rutherford Appleton Laboratory, Didcot, Oxfordshire. OX11 0QX

Keywords: Raman spectroscopy, Kerr-gate, fluorescence, suppression, liver, kidney, tissue.

Corresponding Author's address and contact details:

*Biophotonics Research Group, Pullman Court, Gloucestershire Royal Hospital, Great Western Road, Gloucester. GL1 3NN.

Tel: 01452 395712. Fax: 01452 395713.

E-mail: n.stone@medical-research-centre.com

Abstract.

Kerr-gated Raman spectroscopy was used at wavelengths of 488nm and 532nm to demonstrate both suppression of fluorescence and resonant enhancement of Raman spectra from liver and kidney. These highly absorbing tissues (at visible and NIR wavelengths) prove difficult to measure without the fluorescence significantly swamping the Raman signal. We have shown that we are able to obtain Raman spectra of reasonable quality from dark tissues, by coupling the Kerr-gate with a Raman spectrometer. It is felt that by utilising this technique we will potentially be able to distinguish the subtle changes in Raman spectra that occur between different pathologies within tissues such as the kidney and liver.

Introduction.

Raman spectroscopy is an optical technique that can be used to interrogate biological tissues to help us to understand the changes in molecular structure that occur with disease. By the beginning of the 1990s groups were utilising Raman spectroscopy to distinguish between normal and neoplastic tissue. The first studies looked at differentiating between normal breast tissue and advanced cancers in the breast,[1] as well as diseases of the gynaecological organs.[2,3] As techniques have advanced, the interest has moved to assessing its ability to diagnose cancers at much earlier stages. In this way more cancers could potentially be detected early, and therefore increase the chance of survival from the disease. So far in vitro studies have been performed to differentiate between different pathologies in a number of tissues including colon,[4,5] oesophagus,[6,7,8] brain,[9] skin,[10,11] larynx,[12] bladder,[13,14] and the prostate gland,[13,15]

Dark tissues such as kidney and liver have always caused problems for Raman spectroscopy because they are highly absorbing and fluorescent at most visible and NIR wavelengths. Therefore it has proved difficult to obtain spectra with anything more than the most significant peaks. Because of this the use of Raman spectroscopy in the diagnosis of renal and liver disease has been largely overlooked. There has been some work, however, on near infrared Fourier transform Raman spectroscopy in the liver.[16] These showed characteristic differences between the spectra from different pathological tissues, i.e. normal and cirrhotic liver, but analysis was not performed to evaluate the extent of these differences. Furthermore, acquisition times of 90 to 150 minutes were required to achieve an acceptable signal-to-noise ratio.

Hawi et al also looked at hepatocytes from liver tissue at an excitation wavelength of 632nm and they concluded that there were spectral differences between the cells exhibiting different pathologies, but that also at 632nm there was enhancement of the haem component of the tissue that resulted in marked spectral difference between the tissue and the hepatocytes.[17]

The difficulty of utilising Raman spectroscopy in these darker tissues has held up potential progress in exploring its use for improved diagnostics. If the fluorescence accompanying the Raman spectra of these tissues could be suppressed then the biochemical changes accompanying disease processes can be elucidated. Furthermore, by changing the wavelength of excitation it is possible to obtain resonance Raman signals of specific molecular species. This is usually accompanied by an increased fluorescence signal.

One method to overcome the problem with fluorescence to use picosecond Kerr-gating. This technique utilises impulsive excitation with a picosecond pulsed laser and fast temporal gating of instantaneous Raman scattered light. In this way the signal to noise ratio is increased and the slow emitting fluorescence is minimised.

There have been studies utilising the Kerr-gating technique to improve upon tissue Raman spectra measured at depth, by suppressing the surface signal,[18,19] but there is no published work on utilising this technique to obtain spectra from dark biological tissues. This study has been performed to investigate the use of Kerr gating for fluorescence suppression at different wavelengths in the kidney and the liver. This

will show the potential of the technique to provide wavelength dependent resonance signals with suppressed fluorescence.

Materials and methods.

Tissue collection and preparation.

Pig's liver and kidney were purchased from a local supermarket and kept refrigerated until required. The tissue was cut into thin slices and placed on a glass slide ready for sampling. Samples from the medulla and the cortex of the kidney were both studied.

Instrumentation.

The Kerr-gating system is based on the high throughput 4 picosecond optical Kerr shutter that was described in previous publications by Matousek et al.[20,21] The Kerr-gate is made up of two crossed polarisers (41x 41mm, Glan Taylor polarisers) and a Kerr medium consisting of a 2mm optical cell that is filled with CS_2 (see Figure 1). When the gate is closed, the light collected from the sample is blocked. When the gate is open the polarisation of the collected light is rotated to allow it to pass through the cross polarisers. The gate is opened by a short 1 picosecond gating pulse at 800nm. This bypasses the polarisers and creates a transient anisotropy within the Kerr medium, this then acts to rotate the polarisation of the light from the sample, (Figure 1).

The Raman scattered light was collected in 130º geometry using a lens with an f-number of 2. The spectra were analysed using a dispersive Raman spectrometer (Spex Triplemate) mounted after the Kerr-gate. To prevent residual elastically scattered light from the probe laser from entering the spectrometer a Kaiser holographic notch filter was used. To also prevent the residual 800nm gating beam scatter from entering, a saturated copper sulphate solution in a 1cm thick optical cell was placed in front of the spectrometer slit. A water-heat-exchanger cooled, deep depletion NIR CCD (Andor Technology DU420BR-DD) was used to record the Raman spectra from the tissue.

The probe source (with wavelengths 488 and 532 nm used) was provided by a femtosecond mode-locked Ti:sapphire laser, producing a 1 kHz pulse train, which was then amplified with a Nd:YLF-pumped regenerative amplifier system to produce 1 ps, 800 nm pulses at 2 mJ at 1 kHz. The pulse energy at the sample was around 5 μJ (1 kHz) corresponding to 5 mW of average power. The beam was focused down to 300 μm diameter spot.

To demonstrate the ability to obtain Raman spectra from dark tissue we performed two sets of measurements; the first involved obtaining spectra from the liver and kidney without the use of the Kerr-gate, and the second involved obtaining spectra with the Kerr-gate opening for approximately 4ps a short period after the excitation pulse. The spectra were obtained at two wavelengths to assess whether different components would be resonantly enhanced. Acquisition times varied depending on the strength of the signal measured. These are shown in the result figure captions.

The liver and kidney samples were also measured using a Renishaw System 1000 microspectrometer optimised for tissue measurements at 830nm.[7] This was performed to demonstrate the difficulty of obtaining Raman spectra, even at NIR wavelengths. A x20 0.4 NA ultra long working distance objective was used to illuminate the tissue ands collect the scattered light. Laser power at the sample was approximately 100mW. The spectra were acquired in 1 second for the kidney and 5 seconds for the liver.

Results.

Figure 2 shows the Raman spectra of liver and kidney tissues at 830 nm. The sharp rise seen at around 150cm^{-1} and the ripples at higher wavenumbers are caused by the edge filter used to reject the elastically scattered light. At higher wavenumbers, 900cm^{-1} and above, Raman signal can be seen superimposed on the fluorescence background. Very little of the Raman signal is strong enough to be obtained over the shot noise ($\pm\sqrt{N}$, where N is number of counts).

The spectra obtained using the Kerr-gate have peaks at 665 cm^{-1} and 795 cm^{-1}, these are consistent with Raman peaks of the CS_2 Kerr-medium. The spectra have been truncated to remove these from obscuring the information relevant to this study. There are other peaks labelled with '*' in Figures 4, 6, and 7. These are caused by hot pixels from the detector and are observed to increase in intensity linearly with time and not with signal strength (note they cannot be seen in the Kerr-gate off spectra with a high fluorescence signal).

Figures 3 and 5 show the strength of the fluorescence suppression at 488nm for kidney cortex and liver respectively. In the examples shown the fluorescence signal levels are between 6 and 24 times less (taking into account the time of acquisition as well as the signal on the plot) with the Kerr-gate on.

Figures 4 and 6 show the typical Raman spectral quality from kidney and liver tissues when using the Kerr-gate. There is much fine detail visible, slightly tarnished by the CCD hotpixels. This demonstrates the possibility of utilising Raman spectroscopy in these dark tissues to provides a biochemical information on the tissue state. The true quality of the resonant Raman spectra at both wavelengths with the Kerr-gate on can be seen in Figures 4, 6 and 7. These figures also show that an enhancement of the haemoglobin and carotenoids is obtained at a wavelength of 488nm when compared to a wavelength of 532nm. The peaks for the haemoglobin are at approximately 1356 cm^{-1}, 1547 cm^{-1} and 1605 cm^{-1},[22] whereas the main peak from the carotenoids is at 1003 cm^{-1} (each are labelled h and c respectively in the Figures).

Figure 7 demonstrates that the resonance Raman spectra obtained at 488nm showed a visible difference between tissues from the liver and kidney. The greatest differences appear to be the fatty features found in the liver spectra. This is a first attempt and many further spectra would need to be acquired to provide the relevant statistical confidence for reproducible tissue discrimination using this method.

Conclusion.

Due to the fluorescence of tissues that are extremely vascular and dark, we have historically been unable to obtain good quality spectra. We have shown for the first time, that by incorporating the Kerr-gating technique into the spectral analysis of tissue using Raman spectroscopy, we have been able to suppress the fluorescence and obtain spectra of adequate quality to enable further studies on biological tissue.

The system used has not been optimised for tissue work. Laser pulse repetition rate could be enhanced to raise signal without tissue damage. The spectrometer was not optimised for throughput with the collection optics and geometry and the CCD detector had a number of hot pixels, which blemished the spectra. Improvements in all these areas could see the signal increase between 10 and 100 times, thus facilitating shorter detector integration times.

Other excitation wavelengths can be used, and by tuning these to specific electronic absorption bands, particular species can be resonantly enhanced. With the use of Kerr-gated fluorescence suppression there is the potential for the detection of subtle changes in resonance Raman spectra likely to accompany pathological changes in tissue.

Raman spectroscopy is already being used to distinguish between different pathologies in other tissues such as the bladder,[13,14] prostate,[13,15] cervix,[3] breast,[1] and oesophagus.[6,7,8] Now we will be able to potentially distinguish between different pathologies in more vascular tissue such as the liver and kidney by utilising Kerr-gated Raman spectroscopy.

Further work is planned to compare tissue pathologies in vascular tissues at various wavelengths to evaluate the capacity of Kerr-gated Raman spectroscopy to enhance the ability of RS to distinguish between normal and diseased states.

Acknowledgements.

We gratefully acknowledge the loan of a NIR CCD camera from Andor Technology. Miss M. C. Hart Prieto is supported by the Cobalt Unit Appeal Fund and Dr N. Stone is supported by the PPP foundation and the Department of Health NHS R&D programme.

References.

1. R. Alfano, C.H. Liu, W.L. Sha, H.R. Zhu, D.L. Akins, J. Cleary, R. Prudente and E. Cellmer. Lasers in Life Sciences. **4**(1), 23 (1991).

2. C. Liu, B.B. Das, W.I. Sha Glassmen, G.C. Tang, K.M. Yoo, H.R. Zhu, D.L. Akins, S.S. Lubicz, J. Cleary, R. Prudente, E. Cellmer, A. Caron and R.R Alfano. J Photochem Photobiol B: B. **16**, 187 (1992).

3. A. Mahadevan-Jansen and R. Richards-Kortum. Journal of Biomedical Optics. **1**, 31 (1996).

4. M. S. Feld, R. Manoharan, J. Salenius, J. Orenstein-Carndona, T. J. Romer, J.F. Brennan, et al. Advances in Fluorescence Sensing Technology. **II** (SPIE 2388), 99 (1995).

5. M. Shim, L.M. Song, N.E. Marcon, B.C Wilson. J Photochem Photobiol. **72,** 146 (2000).

6. C. Kendall, N. Stone, N. Shepherd, K. Geboes, B. Warren, R. Bennett, H. Barr. Journal of Pathology. **200,** 602 (2003)

7. N. Stone, C. Kendall, N. Shepherd, P. Crow, H. Barr, Journal of Raman Spectroscopy. **33**, 7, 564 (2002).

8. T.C. Bakker Schut, M.J.H Witjes and H.J.C.M. Sterenborg. Anal Chem. **72**, 6010 (2000).

9. B. Schrader, S. Keller, T. Lochte, S. Fendel, D.S. Moore, A. Simon and I. Sawatzki. Journal of Molecular Structure. **348**, 293 (1995).

10. H. Edwards, A. Williams and B. Barry. Journal of Molecular Structure. **347,** 379 (1995).

11. P.J. Caspers, G.W. Lucassen, R. Wolthuis, H.A. Bruining and G.J. Puppels. Biospectroscopy. **4**, S31 (1998).

12. N. Stone, P. Stravroulaki, C. Kendall, M. Birchall and H. Barr. Laryngoscope. **110,** 1756 (2000).

13. M.C. Hart Prieto, P. Crow, C. Kendall, J. Uff, M. Wright, A.W. Ritchie and N. Stone. Biomedical vibrational spectroscopy and biohazard detection technologies. SPIE. **5321**, 57 (2004).

14. P. Crow, J.S. Uff, J.A. Farmer, M.P. Wright and N. Stone. British Journal of Urology International. **93(9),** 1232 (2004).

15. P. Crow, N. Stone, C.A. Kendall, J.S. Uff, J.A. Farmer, H. Barr and M.P. Wright. British Journal of Cancer. **89(1),** 106 (2003).

16. S. Keller, B. Schrader, A. Hoffman, W. Schrader, K. Metz, A. Rehlaender, J. Pahnke, M. Ruwe and W. Budach. J. Raman Spectrosc. **25,** 663 (1994).

17. S.R. Hawi, W.B. Campbell, A. Kajdacsy-Balla, R. Murphy, F. Adar and K. Nithipatikom. Cancer Letters. **110,** 35 (1996).

18. M.D. Morris, A.E. Goodship, E.R.C. Draper, P. Matousek, M. Towrie and A.W. Parker. Biomedical vibrational spectroscopy and biohazard detection technologies. SPIE. **5321,** 164 (2004).

19. M.C. Hart Prieto, P. Matousek, M. Towrie, A.W. Parker, M. Wright, A.W. Ritchie, N. Stone, **10**, 4, JBO (2005).

20. P. Matousek, M. Towrie, A. Stanley and A.W. Parker. Appl.Spectrosc. **53** (12), 1485 (1999).

21. P. Matousek, M. Towrie, C. Ma, W.M. Kwok, D. Phillips, A.W. Toner and A.W. Parker. J. Raman Spectrosc. **32,** 983 (2001).

22. B.R. Wood, D. McNaughton, J. Raman Spectrosc. **33**, 517 (2002).

Legends:

Fig 1: A schematic diagram and photograph showing the Kerr-gating Raman system at the Rutherford Appleton Laboratory.

Fig 2: Spectra from the cortex of a pig's kidney and liver at a wavelength of 830nm.

Fig 3: Spectra from the cortex of a pig's kidney at a wavelength of 488nm with the Kerr-gate on (20s x 30 accumulations) and off (5s x 30 accumulations).

Fig 4: Spectra from the cortex of a pig's kidney at wavelengths of 488nm (20s x 30 accumulations) and 532nm (30s x 60 accumulations) with the Kerr-gate on.

Fig 5: Spectra from pig's liver at a wavelength of 488nm with the Kerr-gate on (10s x 30 accumulations) and off (5s x 30 accumulations).

Fig 6: Spectra from pig's liver at wavelengths of 488nm (10s x 30 accumulations) and 532nm (20s x 30 accumulations) with the Kerr-gate on.

Fig 7: Spectra from pig's liver (10s x 30 accumulations) and kidney (20s x 30 accumulations) at 488nm with the Kerr-gate on.

Figures:

Fig 1.

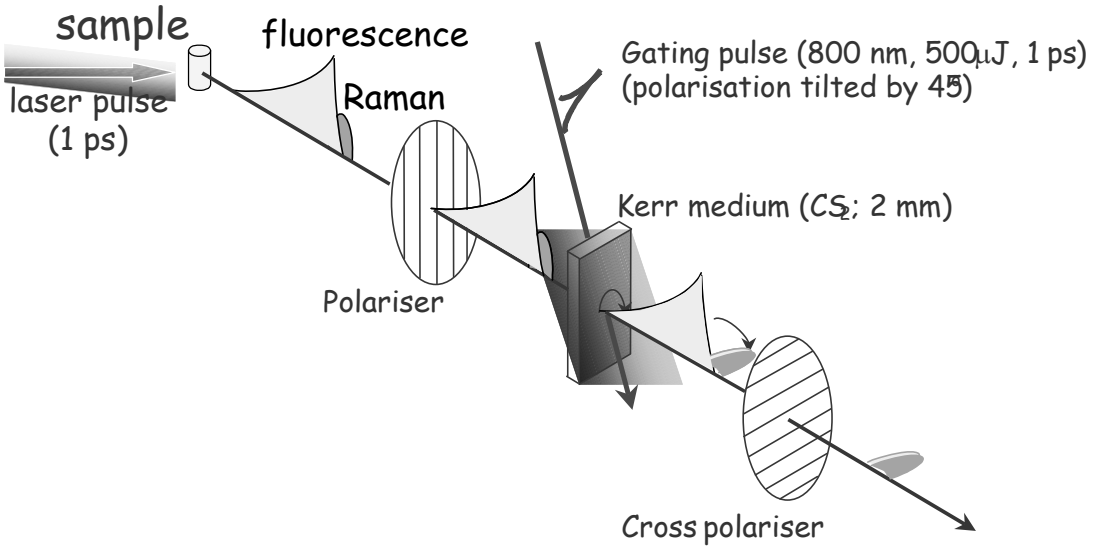

Fig 2.

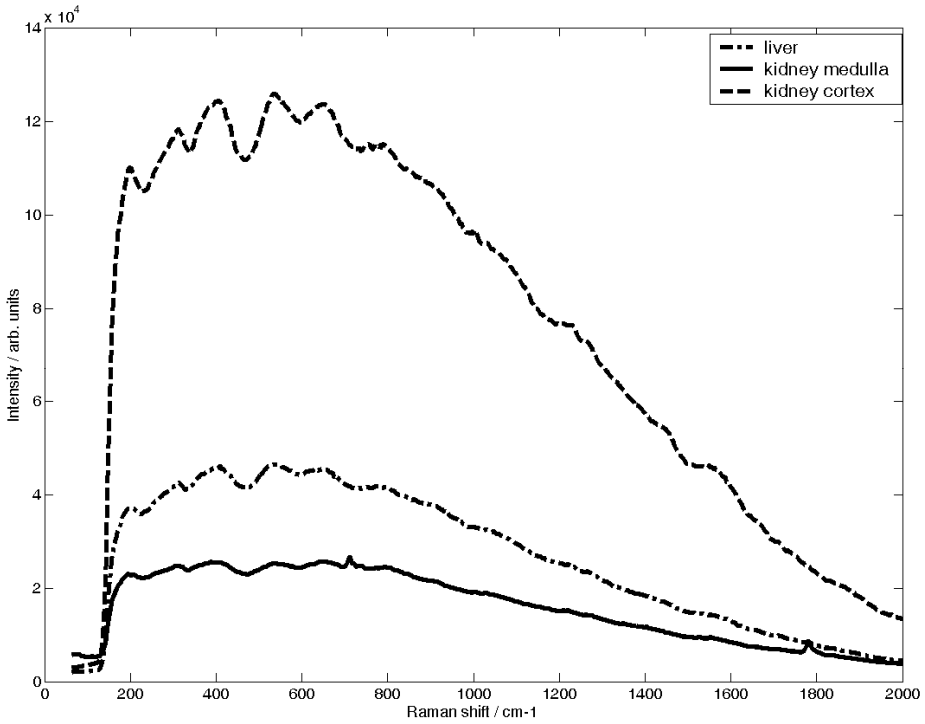
x 10^4
liver
kidney medulla
kidney cortex
Intensity / arb. units
Raman shift / cm-1
0
2
4
6
8
10
12
14
0
200
400
600
800
1000
1200
1400
1600
1800
2000

Fig 3.

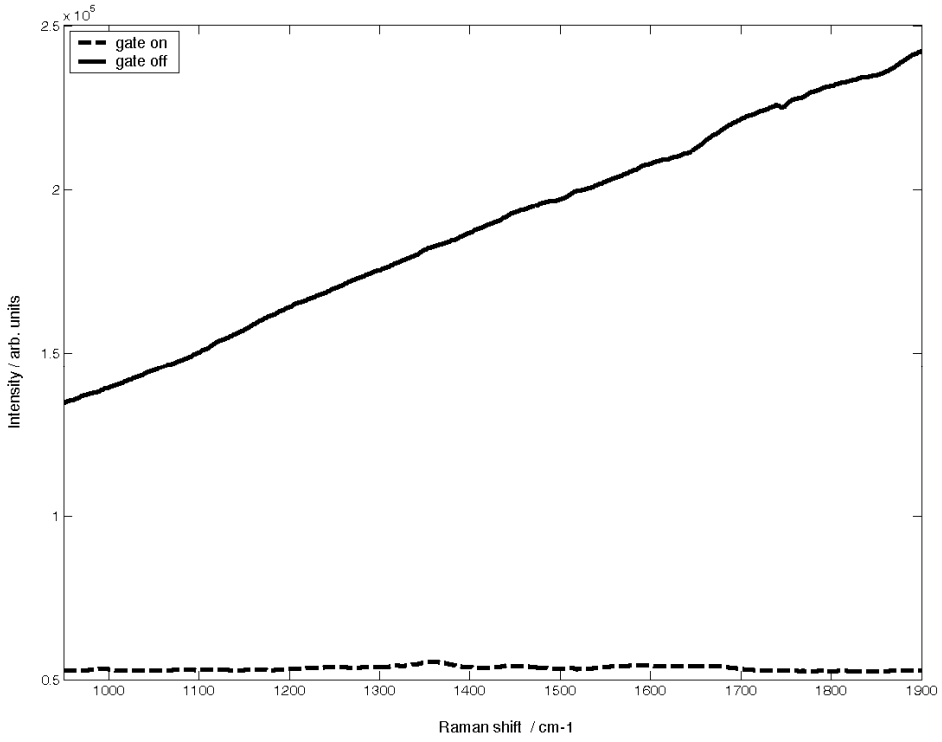
x 10^5
2.5
2
1.5
1
0.5
gate on
gate off
Intensity / arb. units
1000
1100
1200
1300
1400
1500
1600
1700
1800
1900
Raman shift / cm-1

Fig 4.

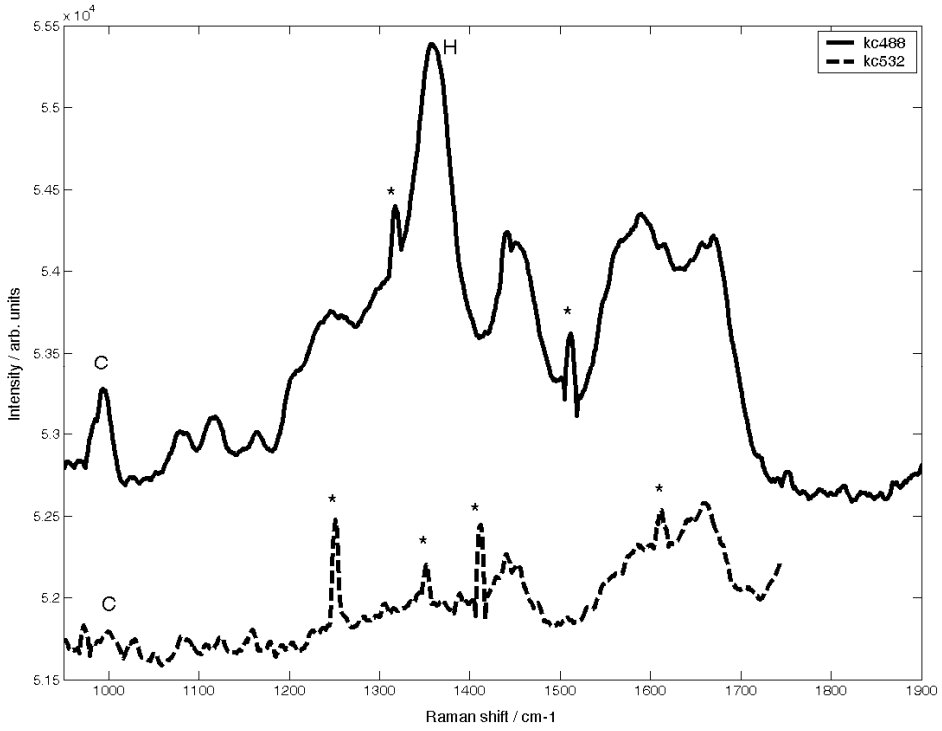
x 10^4
5.55
5.5
5.45
5.4
5.35
5.3
5.25
5.2
5.15
Intensity / arb. units
1000
1100
1200
1300
1400
1500
1600
1700
1800
1900
Raman shift / cm-1
kc488
kc532
H
C
C
*
*
*
*
*

Fig 5.

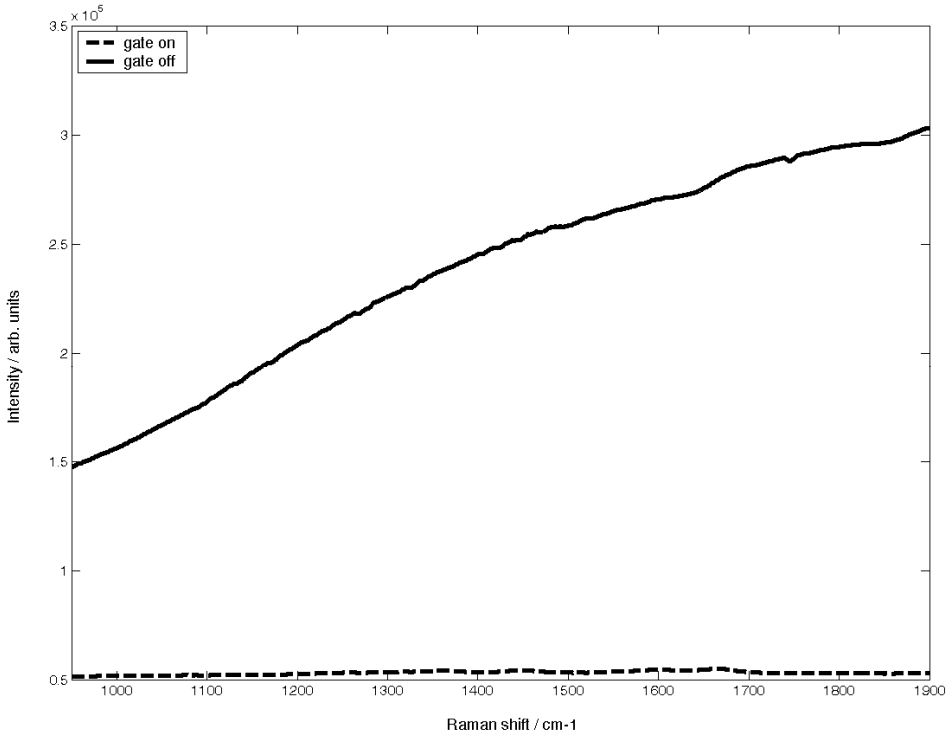
x 10^5
gate on
gate off
Intensity / arb. units
Raman shift / cm-1
3.5
3
2.5
2
1.5
1
0.5
1000
1100
1200
1300
1400
1500
1600
1700
1800
1900

Fig 6.

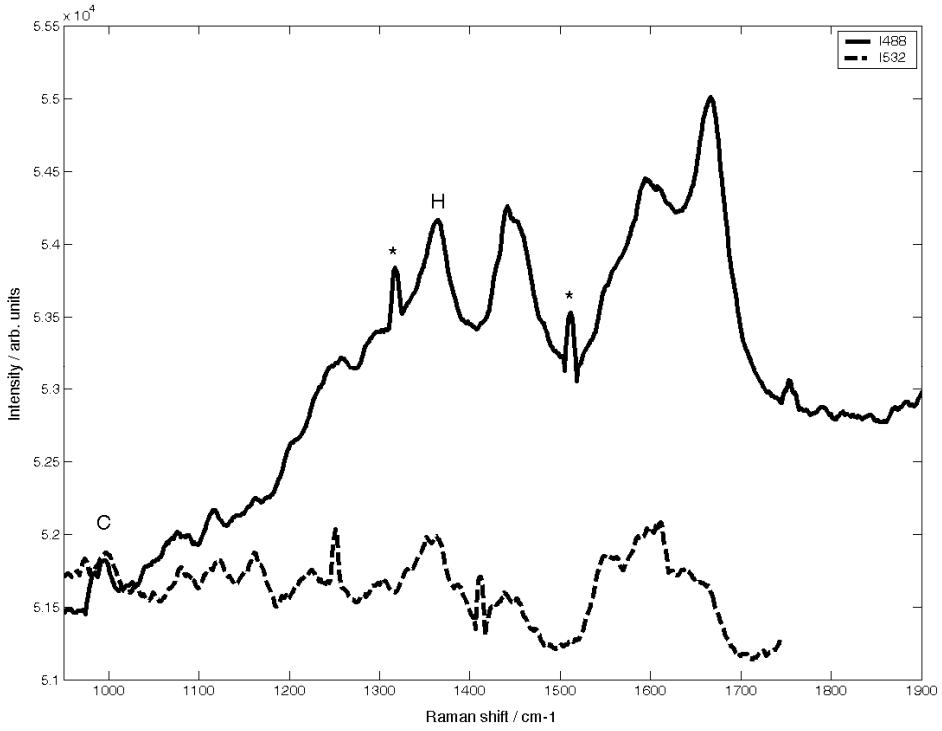
x 10^4
I488
I532
H
C
Intensity / arb. units
Raman shift / cm-1

Fig 7.

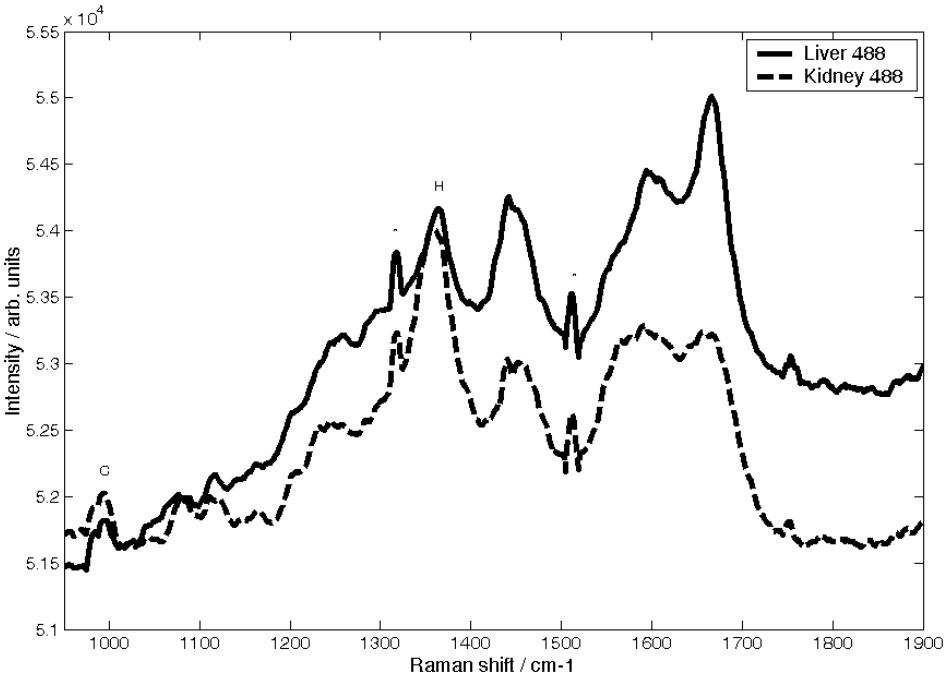
x 10^4
Liver 488
Kidney 488
H
C
Intensity / arb. units
Raman shift / cm-1

The use of Raman spectroscopy to determine the biochemical basis of urological pathologies.

Maria Consuelo Hart Prieto[1], Paul Crow[1], Jeremy Uff[2], Alistair William Ritchie[2], Nicholas Stone[1]*.

1. Biophotonics Research Group, Pullman Court, Gloucestershire Royal Hospital, Great Western Road, Gloucester. GL1 3NN.

2. Gloucestershire Royal Hospital, Great Western Road, Gloucester. GL1 3NN.

Corresponding Author's address and contact details:

* Biophotonics Research Group, Pullman Court, Gloucestershire Royal Hospital, Great Western Road, Gloucester. GL1 3NN.

Tel: 01452 395712. Fax: 01452 395713.

E-mail: n.stone@medical-research-centre.com

Abstract.

Raman spectroscopy is an optical technique that is able to interrogate biological tissues. Prostate samples for this study were obtained by taking a chip at TURP, and bladder samples from a biopsy taken at TURBT and TURP, following ethical approval. Constituents were purchased from Sigma – Aldrich.

Spectra were taken from the constituents and different pathologies within the bladder and the prostate. We were then able to determine the biochemical basis to these pathologies.

We have shown for the first time that we are able to utilise Raman spectroscopy in determining the biochemical basis to the different pathologies within the bladder and prostate gland. In this way we can achieve a better understanding of disease process and carcinogenesis. This could have major implications in the future of the diagnosis of pathologies within the bladder and the prostate gland.

Keywords: Raman spectroscopy, Prostate, Bladder.

Introduction:

Raman Spectroscopy:

Raman spectroscopy is an optical technique that can be used to interrogate biological tissues with chemical specificity. In doing so it gives us an understanding of the changes in the molecular structure that are associated with disease. With this in mind it was felt that Raman spectroscopy could be used to determine the biochemical basis to pathologies in the bladder and the prostate gland.

By the start of the 1990s various groups were using Raman spectroscopy to distinguish between normal and neoplastic tissue. The first studies looked at differentiating between normal tissue and advanced cancers in the breast[1] and gynaecological organs.[2,3] As techniques were refined, interest moved towards diagnosing neoplastic change at progressively earlier stages. To date, in vitro studies have also been undertaken to differentiate between different pathologies in a number of other tissues including colon,[4,5] oesophagus,[6,7,8] brain,[9] skin,[10,11] and larynx.[12]

There has been a lot of research work done on the bladder and the prostate gland in the past, with the aim to provide a specific and sensitive means of distinguishing between the pathologies associated with these organs. It has already been shown that Raman spectroscopy can be used to achieve this however the studies have been exclusively in vitro.[13,14.]

The research to date on the bladder and prostate gland has looked at diagnosis of pathologies rather than at the biochemical basis of the pathologies in question. The biochemical changes that occur are thought to be a gradual continuum from normal to malignant, therefore a means of detecting pre-malignancies within these tissues would be by detecting the biochemical changes that are associated with disease progression before the actual progression has occurred. Raman spectroscopy has the potential to do this through a minimally invasive technique however, the biochemical basis of each of the pathologies within the bladder and the prostate gland must first be ascertained.
To date this has only been done in breast tissue[15].

The Bladder:

The incidence of bladder cancer in the UK is 8% in men and 3% in women. It is the fourth most common cancer in men and the eighth in women. Each year there are 9000 cases diagnosed in men and 3600 diagnosed in women in the UK but although the figures are high there has been a reduction in the age standardised incidence since the 1980's. It is thought that the reason for this is the reduction in smoking and the banning of aromatic amines in the 1980's. Both of these are known risk factors for the development of bladder cancer.[16]

Ninety percent of bladder cancers are transitional cell carcinomas of the bladder, and the majority of these are superficial. They tend to be found in the over 65 year olds.

The Prostate Gland:

27,000 men were diagnosed in the year 2000 in England and Wales with prostate cancer[17]. It is the second leading cause of cancer related death in men in Western Europe and North America,[17,18] and the leading cause of cancer related death in the United States[19]. As many as 40% of men aged between 60 and 70 years, have microscopic foci of well differentiated adenocarcinoma of the prostate gland (CaP). It is also a major cause of morbidity and health care related costs. 3-5% of men will die of CaP and 10% of men diagnosed with CaP will develop clinical disease[18]. The diagnosis of CaP is dependent on an abnormal digital rectal examination (DRE), and / or a raised level of serum prostate specific antigen (PSA). A finding of either of these in men will lead onto transrectal ultrasonography (TRUS), and biopsy. The biopsies tend to be sextant sampling with targeting if a lesion is suspected on TRUS. Unfortunately the biopsies have a high number of false negatives, and therefore a cancer can remain undiagnosed. These false negative results are mainly due to sampling error (in that the CaP may be present as a small focus within the prostate gland and the biopsy may have missed this).[20] It has been shown that even if a man has two sets of negative biopsies with a persistently raised PSA, he has a 10% risk of having a cancer found on the third biopsy.[20]

Materials and methods:

We obtained approval from the Gloucestershire Research Ethics Committee, to obtain samples for experimentation using Raman spectroscopy. The samples used for this study were taken following fully informed consent.

Tissue collection and preparation:

Bladder samples were collected at cystoscopic procedures including transurethral resection of the prostate (normal biopsies) and transurethral resection of bladder tumour. Prostate samples were obtained by taking an extra core from prostate biopsy procedures, or a chip of prostate during transurethral resection of the prostate. The samples were then snap-frozen in liquid nitrogen and transferred to an -80°C freezer for storage.

At the time of the experiment the tissue was passively warmed to room temperature.

Constituents:

The aim of measuring constituents was to assess the biochemical properties of each of the pathologies within the bladder and the prostate gland. In this way it was hoped that it would be possible to quantify the differences between the pathologies.

The following constituents were purchased from Sigma – Aldrich; Actin-from bovine muscle, (A3653). β-carotene- type 1, synthetic, approx 95%, (C9750). Cholesterol sigma grade, 99%+, (C8667). Choline- base, approx 50% (w/w) aqueous solution, (C9154). Collagen- type 1, from human placenta, acid soluble, (C7774), type 3, from human placenta, acid soluble, (C4407), type 4, from human placenta, acid soluble, (C7521). DNA- from human placenta, (D7011). Glycogen- from bovine liver, (G0885). Lycopene-from tomato, (L9879). Oleic Acid- water soluble, (O1257). Prostate Specific Antigen- from human seminal fluid, minimum 95%, (P3338). Triolein (C18:1,(cis)-9)-sigma grade, approx 95%, (T7140).

The above constituents were picked to as they were thought to be representative of different areas within a cell[15]. DNA is representative of the cell nucleus as the other constituents of the nucleus (ribosomes, RNA) have previously been shown to have a minor effect on the spectrum from the nucleus[15]. The other constituents and the region of the cell or sample that they represent is shown below:

Actin- cell cytoplasm, β-carotene- thought to be decreased in malignant tissue[21,22,23], cholesterol-necrosis[15], choline- thought to be abundant in malignant tissue [24], collagen-extracellular matrix/ basement membrane, glycogen- reduced in rapidly dividing cells such as malignant tissue. Only mature cells store glycogen. Lycopene- thought to be decreased in malignant tissue, oleic acid- abundant in urothelium, PSA (prostate specific antigen)- produced by the prostate gland, and triolein- fat.

Raman spectroscopy of the tissue samples and the constituents:

The same system was used for the measurement of both the constituent and tissue spectra. The laser used was a Renishaw high power near infrared diode laser, which supplies the excitation light at a wavelength of 830nm and generates 300mw of power. This is focused through the microscope lens onto the tissue sample or the constituent. The spectrometer then collects the scattered light from the tissue/constituent and detects it. The detected spectrum is recorded on the p.c.

The acquisition of spectra for the tissue samples was performed as follows. A x20 MIRPlan ULWD Olympus microscope objective was used to measure bladder spectra, with an acquisition time of 10secs at full laser power. Approximately 10 spectra were taken from each sample in a random fashion.

For the prostate tissue, an x80 MIRPlan ULWD Olympus microscope objective was used to focus on the prostate and to record the prostate spectra. Once focused for the white light, the focus was moved in to the tissue by 10μm and the acquisition time was set to 60 seconds at full laser power, for 1 acquisition. The spectra were taken randomly with approximately 10 spectra taken per sample.

The solid constituents were placed on a calcium fluoride slide, and the liquid constituents were placed in a cell plate. An x20 MIRPlan ULWD Olympus microscope objective was

then used to focus in on the substance and to measure the spectra. Different acquisition times were used for each constituent.

The laser was always at full power with the monochromator slit set to 50μm for all spectra obtained, and they were centred at 1150cm^{-1} and stored on the system's P.C following acquisition.

The PLS-toolbox® (Eigenvector Technologies, Manson, Washington, USA) for use with Matlab® was adapted for use with the data in these studies[7]. The mean spectra for the pathologies and the constituents were ascertained allowing for further analysis to occur. The fitting of the mean spectra of the constituents to the mean spectra of the different pathologies in the bladder and the prostate gland was done by using 'ordinary least squares' analysis. This is explained simply below:

$$X = cS + E$$

Where S is the matrix of spectral components, c is the matrix of concentrations to be predicted, and X is the measured spectra. This can be used to provide a 'best fit' of the spectral components or basis spectra found within the measured spectra. The assumption is made that the residual is minimised and that the spectral components selected are the main components of the spectra.

$$c = \frac{(X - E)}{S}$$

The disadvantage with this technique is that any co linearity in the components selected will skew the fit. An example being amino acids and the proteins containing them being

used in the model. Observation of the residual E (E=X-cS) enables the quality of the fit to be observed and any remaining features of the spectra to be included in the next iteration of the model.

Results:

Constituent spectra:

The constituent spectra were obtained as described above. The mean of the spectra from each constituent was then obtained by using Matlab® and are shown below in figures 1 to 12.

Constituent analysis of the tissue spectra:

Over 1000 spectra were obtained from both the bladder and the prostate samples and these were analysed to give mean spectra for each of the following pathologies, TCC grades 1 to 3, cystitis, CIS, adenocarcinoma (adenoCa) and normal urothelium, for the bladder and Adenocarcinoma (Gleason score <7, 7 and >7), prostatitis, and normal prostate tissue for the prostate. The constituent spectra were fitted to the mean spectra measured (figs 13 and 15) and an approximate value for the relative constituent concentration (excepting water) was obtained (figs 14 and 16). In this way the biochemical basis for each pathology within the bladder and the prostate was elucidated.

Tables 1 and 2 show the relative percentages of each constituent present in each of the pathologies.

Discussion:

Raman spectroscopy has been in use for chemical analysis in industry for many years now. It wasn't however until recently due to advances in technology that we have been able to apply it to biological tissues.

Shafer – Peltier et al[25,26], have been the only other group in the literature to have looked at the chemical basis of disease using Raman spectroscopy. However this was done in breast tissue, not always with pure standards and has never been done before in urology. This study was performed to determine the biochemical basis of pathologies within the bladder and the prostate gland in order to attain a better understanding of pathogenesis and disease progression.

Firstly the main building blocks or constituents of biological tissue were considered. Spectra were obtained from these constituents and the mean spectrum for each one was derived using empirical analysis. The first derivatives of these were used with 'ordinary least squares' analysis to formulate a biochemical spectral model. In formulating a spectral model containing the main biochemical building blocks (constituents) for tissue we were able to apply it to the mean spectra of different pathologies within the bladder and the prostate gland. In doing so we were able to extract information about the microscopic composition of tissue in different pathologies. Note that the resulting concentrations have been calculated with ordinary least squares, which can be subject to

some errors if significantly collinear constituent spectra are used or if the data is of poor quality, i.e. noisy. Great care was taken to minimise these possible issues.

The results have shown that for pathologies within the bladder and the prostate gland, the DNA content increases as the tissue progresses from normal to malignant, and in the bladder the collagen content decreases. This is as expected as the nuclear to cytoplasm (actin) ratio increases from normal to malignant tissue and DNA is abundant in the nucleus. Also the cells become more abundant and therefore the extracellular matrix is reduced which is abundant in collagen. Until the tumour becomes larger and then you would usually expect more collagen. We found that using collagen types 1 and 4 gave a better spectral fit than by including collagen type 3 suggesting that types 1 and 4 are more abundant in the bladder and prostate tissue. Cholesterol was used in the model as a potential component of necrosis. As a tumour becomes bigger there tends to be necrotic areas within it where it is too big for its blood supply. Interestingly there is no cholesterol in the bladder spectra but it is increased in that of the prostate tissue that is malignant. This may be because a lot of the tumours in the bladder undergoing TURBT are papillary and very vascular; therefore they do not show necrotic areas. The glycogen content appears to increase with malignancy suggesting a higher metabolic rate in malignant tissue which is understandable, although different to that found in some other epithelial tissues such as the oesophagus. The actin level however increases in the bladder but decreases in the prostate gland. This may be because the bladder tumours tend to be papillary and therefore have a larger surface area, however the actin represents the cytoplasm and as the nuclear to cytoplasm ratio increase with malignancy you would expect the actin level to decrease.

Both lycopene and β carotene were thought to be decreased in malignant tissue[21,22,23], however we found that there was none detected using our spectral analysis. This may be because they are in such small concentrations that the other spectra hide them. Also we were unable to measure the PSA for our model as the only samples we could obtain were in such small quantities that we were unable to obtain a usable spectrum.

Conclusion:

We have shown for the first time that we are able to utilise Raman spectroscopy in determining the biochemical basis to the different pathologies within the bladder and prostate gland. In this way we can achieve a better understanding of disease process and carcinogenesis. This could have major implications in the future of the diagnosis of pathologies within the bladder and the prostate gland. Histopathology is at present the 'gold standard' for diagnosis, by utilising Raman spectroscopy and the knowledge we have gleaned from the biochemical studies performed, we potentially will be able to eliminate the intra and inter – observer error that is seen in histopathology.

Acknowledgements:

Miss M C Hart Prieto is supported by the Cobalt Appeal Fund and Dr N Stone is supported by the PPP foundation and the Department of Health NHS R&D programme.

References:

1. Alfano R, Liu C. H, Sha W. L, Zhu H. R, Akins D. L, Cleary J, Prudente R, Cellmer E. 'Human breast tissue studied by IR Fourier transform Raman spectroscopy'. *Lasers in Life Sciences*. **4(1),** 23-28, (1991).

2. Liu C, Das B. B, Sha Glassmen W. l, Tang G. C, Yoo K. M, Zhu H. R, Akins D. L, Lubicz S. S, Cleary J, Prudente R, Cellmer E, Caron A, Alfano R. R. 'Raman, fluorescence and time-resolved light scattering as optical diagnostic-techniques to separate diseased and normal biomedical media'. *J Photochem Photobiol B: Biology*. **16(2),** 187-209, (1992).

3. Mahadevan-Jansen A, Richards-Kortum R. 'Raman spectroscopy for the detection of cancers and pre-cancers'. *J Biomed Optics*. **1**, 31-70 (1996).

4. Feld M. S, Manoharan R, Salenius J, Orenstein-Carndona J, Romer T. J, Brennan J. F, et al. 'Detection and characterization of human tissue lesions with near infra-red Raman spectroscopy'. *Advances in Fluorescence Sensing Technology*. **II** (SPIE 2388), 99-10 (1995).

5. Shim M, Song L. M, Marcon N. E, Wilson B. C. 'In vivo near-infrared Raman spectroscopy: Demonstration of feasibility during clinical gastrointestinal endoscopy'. *J Photochem Photobiol*. **72,** 146-150 (2000).

6. Kendall C, Stone N, Shepherd N, Geboes K, Warren B, Bennett R, Barr H. 'Raman spectroscopy a potential tool for the objective identification and classification of neoplasia in Barrett's oesophagus'. *J Pathology.* **200**, 602-609 (2003).

7. Stone, N. 'Raman Spectroscopy of biological tissue for the application in optical diagnosis of malignancy'. *Department of Environmental and Ordinance Systems R.M.C.S. and Cranfield post graduate medical school*, Cranfield University. *PhD Thesis*. (2001).

8. Bakker Schut T. C, Witjes M. J. H, Sterenborg H. J. C. M, et al. 'In vivo detection of dysplastic tissue by Raman spectroscopy'. *Anal Chem.* **72**, 6010-6018 (2000).

9. Schrader B, Keller S, Lochte T, Fendel S, Moore D. S, Simon A, Sawatzki I. 'FT Raman Spectroscopy in medical diagnostics'. *J Mol Struct*. **348**, 293-296 (1995).

10. Edwards H, Williams A, Barry B. 'Potential applications of FT-Raman spectroscopy for dermatological diagnosis'. *J Mol Struct*. **347,** 379-387 (1995).

11. Caspers P, Lucassen G. W, Wolthuis R, Bruining H. A, Puppels G. J. 'In vitro and in vivo Raman spectroscopy of human skin'. *Biospectroscopy*. **4**, S31-S39 (1998).

12. Stone N, Stravroulaki P, Kendall C, Birchall M, Barr H. 'Raman spectroscopy for early detection of laryngeal malignancy - preliminary results'. *Laryngoscope*. **110**, 1756-1763 (2000).

13. Crow P, Stone N, Kendall C. A, Uff JS, Farmer J. A, Barr H, Wright M. P. 'The use of Raman spectroscopy to identify and grade prostatic adenocarcinoma in vitro'. *BJC*. **89(1),** 106-108 (2003).

14. Stone N, Kendall C, Shepherd N, Crow P, Barr H. 'Near-infrared Raman spectroscopy for the classification of epithelial pre-cancers and cancers.' *JRS.* **33,** 564-573 (2002).

15. Shafer-Peltier, K. E, Haka, A. S, Fitzmaurice, M, Crowe, J, Myles, J, Dasari, R. R, Feld, M. S. 'Raman microspectroscopic model of human breast tissue: implications for breast cancer diagnosis in vivo,' *JRS.* **33**(7): 552-563. (2002).

16. Meyer J. P, Gillat D. 'What's new in bladder cancer?' *Trends in Urol Gynaecol and Sexual Health*. **8 (6),** 25-29, (2003).

17. Cancer Research UK *Cancerstats monograph.* (2004).

18. Kurth, K. H., Mickisch, G.H., Schroder, F.H. *Renal, bladder and prostate cancer - an update*. Parthenon Piblishing. (1998).

19. Tortora, G. J., Grabowski, S.R. *Principles of Anatomy and Physiology*, Harper Collins College. (1996).

20. Kurth, K.H., Mickisch, G.H., Schroder, F.H. *Renal, bladder, prostate and testicular cancer - an update.* Parthenon Publishing. (2000).

21. Hata, T.R., Scholz, T.A., *et al*. "Non-invasive Raman spectroscopic detection of carotenoids in human skin." *Journal of Investigative Dermatology* **115**(3): 441-448. (2000).

22. Toniolo, P., A. L. Van Kappel, et al. "Serum carotenoids and breast cancer." *American Journal of Epidemiology* **153**(12): 1142-1147. (2001).

23. Czeczuga-Semeniuk, E., Wolczynski, S., *et al*. "Preliminary identification of carotenoids in malignant and benign neoplasms of the breast and surrounding fatty tissue." *Neoplasma* **50**(4): 280-286. (2003).

24. Anonymous "MRI technique could replace breast cancer biopsies." Biophotonics international **dec**: 13. (2003).

25. Shafer-Peltier, K. E., A. S. Haka, et al. "Chemical basis for breast cancer diagnosis using Raman spectroscopy." *Lasers in Surgery and Medicine*: 3. (2002).

26. Shafer-Peltier, K. E., A. S. Haka, et al. "Raman microspectroscopic model of human breast tissue: implications for breast cancer diagnosis in vivo." *Journal of Raman Spectroscopy* **33**(7): 552-563. (2002).

Legends:

Fig 1. The mean spectrum of actin.

Fig 2. The mean spectrum of ß carotene.

Fig 3. The mean spectrum of cholesterol.

Fig 4. The mean spectrum of choline.

Fig 5. The mean spectrum of collagen type 1 (col1).

Fig 6. The mean spectrum of collagen type 3 (col3).

Fig 7. The mean spectrum of collagen type 4 (col4).

Fig 8. The mean spectrum of DNA.

Fig 9. The mean spectrum of glycogen.

Fig 10. The mean spectrum of lycopene.

Fig 11. The mean spectrum of oleic acid.

Fig 12. The mean spectrum of triolein.

Fig 13. The mean spectra obtained for each bladder pathology.

Fig 14. A bar graph showing the relative concentration of each constituent for each bladder pathology. Normalised to a total of unity, (the pathology relating to the groups are specified in the table below).

Fig 15. The mean spectra obtained for each prostate pathology.

Fig 16. A bar graph showing the relative concentration of each constituent for each prostate pathology. Normalised to a total of unity. (the pathology relating to the groups are specified in the table below).

Table 1. The relative percentages of each constituent present in each bladder pathology.

Table 2. The relative percentages of each constituent present in each prostate pathology.

Figures:

Figure 1.

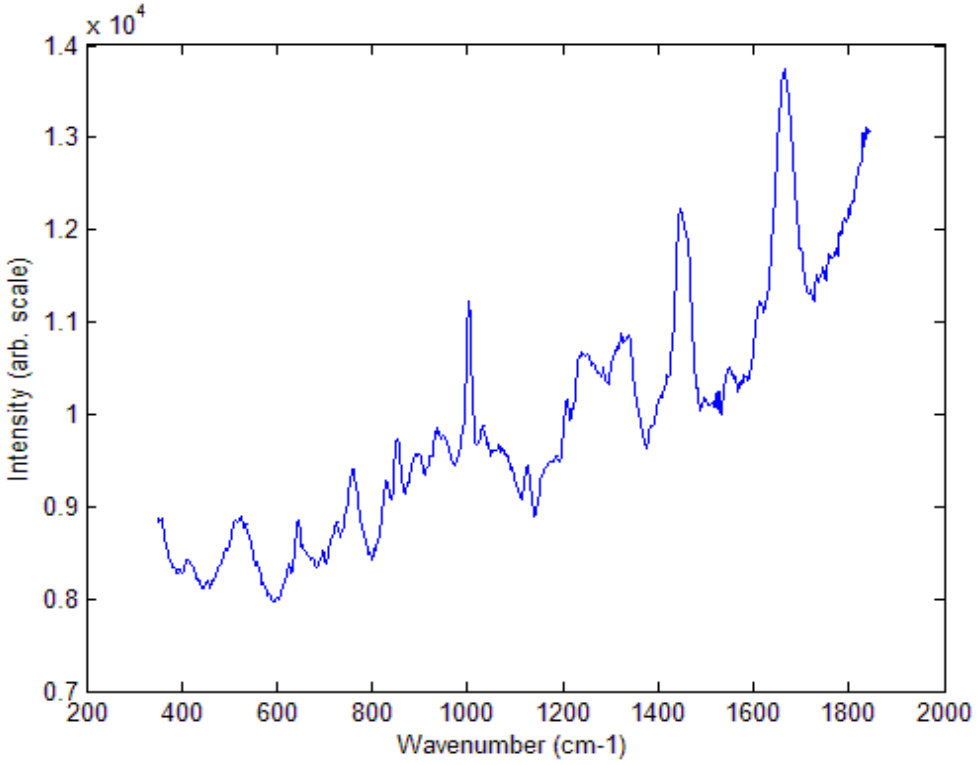

Figure 2.

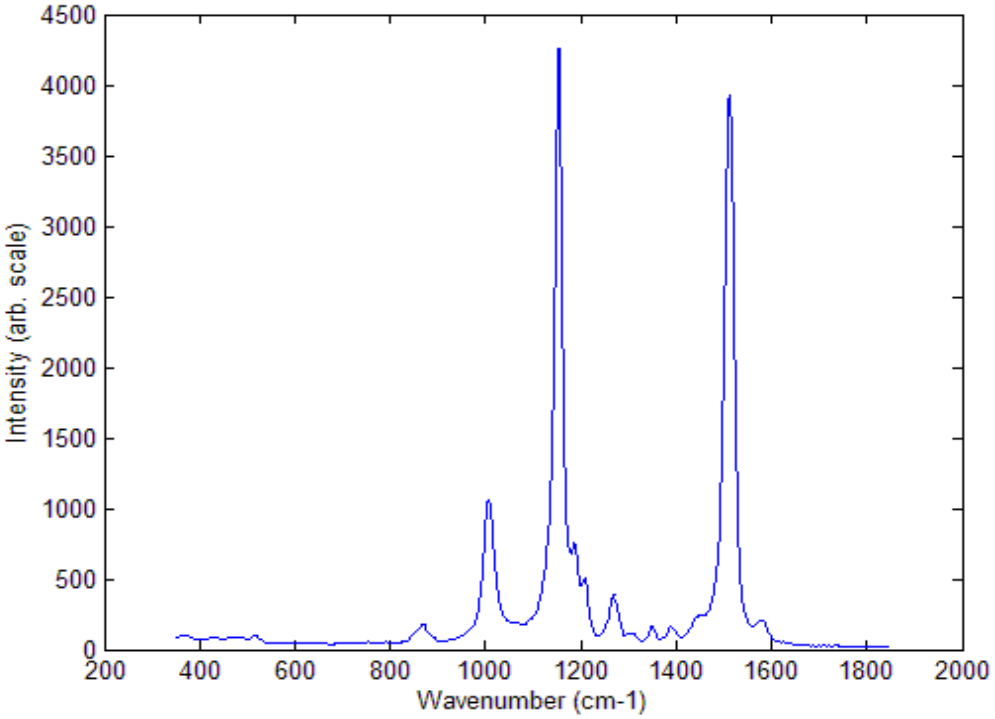

Figure 3.

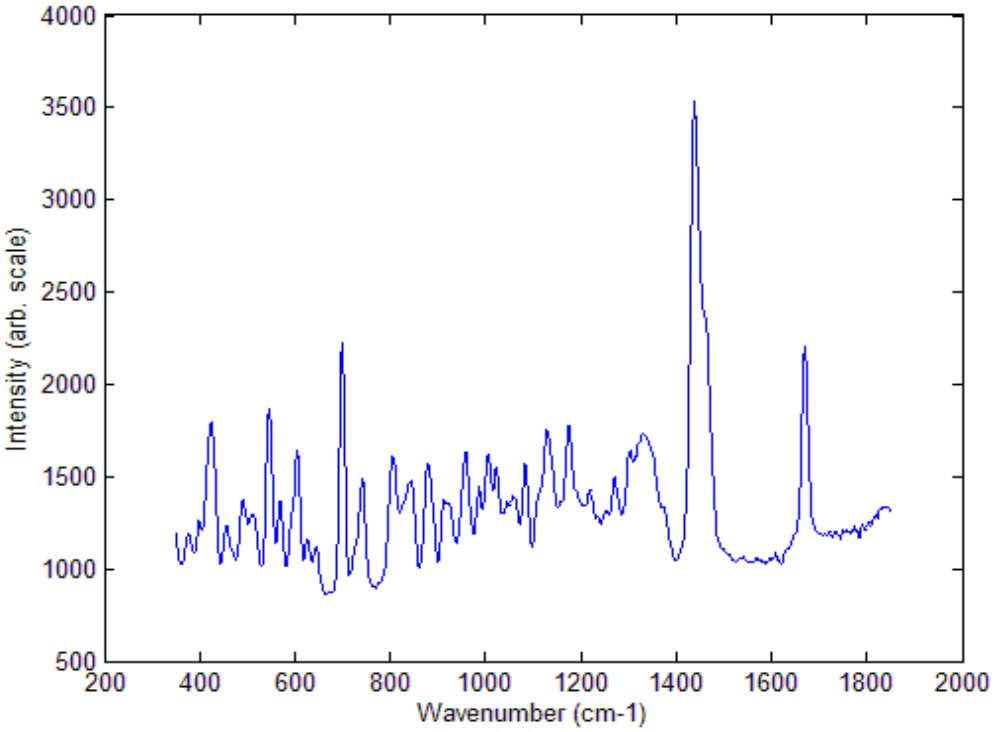

Figure 4.

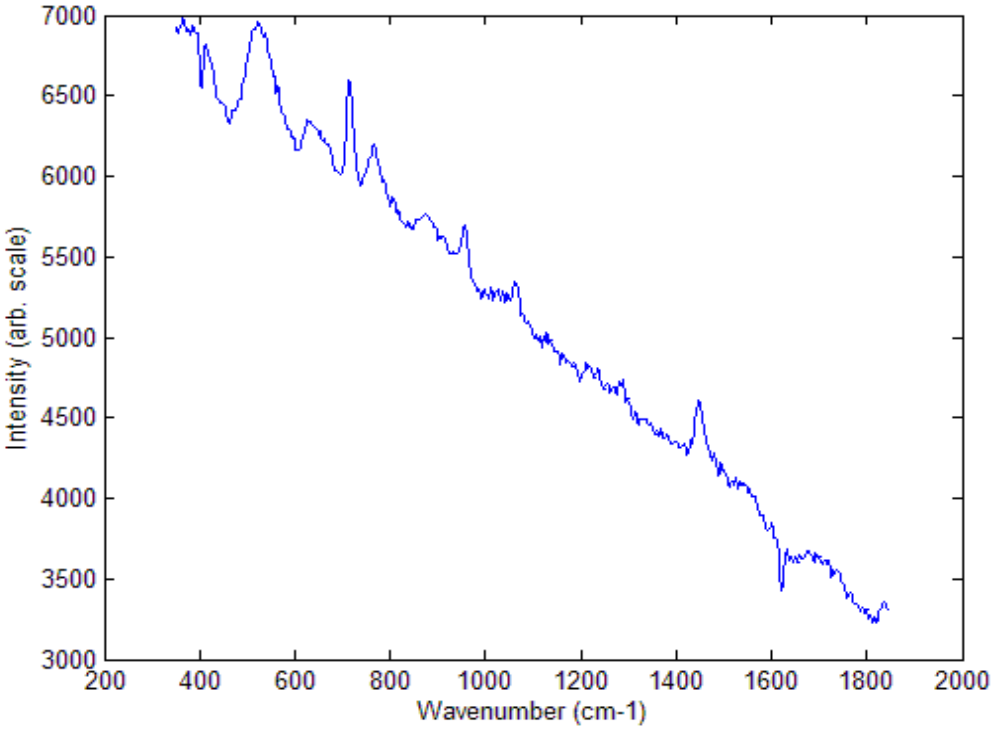

Figure 5.

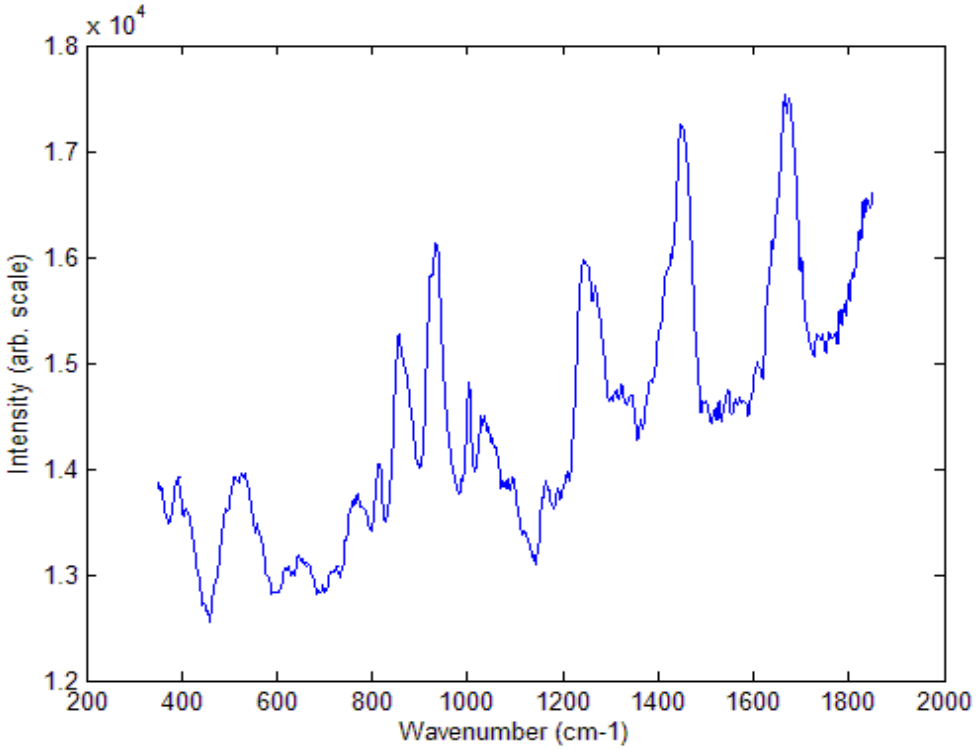

Figure 6.

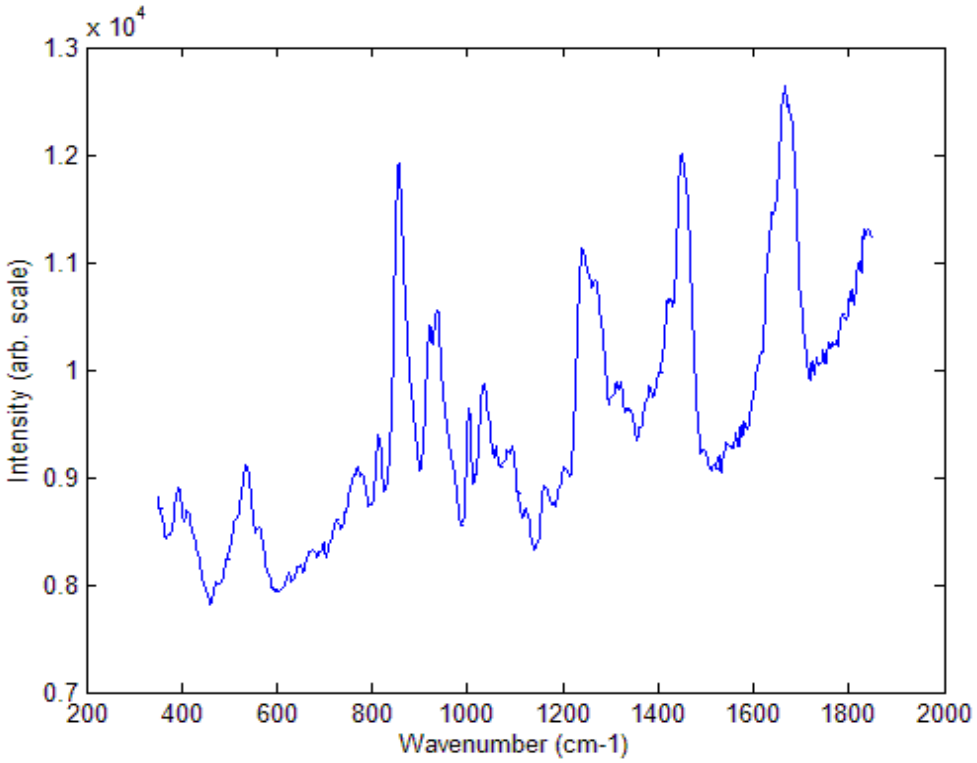
x 10^4
1.3
1.2
1.1
1
0.9
0.8
0.7
Intensity (arb. scale)
200
400
600
800
1000
1200
1400
1600
1800
2000
Wavenumber (cm-1)

Figure 7.

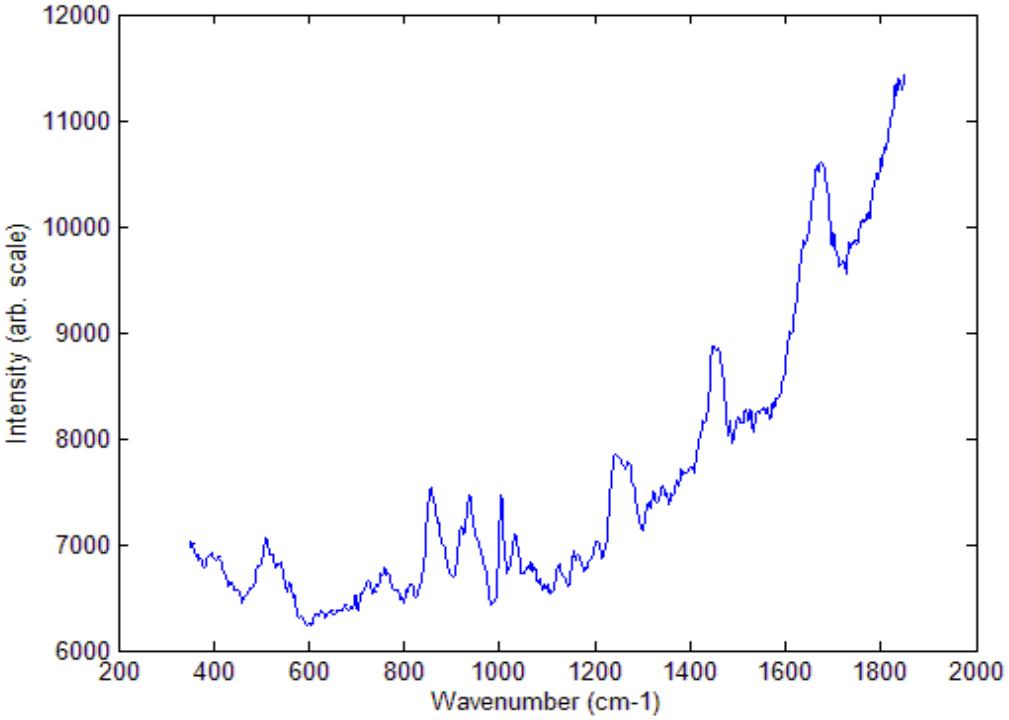
12000
11000
10000
9000
8000
7000
6000
Intensity (arb. scale)
200
400
600
800
1000
1200
1400
1600
1800
2000
Wavenumber (cm-1)

Figure 8.

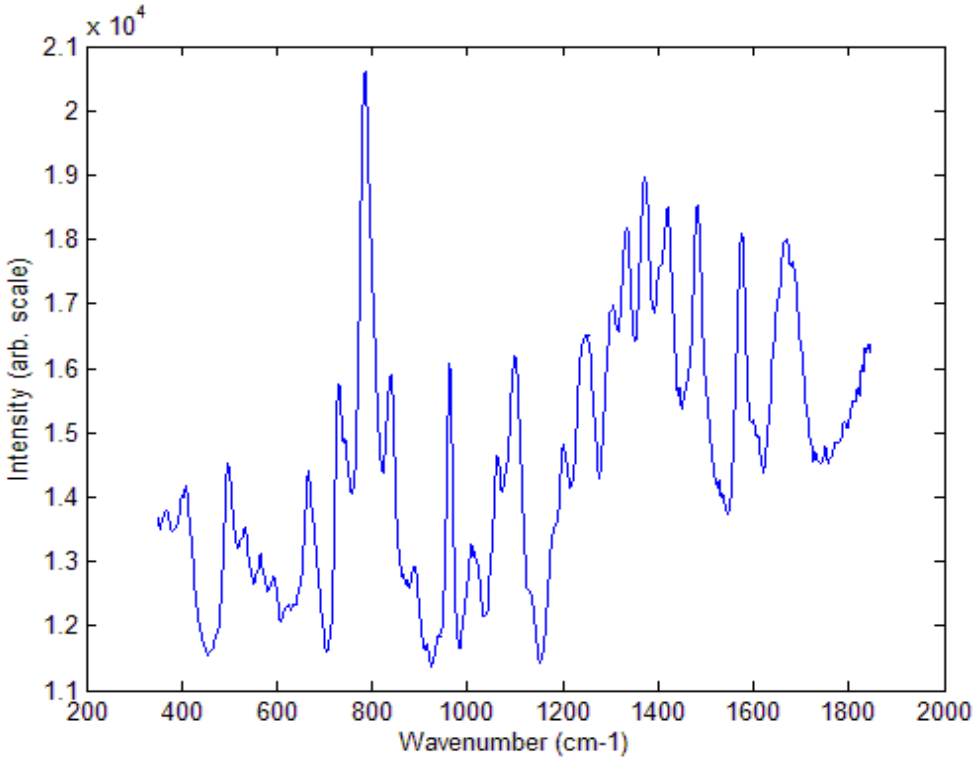

Figure 9.

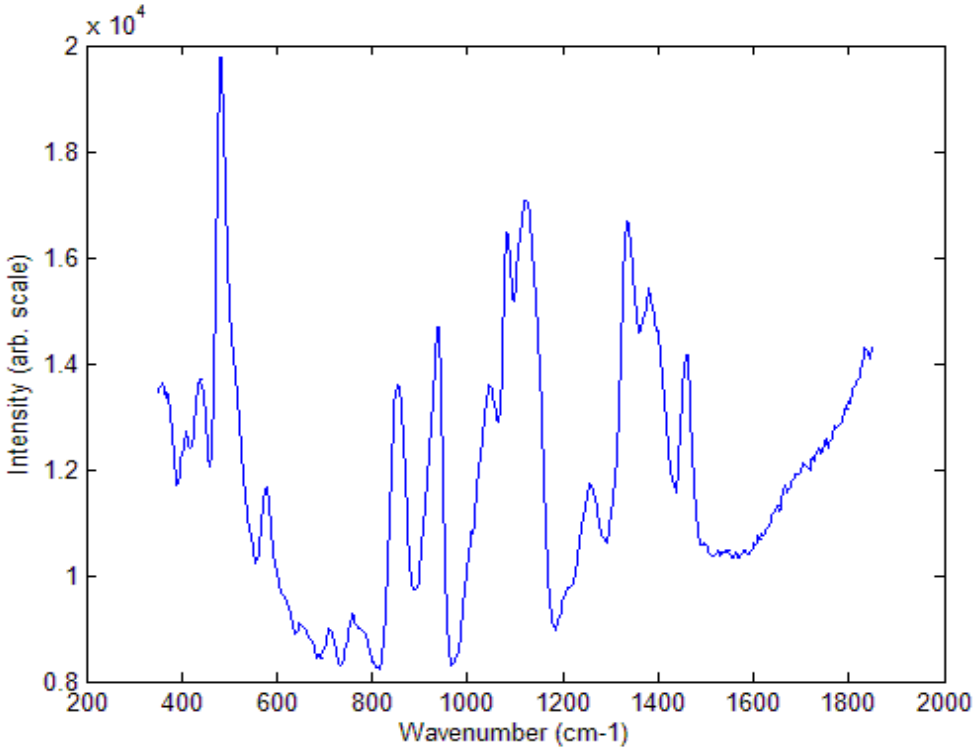

9.

Figure 10.

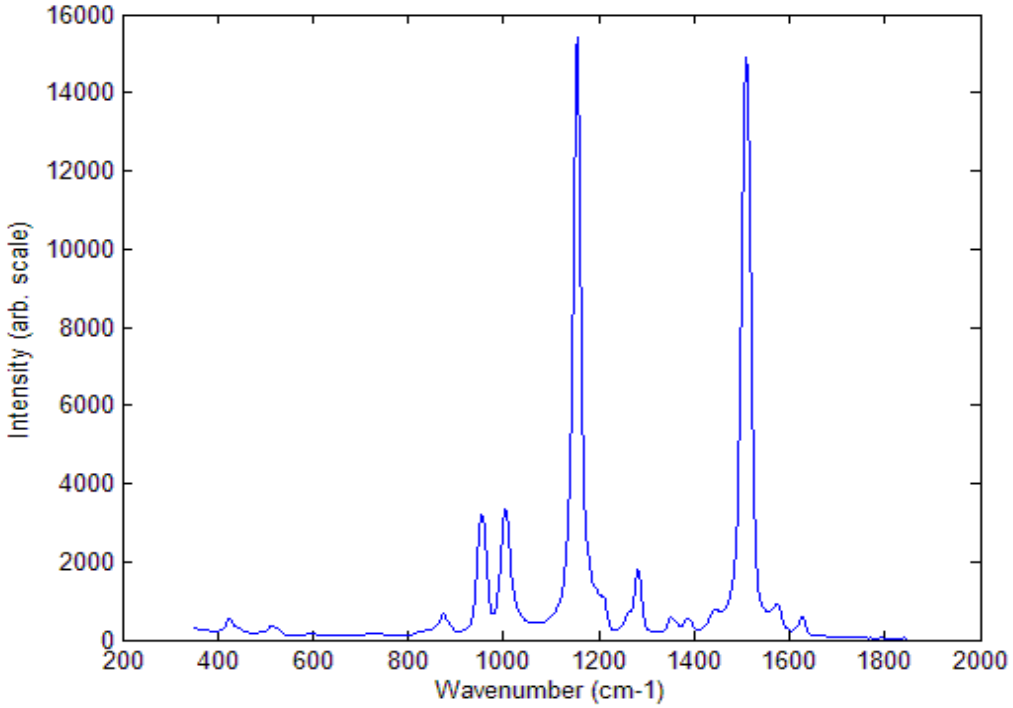
16000
14000
12000
10000
8000
6000
4000
2000
0
Intensity (arb. scale)
200
400
600
800
1000
1200
1400
1600
1800
2000
Wavenumber (cm-1)

Figure 11.

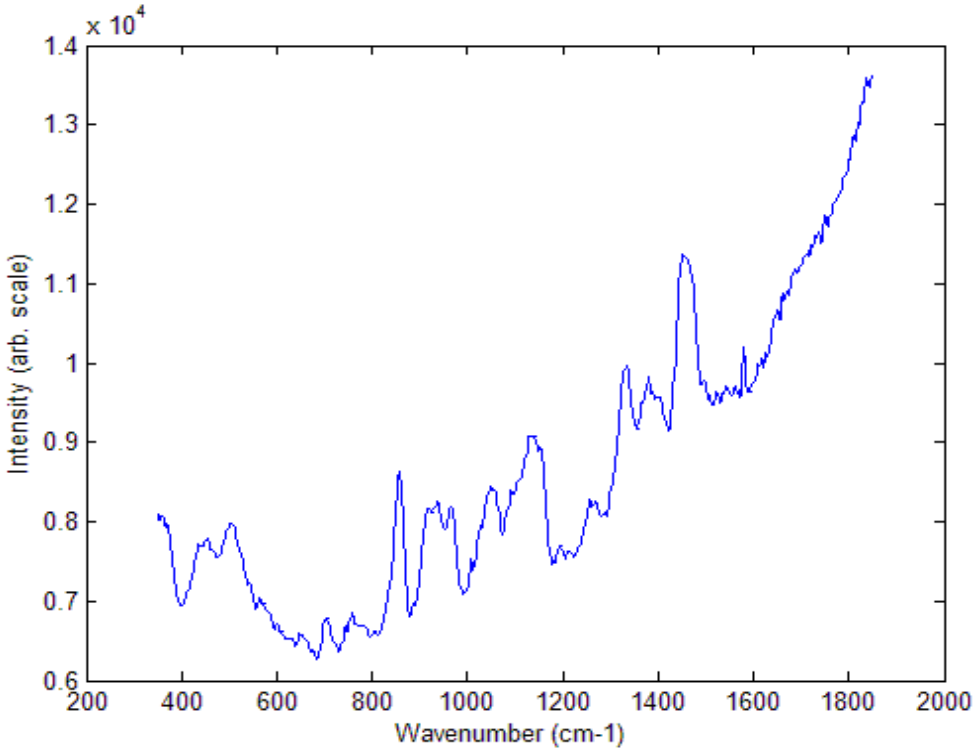
x 10^4
1.4
1.3
1.2
1.1
1
0.9
0.8
0.7
0.6
Intensity (arb. scale)
200
400
600
800
1000
1200
1400
1600
1800
2000
Wavenumber (cm-1)

Figure 12.

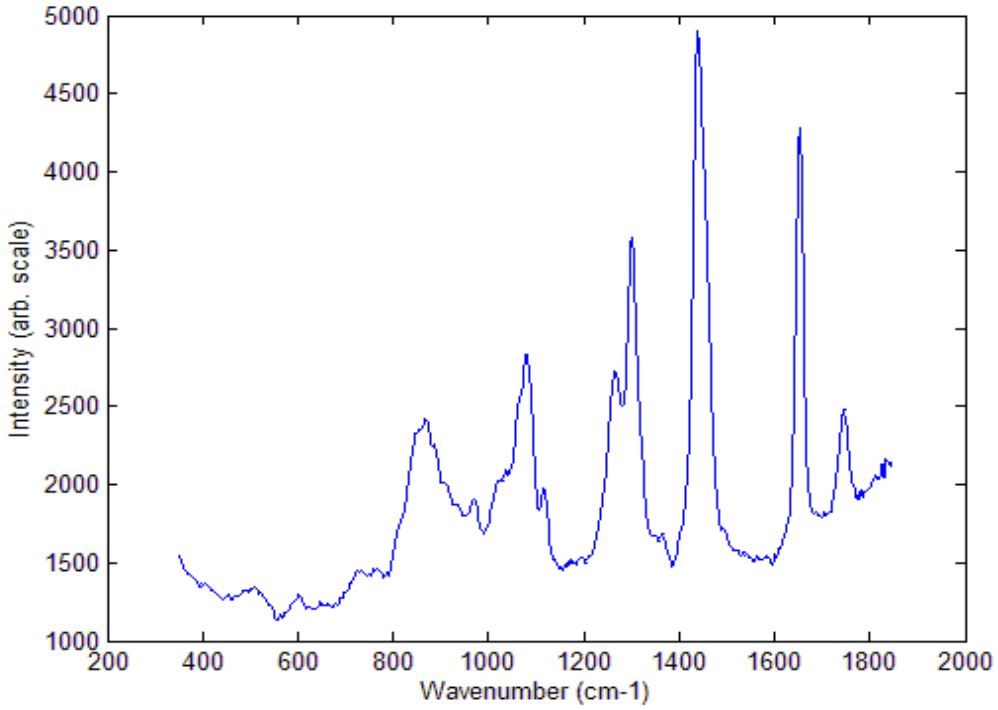

Figure 13.

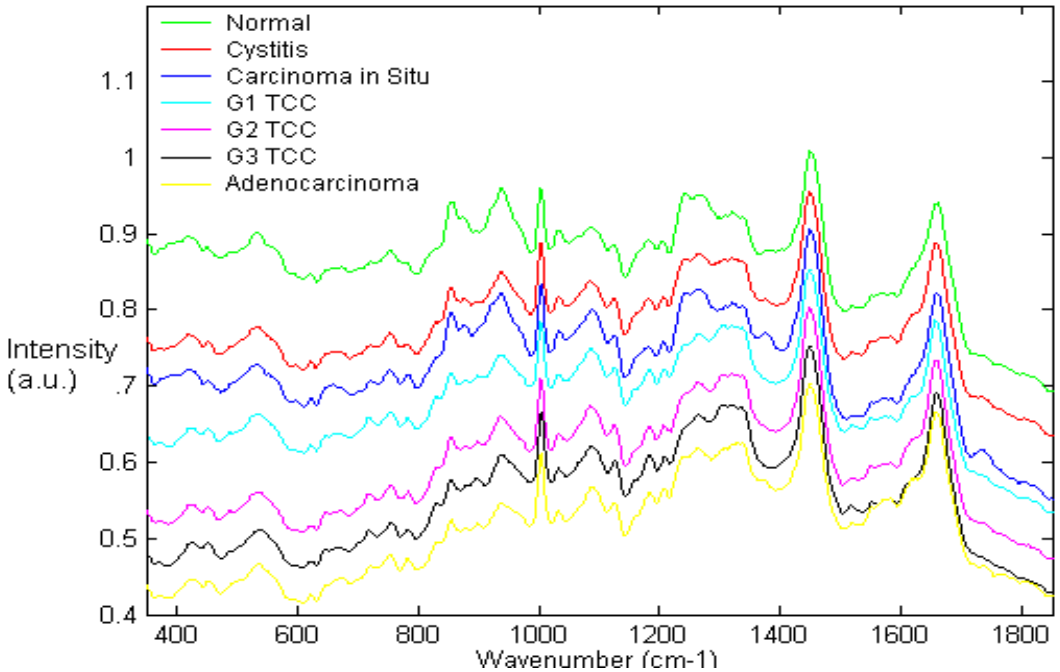

Figure 14.

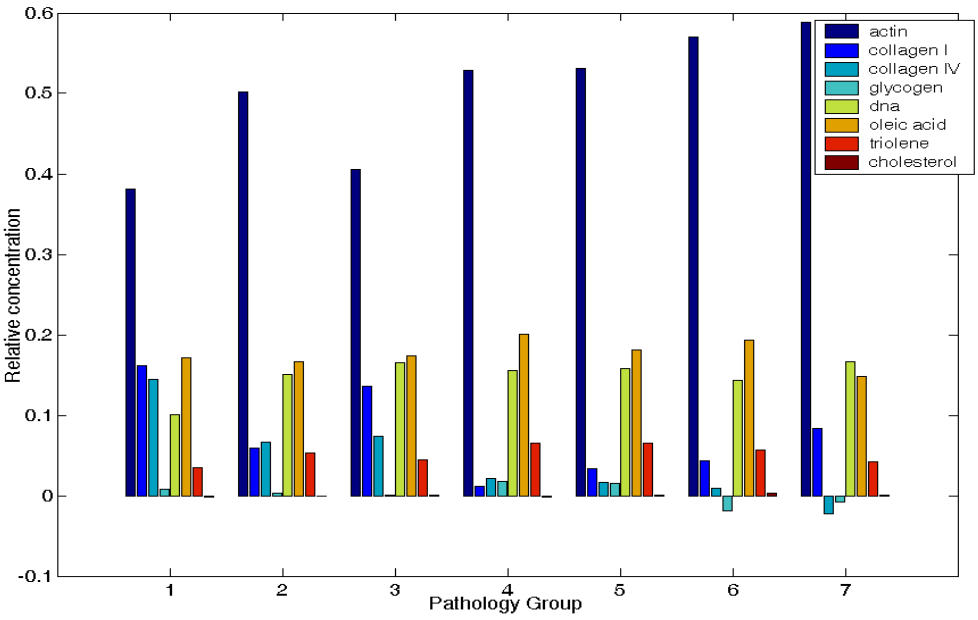

Figure 15.

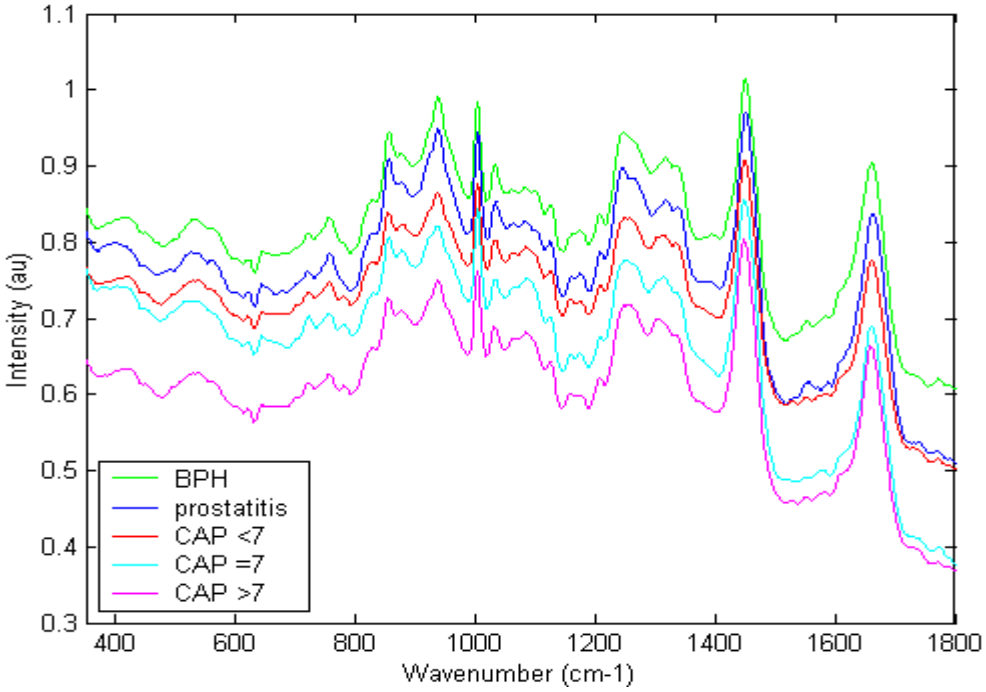

Figure 16.

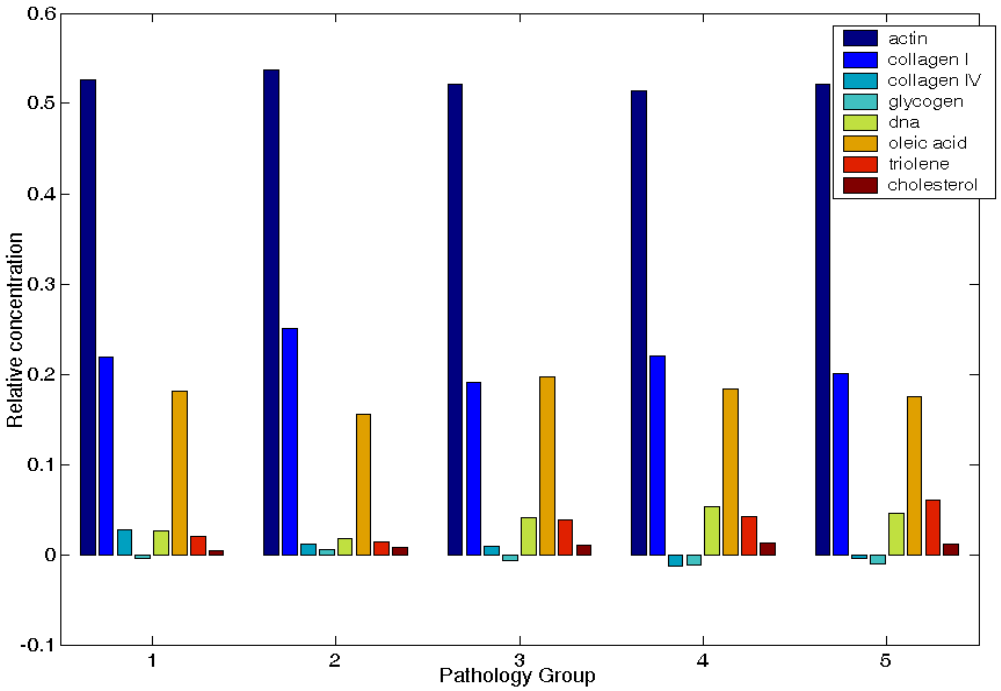

Tables:

Table 1.

Pathology	No	Actin (%)	Col1 (%)	Col4 (%)	Glycogen (%)	DNA (%)	Oleic acid (%)	Triolein (%)	Cholesterol (%)
Normal	1	42.2	17.9	5.4	0.8	11.1	19.0	3.9	-0.2
Cystitis	2	52.5	6.1	2.3	0.4	15.8	17.4	5.6	-0.0
CIS	3	42.6	14.2	2.6	0.1	17.4	18.3	4.7	0.1
G1 TCC	4	53.7	1.2	0.7	1.9	15.8	20.3	6.7	-0.2
G2 TCC	5	53.8	3.4	0.6	1.5	15.9	18.3	6.6	0.0
G3 TCC	6	57.4	4.4	0.3	-2.0	14.5	19.5	5.7	0.3
AdenoCa	7	58.0	8.2	0.7	-0.7	16.4	14.6	4.2	0.0

Table 2

Pathology	No	Actin (%)	Col1 (%)	Col4 (%)	Glycogen (%)	DNA (%)	Oleic acid (%)	Triolein (%)	Cholesterol (%)
BPH	1	52.6	21.9	2.7	-0.4	2.6	18.1	2.0	0.4
Prostatitis	2	53.7	25.1	1.2	0.6	1.8	15.5	1.4	0.7
Gleason <7	3	52.1	19.1	0.9	-0.7	4.1	19.6	3.8	1.1
Gleason 7	4	51.4	22.1	-1.2	-1.2	5.3	18.3	4.2	1.2
Gleason >7	5	52.1	20.1	-0.4	-1.1	4.6	17.5	6.1	1.2